

Proceedings of the
**7th Patras Workshop on Axions,
WIMPs and WISPs**

**27 June - 1 July 2011
Mykonos
Greece**



Editors:
Konstantin Zioutas
Marc Schumann

VERLAG DEUTSCHES ELEKTRONEN-SYNCHROTRON

Proceedings of the
7th Patras Workshop
on Axions, WIMPs and WISPs

PATRAS 2011

June 27–July 1, 2011

Mykonos, Greece

Editors: Marc Schumann, Konstantin Zioutas

Verlag Deutsches Elektronen-Synchrotron

Impressum

Proceedings of the 7th Patras Workshop on Axions, WIMPs and WISPs (PATRAS 2011) June 27–July 1, 2011, Mykonos, Greece

Conference homepage
<http://axion-wimp2011.desy.de/>

Slides at
<http://axion-wimp2011.desy.de/e102694/>

Online proceedings at
<http://www-library.desy.de/confprocs.html>

The copyright is governed by the Creative Commons agreement, which allows for free use and distribution of the articles for non-commercial activity, as long as the title, the authors' names and the place of the original are referenced.

Editors:
Marc Schumann and Konstantin Zioutas
December 2011
DESY-PROC-2011-04
ISBN 978-3-935702-59-1
ISSN 1435-8077

Published by
Verlag Deutsches Elektronen-Synchrotron
Notkestraße 85
22607 Hamburg
Germany

Printed by
Kopierstelle Deutsches Elektronen-Synchrotron

Organizing Committee

Vassilis Anastassopoulos and Konstantin Zioutas (Chairman)
Department of Physics
University of Patras
26504 Patras
Greece

Laura Baudis and Marc Schumann
Physik Institut
University of Zurich
Winterthurerstr. 190
8057 Zurich
Switzerland

Joerg Jaeckel
Institute for Particle Physics Phenomenology (IPPP)
Durham University
South Road
Durham DH1 3LE
United Kingdom

Axel Lindner and Andreas Ringwald
Deutsches Elektronen Synchrotron (DESY)
Notkestraße 85
D-22607 Hamburg
Germany

Conference Secretary and Local Organization

Mary Tsagri
CERN CH-1211
Genève 23
Switzerland

Barbara Wittmann
Deutsches Elektronen Synchrotron (DESY)
Notkestraße 85
D-22607 Hamburg
Germany

Hero Zioutas
Tavropou-Larisou 2
26442 Patras
Greece



7th Patras Workshop on Axions, WIMPs and WISPs

26 June - 1 July 2011
Mykonos (GR)

Programme

- The physics case for WIMPs, Axions, WISPs
- Review of collider experiments
- Signals from astrophysical sources
- Direct searches for Dark Matter
- Indirect laboratory searches for Axions, WISPs
- Direct laboratory searches for Axions, WISPs
- New theoretical developments

Organizing committee:

Vassilis Anastassopoulos (University of Patras)

Laura Baudis (University of Zurich)

Joerg Jaeckel (IPPP/Durham University)

Axel Lindner (DESY)

Andreas Ringwald (DESY)

Marc Schumann (University of Zurich)

Konstantin Zioutas (University of Patras) (chairman)

<http://axion-wimp.desy.de>

Preface

The year 2011 was an exciting period to work on the “dark side” of the Universe. Several experimental claims of the direct detection of WIMP dark matter were challenged by the restrictive limits of several others. Dedicated experiments searching for axions, another well motivated dark matter candidate, and for axion-like particles continued to improve their limits and got an additional boost by puzzling astrophysical observations and new developments in theory. The LHC collected an unexpectedly large amount of data and started to produce results at an amazing speed. And finally, this year’s Nobel price of physics was awarded to the observation of the accelerating expansion of the Universe, an effect which might be related to dark energy, whose nature remain among the biggest mysteries in physics.

These exciting topics and many more important aspects of particle- and astroparticle physics were discussed between experimentalists and theorists at the 7th Patras Workshop on Axions, WIMPs, and WISPs. The workshop took place from June 27 – July 1, 2011, in the Royal Myconian & Myconian Imperial Resorts Hotels on the Greek island of Mykonos. As in the previous years, it was a very fruitful and lively meeting in an inspiring and open atmosphere, which allowed for many open and constructive discussions also on controversial topics. The scientific exchange, the beautiful scenery of the island, the venue itself, the food, an excursion to the ancient ruins of Delos, and finally an amazing conference dinner made this meeting really unique.

The “spirit” of the workshop and its atmosphere cannot be brought to paper, but many of its scientific highlights are collected in these proceedings.

We are looking forward to the 8th Patras Workshop, which will be held in Chicago (USA) July 18–22, 2012. It will be organized jointly by our US colleagues Andrei Afanasev (JLAB), Oliver Baker (Yale), and William Wester (FNAL).

Marc Schumann and Konstantin Zioutas

Acknowledgements

The organizers would like to thank the University of Patras, CAST, DESY, CERN, the IPPP Durham, and the University of Zurich for support. Special thanks also to Mary Tsagri (CERN) for the local support and to Barbara Wittmann (DESY) for creating the online presence of the conference. All participants recognized the engagement of Hero Zioutas during the workshop. We are thankful for her efforts to convince the chairman to organize the workshop on Mykonos. We thank the hotel manager Panagiotis Dahtilidis for the excellent cooperation. Finally, we acknowledge the supporting work from Thanasis Manousos (Thessaloniki) to put these proceedings together.

The organizing committee



Contents

1 WIMP Dark Matter	1
EDELWEISS dark matter search: Latest results and future plans Johann Gironnet	3
Dark Matter Searches with sub-keV Germanium Detectors Hau-Bin Li	7
Dark Matter Search with CRESST-II Raimund Strauss	11
The Search for Dark Matter with XENON Elena Aprile	15
Status of XMASS Yasuhiro Kishimoto	19
DARWIN Marc Schumann	23
Prospects for dark matter searches with CTA Emmanuel Moulin	27
Indirect Dark Matter search with H.E.S.S. Giovanni Lamanna	31
Positronium Portal to the Mirror World Paolo Crivelli	35
2 Axion Dark Matter and Searches for Axions and WISPs	41
Axion BEC Dark Matter Pierre Sikivie	43
The Axion Dark-Matter eXperiment: Results and plans Gray Rybka and David Tanner	47
Preliminary Results from the Yale Microwave Cavity Experiment Andrew J. Martin	51
<i>PATRAS 2011</i>	vii

Cold Dark Matter from the Hidden Sector	56
Paola Arias	
Dark Forces and Dark Matter in a Hidden Sector	60
Sarah Andreas	
Microwave Hidden Sector Photons at UWA	64
Rhys G. Povey	
GammeV: Laser Experiments at Fermilab for WISPs and Other Effects	68
William Wester	
Status of ALPS-II at DESY	72
Jan Eike von Seggern	
Status report of the CERN light shining through the wall experiment with microwave axions and related aspects	76
Michael Betz	
Minicharged particles in light-shining-through-wall experiments and the photon polarization tensor	82
Babette Döbrich and Felix Karbstein	
Notes from the 5th Axion Strategy Meeting	88
Giovanni Cantatore	
3 Solar Axions	91
CAST: Status and Latest Results	93
Theopisti Dafni	
The International Axion Observatory (IAXO)	98
Igor Irastorza	
Solar paraxions	102
Sergey Troitsky	
Search for 5.5 MeV Solar Axions produced in a $p(d, 3He)A$ Reaction with Borexino	107
Alexander Derbin	
A Search for the Resonant Absorption of Solar Axions by Atomic Nuclei	112
Evgeniy Unzhakov	
Solar Chameleons: Production and Detection	116
Philippe Brax	
Solar flares as harbinger of new physics	120
Konstantin Zioutas	
The SphinX Spectrometer for solar soft X-rays	125
Szymon Gburek	

Solar Hidden Photon Search	129
Matthias Schwarz	
The Sun in Hidden Photons	133
Javier Redondo	
4 Cosmological Implications and Constraints	137
Cosmological constraints on thermal relic axions and axion-like particles	139
Davide Cadamuro	
How a cold axion background influences photons	143
Domènec Espriu	
New constraints on very light pseudoscalars	147
Alexandre Payez	
Indications for a suppression of pair production at very high energies	151
Manuel Meyer	
White dwarfs as physics laboratories: the case of axions	158
Jordi Isern	
5 Accelerator Physics and other Topics	163
Z' from GUTs, CPs, Axions, and the μ Problem	165
Jihn E. Kim	
LHCb Physics, Performance, Prospects	169
Olaf Steinkamp	
ATLAS Results on SUSY	174
Bilge M. Demirköz	
Proton EDM Simulations Using Fourth-Order Runge-Kutta Integration	179
Yannis K. Semertzidis	
List of Authors	183
List of Participants	187



Chapter 1

WIMP Dark Matter

EDELWEISS dark matter search: Latest results and future plans

Johann Gironnet

Institut de Physique Nucléaire, Lyon, France

DOI: http://dx.doi.org/10.3204/DESY-PROC-2011-04/gironnet_johann

EDELWEISS is a direct search for WIMP dark matter using cryogenic heat-and-ionization germanium detectors. We report the final results of the second stage of the experiment, EDELWEISS-II, obtained with an array of ten 400 g detectors. A total effective exposure of 384 kg.day has been achieved, obtained following fourteen months of continuous operation at the Laboratoire Souterrain de Modane. Five nuclear recoil candidates are observed above 20 keV, while the estimated background is less than 3 events. We also present the prospects of EDELWEISS-III, which plans to accumulate more than 3000 kg.day of data with forty new 800 g detectors.

1 The EDELWEISS-II experiment

The EDELWEISS [2] experiment is dedicated to the direct detection of WIMPs trapped in the Milky Way halo. The detection is performed through the measurement of the recoil energy produced by the elastic scattering of a WIMP off target nuclei. The main constraints are the extremely low event rate (<1 evt/kg/year) and relatively small deposited energy (in the tens of keV range). The goal of the phase II of the project is to explore wimp-nucleon cross section of a few 10^{-8} pb, thus requiring a background of less than 10^{-3} nuclear recoil candidate per kg.day above 10keV. For the search, the detectors are operated in a radiopure underground environment located in the Laboratoire Souterrain de Modane (LSM) where the 4850 meter-water-equivalent rock cover reduces the cosmic-ray background by six order of magnitude. The experiment is protected by the *gamma*-ray background with a 20 cm lead shield and through a very careful selection of all materials. A clean room surrounds the whole experiment and a class 100 laminar flow with deradonised air (<0.1 Bq/m³) is used when mounting the detectors. Fast neutrons are a particular background as their scattering in the detector can induce germanium recoil similar to those expected from WIMPs. The fast neutron flux is moderated through a 50 cm polyethylene shield surrounding the lead shield. It has been measured to be 10^{-6} n/cm²/s above 1 MeV. A muon veto with a 98% geometric efficiency surrounds the polyethylene shield, in order to tag neutrons created by muon interactions inside the lead shield. The experimental volume is about 50 liters allowing the installation of up to 40 kg of detectors in a compact arrangement for self shielding and multiple interaction identification. EDELWEISS uses high purity Germanium cryogenic detectors with simultaneous measurement of phonon and ionization signals at ≈ 20 mK. A nucleus recoil produces approximately three times less ionization than an electron recoil does, allowing an excellent event-by-event discrimination between nuclear recoils (induced by WIMPs or neutron scattering) and electron recoils (induced

by α , β and γ radioactivity). The actual limitation of this technique arises from incomplete charge collection for near-surface events (mainly low energy electrons from residual ^{210}Pb , a daughter of radon that is present on all surfaces): because of diffusion, recombination and trapping processes a small fraction of surface events could be miscollected and even mimic nuclear recoil interactions. The EDELWEISS collaboration has recently developed a new type of detectors, the so-called ID (InterDigit) detectors [1] with an active surface event rejection based on a special interdigitized electrodes scheme. The detectors are made from hyperpure germanium crystal of cylindrical shape with a diameter of 70mm and a height of 20mm. Each flat surface is covered with concentric aluminum ring electrodes of 2mm pitch regrouped in two sets of electrodes connected alternatively by ultrasonic bonding. Two additional plain guard electrodes cover the outer edges of the crystal. With the additional cut on the interleaved electrodes, corresponding to depth down to 1mm below the flat surfaces, the resulting fiducial volume per detector is 165 g.

2 EDELWEISS-II results

A WIMP search was carried out using ten 400-g ID detectors from April 2009 to May 2010. During the whole acquisition period, the cryogenic conditions were maintained stable at 18 mK.

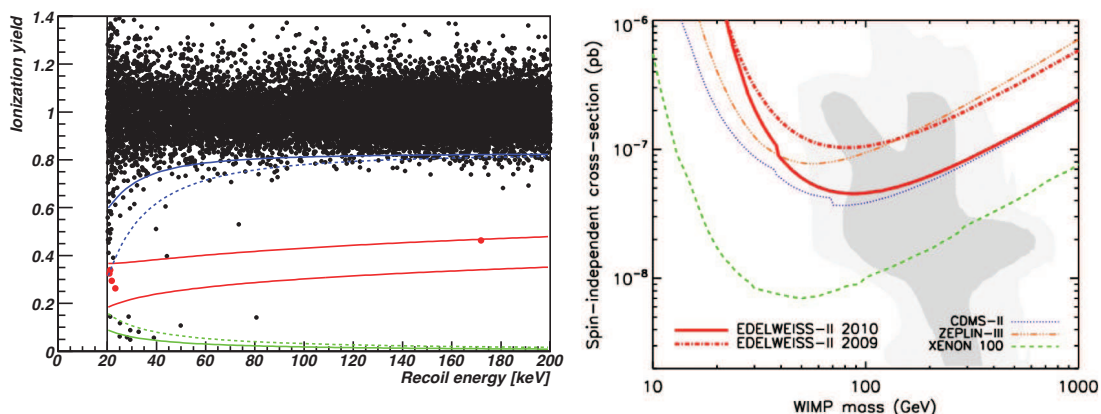


Figure 1: Left pannel: Ionization yield as a function of recoil energy for the 384 kg.d exposure collected by EDELWEISS for its WIMP search with ten 400g ID detectors. Right pannel: Limits on the cross-section for spin-independent scattering of WIMPs on the nucleon as a function of WIMP mass, derived from the present work, together with the limits from CDMS [4], ZEPLIN [5] and XENON100 [6]. The shaded area correspond to the 68% and 95% probability regions of the cMSSM scan from Ref. [8].

Most of the time was devoted to WIMP search (325 days), and a small fraction to gamma and neutron calibrations (10.1 and 6.4 days). The data were analysed using two independent pipelines which yield consistent results. The average baseline resolutions of heat and fiducial ionization channels were of ≈ 1.2 keV FWHM and ≈ 0.9 keV FWHM, respectively. WIMPs interaction candidates were searched among fiducial events in the 90% CL nuclear recoil band. Tagging of coincident events in bolometers and the muon veto allowed to reject neutron-induced

recoils. A WIMP- search energy threshold was set a priori to 20 keV, energy above which efficiency is independent of the energy. After all cuts, the effective exposure obtained is 384 kgd. The analysis procedures and results are described in details in [2]. From the γ -ray calibration we obtain a γ rejection factor of $\approx 3.10^{-5}$. The origin of the six events leaking into the nuclear recoil band is being investigated but we can see on Figure 1. that the rejection is improved significantly with the new FID detectors without guard rings. Five events are found in the nuclear recoil band: four of them have energies between 20 and 23 keV, and one has 172 keV. All of them are well-reconstructed events, which lie well above the noise level of the detectors. Background studies are still ongoing to fully understand their origin. Upper limits may be derived from the known residual gamma, beta and neutron backgrounds, using calibration data, material radioactivity measurements and Monte Carlo simulation of the detectors. Overall, less than 3 events (90% CL) from known origin are expected. The spin-independent cross-section upper limit for WIMP-nucleon elastic scattering is calculated using the standard Yellin prescription [8] and halo model and parameters. The best sensitivity obtained by EDELWEISS-II is $4.4.10^{-8}$ pb at $M_\chi=85$ GeV. These data have been also interpreted in the inelastic dark matter scenario [2]. The resulting limits are shown in the right panel of Figure 1, compared with those of other direct WIMP searches [4, 5, 6]. The data has a significant impact on the total sensitivity obtained when combining it with the results of the other search using cryogenic germanium detectors, CDMS [7].

3 The EDELWEISS-III project: setup and detectors

The Inter-Digit detector technology has proven to be reliable and robust enough to perform direct detection of WIMPs at the highest level of the competition. To go beyond the present performances, a new generation of detectors has been developed with interleaved electrodes covering also the lateral surfaces of the crystal: the Full Inter-Digit (FID). A first series of four detectors has been tested. The combination of an unprecedented mass of 800 g and the FID technology increases significantly the fiducial mass of the detectors to ≈ 600 g (it was ≈ 165 g for the ID). In addition to this, the FID800 series benefits from two NTD sensors to have redundancy also in the heat measurement and new surface treatments to increase the surface event rejection [3]. The construction of an array of forty 800 g detector, to be completed by 2012, is in progress, with a projected sensitivity of WIMP scattering cross-section of 5×10^{-9} pb. This third stage of EDELWEISS will also see its cryogenics and electronics being upgraded for achieving a recoil energy analysis threshold below 15 keV. Further developments are being studied in the framework of the EURECA [9] collaboration, aiming for an experiment in the future extension of the underground laboratory at LSM, with a sensitivity goal of 10^{-11} pb . This project brings together the European efforts of EDELWEISS and also of the CRESST and ROSEBUD teams working on heat-and-scintillation detectors, to built a ton-scale multi-target array of cryogenic detectors.

4 Acknowledgments

The help of the technical staff of the Laboratoire Souterrain de Modane is gratefully acknowledged. This project is supported in part by the Agence Nationale pour la Recherche under contract ANR-06- BLAN-0376-01, by the Russian Foundation for Basic Research and by the Science and Technology Facilities Council, UK.

References

- [1] A. Broniatowski *et al.* [EDELWEISS Collaboration], PLB **681** (2009) 305.
- [2] E. Armengaud *et al.* [EDELWEISS collaboration], Phys. Lett. B **702** (2011) 329.
- [3] S. Marnieros *et al.*, AIP Conf. Proc. **635**, 1185 (2009).
- [4] Z. Ahmed *et al.*, Science **327** (2010) 1619.
- [5] V.N. Lebedenko *et al.*, Phys. Rev. D **80** (2009) 052010.
- [6] E. Aprile *et al.* [XENON Collaboration], Phys. Rev. Lett. **107** (2011) 131302.
- [7] Z. Ahmed *et al.* [CDMS and EDELWEISS Coll.], Phys. Review D **84** (2011) 011102.
- [8] L. Roszkowski *et al.*, JHEP **07** (2007) 075.
- [9] H. Kraus *et al.*, J. Phys. Conf. Ser. **39** (2006) 139.

Dark Matter Searches with sub-keV Germanium Detectors

Hau-Bin Li, Henry T. Wong

Institute of Physics, Academia Sinica
Taipei 11529, Taiwan

DOI: http://dx.doi.org/10.3204/DESY-PROC-2011-04/li_hau-bin

The theme of the TEXONO-CDEX research program is on the studies of low energy neutrino and dark matter physics at Kuo-Sheng Reactor Neutrino Laboratory and China Jin-Ping Underground Laboratory. The current goal is to open the “sub-keV” detector window with germanium detectors for dark matter searches. We highlight the status, results and plans in this article.

1 Physics Motivations and Goals

There are compelling evidence that about 20% of the energy density in the universe is composed of Cold Dark Matter[1] due to a not-yet-identified particle, generically categorized as Weakly Interacting Massive Particle (WIMP, denoted by χ). A direct experimental detection of WIMP is one of the biggest challenges in the frontiers of particle physics and cosmology.

The TEXONO Collaboration has contributed in formulating the physics program and in making technical advances to open a detector window in the previously unexplored “sub-keV” regime[2] with low-energy germanium detectors. The generic goals in terms of detector performance are: (1) modular target mass of order of 1 kg; (2) detector sensitivities reaching the range of 100 eV; (3) background at the range of $1 \text{ kg}^{-1}\text{keV}^{-1}\text{day}^{-1}$ (cpk/d). The neutrino physics program and dark matter searches is being pursued at the established Kuo-Sheng Reactor Neutrino Laboratory (KSNL), while underground dark matter searches will be conducted at the new China Jin-Ping Underground Laboratory (CJPL)[3]. The two facilities are depicted schematically in Figures 1a&b.

1.1 Cold Dark Matter Searches at KSNL and CJPL

The WIMPs interact with matter pre-dominantly via: $\chi + N \rightarrow \chi + N$. There may be both spin-independent and spin-dependent interactions.

Most experimental programs optimize their design in the high-mass region and exhibit diminishing sensitivities for $m_\chi < 10 \text{ GeV}$, where there is an allowed region if the annual modulation data of the DAMA experiment[4] are interpreted as WIMP signatures. There are increasing theoretical interest in this light-WIMP region[5, 6], which include models on light neutralinos, non-pointlike SUSY candidates like Q-balls, as well as WIMPlless, mirror, asymmetric, and singlet fermionic dark matter.

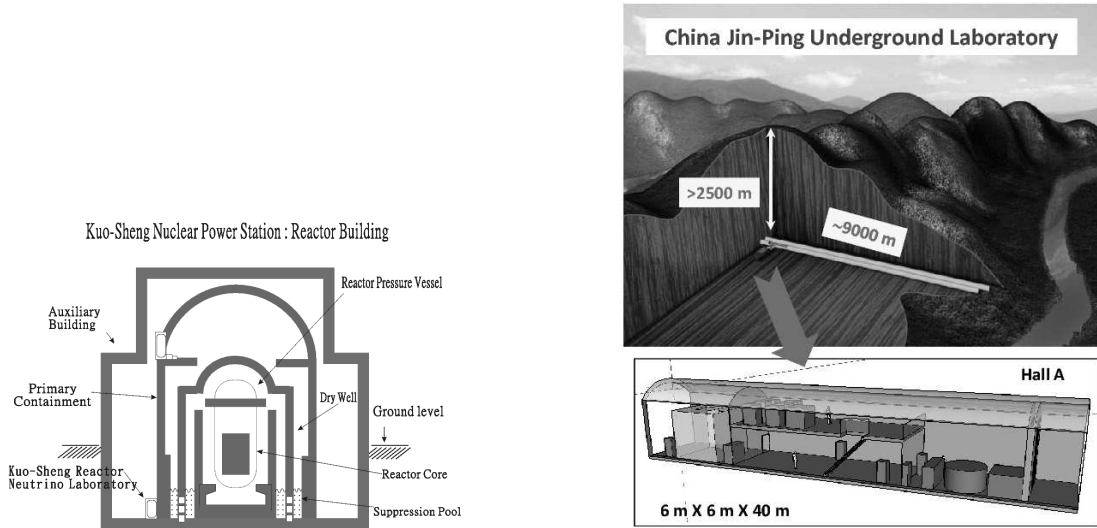


Figure 1: Schematic diagrams of the two facilities where our experiments are conducted: (a) Left: Kuo-Sheng Reactor Neutrino Laboratory (KSNL) (b) Right: China Jin-Ping Underground Laboratory (CJPL).

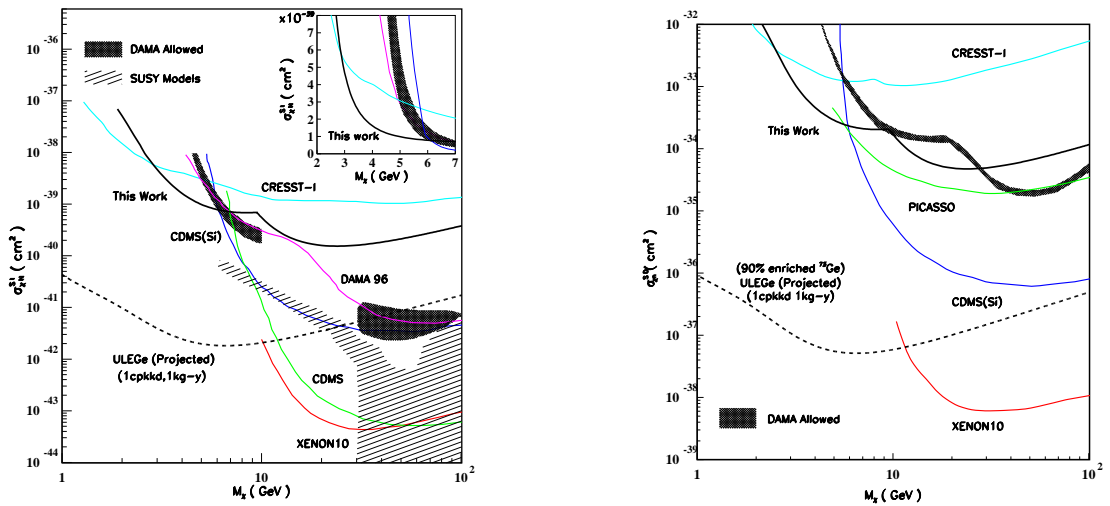


Figure 2: Exclusion plots of (a) Left: spin-independent χN and (b) Right: spin-dependent χN cross-sections versus WIMP-mass, displaying the KSNL-ULEGe limits and those defining the current boundaries. The DAMA allowed regions are superimposed. The striped region is that favored by SUSY models. Projected reach of experiments at benchmark sensitivities are indicated as dotted lines. The relevant region is presented with linear scales in the inset.

A detector with 100 eV threshold will therefore open a window for Cold Dark Matter WIMP searches[1] in the unexplored mass range down to several GeV[2]. The uniqueness and advantages of having a low-threshold detector are twofold. Firstly, a new window of observation is opened for low-mass WIMPs. Secondly, the minimum velocity of WIMPs that produces χN is proportional to the recoil energy. Therefore, a lower threshold allows a larger range of WIMPs to contribute in an observable interaction and hence results in better sensitivities for all values of m_χ .

Based on data taken at KSNL with the 20-g prototype Ultra-Low-Energy Germanium detector (ULEGe), competitive limits were derived in the low WIMP mass region ($3 < m_\chi < 6$ GeV)[7]. The $\sigma_{\chi N}^{\text{SI}}$ versus m_χ and $\sigma_{\chi N}^{\text{SD}}$ versus m_χ exclusion plots are depicted in Figures 2a&b, respectively. The various results[8][9][10] defining the exclusion boundaries are also shown.

The underground facility CJPL[3], shown in Figure 1b, is located at Sichuan, China, with ~ 2500 meter of rock overburden and tunnel drive-in access. It is owned by the Ertan Hydropower Development Company, and managed by Tsinghua University, China. Construction of the first experimental hall (“Hall A”) of dimension 6 m(width) \times 6 m(height) \times 40 m(length) and the first shielding structures were completed in September 2010. By the mid of 2011, the necessary infrastructures, office and dormitory spaces are being installed. The first experiment with the 20 g ULEGe and 1-kg PCGe are being set up in 2011. Upgrades of detector to the 10-kg mass range at the 2012–2013 frame are planned. Potential reaches with benchmark sensitivities are depicted by dotted lines in Figures 2a&b.

2 Sub-keV Germanium Detectors

Several R&D directions are intensely pursued towards improvement on the threshold and background for sub-keV germanium detectors:

1. Pulse Shape Analysis of Near Noise-Edge Events:

It has been demonstrated that by studying the correlation of the Ge signals in two different shaping times[7] as depicted in Figure 3a, the threshold can be further reduced below the hardware noise edge via Pulse Shape Discrimination (PSD). The achieved thresholds at 50% signal efficiency are 220 eV and 310 eV for 20-g ULEGe and 500-g PCGe, respectively. The PSD selection efficiencies were derived from the survival probabilities of these anti-Comptoni(AC)-tagged samples in the coincidence window[7]. The trigger efficiencies were measured with the fractions of calibrated pulser events above the discriminator threshold provided the first measurement and the studies on the amplitude distributions of *in situ* background[7].

2. Pulse Shape Analysis of Surface Vs Bulk Events:

The surface and bulk events in PCGe can be separated by the rise time of the pulses as characterized by the amplitude of timing amplifier (TA) signals. It is illustrated in Figure 3b.

3. Background Understanding and Suppression:

The measured sub-keV spectrum at KSNL [7] could not be explained with standard background modeling on ambient radioactivity. Intense efforts on hardware cross-checks, further simulation and software analysis are underway.

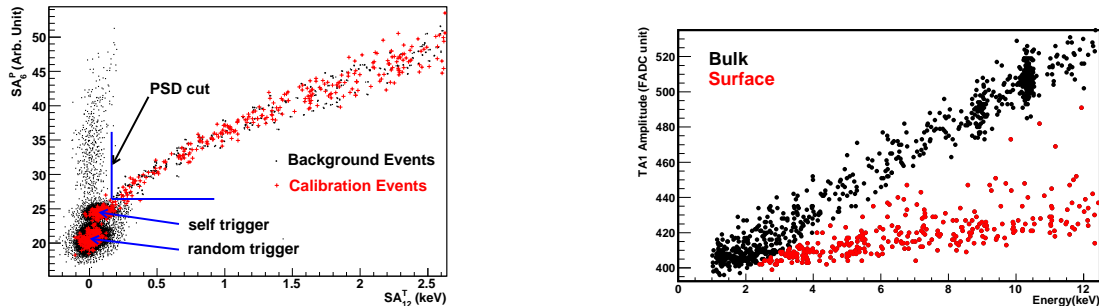


Figure 3: (a) Left: Scattered plots of the SA_6^P (shaping time $6 \mu s$ with partial integration) versus SA_{12}^T (shaping time $12 \mu s$ with partial integration) signals, for both calibration and physics events. The PSD selection is shown. (b) Right: Rise time plots, as characterized by the amplitude of timing amplifier (TA) signals, showing different behaviour between surface (faster) and bulk (slower) events.

3 Prospects and Outlook

A detector with 1 kg mass, 100 eV threshold and 1 cpkkd background level has important applications in dark matter physics. Crucial advances have been made in adapting the Ge detector technology towards these requirements. Relevant limits have been achieved in prototype studies at KSNL on the WIMP couplings with matter. The sub-keV events are still to be understood. Intensive research programs are being pursued along various fronts towards realization of experiments which can meet all the technical challenges. Detectors with kg-scale are being deployed at KSNL and CJPL.

References

- [1] M. Drees and G. Gerbier, *Review of Particle Physics*, Phys. Lett. **B 667**, 241 (2008), and references therein.
- [2] H.T. Wong et al., J. Phys. Conf. Ser. **39**, 266 (2006); H.T. Wong et al., J. Phys. Conf. Ser. **120**, 042013 (2008).
- [3] D. Normile, Science Vol. **324**, 1246 (2009); K.J. Kang et. al., J. Phys. Conf. Ser. **203**, 012028 (2010); T. Feder, Physics Today, **Sept 2010**, 25 (2010).
- [4] C. Savage, P. Gondolo and K. Freese, Phys. Rev. **D 70**, 123513 (2004); P. Gondolo and G. Gelmini, Phys. Rev. **D 71**, 123520 (2005).
- [5] A. Bottino et al., Phys. Rev. **D 72**, 083521 (2005);
- [6] G. Fleming, A. Kusenko and S. Nussinov, Phys. Rev. Lett. **89**, 101302 (2002); X.G. He et al., Mod. Phys. Lett. **A 22**, 2121 (2007); J.L. Feng, J. Kumar, and L.E. Strigari, Phys. Lett. **B 670**, 37 (2008); D.E. Kaplan, M.A. Luty, K.M. Zurek, Phys. Rev. **D 79**, 115016 (2009); R. Foot, Phys. Rev. **D 80**, 091701 (2009); Y.G. Kim and S. Shin, JHEP **0905**, 036 (2009). L. Fitzpatrick, D. Hooper, K.M. Zurek, arXiv:1003.0014 (2010).
- [7] H.T. Wong, Mod. Phys. Lett. **A 23**, 1431 (2008); S.T. Lin et al., Phys. Rev. **D 76**, 061101(R) (2009).
- [8] G. Angloher et al., Astropart. Phys. **18**, 43 (2002).
- [9] R. Bernabei et al., Phys. Lett. **B 389**, 757 (1996); D.S. Akerib et al., Phys. Rev. Lett. **96**, 011302 (2006); J. Angle et al., Phys. Rev. Lett. **100**, 021303 (2008).
- [10] C.E. Aalseth et al. Phys. Rev. Lett. **101**, 251301 (2008); C.E. Aalseth et al.. arXiv:1002.4703 (2010).

Dark Matter Search with CRESST-II

R. Strauss¹, G. Angloher², M. Bauer³, I. Bavykina², A. Bento^{2,5}, C. Bucci⁴, C. Ciemiak¹, G. Deuter³, F. von Feilitzsch¹, D. Hauff², C. Isaila¹, J. Jochum³, M. Kiefer², M. Kimmerle³, J.-C. Lanfranchi¹, F. Petricca², S. Pfister¹, W. Potzel¹, F. Pröbst², F. Reindl², S. Roth¹, K. Rottler³, C. Sailer³, K. Schäffner², J. Schmalzer², S. Scholl^{2,3}, W. Seidel², M. von Sivers¹, L. Stodolsky², C. Strandhagen³, A. Tanzke², I. Usherov³, S. Wawoczny¹, M. Willers¹, A. Zöller¹

¹Physik-Department E15, Technische Universität München, D-85747 Garching, Germany

²Max-Planck-Institut für Physik, D-80805 München, Germany

³Eberhard-Karls-Universität Tübingen, D-72076 Tübingen, Germany

⁴Laboratori Nazionali del Gran Sasso, INFN, I-67010 Assergi, Italy

⁵Departamento de Física, Universidade de Coimbra, P3004 516 Coimbra, Portugal

DOI: http://dx.doi.org/10.3204/DESY-PROC-2011-04/strauss_aimund

The CRESST-II Dark Matter experiment aims at the direct detection of WIMPs via scattering off nuclei in CaWO_4 crystals which are operated as cryogenic detectors. The phonon signal and the scintillation light signal are recorded simultaneously. The light output of these crystals is used for active discrimination between background events and possible WIMP-induced nuclear recoils. The recently finished 730 kg-days experimental run indicates an excess of events in the signal region which is hard to explain with known backgrounds and could hint towards light WIMPs.

1 Experimental approach of CRESST

Astrophysical experiments and observations indicate a large abundance of non-baryonic matter in the Universe. Well motivated theoretical concepts propose weakly-interacting massive particles (WIMPs) to be the origin of the *Dark Matter*. So far it has not been clearly verified despite a large variety of experiments aiming at its direct detection [1].

The **CRESST-II** (Cryogenic Rare Event Search with Superconducting Thermometers) experiment, located at the Laboratori Nazionali del Gran Sasso (LNGS), Italy, attempts to measure the very rare interactions expected between ordinary matter and WIMPs via elastic scattering off nuclei [2, 3, 4]. Tiny energy transfers to the recoiling nucleus ($\mathcal{O}(10 \text{ keV})$) and ultra-low event rates ($<0.1 \text{ events/kg/day}$) require very sensitive detectors with low-energy thresholds as well as excellent shielding against environmental radiation and an active background discrimination technique. Scintillating CaWO_4 crystals as target material operated as cryogenic detectors are suitable for this challenging approach. These crystals are cylindrically shaped, $\sim 40 \text{ mm}$ in diameter and height ($\sim 300 \text{ g}$), each equipped with a tungsten (W) transition edge sensor (TES) stabilized in its transition between the superconducting and the normal-conductive state at a temperature of typically $10\text{-}20 \text{ mK}$. This allows to measure the total energy deposition in the crystal (phonon channel). The resulting temperature rise after a particle interaction in the target crystal causes a significant change in resistance of the TES which is read out by a SQUID

system. Thereby sub-keV thresholds and energy resolutions of <500 eV FWHM are achieved in the region of interest for Dark Matter search (typically 10-40 keV).

The kind of interaction can be identified by simultaneously measuring the **scintillation light** output of the CaWO_4 crystal, which is typically only a small fraction ($\mathcal{O}(1\%)$) of the total energy deposition. The light output (*light yield*) for electron recoils induced by 122 keV γ 's from a ^{57}Co source is normalized to one. Due to quenching effects the light output is further reduced for nuclear recoil events, which is quantified by *Quenching Factors* (QF). During dedicated measurement campaigns the QFs were precisely measured [2]: $\text{QF}_O=(10.4\pm 0.5)\%$, $\text{QF}_{\text{Ca}}=(6.38\pm 0.65)\%$, $\text{QF}_W=(3.91\pm 0.48)\%$ and $\text{QF}_{e/\gamma}:=100\%$ (by definition). This active discrimination technique features an excellent separation of the dominant e/γ background from possible WIMP-induced nuclear recoils on the individual components O, Ca and W (WIMP mass spectroscopy) and a characterization of neutron backgrounds. The light is collected with a separate cryogenic detector, a silicon on sapphire (or pure Si) disc of 40 mm diameter, again equipped with a W-TES. Target crystal and light absorber are placed in a housing covered by a reflective and scintillating polymeric foil in order to increase the light collection efficiency and to discriminate α -decay events [2]. Up to 33 *detector modules* (see Fig. 1, left) can be installed in the CRESST-II setup for up to 10 kg active target mass.

The detector volume is coupled via a longish (1.3 m) copper cold finger to a ^3He - ^4He dilution refrigerator in order to avoid the presence of non-radiopure materials of the cryostat near the detectors. Layers of ultra-pure copper and lead, active muon veto panels and polyethylene surround the detectors [2, 3, 4]. Together with the 1400 m of rock overburden (3500 m.w.e.) in the underground facilities of the LNGS, the setup provides an efficient **shielding** against ambient and cosmic radiation.

2 Recent experiment: Run32

CRESST-II was successfully commissioned in 2007 [3]. Run32 was the first extensive physics run of CRESST-II with a net exposure of 730 kg-days and a runtime of almost 2 years from June 2009 to April 2011. Eight fully functional detector modules have been used for the Dark Matter analysis and were calibrated by AmBe, ^{57}Co and ^{232}Th sources during dedicated campaigns. Here a brief qualitative discussion of background sources and the final results derived from an extensive likelihood analysis are presented. A detailed description of the analysis is given in [2].

2.1 Backgrounds

In Fig. 1, right a light yield plot of a typical detector module (channel 20) is shown with the relevant event bands to illustrate the background distribution discussed in this section. The acceptance region for WIMP search is defined for this particular module from 12.9 keV to 40 keV including the contributions of the O, Ca and W recoil bands.

The dominant **e/γ background** (~ 0.3 events/keV/kg/day) can be well discriminated from the nuclear recoil bands due to its relatively high light output ($\text{QF}_{e/\gamma}:=1$). Nevertheless there is an overlap between the bands at low recoil energies which fixes the lower boundary of the WIMP-acceptance region individually [2] for each module (typically 10-20 keV).

Discrete **alpha** lines are observed at MeV energies (e.g. ^{210}Po decay with 5.3 MeV α) at a QF of $\sim 22\%$ and can thus be well distinguished from the nuclear recoil events. If the α emitter is implanted in the surface of the material surrounding the crystal (e.g. bronze clamps that

DARK MATTER SEARCH WITH CRESST-II

	e/γ	α	n	^{206}Pb	signal
M1	$8.00^{+0.05}_{-0.05}$	$11.5^{+2.6}_{-2.3}$	$7.5^{+6.3}_{-5.5}$	$15.0^{+5.2}_{-5.1}$	$29.4^{+8.6}_{-7.7}$
M2	$8.00^{+0.05}_{-0.05}$	$11.2^{+2.5}_{-2.3}$	$9.7^{+6.1}_{-5.1}$	$18.7^{+4.9}_{-4.7}$	$24.2^{+8.1}_{-7.2}$

Table 1: Contributions of the considered backgrounds and a possible WIMP-induced signal obtained by the maximum likelihood analysis for the two fit maxima M1 and M2 [2].

hold the crystal), α 's can lose energy before reaching the detector. These degraded α 's are a harmful background as they can leak into the acceptance region due to an overlap of the bands at low energies. The leakage can be estimated using an overlap-free α -reference region of an energy range of 100 keV [2].

An accumulation of nuclear recoil events at ~ 103 keV slightly below the W-band is observed which were identified as ^{206}Pb recoils originating from ^{210}Po decays in the clamps holding the crystal. Again an overlap-free reference region is defined and, combined with a SRIM simulation which models the implantation-depth distribution of the ^{210}Po mother nuclei in the clamp material, the leakage into the acceptance region can be derived.

Ambient **neutrons** from spontaneous fission or α - n reactions in the materials surrounding the detector volume are highly degraded and appear mainly as oxygen recoils. As 8 detector modules are operated one can look for multiple detector hits which can be induced by n 's but not by WIMPs. The *multiplicity structure* of source-like n -events was determined by neutron calibration campaigns [2]. Another class of events are unvetted muon induced neutrons as the muon-veto system is not 100% efficient. The multiplicity structure can be studied by analyzing the response of the detectors for events in coincidence with the muon veto. For both classes of n -events the number of (WIMP-like) single hits can be estimated by the observed multiplicity distributions. High-energy neutrons (>10 MeV) generated by muons in the rock surrounding the experiment have been studied in Monte Carlo simulations [2].

2.2 Results and discussion

The contributions of the backgrounds discussed above as well as a possible contribution of a WIMP signal are fully implemented in a maximum likelihood analysis. In total, 67 events are

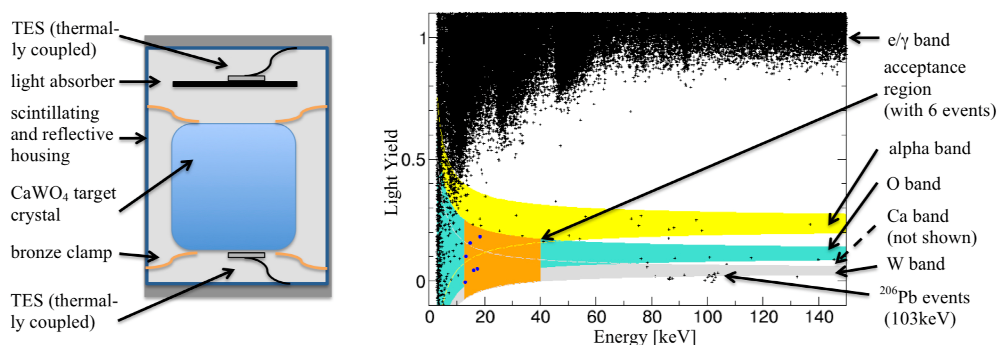


Figure 1: Left: Scheme of a CRESST-II detector module. Right: Typical light yield plot (channel 20) showing the relevant event bands.

observed in the acceptance regions of the individual detectors. The α and ^{206}Pb recoil events are identified to originate from a contamination in the bronze clamps holding the CaWO_4 crystals (see Fig. 1, left). The acceptance region is defined such that one γ event per detector module is expected in the acceptance region. The shape of the neutron background is obtained by the calibration. The final result of the maximum likelihood analysis [2, 4] for the contribution of the considered backgrounds and a possible signal is summarized in table 1. Two fit maxima M1 and M2 have been found.

The observed events in the acceptance region cannot be explained by the considered backgrounds only. An additional exponential contribution is needed at a significance level of 4.7σ for M1 (4.2σ for M2). If this excess is interpreted as an indication for a Dark Matter signal the corresponding WIMP parameters can be obtained by the fit for both maxima as listed in table 2.

Such a WIMP signal would be in serious tension with the results of the XENON-100 and CDMS-II experiments [1], while it is consistent with earlier CRESST-II results [3] and their recent re-analysis [5]. Our results - if not an unknown background - would hint to light WIMPs similar to DAMA/LIBRA and CoGeNT [1]. To clarify the origin of the observed excess of events much effort is currently being put into background reduction for the upcoming Run33.

	$m_\chi[\text{GeV}]$	$\sigma_{\text{WN}}[\text{pb}]$	O	Ca	W
M1	25.3	$1.6 \cdot 10^{-6}$	$\sim 7\%$	$\sim 25\%$	$\sim 69\%$
M2	11.6	$3.7 \cdot 10^{-5}$	$\sim 52\%$	$\sim 48\%$	$\sim 0\%$

Table 2: Results of the maximum likelihood fit [2] interpreting the signal excess as WIMPs of mass m_χ and elastic WIMP-nucleon scattering cross section σ_{WN} . For both likelihood maxima (M1, M2) the contributions of O, Ca and W events to the signal are listed.

Acknowledgements

We thank for the support by the DFG (Transregio 27), the Munich Cluster of Excellence (Universe), the MLL (Garching), the STFC UK, the DFG Kolleg GRK 683 and the LNGS.

References

- [1] J. Kopp *et al.*, “Light Dark Matter in the light of CRESST-II” [arXiv:1110.2721 [astro-ph]].
- [2] G. Angloher *et al.* [CRESST collaboration], “Results from 730kg days of the CRESST-II Dark Matter Search” [arXiv:1109.0702 [astro-ph]].
- [3] G. Angloher *et al.* [CRESST collaboration], “Commissioning Run of the CRESST-II Dark Matter Search” *Astropart. Phys.* **13**, 270 (2009) [arXiv:0809.1829 [astro-ph]].
- [4] F. Petricca *et al.* [CRESST collaboration], “Dark Matter Search with CRESST-II”, TAUP 2011 proceedings
- [5] A. Brown *et al.*, “Extending the CRESST-II commissioning run limits to lower masses” [arXiv:1109.2589 [astro-ph]].

The Search for Dark Matter with XENON

Elena Aprile¹

On Behalf of the XENON100 Collaboration

¹Physics Department, Columbia University, 550 W 120th Street

New York, NY 10027, USA

E-mail: age@astro.columbia.edu

DOI: http://dx.doi.org/10.3204/DESY-PROC-2011-04/aprile_elena

The XENON100 experiment aims at detecting cold dark matter particles via their collisions with xenon nuclei in a two-phase time projection chamber filled with a total of 165 kg of ultra pure liquid xenon. The detector sensitive target mass is about 65 kg, surrounded by about 100 kg of active veto. The detector has been installed underground at the Gran Sasso National Laboratory (LNGS) since 2008 and after a successful calibration, dark matter data taking has started. The current status of the XENON100 as well as future plans for the upgrade are presented.

1 Introduction

There is an increasing number of astrophysical and astronomical observations pointing to the existence of a non-luminous, non-baryonic and cold (i.e. non-relativistic) matter component in the universe, called Cold Dark Matter (CDM) [1, 2]. The most appealing candidates for CDM are Weakly Interactive Massive Particles (WIMPs) predicted by supersymmetric theories (SUSY), models with extra dimensions and little Higgs models [3, 4, 5].

The XENON project is currently one the most promising experiments for the direct detection of dark matter. After the successful results of the first 10 kg scale detector XENON10 [6, 7], the collaboration has designed and built a second-generation experiment exploiting the two-phase time projection chamber (TPC) technique based on liquid xenon (LXe). The XENON100 detector features an increase in mass by a factor of 10 and a reduction of the radioactive background level by a factor of 100, as shown by the first measured scientific data [8]. XENON100 sensitivity reach is a factor of 50 better than that of XENON10.

2 Detector Operation

Liquid xenon is appealing as a target material for dark matter direct detection. It is a heavy ($A = 131$) and dense ($\rho \sim 3 \text{ g/cm}^3$) medium and an efficient scintillator (80% of NaI). The high mass number provides excellent detection capabilities for the spin-independent WIMP-nucleon scattering ($\sigma \propto A^2$). The abundance of odd isotopes (about 50%) allows the detection of spin-dependent interactions ($\sigma \propto J(J+1)$). The high density and high Z provide self shielding against external gamma radiation. Xenon has no long lived isotopes and purification of krypton

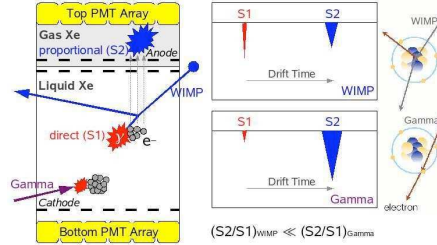


Figure 1: Principle of a two-phase liquid xenon TPC. A particle generates primary scintillation light (S1) and ionization electrons. These are drifted upwards with the field and detected via secondary scintillation light in the gas phase (S2). The S2 hit pattern (xy) and the drift time (z) give complete information for the position of events. Additionally, the ratio S2/S1 allows event discrimination between nuclear recoils (WIMPs, neutrons) and electron recoils (γ , β).

in xenon has been shown down to the level of a few ppt, which is an important advantage in the search for rare dark matter induced events.

The XENON100 detector is a two-phase (liquid-gas) time projection chamber (TPC). A particle interacting with the target generates electron ion pairs and excited xenon atoms, which produce scintillation light and free electrons in the medium (Figure 1). The primary light (S1) is detected immediately by the two photomultiplier (PMT) arrays above and below the target. An electric field (~ 0.53 kV/cm) across the TPC drifts the free ionization electrons upwards, where they are extracted into the gas phase by an even stronger extraction field. In the gas phase, the electrons generate very localized proportional scintillation light (S2). The PMT hit pattern of the S2 signal can be used to determine the xy-position of the interaction point and since the z-position is known from the drift time, the event positions can be reconstructed in three dimensions. This allows to select an inner fiducial volume in our target which together with the self shielding capability of liquid xenon drastically reduces the radioactive background from external sources.

The high ionization density of nuclear recoils in liquid xenon leads to a smaller S2/S1 ratio compared to electron recoils. The simultaneous measurement of charge and light provides a powerful discrimination between signal (nuclear recoils) and background events (electron recoils) via the ratio S2/S1. A discrimination of 99.5-99.9% has been achieved, for 50% nuclear recoil acceptance, in both XENON10 and XENON100.

3 Detector Setup

The XENON100 detector consists of 165 kg of liquid xenon divided in two concentric cylinders. The inner sensitive volume contains 65 kg of Xenon and is separated from the outer volume by a PTFE cage on the sides, a diving bell on the top and a PMT array in the bottom. Two electric field regions are created in this volume with one mesh in the bottom and three in the top, near the liquid gas interface. These electric fields allow electrons produced in interactions to drift in the main volume and be extracted to the gas where they produce proportional scintillation light. The PTFE cage acts as a reflector for the UV light from the liquid xenon and also accommodates a set of 40 field shaping rings and their resistive divider chain to improve the homogeneity of the field. The outer volume acts as an active veto reducing the amount of

interactions in the inner volume and allowing to identify multiple scatter events. This in fact reduces the DAQ rate and the amount of data collected and improves our ability to reject gamma events as WIMP candidates.

The light readout is based on 1" \times 1" Hamamatsu R8520-06-A1 low-radioactive PMTs with quantum efficiencies up to $\sim 35\%$. 98 PMTs in the top array above the anode mesh are arranged in a circular pattern to improve position reconstruction, while 80 PMTs on the bottom are arranged in a compact grid to optimize the light collection. 64 PMTs in the active veto allow to detect energy depositions as low as 100 keVee reducing the overall background by a factor 4.

The detector is surrounded by a passive shield consisting, from the inside to the outside of 5 cm copper, 20 cm polyethylene and 20 cm lead (which has a low concentration of ^{210}Pb) and 20 cm of water. All the systems associated with the cooling and the purification of the xenon are placed outside this shield in order to minimize the background level.

The cryostat and detector production was completed in early 2008 and the detector was installed underground at LNGS. An extensive calibration of the detector systems has been performed in 2009 and blind dark matter data taking started in January 2010.

4 Detector Calibration

The XENON100 detector has been installed underground in LNGS since the middle of 2008, and has been tested in a series of successful calibrations during this period. Monitoring of the detector performance has been done on a regular basis using ^{137}Cs and blue LEDs to study the PMT gain, the light collection efficiency and the electron absorption. For dark matter detection one of the most important features of a two-phase liquid xenon TPC is the ability to distinguish between electronic and nuclear recoils. In order to characterize the electron recoil regions several calibrations with a ^{60}Co source have been performed. A high energy veto has been used to acquire only the lower part of the spectrum ≤ 150 keV.

To study the response to nuclear recoils, during December 2009 and for three days a calibration was performed with an AmBe neutron source. This allowed us to collect a large sample of elastic nuclear recoils, but also a rather homogeneous sample of 40 keV and 80 keV gamma-rays from inelastic scatterings which have been used to measure the energy resolution of the detector down to this energy.

5 XENON100 First Results

During the detector calibration period in 2009 some data were taken when no source was present and in ideal detector conditions. While this data were not originally blinded, we decided to perform a blind analysis on them by defining selection cuts only on the calibration data [8]. 11.2 days of data were analysed with a fiducial volume of 40 kg. Only very basic cuts were defined, aiming to remove noisy events, events interacting in the gas or events with multiple interactions in the detector. After applying these cuts a total of 22 events were observed in the fiducial volume and the energy region preselected for the signal, corresponding to a background level of ~ 7 mdr, which is the lowest measured in a dark matter search up to date. None of the measured events lies in the nuclear recoil band, showing for the first time the successful background free operation of a liquefied noble gas TPC. Figure 2 shows the limit for spin

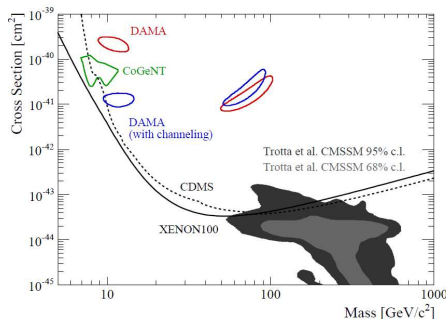


Figure 2: Exclusion plots for spin independent WIMP-nucleon interactions. The current limits are the curves around 10^{-43} cm^2 , given by XENON100 (solid,[8]) and CDMS II (dashed,[9]). The projected sensitivity for XENON100 is one order of magnitude lower. The shaded regions are theoretical expectations of CMSSM.

independent dark matter parameter space established from this result, which already at this early stage of operation is comparable to the best exclusion limit to date.

Blind data acquisition started at the beginning of 2010 and to date more than 10 times the exposure used for this analysis has been completed and analysed [10]. Currently (2011) we are taking new set of blind data.

6 XENON1T

The XENON100 gamma background is dominated by the PMTs and the PMT bases, followed by the polyethylene of the shield and the stainless steel of the cryostat. The next step in the XENON dark matter project will be XENON1t, with a fiducial mass of ~ 1.1 ton. In order to achieve reduced background, PMT arrays will be replaced by QUPIDs [11], novel photosensors with an extremely low intrinsic radioactivity, developed by UCLA and Hamamatsu for this experiment. Additionally, a copper cryostat and 10 meter diameter water shield acting also as an active muon veto will be implemented. This detector will bring an improvement in the spin-independent WIMP-nucleon sensitivity of 2 orders of magnitude by 2015.

References

- [1] W. Freeman and M. Turner, *Rev. Mod. Phys.*, **75**, 1433 (2003).
- [2] M. J. Jee et al., <http://xxx.lanl.gov/abs/0705.2171>
- [3] A. Bottino et al., *Phys. Rev. D* **69**, 037302 (2004).
- [4] J. Ellis et al., *Phys. Rev. D* **71**, 095007 (2005).
- [5] A. Birkedal-Hansen and J. G. Wacker, *Phys. Rev. G* **69** 065022 (2004).
- [6] J. Angle et al., [XENON10 collaboration], *Phys. Rev. Lett.*, **100**, 021303 (2008).
- [7] J. Angle et al., [XENON10 collaboration], *Phys. Rev. Lett.*, **101**, 091301 (2008).
- [8] E. Aprile et al. [XENON100 collaboration], *Phys. Rev. Lett.* **105**, 131302 (2010)
- [9] Z. Ahmed et al. [CDMS II collaboration], *Science* **327**, 1619 (2010).
- [10] E. Aprile et al. [XENON100 collaboration], arXiv:1104.2549v2 (2011)
- [11] K. Arisaka et al., arXiv:0808.3968 (2008).

Status of XMASS

Yasuhiro Kishimoto^{1 2} for the XMASS collaboration

¹Kamioka Observatory, ICRR, University of Tokyo, Kamioka, Gifu, Japan

²Institute for the Physics and Mathematics of the Universe, Kashiwa, Chiba, Japan

DOI: http://dx.doi.org/10.3204/DESY-PROC-2011-04/kishimoto_yasuhiro

The XMASS project aims to direct ${}^7\text{Be}/pp$ -solar neutrinos, neutrino-less double beta decay, and darkmatter searches using ultra-pure liquid xenon. The first stage of the XMASS searches for darkmatter with 800 kg single-phase xenon-scintillator detector, whose construction was started in April 2007 and completed in September 2010. After installation of purified xenon, commissioning runs have been started since October 2010. Status of the current XMASS detector was reported, especially about evaluation of performance of event vertex reconstruction and amount of internal contamination in the liquid xenon.

1 Introduction

The XMASS project aims to direct ${}^7\text{Be}/pp$ -solar neutrinos, neutrino-less double beta decay, and darkmatter searches using ultra-pure liquid xenon [1]. The first stage of the XMASS project is for direct darkmatter searches. The XMASS detector with 800 kg ultra-pure liquid xenon is located in Kamioka mine(2,700 m.w.e), Japan. The liquid xenon was chosen as target material because it has large photon yield and high mass number ($A=131.29$). The 800 kg detector construction was started in April 2007 and it was completed in September 2010. After installation of purified xenon, commissioning run has been running since October 2010. In the commissioning run, we carried out calibration using radioactive sources to study for energy and position resolution. We put several kinds of sources inside the detector and evaluated the performance of the vertex reconstruction. We also evaluated internal contamination, such as radon (${}^{222}\text{Rn}$ and ${}^{220}\text{Rn}$) and krypton(${}^{85}\text{Kr}$). In this paper, the performance of the reconstruction and the evaluation of the internal contaminations will be described.

2 XMASS detector

The XMASS detector consists of oxygen-free high conductivity (OFHC) copper vessel with about 1.2 m diameter and 642 photomultiplier tubes (PMTs) immersed in liquid xenon.

The total amount of liquid xenon for active volume is 835 kg. Ultra-low background 630 hexagonal PMTs and 12 round ones are mounted in an approximately spherical-shape holder made of OFHC copper. The photo coverage of the PMTs is about 64%. The detector employs a single-phase technology and observe only scintillation lights emitted by the interaction of darkmatter. Vertexes of events are reconstructed using photo electron distribution observed by PMTs. The key idea of the background (BG) reduction in XMASS is "self-shielding". External gamma-rays can be absorbed by the outer surface of the liquid xenon owing to the

high atomic number ($Z=53$). On the other hand, the darkmatter particles can give uniform vertex distributions over the detector. By extracting events that occur only deep inside the detector, therefor, a sensitive search for darkmatter can be conducted.

Almost all of the material used for the detector were carefully selected with a high purity germanium detector and induced coupled plasma mass spectrometers. More than 250 samples were measured. The main BG is coming from the PMTs although their radioactive impurities are two orders magnitude less than those of ordinary ones. Monte Carlo simulations (MCs) were performed to estimate the BG from PMTs and found about 0.1 counts/day/kg/day in the whole volume and less than 10^{-4} counts/day/kg/day in the fiducial volume with 20 cm radius (100 kg sensitive volume).

Xenon does not have long-lived radioactive isotopes, which is one of the most important advantage for rare event search experiments like darkmatter search. Commercial xenon, however, contains small amount (about 0.1 ppm) of krypton which has radioactive ^{85}Kr (half-live of 10.76 years). Our requirement for contamination of ^{85}Kr is less than 2 ppt. We have developed a distillation tower purification system and achieved ^{85}Kr contamination of 3.3 ± 1.1 ppt for prototype detector [2], which was very close to the goal of our requirement. A new distillation tower was build with about 4 m length of a tower column and about 1.2 ton of xenon gas has been processed in September 2010 for 10 days.

With BG level of 10^{-4} counts/day/kg/day, expected sensitivity of WIMP-nucleon cross section for the spin independent case is presented in Fig.1 with some experimental results and one of theoretical predictions.

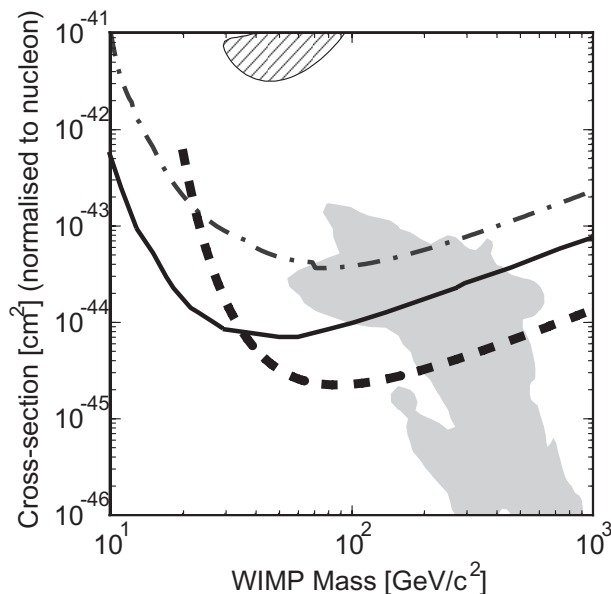


Figure 1: Measured and expected sensitivities of WIMPs-nucleon cross section as a function of WIMP mass. Hatched region is 3σ arrowed region by DAMA/LIBRA with no ion channeling[3]. Shaded region is a result of a theoretical calculation in [4]. Upper region of a solid thin line and a line-dashed lines are excluded by XENON100[5] and CDMS[6], respectively. XMASS expected sensitivity is plotted in thick dash line.

3 Detector calibration

Radioactive sources are introduced into the active volume using XMASS calibration system. The XMASS calibration system consists of several kind of sources (^{57}Co , ^{55}Fe , ^{109}Cd , and ^{137}Cs), OFHC copper rod, thin stainless wire, and a stepping motor. One of the radioactive sources is put on the edge of the copper rod. The rod is hung with thin stainless wire and lifted up and down from the outside of the detector with a motion feed-through and stepping motor located on the top of the water tank. The sources position can be controlled along z axis of the active volume inside the detector within ± 1 mm accuracy. The radioactive sources can be exchanged without any influence on the detector owing to gate valve isolation.

The left panel of Fig. 2 plots energy spectrum obtained using ^{57}Co source at the center of the detector ($z = 0$ cm). The photoelectron distribution was well reproduced by a MC, and

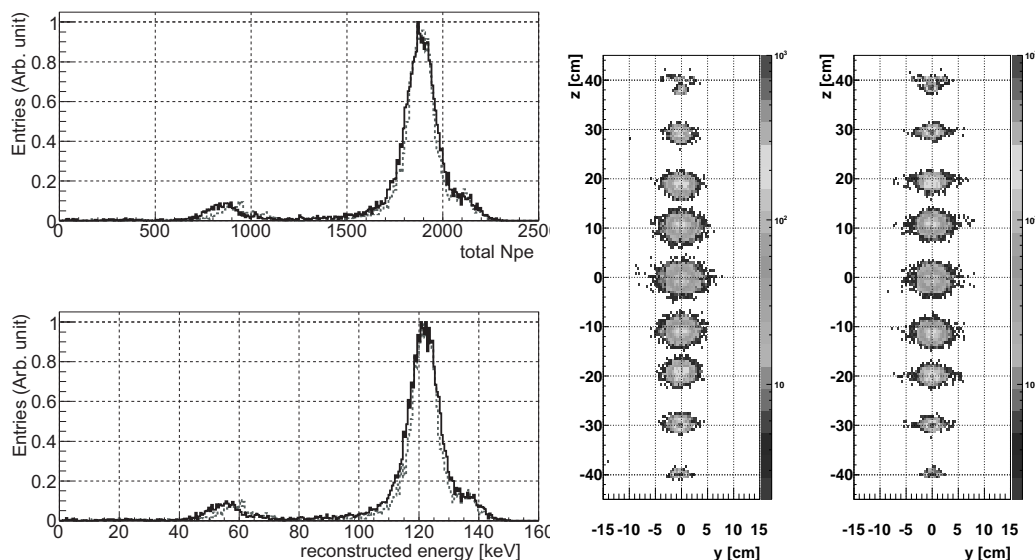


Figure 2: The left panel shows observed photoelectron (upper) and reconstructed energy (lower). Calibration data and MC results are plotted by solid line and dashed one, respectively. Reconstructed vertex distributions of calibration data (left) and MC results (right) are compared in the right panel.

high light yield which is 15.1 ± 1.2 photoelectrons/keV was obtained. The right panel of Fig. 2 shows reconstructed vertices for various position of the ^{57}Co source. The position and energy are reconstructed from PMT charge patterns which are function of position and energy in the detector by using a likelihood method. Obtained position resolution (RMS) are 1.4 cm at $z = 0$ cm and 1.0 cm at $z = \pm 20$ cm for 122 keV gamma-rays.

4 Evaluation of internal BG

External BGs can be effectively reduced by the "self-shielding" of liquid xenon. Internal BGs, however, need to be reduced by other means. Possible internal BG sources are radon (^{222}Rn

and ^{220}Rn) and krypton ^{85}Kr .

The evaluation of radon was done through the following coincidence reaction.

- For ^{222}Rn : $^{214}\text{Bi}(\beta, E_{\text{max}} = 3.3\text{MeV}) \rightarrow ^{214}\text{Po}(\alpha, E = 7.7\text{MeV}, \tau = 164\mu\text{sec}) \rightarrow ^{210}\text{Pb}$
- For ^{220}Rn : $^{220}\text{Rn}(\alpha, E = 6.3\text{MeV}) \rightarrow ^{216}\text{Po}(\alpha, E = 6.8\text{MeV}, \tau = 0.14\text{sec}) \rightarrow ^{212}\text{Pb}$

The obtained ^{222}Rn concentration was 8.2 ± 0.5 mBq which was close to PMT's BG level. For ^{220}Rn , we did not find any candidate events. Then, we have set a limit as < 0.28 mBq(90%C.L.), which is lower than our goal (0.43 mBq).

The krypton contamination is now being evaluated with a combined system of an atmospheric pressure ionization mass spectrometer (API-MS) and a gas chromatography. Current sensitivity of the system is about 10 ppt which is very close to our target value (2 ppt). More sensitive measurement (< 1 ppt) is under preparation with more proper measurement parameters and will start soon.

The krypton contamination is also evaluated from data analysis of the following delayed coincidence events:

- $^{85}\text{Kr}(\beta, E_{\text{max}} = 173 \text{ keV}) \rightarrow ^{85}\text{Rb}^*(\gamma, E = 514 \text{ keV}, \tau = 1.9 \mu\text{sec}) \rightarrow ^{85}\text{Rb}$.

This analysis is being studied.

5 Conclusions

The construction of XMASS 800 kg detectors was completed in September 2010 and commissioning run has been started since October 2010. The main component of BG of this darkmatter detector is expected to be gamma-rays coming from PMTs, and estimated BG rate is less than 10^{-4} events/day/kg/keV. The corresponding sensitivity of WIMP-nucleon cross section for the spin independent case will be $2 \times 10^{-45} \text{ cm}^2$ at $100 \text{ GeV}/c^2$ WIMP mass. Commissioning runs are being carried out to confirm the detector performance and low BG properties. Energy and vertex resolution were as expected. The radon BG level is close to the target values and krypton contamination will be evaluated. Physics run will be start after commissioning runs.

References

- [1] Y. Suzuki *et al.*, "Low energy solar neutrino detection by using liquid xenon", [arXiv: 0008296 [hep-ph]].
- [2] K. Abe *et al.*, "Distillation of Liquid Xenon to Remove Krypton", *Astroparticle physics* **31**, 290 (2009).
- [3] R. Bernabei *et al.*, "First results from DAMA/LIBRA and the combined results with DAMA/NaI", *Eur. Phys. J. C* **56**, 333 (2008) as interpreted in Savage *et al.*, "Compatibility of DAMA/LIBRA dark matter detection with other searches", *JCAP*, **04**, 010 (2009).
- [4] R. Trotta *et al.*, "The impact of prior and observables on parameter inferences in the Constraint MSSM", *JHEP* **0812**, 024 (2008)
- [5] E. Aprile *et al.*, "First Dark Matter Results from the XENON100 Experiment", *Phys. Rev. Lett.* **105**, 131302 (2010)
- [6] Z. Ahmed *et al.*, "A Search for WIMPs with the First Five-Tower Data from CDMS" *Phys. Rev. Lett.* **102**, 011301 (2009)

DARWIN

Marc Schumann for the DARWIN consortium*

Physics Institute, University of Zürich, CH-8057 Zürich, Switzerland

DOI: http://dx.doi.org/10.3204/DESY-PROC-2011-04/schumann_marc

DARWIN is a design-study for a next-to-next generation experiment to directly detect WIMP dark matter in a detector based on a liquid xenon/liquid argon two-phase time projection chamber. This article describes the project, its goals and challenges, and presents some of the recent R&D highlights.

1 Introduction

Even though the existence of dark matter in the Universe is well established since many years [1], the nature of the dark matter particle remains unknown and has not been detected convincingly yet. One of the most promising particle candidate is the weakly interacting massive particle (WIMP), which arises naturally in many extensions of the standard model.

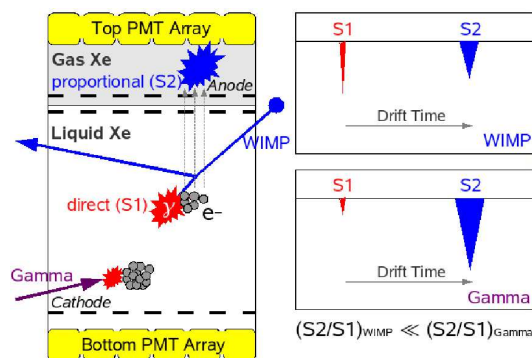


Figure 1: Principle of a two-phase liquid-noble gas TPC: Interactions generate prompt scintillation light (S1) and ionize the liquid target. The ionization electrons (charge signal, S2) are drifted upwards and detected in the gas volume. The event vertex is reconstructed from the S2 pattern and the electron drift time. The S2/S1 ratio is used for signal/background discrimination. In LAr, the S1 pulse-shape provides another powerful discrimination channel.

Detectors using the liquid noble gases xenon (LXe) [2, 3] and argon (LAr) [4] as a WIMP target in a two-phase time projection chamber (TPC), see Fig. 1, have already delivered very competitive results. They are also among the most promising techniques to build future detectors with a multi-ton target mass and an ultra-low background. These are the crucial requirements in order to be able to detect a significant number of WIMPs to allow for a clear dark matter detection. If the WIMP is found with the current or next generation detectors, it would allow for “WIMP spectroscopy” to constrain its properties.

*The following institutions are members of the DARWIN consortium (status October 2011): ETH Zürich, U Zürich (CH); Karlsruhe, Mainz, MPIK Heidelberg, Münster (DE); Subatech (FR); Weizmann Institute of Science (IL); INFN (IT): Bologna, L’Aquila, LNGS, Milano, Milano Bicocca, Napoli, Padova, Pavia, Perugia, Torino; Nikhef (NL); Associated US Groups: Columbia, Princeton, UCLA, Arizona State.

DARWIN (dark matter WIMP search with noble liquids) [5] is an international consortium which brings together experts from the LAr experiments WARP [4], ArDM [6] and DarkSide [7] and from the LXe experiment XENON [2], as well as new particle physics groups, in order to design Europe’s next-to-next generation dark matter facility based on LXe and/or LAr. DARWIN is supposed to be an ultimate WIMP detector, limited only by irreducible neutrino backgrounds and finite rejection of background events from the bulk. The outcome of the design study, which is funded by ASPERA since late 2009, is a proposal for an experiment. The details, including the decision whether the facility will be based on LXe and/or LAr and at which target mass, are not decided yet and are part of the study. The idea behind the combination of LXe and LAr in one experiment is to use synergies between both communities and to exploit some complementarity of the different targets [5, 8, 9].

2 Goals, Challenges and Progress

R&D within the DARWIN project is organized in seven work packages (plus one for management): Detector Infrastructure, Light Readout and Light Response, Charge Readout, Electronics and Trigger, Underground Site, Shields and Background, Material Selection and Screening (plus measurement of minute radioactive traces), and Science Impact. A biased selection of intermediate results is presented in the remaining part of this section.

Background: A next-to-next generation dark matter experiment must aim at a sensitivity to spin-independent WIMP nucleon cross sections around 10^{-48} cm², well below the goal of the next generation experiments such as XENON1T, DarkSide, and SuperCDMS. Besides the target mass, for which we assume as benchmark cases at least 5 tons of LXe and ~ 10 tons of LAr after fiducial volume cuts, one of the most crucial requirements is an extremely low background.

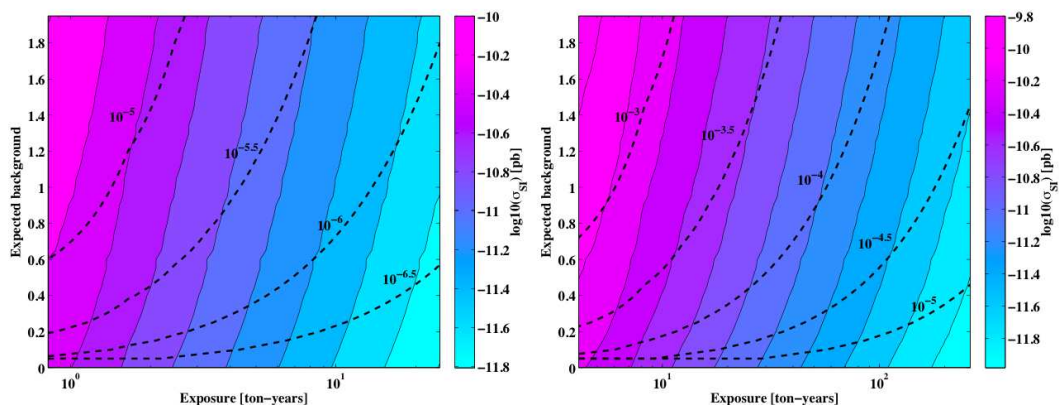


Figure 2: Background requirements for a multi-ton LXe (left) and LAr TPC (right). Shown is the number of background events vs exposure (the dashed lines show the background in dru = evts \times keV⁻¹ \times kg⁻¹ \times day⁻¹). The z-axis gives the sensitivity to spin-independent WIMP nucleon cross sections σ (in pb). The state-of-the-art values for background, acceptance, threshold (10 keVr/30 keVr for LXe/LAr), and background rejection (99.5%/ 3×10^{-7}) are used in the study. To reach $\sigma \sim 10^{-11}$ pb= 10^{-47} cm², a background level of $10^{-5.5}$ – 10^{-6} dru is required for LXe in a 5 ton \times year exposure and about 10^{-4} for LAr in a 40 ton \times year exposure.

DARWIN

Radioactivity from the detector itself can be reduced very efficiently by a fiducial volume cut and background from neutrons can be tackled by large water- or scintillator-based shields and a muon veto, as well as exploiting the possibility to detect and reject multiple-scatter interactions with the TPC. The remaining background is from intrinsic radioactive contamination in the target itself, which is mainly ^{85}Kr and ^{222}Rn for LXe and ^{39}Ar (and to a lower extent also ^{85}Kr and ^{222}Rn) in LAr. Fig. 2 shows the impact of background on DARWIN's sensitivity. It becomes clear that the background reduction and discrimination standards, which have been achieved by the current generation of experiments, are not yet sufficient for DARWIN. The Kr concentration in LXe, for example, must be reduced to below 1 ppt, and the background rejection by the pulse-shape analysis method in LAr must be improved by an order of magnitude.

Progress is also made regarding the development of the tools to measure minute traces of radioactivity in liquid noble gases at several member institutions (MPIK, Münster, Columbia) using different methods such as mass spectroscopy, gas chromatography, atom trapping etc.

Light response of LXe/LAr to low energy interactions: Several experiments are ongoing in order to study the response of the noble liquid targets to low energy nuclear recoils (from neutron or WIMP interactions) or electronic recoils (from γ -interactions). The Columbia group has recently published a new measurement of the relative scintillation efficiency \mathcal{L}_{eff} in LXe [10] which clearly shows non-zero values down to the lowest measured data-point of 3 keVr (keV nuclear recoil energy). A similar measurement for LAr is currently ongoing at CERN/U Zürich [11]. A measurement of the LXe response to electronic recoils down to 2.5 keV is currently performed at U Zürich [12] and also indicates non-zero values.

Light and charge readout: Two main avenues are currently pursued to detect the prompt scintillation light from the interactions. One involves the QUPID, a novel hybrid photodetector with very low intrinsic radioactivity [13] which has been developed by UCLA for use in LXe and LAr. Another approach is the commercial 3" photomultiplier tube R11410/R11065 (LXe/LAr) from Hamamatsu, which is extensively tested at several member institutions (see e.g. [14]).

Alternatives to the currently employed charge readout via a secondary scintillation process

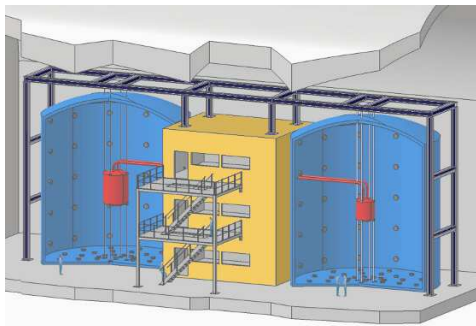


Figure 3: Illustration of a possible layout of the DARWIN facility: A 10 ton LXe detector (5 ton fiducial mass) and a 20 ton LAr detector (10 ton fiducial mass). In the final realization, the two detectors do not necessarily need to be placed directly next to each other.

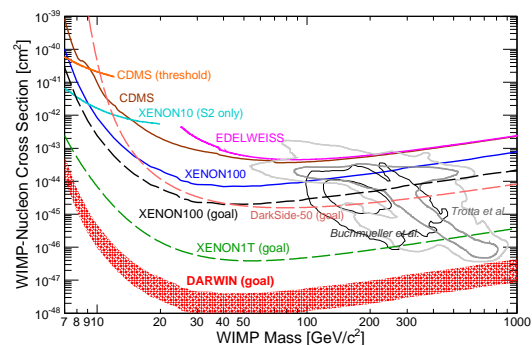


Figure 4: DARWIN's sensitivity goal is in the low 10^{-48} cm^2 range for spin-independent WIMP nucleon cross sections, more than one order of magnitude below the goals of the next-generation experiments. Solid curves indicate published results.

are interesting when large areas have to be covered and single electron sensitivity and fine spatial granularity are desirable. R&D towards this goal is performed at several institutions, focussing mainly on large cryogenic LEMs/ThickGEMs/Micromegas for noble liquids [15] (ETHZ), on gaseous PMTs (GPMs) without dead zones [16] (Subatech/WIS), and on CMOS pixel detectors coupled to electron multipliers (GridPix [17], Nikhef).

Science impact: Several questions have been addressed within the context of this work package. One is the optimum scaling of the LXe/LAr target mass in order to reach a similar sensitivity (to a $100 \text{ GeV}/c^2$ WIMP). It turns out that the optimum ratio would be 1:7, assuming a lower threshold of 10 keVr and 30 keVr for LXe and LAr, respectively. For a target mass of 5 tons of LXe, this would mean a LAr target of 35 tons, challenging in terms of threshold and light detection (necessary for background reduction by the S1 pulse shape analysis). Another topic is the complementarity of the targets, this has been studied in a dedicated publication [8].

3 The Future

The outcome of the DARWIN project will be a design report for a multi-ton LXe/LAr dark matter detection experiment, therefore the details are not yet finalized. Nevertheless, Fig. 3 illustrates how the future DARWIN facility might look like. The Figure shows two separate large water shields – instrumented as active Čerenkov muon veto – housing a 10 ton LXe detector and a 20 ton LAr detector with 5 tons and 10 tons fiducial mass, respectively. If the background requirements as mentioned in Sect. 2 are achieved, this facility will be able to probe spin-independent WIMP nucleon cross sections around 10^{-48} cm^2 . This is illustrated in Fig. 4, together with results which have already been achieved (solid lines) and the goals of upcoming experiments (dashed). Also indicated are expectations from some supersymmetric models (gray contours). These predict the WIMP to be in a region of the parameter space which will be completely covered by DARWIN.

References

- [1] K. Nakamura et al. (Particle Data Group), *J. Phys.* **G 37**, 075021 (2010) and references therein.
- [2] J. Angle et al. (XENON10), *Phys. Rev. Lett.* **100**, 021303 (2008);
E. Aprile et al. (XENON100), *Phys. Rev. Lett.* **107**, 131302 (2011).
- [3] D.Yu Akimov et al., (ZEPLIN-III), [arXiv:1110.4769](https://arxiv.org/abs/1110.4769) (2011).
- [4] R. Brunetti et al. (WARP), *Astropart. Phys.* **28**, 495-507 (2008).
- [5] L. Baudis (DARWIN), PoS(IDM2010)122 (2010). <http://darwin.physik.uzh.ch>
- [6] A. Rubbia et al. (ArDM), *J. Phys. Conf. Ser.* **39**, 129 (2006).
- [7] A. Wright (DarkSide), [arXiv:1109.2979](https://arxiv.org/abs/1109.2979) (2011).
- [8] M. Pato et al., *Phys. Rev.* **D83**, 083505 (2011).
- [9] K. Arisaka et al., [arXiv:1107.1295](https://arxiv.org/abs/1107.1295) (2011).
- [10] G. Plante et al., *Phys. Rev.* **C84**, 045805 (2011).
- [11] C. Regenfus, talk presented at TAUP2011 (2011).
- [12] A. Manalaysay, talk presented at TAUP2011 (2011).
- [13] A. Teymourian et al., *Nucl. Instr. Meth. A* **654**, 184 (2011).
- [14] R. Acciarri et al. (WARP), [arXiv:1108.5584](https://arxiv.org/abs/1108.5584) (2011).
- [15] A. Badertscher et al, *Nucl. Instr. Meth. A* **641**, 48 (2011).
- [16] S. Duval et al., [arXiv:1110.6053](https://arxiv.org/abs/1110.6053) (2011).
- [17] V. Blanco Carballo et al., *JINST* **5**, P02002 (2010).

Prospects for dark matter searches with CTA

Emmanuel Moulin

Irfu, Service de Physique des Particules, CEA Saclay, F-91191 Gif-sur-Yvette, Cedex, France

DOI: http://dx.doi.org/10.3204/DESY-PROC-2011-04/moulin_emmanuel

Dark matter particle annihilations are expected to occur in dense regions of the universe. Among the final annihilation products are very high energy gamma rays. The future array of Imaging Atmospheric Cherenkov Telescopes (IACTs), *i.e.* the Cherenkov Telescope Array (CTA), is a well-suited instrument to look further for particle dark matter annihilations in the 10 GeV - 100 TeV range. Here, I will present CTA prospective studies for targeted and wide-field survey searches.

1 Dark matter annihilations searches with IACTs

In the context of gamma-ray astronomy, the gamma-ray flux from self-annihilations of dark matter (DM) particles of mass m towards a given astronomical target can be written as:

$$\frac{d\Phi_\gamma(\Delta\Omega, E_\gamma)}{dE_\gamma} = \frac{1}{8\pi} \frac{\langle\sigma v\rangle}{m^2} \underbrace{\sum_i BR_i \frac{dN_\gamma^i}{dE_\gamma}}_{\text{Particle Physics}} \times \underbrace{\int_{\Delta\Omega} \int_{LOS} \rho(r[s])^2 ds d\Omega}_{\text{Astrophysics}}, \quad (1)$$

where $\langle\sigma v\rangle$ is the velocity-weighted annihilation cross section of the DM particle and $dN_\gamma/dE_\gamma = \sum_i BR_i dN_\gamma^i/dE_\gamma$ is the annihilation spectrum summed over all the possible annihilation channels i with branching ratios BR_i . The astrophysical factor corresponds to the integration of the square of the density ρ over the line of sight (LOS) and the solid angle $\Delta\Omega$. In the absence of a clear gamma-ray signal, the DM constraints are expressed in terms of the remaining particle physics parameters $\langle\sigma v\rangle$ and m for given annihilation spectrum and DM halo profile.

The DM searches with very high energy (VHE) gamma rays focus on regions with expectedly high DM density. Among them are the dwarf spheroidal galaxy (DSG) satellites of the Milky Way, and DM subhalos populating the Milky Way halo. Current IACTs, *i.e.* HESS, MAGIC and VERITAS, are actively searching for DM signals towards a variety of astronomical targets. Even though competitive limits are obtained, the present generation does not have the required sensitivity to probe natural value of $\langle\sigma v\rangle$ for thermally-produced DM. The next generation of IACTs, *i.e.* the Cherenkov Telescope Array [1], will consist of a large array with improved overall performances over present IACTs: i) The extended energy range from a few tens of GeV to several tens of TeV will allow to connect with the Fermi-LAT instrument at low energies, and for an improved sensitivity for DM masses above 100 GeV. ii) The probability of detection will be evidently increased by the improved sensitivity over the whole energy range. iii) The increased field of view will allow to efficiently search for extended DM emissions. iv) The better energy resolution should make easier the detection of possible spectral features in the DM-induced gamma-ray spectrum.

2 Dwarf spheroidal galaxies

DSGs have concentrated a lot of interest to search for DM with VHE gamma rays: i) Stellar dynamic measurements show that DSGs are among the most DM-dominated systems in the universe. Stellar dynamics also allow to control the astrophysical factor. ii) They show favorably low astrophysical background gamma-ray environments. These galaxies are expected to harbor no strong astrophysical VHE gamma-ray emitters due to the lack of recent star formation history (supernova remnants, pulsar wind nebula,...) and little or no gas acting as target material for cosmic rays. iii) Baryon-DM interaction is not expected to play an important role in the DM distribution. iv) Many of them lie in the 100 kpc from the Sun.

The nearest objects are in principle the best targets. They may however experience tidal effects from the Milky Way. It has been shown recently that one could take advantage of this effect to trace back the evolution history of the object [2]. During the orbital motion of a DSG, multiple crossings of the dwarf galaxy through the galactic disc of the Milky Way give rise to the formation of tidal streams. Their careful study allows to infer its gravitational potential. In the case of the Sagittarius Dwarf galaxy (SgrDw), the tidal streams have been detected with multiple tracer populations and used to derive the DM halo potential. Furthermore, measurements of stars within SgrDw and the luminosity of its core and surrounding debris, allows the estimate of the DM content prior to tidal disruption [3, 4]. Other peculiar features of SgrDw include the presence of the globular cluster M 54 coincident in position with its gravity centre, and hints for the presence of a central Intermediate Mass Black Hole (IMBH) [5]. Figure 1 (left) shows 95% C.L. sensitivity towards SgrDw for a CTA-like instrument for NFW and isothermal (ISO) DM halo profiles¹. For 200 h observation time, the sensitivity reaches a few 10^{-25} cm^3s^{-1} for TeV DM masses [6]. Assuming that the DM velocity dispersion is close to that of stars, the *Sommerfeld* effect can substantially boost the annihilation cross section in DSGs (see, for instance, Ref. [7]), since it is particularly effective in the low velocity regime. The value of the DM velocity dispersion in SgrDw is fixed at 11 km s^{-1} . Figure 1 (right) presents the 95% C.L. sensitivity assuming the *Sommerfeld* enhancement for the ISO DM profile and 200 h observation time [6]. The values of $\langle\sigma v\rangle$ corresponding to thermally-produced DM can be probed for specic wino masses in the resonance regions of the *Sommerfeld* effect. Outside the resonances the sensitivity reaches the level of 10^{-26} cm^3s^{-1} for TeV DM masses.

The issue of possible standard astrophysical gamma-ray background in the search for DM annihilation signal towards DSGs has been first addressed in the case of SgrDw. Even though DSGs are believed to harbor little standard astrophysical emitters at VHE, some gamma-ray emission may still be expected, in particular from pulsars, and black hole accretion and/or jet emission processes². Conservative models for the collective VHE emission from millisecond pulsars in M 54 would give a signal with a significance of about 4σ in 200 h observation time. With long-enough observation times, gamma-ray background from millisecond pulsars in M 54 may limit the sensitivity to DM annihilations (see Ref. [6] for more details). SgrDw may also host a $10^4 M_{\odot}$ IMBH. The modeled gamma-ray emission based on relativistic jets associated with active galactic nuclei has been done in [6] assuming that the IMBH is active and has a jet inclined towards the line of sight. The emission from *pp* interactions is dominant in the CTA energy range. For a reasonable set of parameters, the emission is too faint to be detected by CTA. However, under favorable circumstances (active black hole and jet aligned towards the

¹The sensitivity is computed here with more realistic DM halo profiles than used in Ref. [8]

²The collective emission of high energy gamma rays by millisecond pulsars in Galactic globular clusters has been detected by Fermi-LAT [9] and recently by HESS from Terzan 5 [10].

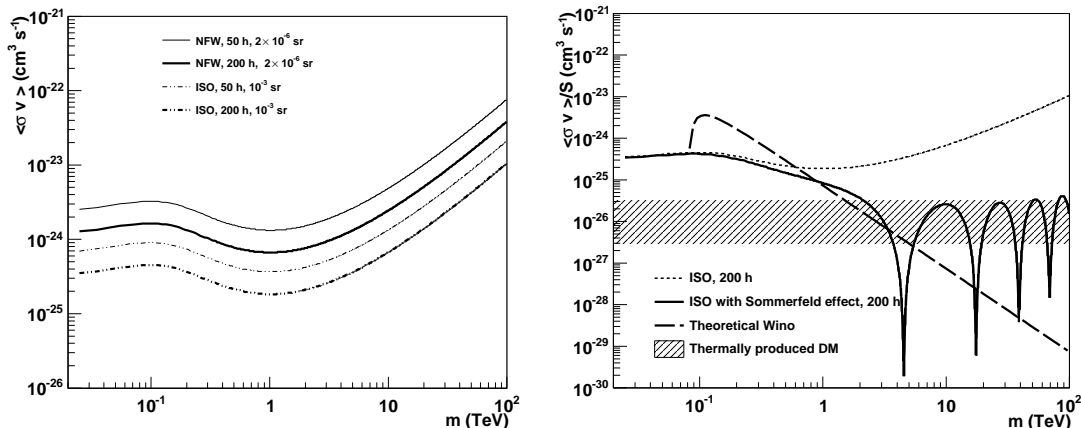


Figure 1: Left: 95% C.L. sensitivity on $\langle\sigma v\rangle$ towards SgrDw for a CTA-like instrument for an NFW (solid line) and an Isothermal (ISO) (dashed line) DM halo profiles, respectively. The sensitivity is shown for 50 and 200 h observation times. The solid angle of observation is taken as $\Delta\Omega = 2 \times 10^{-6}$ sr for the NFW profile and $\Delta\Omega = 10^{-3}$ sr for the ISO profile. Right: 95% C.L. sensitivity on $\langle\sigma v\rangle/S$ enhanced by the Sommerfeld effect for the ISO profile (solid line). Figures extracted from Ref. [6].

line of sight), it might nevertheless be detectable in observations of SgrDw.

3 Blind searches for dark matter subhalos

Thanks to their very large collection area, IACTs are very well suited for deep observations of pointed DM sources associated with standard astrophysical counterparts. However, HESS has demonstrated the ability to accurately map large regions of the sky, as obtained from the Galactic Plane Survey (GPS) [11, 12]. The GPS have been used to perform for the first time a blind search for DM substructures (DM spikes around galactic IMBHs) using an IACT wide-field survey [13]. Constraints have been then derived from the HESS GPS on the conventional CDM subhalo distribution obtained by the cosmological N-body simulation Via Lactea II [14]. Values of $\langle\sigma v\rangle$ at the level of 10^{-23} cm³s⁻¹ can be tested [15]. A projected sensitivity map for a GPS for CTA have been computed. Figure 2 (left) shows that the 90% C.L. sensitivity reaches a few 10^{-25} cm³s⁻¹ in the TeV mass range [15]. However, the flux sensitivity along the Galactic plane is limited by the new population of sources that will be detected at a flux level of 10^{-12} cm⁻²s⁻¹. The Galactic plane might also not be the best place to look for DM subhalos since they could have been tidally affected by the Galactic disk.

Larger scans of the sky will most likely be conducted by CTA. In particular, a more extended survey of the order of a quarter-sky size is foreseen. A large survey increases the probability to find bright DM subhalos in the field of view, which thus translates into better constraints. Such a survey should not include the Galactic plane where numerous standard astrophysical sources are expected to shine and therefore decrease the sensitivity to DM clumps. On the other hand, the central region of the Milky Way is attractive since the Via Lactea-II subhalo distribution is

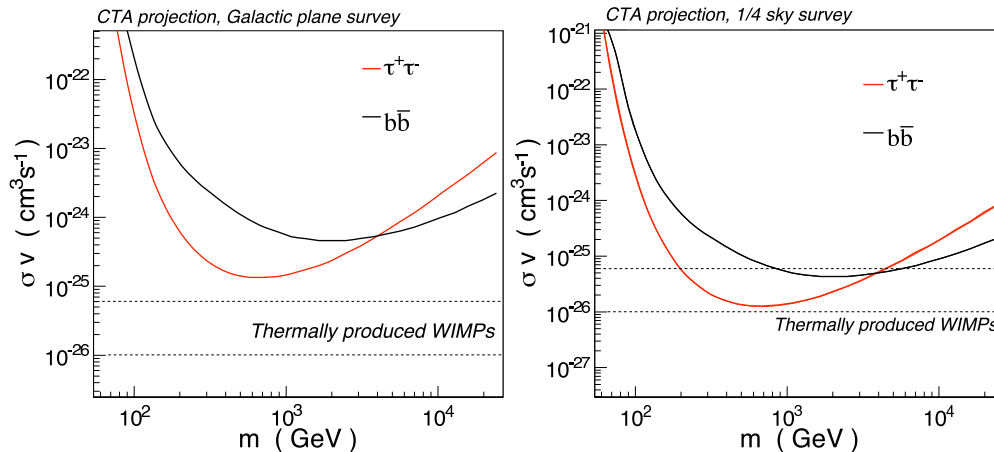


Figure 2: Sensitivity on σv versus the DM particle mass m for a CTA GPS (left) and for a CTA survey of a one-fourth of the sky (right). The sensitivity is calculated at 90% C.L. for the DM clumps provided by the VL-II simulation. The DM particle is assumed to annihilate into purely $b\bar{b}$ and $\tau^+\tau^-$ pairs, respectively. The region of natural values of σv for thermally produced WIMPs is also plotted. Figures extracted from Ref. [15].

peaked towards the centre. A prospective study has been conducted selecting the region from -90° to $+90^\circ$ in Galactic longitude and from -45° to $+45^\circ$ in Galactic latitude, excluding the Galactic plane between $\pm 1.5^\circ$ [15]. A constant flux sensitivity of about $5 \times 10^{-13} \text{ cm}^{-2} \text{ s}^{-1}$ is taken over the entire field of view. Figure 2 (right) shows the 90% C.L. sensitivity on σv as a function of the DM particle mass. It is shown that thermally-produced DM can be probed with an ambitious quarter-of-the-sky survey with CTA.

References

- [1] The CTA Consortium, arXiv:1008.3703 [astro-ph.IM].
- [2] J. Penarrubia, J. Navarro and A. McConnachie, *Astrophys. J.* **673**, 226 (2008).
- [3] M. Niederste-Ostholt, V. Belokurov, N. W. Evans, and J. Peñarrubia, *Astrophys. J.* **712**, 516, (2010).
- [4] J. Peñarrubia, *et al.*, *MNRAS*, **408**, L26 (2010).
- [5] R. Ibata *et al.*, *Astrophys. J.* **699**, L169 (2009).
- [6] A. Viana *et al.*, *accepted in Astrophys. J.* (2011), arXiv:1103.2627 [astro-ph.HE].
- [7] M. Lattanzi, J. I. Silk, *Phys. Rev.* **D79**, 083523 (2009).
- [8] F. Aharonian, *et al.*, *Astropart. Phys.* **29**, 55 (2008). Erratum-ibid: 33, 274 (2010).
- [9] A. Abdo, *et al.*, [Fermi-LAT Collaboration] *A&A*, **524**, A75 (2010).
- [10] A. A. Abramowski, *et al.*, [HESS Collaboration] arXiv:1106.4069 [astro-ph.HE].
- [11] F. Aharonian *et al.* [H.E.S.S. Collaboration], *Science* **307**, 1938-1942 (2005).
- [12] F. Aharonian *et al.* [HESS Collaboration], *Astrophys. J.* **636**, 777-797 (2006).
- [13] F. Aharonian *et al.* [HESS Collaboration], *Phys. Rev.* **D78**, 072008 (2008).
- [14] J. Diemand, M. Kuhlen, P. Madau, M. Zemp, B. Moore, D. Potter, J. Stadel, *Nature* **454**, 735-738 (2008).
- [15] P. Brun, E. Moulin, J. Diemand, J. -F. Glicenstein, *Phys. Rev.* **D83**, 015003 (2011).

Indirect Dark Matter search with H.E.S.S.

Giovanni Lamanna¹ for the H.E.S.S. collaboration

¹Laboratoire d'Annecy-le-Vieux de Physique des Particules (LAPP), Université de Savoie, CNRS/IN2P3, F-74941 Annecy-le-Vieux, France

DOI: <http://dx.doi.org/10.3204/DESY-PROC-2011-04/lamanna-giovanni>

Dark Matter (DM) accounts for 25% of the mass-energy budget of the Universe but its nature is still to be discovered. The hypothesis that DM is made of Weakly Interacting Massive Particles (WIMPs) is explored by the latest generation of Astroparticle experiments. The indirect DM search methods are sensitive to self-annihilating/decay DM candidates leading also to the production of GeV-TeV gamma-rays in the final state. In particular these photons may be detected by Imaging Atmospheric Cherenkov Telescopes (IACT) like H.E.S.S.. Searches for WIMP-annihilation signatures from various candidate regions with enhanced DM density and related observations performed with H.E.S.S. are reviewed.

1 Introduction

The existence of DM assumed in the Standard Cosmological Model is supported by a series of observations such as rotation curves in spiral galaxies and velocity dispersion in elliptical galaxies, gravitational lensing and large scale distribution of galaxies. However, the nature of the DM remains unknown. Among many theoretical candidates for the DM particle, WIMPs predicted in theories beyond the Standard Model (SM) of particle physics such as the neutralinos introduced in Supersymmetry, are among the best motivated. A pair of WIMPs can annihilate and produce SM particles including photons. Unfortunately, potential direct annihilations into $\gamma\gamma$ or $Z\gamma$ producing a sharp line photon spectrum with a photon energy depending on the neutralino mass, are very rare because loop-suppressed. However DM can also annihilate to pairs of leptons or quarks, leading in subsequent processes to π^0 decays, resulting in a continuous photon spectrum.

2 The H.E.S.S. observations towards potential targets

The High Energy Stereoscopic System (H.E.S.S.) located in Namibia is an array composed of four IACTs of large collection surface (107 m² per telescope) and fine pixelated cameras (960 PMTs). It is designed for high sensitivity measurements in the energy range from 100 GeV to 10 TeV (e.g. 1% of the Crab Nebula flux is detected after ~ 25 h observation [1]). H.E.S.S. has started its observations in 2003; since then it has deeply explored a large fraction of the galactic sky accessible from the southern hemisphere and it has investigated, among other targets, the potential TeV γ -ray emission of exotic origin bringing a potential signature of WIMPs annihilations. Such a signal would depend on: 1) the intrinsic DM density distribution in the observed source; 2) the particle physics coupling of the WIMP; 3) the field of view $\Delta\Omega$ within

which the signal is integrated. The resulting γ -ray flux is then usually factorized in two terms: $\Phi_{pp}(E_\gamma) \times J(\Omega) \Delta\Omega$. The first factor accounts for the particle physics, while the second factor is about the nature of the DM density distribution. In particular $\Phi_{pp}(E_\gamma) = 1/8\pi \langle \sigma v \rangle / m_\chi^2 \times dN_\gamma/dE_\gamma$, where $\langle \sigma v \rangle$ is the velocity averaged annihilation cross section, m_χ is the WIMP particle mass, and dN_γ/dE_γ is the differential γ -ray spectrum summed over the whole final states with their corresponding branching ratios. In the astrophysical factor $J(\Omega) \Delta\Omega$, the integral along the line-of-sight (l.o.s.) of the squared density of the DM distribution in the object is averaged over the instrument solid angle of the integration region. Therefore the best places to look for DM will be those with the highest DM concentrations. Distance is also very important, since candidate DM-dominated systems that are located too far from us will yield too low WIMPs annihilation fluxes at Earth. For those reasons H.E.S.S. searches have focused on the Galactic Center and dwarf galaxy satellites of the Milky Way. Nearby Globular Clusters have been considered more recently as very suitable targets, since they may also yield similar γ -ray fluxes despite their distance. No signals have been found in the H.E.S.S. DM searches and upper limits on the $\langle \sigma v \rangle$ value as a function of m_χ and under specific assumptions on the DM density profile (e.g. $J(\Omega)$) are derived.

2.1 The Galactic Center region

One of the closest in distance and the most dense region of our Galaxy is its center, located at 8.5 kpc from the Earth, and potentially populated by an over-density of relic annihilating WIMPs. H.E.S.S. dedicated more than 100 hrs of observation to the Galactic center, and it is a target from which a γ -ray emission has actually been measured (i.e. source HESS J1745-290) coincident with the position of the supermassive black hole Sgr A* [2]. Although its temporal stability is consistent with a WIMP annihilation signal and the morphology is not excluding a potential consistency with the DM halo shapes predicted by some structure formation simulations, the detected emission shows an energy spectrum which extends beyond 10 TeV (requiring WIMP masses which are uncomfortably large) and a shape more consistent with an astrophysical origin. One should note also that several astrophysical objects are indeed present in the same field of view and that the galactic γ -ray diffuse emission is also contributing to the general picture. Assuming a NFW dark matter halo profile, 99% CL upper limits on the velocity-weighted annihilation cross section $\langle \sigma v \rangle$ are of the order of 10^{-24} - 10^{-23} $\text{cm}^3 \text{s}^{-1}$. These limits can vary by plus or minus three orders of magnitude if one assumes other DM halo shapes. In particular large differences among different parametrisation occur if they are extrapolated down to the very center of the halo (e.g. where the NFW profile is more strongly peaked). At distances >10 pc, however, these differences are less pronounced, allowing one to put limits on $\langle \sigma v \rangle$ which do not depend strongly on the

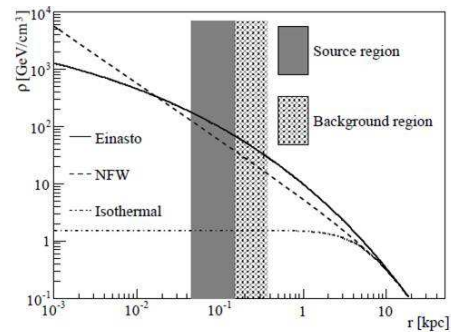


Figure 1: Galactic halo analysis: the source region and the region used for background estimation are indicated. NFW, Einasto and an isothermal profiles are shown for comparison.

shapes. In H.E.S.S. this fact was exploited by searching for a VHE γ -ray signal from DM annihilation in a region with a projected galactocentric distance of 45 pc - 150 pc excluding the Galactic plane [3]. The target region (observed for 112 h) corresponds to a circular source region of radius 1.0° centered at the Galactic Center. Contamination of the DM signal by local astrophysical γ -ray sources is excluded by restricting the analysis to Galactic latitudes $|b| > 0.3^\circ$, effectively cutting the source region into two segments above and below the Galactic plane. For the data analysis, background regions are located further away from the Galactic Center than the source region. This is an important aspect, since, unavoidably, a certain amount of DM annihilation events would be recorded in the background regions, too, reducing a potential excess signal obtained in the source region. For the two studied halo profiles, NFW and Einasto, the expected DM annihilation flux is thus smaller in the background regions than in the source region (see Figure 1), making the measurement of a residual annihilation flux possible. Both source and background analysed spectra agree well within the errors, resulting in a null measurement for a potential DM annihilation signal, from which upper limits on $\langle\sigma v\rangle$ can be determined. These are among the best reported so far for the energy range 300 GeV - 10 TeV. In particular, for the DM particle mass of ~ 1 TeV, values for $\langle\sigma v\rangle$ above $3 \times 10^{-25} \text{ cm}^3 \text{ s}^{-1}$ are excluded for the Einasto density profile (see Figure 2 - left).

2.2 The Dwarf galaxies

Dwarf galaxies are considered DM-dominated objects, having a reduced astrophysical background since they have little or no recent star formation activity. Nearby dwarf galaxies in the Local Group have been observed with H.E.S.S.. The *Sagittarius Dwarf* (Sgr dSph) was observed in the 2006-2010 period for 45 h. No significant γ -ray excess was found above the estimated background at the nominal target position (RA = $18^{\text{h}}55^{\text{m}}59.9^{\text{s}}$, Dec = $-30^\circ 28' 59.9''$, J2000.0). A 95% confidence level upper limit on the total observed numbers of γ -rays is computed. For that two different modelling of the dark matter halo of Sgr dSph have been considered: the NFW and an isothermal profile taking into account also disruptions by tidal winds by imposing a truncation in the dark matter density profiles [4]; both result in similar values for the J -factor yielding two exclusion limits of the same order $\sim 10^{-22} \text{ cm}^3 \text{ s}^{-1}$ (Figure 2). The *Sculptor* and *Carina* Dwarf spheroidal galaxies were observed between 2008 and 2009 for 11.8 and 14.8 hours respectively. No gamma-ray signal was detected at the nominal positions of these galaxies. 95% CL constraints on the velocity weighted WIMP annihilation cross section for both Sculptor and Carina range from $\langle\sigma v\rangle \sim 10^{-21} \text{ cm}^3 \text{ s}^{-1}$ down to $\langle\sigma v\rangle \sim 10^{-22} \text{ cm}^3 \text{ s}^{-1}$ depending on the dark matter halo model used. Possible enhancements of the γ -ray flux are studied: the Sommerfeld effect, which is found to exclude some dark matter particle masses, the internal Bremsstrahlung and clumps in the dark-matter halo distributions [5]. The *Canis Major* (CMA) overdensity has been observed by H.E.S.S. as a potential target for indirect DM search. The nature of CMA is still controversial and one scenario represents it as a dwarf galaxy. A total of 9.6 h of data were collected and no evidence for a very high energy γ -ray signal is found. Constraints on $\langle\sigma v\rangle$ are calculated using a NFW DM-halo model: assuming a total halo mass of $3 \times 10^8 M_\odot$, 95% CL exclusion limits of the order of $\sim 5 \times 10^{-24} \text{ cm}^3 \text{ s}^{-1}$ are reached in the 500 GeV - 10 TeV WIMP particle mass interval [6]. Although these are competitive limits on DM annihilation cross sections (as summarised in Figure 2) the present IACT instruments like H.E.S.S. do not have yet the required sensitivity to probe thermally-produced DM limit (of the order of $\sim 3 \times 10^{-26} \text{ cm}^3 \text{ s}^{-1}$).

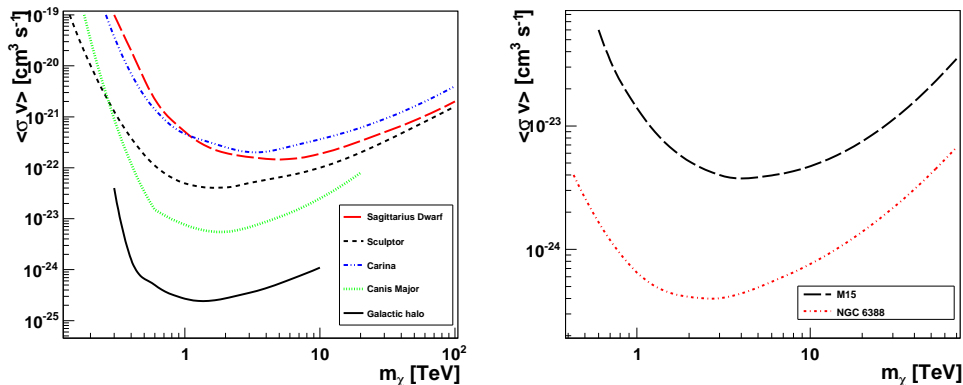


Figure 2: Left) Compilation of H.E.S.S. constraints in the DM search: 95% CL upper limits on $\langle\sigma v\rangle$ as a function of the WIMP mass. Right) 95% CL limits for M15 and NGC 6388 in the final state and starting with an initial NFW dark matter density profile.

2.3 Globular Clusters

Globular Clusters (GCs) are dense stellar systems found in halos of galaxies, with typical masses similar to dwarf galaxies but much more compact and dominated by a baryonic environment. However GCs are suggested as potential targets for indirect DM searches since in the primordial formation scenario they could have been formed in DM minihalos, before or during the reionization, before formation of galaxies and WIMPs could still be present in their environment. Under such hypothesis H.E.S.S. has observed M 15 which is a metal-poor GC (therefore of cosmological origin), and NGC 6388, which although metal-rich might host a $>10^3 M_\odot$ black hole suggested to be of primordial origin. The DM content of the globular clusters NGC 6388 and M 15 (observed for 27.2 and 15.2 hours respectively) is modelled taking into account the astrophysical processes that can be expected to influence the WIMPs distribution during the evolution of the globular cluster: the DM adiabatic contraction by baryons, the adiabatic growth of a black hole in the DM halo and the kinetic heating of DM by stars. The 95% confidence level exclusion limits on $\langle\sigma v\rangle$ are derived at the level of $10^{-25} \text{ cm}^3 \text{ s}^{-1}$ and few $10^{-24} \text{ cm}^3 \text{ s}^{-1}$ for NGC 6388 and M 15 respectively [7] (Figure 2). The upgrading of the H.E.S.S. system with a fifth telescope of larger size will provide observations at energies as low as 30 GeV addressing DM search at lower values of the candidate WIMP mass. First results are expected in 2012.

References

- [1] F. Aharonian *et al.* (H.E.S.S. Collaboration), *A&A*, 2006, 457, 899-915
- [2] F. Aharonian *et al.* (H.E.S.S. Collaboration), *Phys. Rev. Let.*, 2006, 97, 221102
- [3] A. Abramowski *et al.* (H.E.S.S. Collaboration), *Phys. Rev. Let.*, 2011, 106, 161301
- [4] J. Masbou *et al.* (H.E.S.S. Collaboration), *Proceedings 1078, ICRC 2011*
- [5] A. Abramowski *et al.* (H.E.S.S. Collaboration), *Astropart. Phys.*, 2011, 34, 608
- [6] F. Aharonian *et al.* (H.E.S.S. Collaboration), *Astroph. J.*, 2009, 691, 175181
- [7] A. Abramowski *et al.* (H.E.S.S. Collaboration), *Astroph. J.*, 2011, 735, 12

Positronium Portal to the Mirror World

Paolo Crivelli¹

¹ETH Zurich, Institute for Particle Physics, 8093 Zurich, Switzerland

DOI: http://dx.doi.org/10.3204/DESY-PROC-2011-04/crivelli_paolo

It was realized sometime ago by Glashow that the mirror matter could have a portal to our world through photon-mirror photon mixing (ϵ) which would lead to orthopositronium (oPs) to mirror orthopositronium oscillations. This would result in a modification of the oPs decay rate however this effect is too small to be observed. Another experimental signature of this process is the apparently invisible decay of oPs. In this paper, we describe an experiment to search for the decay oPs \rightarrow invisible in a vacuum cavity with an expected sensitivity in the mixing strength of $\epsilon \simeq 10^{-9}$. This is more than one order of magnitude below the current Big Bang Nucleosynthesis limit and it is in a region of parameter space of great theoretical and phenomenological interest. An experiment with such a sensitivity is particularly timely in light of the recent claims for the observations of the annual modulation signal consistent with a mirror type dark matter interpretation.

1 Introduction

Cosmological observations of galactic rotational curves [1] and the gravitational lensing [2, 3] give strong evidence for the existence of dark matter [4]. This is one of the strongest indications for the existence of new physics beyond the standard model because within this theory no candidates can be found, thus, the identification of the origin of dark matter is a task of enormous importance for both particle physics and cosmology. At present, the most popular candidates for the (thermal-produced) dark matter are the so-called weakly interacting massive particles (WIMPs), which are e.g. lightest supersymmetric particles, Kaluza-Klein particles in universal extra dimension models or axions. However, despite of significant efforts the experiments looking for WIMPs lead so far to negative results, thus, pushing further possible WIMP searches into higher energy and/or higher sensitivity frontiers. The confirmation by the DAMA/LIBRA experiment [5] of the annual modulation signal observed by the DAMA/NaI [6] could potentially be the first direct terrestrial experimental detection of the existence of non-baryonic dark matter in our galactic halo. Very recently, also the CoGeNT collaboration [7] claimed the observation of a modulation and the CRESST-II experiment reported more than 4 sigma excess of events above their expected background [8]. However, standard WIMPs cannot explain these observations. A possibility is to conclude that those observations are originated by poorly understood background. Another approach is to look for a different model that could explain these results. Among numerous alternatives that have been discussed, one of the most promising, which could reconcile the DAMA and CoGeNT annual modulation signals, the CRESST excess and the negative results of higher thresholds experiments [9]-[11], is mirror type dark matter [12]-[14]. Mirror matter is an exact copy of the ordinary matter (e.g the mirror electron would have the same mass of the electron) with the same physics (i.e. the same couplings)

but in this model the particles have the left and right chiral properties interchanged. Therefore, if mirror matter is present in our universe it would mean that parity (spatial-inversion) is an unbroken symmetry of nature. Mirror baryons are naturally dark, stable and massive. Currently, it seems that this concept could also explain in a natural way the visible and dark matter densities in the universe ($\Omega_B = 0.044$ and $\Omega_{DM} = 0.26$) [15, 16]. The mirror matter, in addition to gravity, could communicate with our world through photon-mirror photon kinetic mixing (with strength ϵ) [17] or the Higgs- mirror Higgs quartic couple $\lambda\phi\phi^\dagger\phi'\phi'^\dagger$ [18, 19]¹. These are the only renormalizable and gauge invariant terms that can be added to the standard model Lagrangian.

2 Experimental technique and setup

The experiment presented here is based on the ETHZ slow positron beam to form Ps in a vacuum cavity combined with the BGO calorimeter used in our previous search for $Ps \rightarrow invisible$ decays [21] with a modified geometry to accommodate the beam pipe [22, 23]. The photon mirror-photon kinetic mixing would break the degeneracy between Ps and Ps' so that the vacuum energy eigenstates are a linear combination of the mass eigenstates $(Ps \pm Ps')/\sqrt{2}$. This would lead to orthopositronium to mirror orthopositronium Rabi oscillations [24]. The experimental signature of this process is the apparently invisible decay of Ps. By invisible is meant that the energy $2m_e$ expected for ordinary decays is not detected in a hermetic calorimeter surrounding the Ps formation target. Therefore, the occurrence of the $Ps \rightarrow Ps' \rightarrow invisible$ conversion would appear as an excess of events with zero-energy deposition in the calorimeter above those expected either from Monte Carlo prediction of the background or from direct background measurements. Compared to our previous search for $Ps \rightarrow invisible$ this experiment present many advantages. A factor 10^2 more statistics can be collected with the same number of positrons because of the much more efficient trigger system, a gain of almost a factor 10 in the fraction of Ps atoms produced per impinging positron (this concomitantly reduces the background from 2 photons annihilations) and a higher efficiency for signal detection. Furthermore, because the number of collisions per lifetime (N_{coll}) of the Ps with the cavity walls affects the coherence of oscillation [25], the probability of oscillation ($\sim \sqrt{N_{coll}}$) will be about 100 times higher than in the previous search where Ps was produced and confined in the pores of an aerogel target ($N_{coll} \sim 10^4$) instead of a vacuum cavity ($N_{coll} \sim 1$) as proposed here. Another great advantage is the fact that the number of collisions is an experimental parameter that can be tuned taking runs at different positron implantation energies. From 3 to 5 keV the mean velocity of the created Ps increases by about a factor of two, thus, the collision rate with the walls is 2 times bigger and the signal is suppressed by the same factor. This without affecting the background level since the fraction of Ps will just vary by a few % [26]. However, compared to the previous experiment, there is a clear disadvantage: the calorimeter must be mounted outside the vacuum chamber so that the vacuum pipe introduces a loss of the photon energy.

¹This may result in dramatic consequences for the LHC, making the significance of the Higgs signal lower due to decreasing of the *Signal/Background* ratio if the mass splitting is large compared to the Higgs LHC experiments mass resolution [20].

3 Expected background level and sensitivity

In Table 1, we summarize the estimated contributions of the expected background sources of the experiment. The main contribution to the first background is coming from the losses of annihilation energy coming in the vacuum beam pipe. This was estimated with the help of the simulation using a beam pipe made of 0.04 mm aluminum and 0.80 mm thick carbon (similar to the one produced at ETHZ that was used at the H1 experiment at DESY). The target substrate and the copper wire surrounding the beam pipe were also included. We will investigate other possibilities, e.g. to use an “active” beam pipe in which the energy lost by the photons is measured. This could be a scintillating crystal with a bore to be used as a vacuum cavity with an internal coating compatible with a good vacuum. The most dangerous background source is due to the backscattered positrons, either from the carbon foil or from the target. A possible way to further suppress this background is the installation of an electrode to which a pulsed voltage is applied in order to redirect back the positrons in the target avoiding them to escape detection region [22].

	BACKGROUND SOURCE	expected
1)	Photon detection loss:	$\simeq 10^{-8}$
2)	Positron backscattered from carbon foil	$< 10^{-7}$
3)	Positron Backscattered from SiO ₂	$< 10^{-7}$
4)	Fast Ps from carbon foil	$< 5 \times 10^{-8}$
5)	Fast Ps from target	$<< 10^{-8}$

Table 1: *Summary of the expected background level for the different background sources.*

The sensitivity of the experiment is defined as the level at which the first background event is expected:

$$S_{\text{Ps} \rightarrow \text{invisible}} = 1/(N_{\text{Ps}} \cdot \epsilon_{\text{tot}}) \quad (1)$$

where the terms in the denominator are the integrated number of produced Ps (N_{Ps}) and $\epsilon_{\text{tot}} \simeq 0.95$ is the total efficiency to detect an invisible decay. The losses in signal efficiency of about 4.5% arise from the possibility of having 2 or more positrons per bunch. We estimated the rate of these events using $R_{2e^+} = 2 \cdot \tau_{\text{bunch}} \cdot R_{e^+}$ where $\tau_{\text{bunch}} = 300$ ns and $R_{e^+} = 7.5 \times 10^4/s$ is the number of delivered positrons per second on the target in continuous mode. For two or more positrons there is always annihilation energy deposition in the ECAL, hence this effect does not result in a background. The number of Ps/s, R_{Ps} , is defined as a product

$$R_{\text{Ps}} = R_{e^+} \cdot \epsilon_{\text{Ps}} \cdot \epsilon_{\text{tagging}} \cdot \epsilon_{\text{Bunching}} \quad (2)$$

where the first factor was defined above, the second one is the efficiency for Ps production (about 30%), the third one $\epsilon_{\text{tagging}} = 0.04$ is the efficiency of the tagging system and the last one, $\epsilon_{\text{Bunching}} = 0.1$, are the losses due to the duty cycle of the bunching system. As in our previous search, the length of the gate for the ADCs has to be at least $3 \mu\text{s}$ in order to suppress the probability for Ps to decay after this time to a level of 10^{-9} . Therefore, a limit on the branching ratio of 4×10^{-8} , which is 10 times more stringent than the current one², can be reached in less than a 8 days run ($\approx 6 \times 10^7$ observed Ps annihilations). Assuming

²For comparison, it took us 6 months of data taking to set the current limit.

that the DAMA/LIBRA and the CoGeNT annual signal modulations and the CRESST excess are generated by elastic scattering of mirror matter, the mixing strength should be of the order of $\epsilon \simeq 10^{-9}$ [14]. With the estimated average number of Ps collisions in the vacuum cavity we plan to use $N_{coll} \simeq 0.5$ (for 5 keV implantation energy of the positrons), the expected branching ratio for this process will be $Br(\text{Ps} \rightarrow \text{invisible}) \simeq 5 \times 10^{-8}$ (we assume $\epsilon = 2 \times 10^{-9}$ for the following estimation), thus, a total number of $\simeq 35$ signal events would be detected in the ECAL during 3 months of data taking. We are expecting a background level comparable with the signal rate, thus, about the same amount of background events are expected which means that a discovery with about 6σ significance is possible. As explained above, a unique feature of our proposal is the possibility to change the experimental conditions (i.e. the number of the Ps collisions with matter), and hence to cross check the results without affecting the background. For an implantation energy of the positrons of 3 keV, the number of excess events will be 2 times smaller compared to 5 keV positrons.

4 Conclusions

The proposed experiment to search for invisible decays of positronium is designed with the goal to confront directly the interpretation of the dark matter direct searches in terms of mirror dark matter. In case of a signal detection, this will prove unambiguously that dark matter should be identified with mirror matter solving this very important problem of cosmology and particle physics. Furthermore, the value of the coupling (ϵ) of matter to their mirror counterpart via photon mirror-photon kinetic mixing will be precisely determined. In case that no signal will be observed, this measurement will exclude that the DAMA/LIBRA and CoGeNT annual signal modulation is generated by elastic scattering of mirror matter in their detectors and will provide an improvement of more than a factor of 10 on the branching ratio for Ps \rightarrow invisible. This will place stringent limits for possible new physics beyond the standard model like for example extra-dimensions, milli-charged particles and hidden sectors.

5 Acknowledgments

This work was funded by the Swiss National Science Foundation under the grant PZ00P2_132059.

References

- [1] A. Borriello and P. Salucci, *Mon. Not. Roy. Astron. Soc.* **323**, 285 (2001) [arXiv:astro-ph/0001082].
- [2] H. Hoekstra, H. Yee and M. Gladders, *New Astron. Rev.* **46**, 767 (2002) [arXiv:astro-ph/0205205].
- [3] R. B. Metcalf, L. A. Moustakas, A. J. Bunker and I. R. Parry, *Astrophys. J.* **607**, 43 (2004) [arXiv:astro-ph/0309738]; L. A. Moustakas and R. B. Metcalf, *Mon. Not. Roy. Astron. Soc.* **339**, 607 (2003) [arXiv:astro-ph/0206176].
- [4] G. Bertone, D. Hooper and J. Silk, *Phys. Rept.* **405**, 279 (2005) [arXiv:hep-ph/0404175].
- [5] R. Bernabei et al. [DAMA Collaboration], *Eur. Phys. J. C* **56**, 333 (2008) [arXiv:0804.2741 [astro-ph]].
- [6] R. Bernabei et al. (DAMA Collaboration), *Riv. Nuovo Cimento* **26**, 1 (2003);
- [7] C.E. Aalseth et al., *Phys. Rev. Lett.* **106**, 131301 (2011);
C.E. Aalseth et al., arXiv:1106.0650
- [8] G. Angloher et al., arXiv:1109.0702
- [9] Z. Ahmed et al., *Science* **327**, 1619 (2010)

POSITRONIUM PORTAL TO THE MIRROR WORLD

- [10] J. Angle et al., Phys. Rev. Lett. 107, 051301 (2011)
- [11] E. Aprile et al., Phys. Rev. D84, 061101 (2011)
- [12] R. Foot, Phys. Rev. D78, 043529 (2008) [arXiv:0804.4518 [hep-ph]].
- [13] R. Foot, Phys.Rev. D82, 095001 (2010)
- [14] R. Foot, Phys.Lett. B703, 7 (2011)
- [15] Z. Berezhiani, Int. J. Mod. Phys. A19, 3775 (2004)
- [16] P. Ciarcelluti and A. Lepidi, Phys. Rev. D78, 123003 (2008) [arXiv:0809.0677 [astro-ph]].
- [17] B. Holdom, Phys. Lett. B166, 196 (1986).
- [18] R. Foot, H. Lew and R. R. Volkas, Phys. Lett. B272, 67 (1991),
R. Foot, H. Lew and R. R. Volkas, Mod. Phys. Lett. A7, 2567 (1992),
A. Y. Ignatiev and R. R. Volkas, Phys. Lett. B487, 294 (2000), [arXiv:hep-ph/0005238].
- [19] Wen-sheng Li, Peng-fei Yin, and Shou-hua Zhu, Phys. Rev. D76, 095012 (2007), arXiv:0709.1586 [hep-ph]; R. Barbieri, T. Gregoire and L. J. Hall, arXiv:hep-ph/0509242; Z. Chacko, Y. Nomura, M. Papucci and G. Perez, JHEP 0601, 126 (2006) [arXiv:hep-ph/0510273]; B. Patt and F. Wilczek, arXiv:hep-ph/0605188; J. March-Russell, S. M. West, D. Cumberbatch and D. Hooper, arXiv:0801.3440. J.D. Wells, arXiv:0803.1243[hep-ph]
- [20] R. Foot, A. Kobakhidze, R. R. Volkas, arXiv:1109.0919 [hep-ph]
- [21] A. Badertscher, P. Crivelli, W. Fetscher, U. Gendotti, S. Gninenko, V. Postoev, A. Rubbia, V. Samoylenko, D. Sillou, Phys. Rev. D 75, 032004 (2007) [arXiv:hep-ex/0609059].
- [22] P. Crivelli, A. Belov, U. Gendotti, S. Gninenko and A. Rubbia, JINST 5, P08001 (2010) [arXiv:1005.4802 [hep-ex]].
- [23] A. Badertscher, A. Belov, P. Crivelli, S. N. Gninenko, J. P. Peigneux, A. Rubbia and D. Sillou, Int. J. Mod. Phys. A 19, 3833 (2004).
- [24] S. L.Glashow, Phys. Rev. Lett. 167, 35 (1986)
- [25] S. N. Gninenko, Phys. Lett. B326, 317 (1994).
R. Foot and S. N. Gninenko, Phys. Lett. B480, 171 (2000).
- [26] P. Crivelli, U. Gendotti, A. Rubbia, L. Liskay, P. Perez, C. Corbel, Phys. Rev. A 81, 052703 (2010) [arXiv:1001.1969 [physics.atom-ph]].

Chapter 2

Axion Dark Matter and Searches for Axions and WISPs

Axion BEC Dark Matter

Ozgur Erken, Pierre Sikivie, Heywood Tam, Qiaoli Yang

Department of Physics, University of Florida, Gainesville, FL 32611, USA

DOI: http://dx.doi.org/10.3204/DESY-PROC-2011-04/sikivie_pierre

Cold dark matter axions thermalize through gravitational self-interactions and form a Bose-Einstein condensate when the photon temperature reaches approximately 500 eV. Axion Bose-Einstein condensation provides an opportunity to distinguish axions from the other dark matter candidates on the basis of observation. The rethermalization of axions that are about to fall in a galactic potential well causes them to acquire net overall rotation, whereas ordinary cold dark matter falls in with an irrotational velocity field. The inner caustics of galactic halos are different in the two cases.

1 Introduction

Both axions and weakly interacting particles (WIMPs) are considered forms of cold dark matter (CDM). Furthermore, until recently, axions and WIMPs were thought to be indistinguishable on observational grounds, i.e. indistinguishable on the basis of purely astronomical data. The discovery [1] that dark matter axions form a Bose-Einstein condensate (BEC) has changed this view since axion BEC is claimed to have observable consequences [1, 2, 3]. This raises the question: When do axions behave as ordinary CDM and when do they not?

To start off it is worth emphasizing that, at the fundamental level, axions and WIMPs are very different. The surprise is really that they have similar properties as far as large scale structure is concerned. Both axions and WIMPs are described by quantum fields. Furthermore, both are excellently described by classical limits of quantum fields. But the classical limits are different in the two cases: WIMPs are in the classical particle limit whereas (decoupled) axions are in the classical field limit. In the classical particle limit one takes $\hbar \rightarrow 0$ while keeping $E = \hbar\omega$ and $\vec{p} = \hbar\vec{k}$ fixed. Since $\omega, \vec{k} \rightarrow \infty$, the wave nature of the quanta disappears. WIMPs are to excellent approximation classical point particles. In the classical field limit, on the other hand, one takes $\hbar \rightarrow 0$ for constant ω and \vec{k} . $E = \mathcal{N}\hbar\omega$ and $\vec{p} = \mathcal{N}\hbar\vec{k}$ are held fixed by letting the quantum state occupation number $\mathcal{N} \rightarrow \infty$. This is the limit in which quantum electrodynamics becomes classical electrodynamics. It is the appropriate limit for (decoupled) cold dark matter axions because they are a highly degenerate Bose gas. The axion states that are occupied have huge occupation numbers, $\mathcal{N} \sim 10^{61}$ [1]. The need to restrict to *decoupled* axions will be explained shortly.

So axions and WIMPs are fundamentally different even if both can legitimately be called CDM. The distinction is not just academic, and is certainly important if axions thermalize, i.e. if axions find a state of larger entropy through self-interactions. Recall that, whereas statistical mechanics makes sense of the behaviour of large aggregates of classical particles (it was invented by Boltzmann to derive the properties of atoms in the gaseous state) it fails to make sense of

classical fields. In thermal equilibrium every mode of a classical field would have average energy $k_B T$. As Rayleigh pointed out, the energy density is infinite then at finite temperature due to the contributions from short wavelength modes. Thus the application of statistical mechanics to classical field theory (classical electrodynamics in particular) is in direct disagreement with observation. As is well-known, the disagreement is removed because of, and only because of, quantum mechanics.

In summary, if the axions are decoupled (i.e. do not interact and hence do not thermalize), they behave to excellent approximation like a classical field. However, if the axions thermalize, they are not described by a classical field. Instead they form a Bose-Einstein condensate, an essentially quantum-mechanical phenomenon.

2 Axion Bose-Einstein Condensation

Axions were originally introduced [4] as a solution to the strong CP problem. It was later found that they are a cold dark matter candidate [5]. Cold axions are produced when the axion mass turns on during the QCD phase transition. The critical time, defined by $m(t_1)t_1 = 1$, is $t_1 \simeq 2 \cdot 10^{-7} \text{ sec } (f/10^{12} \text{ GeV})^{\frac{1}{3}}$, where f is the axion decay constant. The zero temperature axion mass is given in terms of f by

$$m \simeq 6 \cdot 10^{-6} \text{ eV } \frac{10^{12} \text{ GeV}}{f} \quad . \quad (1)$$

At temperatures well above 1 GeV, the axion mass is practically zero. It increases from zero to m during the QCD phase transition. The cold axions are the quanta of oscillation of the axion field that result from the turn on of the axion mass. They have number density [5]

$$n(t) \sim \frac{4 \cdot 10^{47}}{\text{cm}^3} \left(\frac{f}{10^{12} \text{ GeV}} \right)^{\frac{5}{3}} \left(\frac{a(t_1)}{a(t)} \right)^3 \quad (2)$$

where $a(t)$ is the cosmological scale factor. Because the axion momenta are of order $\frac{1}{t_1}$ at time t_1 and vary with time as $a(t)^{-1}$, the velocity dispersion of cold axions is

$$\delta v(t) \sim \frac{1}{mt_1} \frac{a(t_1)}{a(t)} \quad (3)$$

if each axion remains in whatever state it is in, i.e. if axion interactions are negligible. We refer to this case as the limit of decoupled cold axions. If decoupled, the average state occupation number of cold axions is

$$\mathcal{N} \sim n \frac{(2\pi)^3}{\frac{4\pi}{3}(m\delta v)^3} \sim 10^{61} \left(\frac{f}{10^{12} \text{ GeV}} \right)^{\frac{8}{3}} \quad . \quad (4)$$

Clearly, the effective temperature of cold axions is much smaller than the critical temperature

$$T_c = \left(\frac{\pi^2 n}{\zeta(3)} \right)^{\frac{1}{3}} \simeq 300 \text{ GeV } \left(\frac{f}{10^{12} \text{ GeV}} \right)^{\frac{5}{9}} \frac{a(t_1)}{a(t)} \quad (5)$$

for BEC. Axion number violating processes, such as their decay to two photons, occur only on time scales vastly longer than the age of the universe. The only condition for axion BEC that is not manifestly satisfied is thermal equilibrium.

Axions are in thermal equilibrium if their relaxation rate Γ is large compared to the Hubble expansion rate $H(t) = \frac{1}{2t}$. However, the usual techniques of non-equilibrium statistical mechanics are not applicable to dark matter axions. On the one hand, cold axions are highly condensed in phase space ($\mathcal{N} \gg 1$), which greatly exaggerates the quantum effect of Bose-enhancement in their scattering processes. On the other, because their energy dispersion is very small, they are outside the ‘particle kinetic regime’. The picture of instantaneous collisions breaks down, and the usual Boltzmann equation no longer applies. The particle kinetic regime is defined by $\delta\omega \gg \Gamma$ where $\delta\omega$ is the energy dispersion of the particles. Axions are in the opposite regime, $\delta\omega \ll \Gamma$, which we call the ‘condensed regime’. Thermalization in the condensed regime is discussed in detail in ref. [6], which gives an estimate for the relaxation rate of cold dark matter axions due to their gravitational self-interactions:

$$\Gamma \sim 4\pi Gnm^2\ell^2 \quad (6)$$

where $\ell \sim (m\delta v)^{-1}$ is the axion correlation length. $\Gamma(t)/H(t)$ is of order $5 \cdot 10^{-7}(f/10^{12} \text{ GeV})^{\frac{2}{3}}$ at time t_1 but grows as $ta^{-1}(t) \propto a(t)$. Thus gravitational interactions cause the axions to thermalize and form a BEC when the photon temperature is of order 500 eV $(f/10^{12} \text{ GeV})^{\frac{1}{2}}$.

The question is then whether axion BEC has observable consequences. It is shown in refs. [1, 6] that cold dark matter axions behave as ordinary cold dark matter on all scales of observational interest when they are non-interacting. Observable differences between cold axions and ordinary CDM occur only when the axions self-interact or interact with other species. Before Bose-Einstein condensation, cold axions are described by a free classical field and are indistinguishable from ordinary cold dark matter on all scales of observational interest. After Bose-Einstein condensation, almost all axions are in the same state. In the linear regime of evolution of density perturbations and within the horizon, the lowest energy state is time independent and no rethermalization is necessary for the axions to remain in the lowest energy state. In that case, axion BEC and ordinary CDM are again indistinguishable on all scales of observational interest [1]. However, beyond first order perturbation theory and/or upon entering the horizon, the axions rethermalize to try and remain in the lowest energy available state. Axion BEC behaves differently from CDM then and the resulting differences are observable.

An example of an observable distinction between axion BEC and ordinary CDM is given in the next section. Another possible observable distinction is the cooling of cosmic photons by thermal contact with the axion BEC. If this happens, the baryon-to-photon ratio at nucleosynthesis and the effective number of neutrinos (a measure of the radiation density at recombination) are modified compared to their values in the standard cosmological model [3].

3 Tidal torquing with axion BEC

Let us consider axion BEC dark matter as it is about to fall into the gravitational potential well of a galaxy. The gravitational field of neighbouring galaxies applies a tidal torque [7] to the axion BEC. Under what conditions is thermalization by gravitational self-interactions sufficiently fast that the condensed axions remain in the lowest energy available state as the space-time background evolves? Following the arguments of ref. [6], we expect that the axion BEC rethermalizes provided the gravitational forces produced by the BEC are larger than the typical rate \dot{p} of change of axion momenta required for the axions to remain in the lowest energy state. The gravitational forces are of order $4\pi Gnm^2\ell$. In this case, the correlation length ℓ must be taken to be of order the size L of the region of interest since the gravitational fields

due to axion BEC outside the region do not help the thermalization of the axions within the region. Hence the condition is

$$4\pi Gnm^2 L \gtrsim \dot{p} \quad . \quad (7)$$

The self-similar infall model [8] was used [6] to estimate L and \dot{p} as functions of time. Furthermore, assuming that most of the dark matter is axions, the Friedmann equation implies

$$4\pi Gnm \simeq \frac{3}{2}H(t)^2 \simeq \frac{2}{3t^2} \quad (8)$$

after equality between matter and radiation. It is found [6] that Eq. (7) is satisfied at all times from equality till today by a margin of order 30.

We conclude that the axion BEC does rethermalize before falling into the gravitational potential well of a galaxy. Most axions go to the lowest energy state consistent with the total angular momentum acquired from neighboring inhomogeneities through tidal torquing [7]. That state is a state of rigid rotation on the turnaround sphere, implying $\vec{\nabla} \times \vec{v} \neq 0$ where \vec{v} is the velocity field of the infalling axions. In contrast, the velocity field of WIMP dark matter is irrotational. The inner caustics of galactic halos are different in the two cases. Axions produce caustic rings [9, 10] whereas WIMPs produce the ‘tent-like’ caustics described in ref. [11]. There is evidence for the existence of caustic rings in various galaxies at the radii predicted by the self-similar infall model. For a review of this evidence see ref. [12]. It is shown in ref. [2] that the phase space structure of galactic halos implied by the evidence for caustic rings is precisely and in all respects that predicted by the assumption that the dark matter is a rethermalizing BEC.

4 Acknowledgments

This work was supported in part by the U.S. Department of Energy under grant DE-FG02-97ER41209.

References

- [1] P. Sikivie and Q. Yang, Phys. Rev. Lett. 103 (2009) 111301.
- [2] P. Sikivie, Phys. Lett. B 695 (2011) 22.
- [3] O. Erken, P. Sikivie, H. Tam and Q. Yang, arXiv:1104.4507.
- [4] R.D. Peccei and H. Quinn, Phys. Rev. Lett. 38 (1977) 1440 and Phys. Rev. D16 (1977) 1791; S. Weinberg, Phys. Rev. Lett. 40 (1978) 223; F. Wilczek, Phys. Rev. Lett. 40 (1978) 279.
- [5] J. Preskill, M. Wise and F. Wilczek, Phys. Lett. B120 (1983) 127; L. Abbott and P. Sikivie, Phys. Lett. B120 (1983) 133; M. Dine and W. Fischler, Phys. Lett. B120 (1983) 137.
- [6] O. Erken, P. Sikivie, H. Tam and Q. Yang, arXiv:1111.1157.
- [7] P.J.E. Peebles, Ap. J. 155 (1969) 2, and Astron. Ap. 11 (1971) 377.
- [8] J.A. Fillmore and P. Goldreich, Ap. J. 281 (1984) 1; E. Bertschinger, Ap. J. Suppl. 58 (1985) 39; P. Sikivie, I. Tkachev and Y. Wang, Phys. Rev. Lett. 75 (1995) 2911; Phys. Rev. D56 (1997) 1863.
- [9] P. Sikivie, Phys. Lett. B432 (1998) 139.
- [10] P. Sikivie, Phys. Rev. D60 (1999) 063501.
- [11] A. Natarajan and P. Sikivie, Phys. Rev. D73 (2006) 023510.
- [12] L. Duffy and P. Sikivie, Phys. Rev. D78 (2008) 063508.

The Axion Dark-Matter eXperiment: Results and plans

S.J. Asztalos,¹ R. Bradley,² G. Carosi,¹ J. Clarke,³ C. Hagmann,¹ J. Hoskins,⁴ M. Hotz,⁵ D. Kinion,¹ C. Martin,⁴ L. J. Rosenberg,⁵ G. Rybka,⁵ P. Sikivie,⁴ N.S. Sullivan,⁴ D.B. Tanner,⁴ K. van Bibber,¹ and A. Wagner⁵

¹Lawrence Livermore National Laboratory, Livermore, CA, 94550

²National Radio Astronomy Observatory, Charlottesville, VA 22903

³University of California and Lawrence Berkeley National Laboratory, Berkeley, CA 94720

⁴University of Florida, Gainesville, FL 32611

⁵University of Washington, Seattle, WA 98195

DOI: http://dx.doi.org/10.3204/DESY-PROC-2011-04/rybka_gray

The axion affects issues of the origin of CP symmetry in the strong interactions and the composition of the dark matter of the universe; current constraints limit its mass to $1\ \mu\text{eV}$ – $10\ \text{meV}$, with the low end of this range (1 – $10\ \mu\text{eV}$) especially significant for dark-matter axions. Axions may be detected by their coupling to photons in a resonant cavity in a strong magnetic field. The Axion Dark-Matter eXperiment (ADMX) recently completed Phase I of an upgrade to its detector, incorporating SQUID electronics in the receiver front end and conducting a year-long data run. Phase II of the upgrade will install a high-capacity dilution refrigerator to cool the SQUID and cavity to $\sim 100\ \text{mK}$.

1 Introduction

The discovery of the axion, or placing unambiguous limits on its existence, would have profound implications for two of the most important problems in contemporary physics: (i) the origin of parity (P) and the product of charge conjugation with parity (CP) symmetry in the strong interactions and (ii) the composition of the dark matter of the universe. The Axion Dark-Matter eXperiment (ADMX) searches for axions in the dark-matter halo of our galaxy. Many observations imply the existence of large halos of non-luminous matter in galaxies. The composition of this dark matter is a mystery whose solution is one of the most exciting challenges in science today. It seems probable that much of the dark matter is non-baryonic; the leading candidates are finite-mass neutrinos, weakly interacting massive particles, and axions. Only the latter two candidates could be cold dark matter, preferred in most scenarios. Between these two, the axion is special in the sense that a laboratory experiment can be carried out with current technology that can detect or rule out axions at the expected level of abundance.

ADMX detects axions by their stimulated conversion into microwave photons in a high Q cavity permeated by a large magnetic field. [1] This detector [2, 3] consists of a large superconducting magnet containing one or more microwave cavities. Axions in the high-field region will be stimulated to decay into microwave photons (which have a frequency equal to the rest mass of the axions) when the resonant frequency of the cavity equals the mass of the axion.

The cavity frequency is slowly tuned to search for this resonant conversion. Over the past few years, the detector has scanned the 1.9–3.5 μeV axion mass range; its sensitivity is such that the detector could find a signal, given the constraints on dark matter density set by astrophysical and cosmological considerations. [4–9, 11]

ADMX was recently upgraded to incorporate superconducting quantum interference device (SQUID) amplifiers into the front end of the receiver. This upgrade is based on a remarkable breakthrough in making SQUIDs operate as high-gain, low-noise amplifiers into the GHz range [14] with measured SQUID noise temperatures of $T_N = 70$ mK. This noise, which is close to the quantum limit and which compares very well to the $T_N = 1.5$ K of the earlier HEMT amplifiers, requires the cavity and amplifier be cooled to 100 mK. The collaboration planned and proposed a conservative, two-step approach to this upgrade. First (as Phase I), the experiment was retrofitted to operate with SQUID amplifiers, but at the same physical temperature of $T \sim 1.5$ K. In this case the system background temperature is dominated by the physical temperature. The Phase I construction and commissioning ended in 2008 and was followed by a science run with the SQUID amplifiers prior to moving from LLNL to UW. Axion search results using the SQUID have been published [11], as well as results from searches for axion-like particles [12, 13].

Phase II will add a high-circulation-rate dilution refrigerator to the detector, reducing the physical temperature to $T \sim 100$ mK. The system noise temperature after Phase II is expected to be $T_s \sim 200$ mK. The upgrade will improve system noise performance to an extent that ADMX will be sensitive to—or be able to rule out—axions as a component of the halo of our galaxy with *all* plausible coupling strengths in the lowest decade of the allowed mass range, ($\sim 1\text{--}10$ μeV).

2 ADMX Phase 1

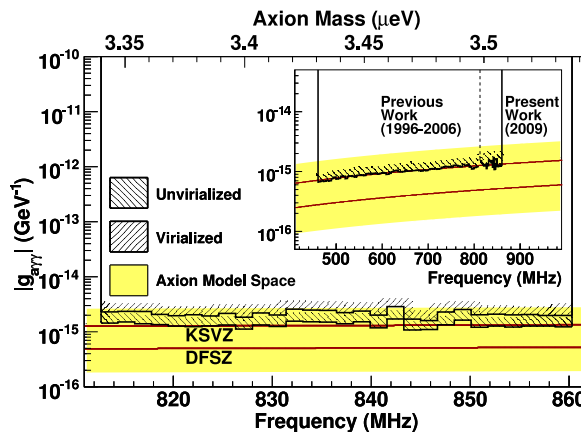


Figure 1: Axion couplings and masses excluded at the 90% confidence level by the experiment. The main figure shows the results from the Phase I upgrade and the inset the limits from all data by ADMX.

Figure 1 shows the axion couplings and masses excluded at the 90% confidence level by

ADMX. [4–9, 11] The plot shows the axion-to-photon coupling $g_{a\gamma\gamma}$ as a function of the axion mass $m_a = hf/c^2$ and photon frequency f . ADMX is 100 times more sensitive than earlier microwave cavity experiments, [15, 16] and is the first to exclude realistic axion couplings: KSVZ axions of mass between 1.9 and 3.5 μeV . If a significant fraction of halo axions are distributed in a few narrow peaks, weaker axion two-photon couplings are excluded. [8–10]

3 ADMX Phase 2

Work is already underway on ADMX Phase II, which will have numerous improvements over the previous version. Foremost of the improvements is the addition of a dilution refrigerator, lowering the system (physical plus amplifier) noise temperature to 200 mK and allowing a scan rate 100 times that of ADMX Phase I. Also notable is the addition of a second, higher frequency, data taking channel. Dark matter axions incident on the ADMX cavity can excite the TM_{010} mode, which was used in previous experiments, but also can excite the TM_{020} mode. The coupling to the TM_{020} mode is weaker than that of the TM_{010} , but the frequency (and hence the detectable axion mass) is nearly twice that of the TM_{010} mode, doubling the axion mass range that can be covered in a single sweep. The expected sensitivity for both modes with the dilution refrigerator installed after one year of running is shown in Figure 2. This covers nearly the entire first decade of the favored axion mass range even for pessimistic axion-photon couplings.

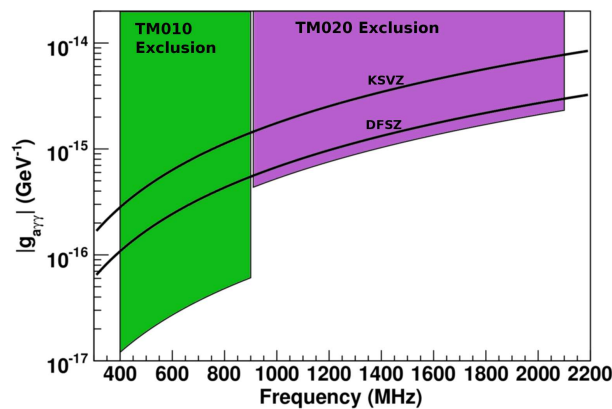


Figure 2: Target exclusion region for TM_{010} and TM_{020} modes of ADMX Phase 2 with dilution refrigerator installed after one year of running.

4 Conclusions

The QCD axion is a compelling dark matter candidate, and ADMX has proven it has the sensitivity necessary to find or exclude dark matter axions. The combination of SQUID technology established in Phase 1 and a dilution refrigerator upgrade in Phase 2 will allow ADMX to explore a significant fraction of allowed dark matter axion masses and couplings in the near future. With future work on high frequency cavities and amplifiers, it is likely ADMX will be

able to cover the entire plausible range of masses and couplings and definitively answer the question of whether or not dark matter is made of axions.

5 Acknowledgments

This work has been supported by the U.S. Department of Energy through grant numbers DE-FG02-97ER41029, DE-FG02-96ER40956, and DE-AC52-07NA27344 as well as through the LDRD program at Lawrence Livermore National Laboratory.

References

- [1] P. Sikivie, *Phys. Rev. Lett.* **51**, 1415 (1983).
- [2] H. Peng, S. Asztalos, E.J. Daw, N.A. Golubev, C.A. Hagmann, D. Kinion, J. LaVeigne, D.M. Moltz, F.A. Nezrick, J. Powell, L.J. Rosenberg, P. Sikivie, W. Stoeffl, N.S. Sullivan, D.B. Tanner, M.S. Turner, and K. van Bibber, *Nucl. Instrum. Methods A*, **444**, 569–583 (2000).
- [3] Richard Bradley, John Clarke, Darin Kinion, Leslie J Rosenberg, Karl van Bibber, Seishi Matsuki, Michael Mück, and Pierre Sikivie, *Rev. Mod. Phys.* **75**, 777 (2003).
- [4] C.A. Hagmann, D. Kinion, W. Stoeffl, K. van Bibber, E.J. Daw, H. Peng, L.J. Rosenberg, J. LaVeigne, P. Sikivie, N.S. Sullivan, D.B. Tanner, F.A. Nezrick, M.S. Turner, D.M. Moltz, J. Powell, and N.A. Golubev, *Phys. Rev. Lett.* **80**, 2043, (1998).
- [5] S. Asztalos, E. Daw, H. Peng, L.J. Rosenberg, C. Hagmann, D. Kinion, W. Stoeffl, K. van Bibber, P. Sikivie, N.S. Sullivan, D.B. Tanner, F. Nezrick, M.S. Turner, D.M. Moltz, J. Powell, M.-O. André, J. Clarke, and M. Mück, *Phys. Rev. D* **64**, 092003 (2001).
- [6] S.J. Asztalos, E. Daw, H. Peng, L.J. Rosenberg, C. Hagmann, D. Kinion, W. Stoeffl, K. van Bibber, J. LaVeigne, P. Sikivie, N.S. Sullivan, D.B. Tanner, F. Nezrick, M.S. Turner, and D.M. Moltz, *Ap. J. Lett.* **571**, L27 (2002).
- [7] S.J. Asztalos, R.F. Bradley, L. Duffy, C. Hagmann, D. Kinion, D.M. Moltz, L.J. Rosenberg, P. Sikivie, W. Stoeffl, N.S. Sullivan, D.B. Tanner, K. van Bibber, and D.B. Yu, *Phys. Rev. D* **69**, 011101(R) (2004).
- [8] L. Duffy, P. Sikivie, D.B. Tanner, S. Asztalos, C. Hagmann, D. Kinion, L.J. Rosenberg, K. van Bibber, D. Yu, and R.F. Bradley, *Phys. Rev. Lett.* **95**, 091304 (2005).
- [9] L.D. Duffy, P. Sikivie, D.B. Tanner, S.J. Asztalos, C. Hagmann, D. Kinion, L.J. Rosenberg, K. van Bibber, D.B. Yu, and R.F. Bradley, *Phys. Rev. D* **74**, 012006 (2006).
- [10] J. Hoskins, J. Hwang, P. Sikivie, N.S. Sullivan, D.B. Tanner, M. Hotz, L.J. Rosenberg, G. Rybka, A. Wagner, S.J. Asztalos, G. Carosi, C. Hagmann, D. Kinion, K. van Bibber, R. Bradley, and J. Clarke, *arXiv:1109.4128v1 [astro-ph.CO]*.
- [11] S.J. Asztalos, G. Carosi, C. Hagmann, D. Kinion, K. van Bibber, M. Hotz, L.J. Rosenberg, G. Rybka, J. Hoskins, J. Hwang, P. Sikivie, D.B. Tanner, R. Bradley, and J. Clarke, *Phys. Rev. Lett.* **104**, 041301 (2010).
- [12] G. Rybka, M. Hotz, L.J. Rosenberg, S.J. Asztalos, G. Carosi, C. Hagmann, D. Kinion, K. Van Bibber, J. Hoskins, C. Martin, P. Sikivie, D.B. Tanner, R. Bradley, and J. Clarke, *Phys. Rev. Lett.* **105**, 051801 (2010).
- [13] A. Wagner, G. Rybka, M. Hotz, L.J. Rosenberg, S.J. Asztalos, G. Carosi, C. Hagmann, D. Kinion, K. Van Bibber, J. Hoskins, C. Martin, P. Sikivie, D.B. Tanner, R. Bradley, and J. Clarke, *Phys. Rev. Lett.* **105**, 171801 (2010).
- [14] M. Mück, M.-O. André, J. Clarke, J. Gail and C. Heiden, *Applied Phys. Lett.* **72**, 2885 (1998); *Applied Phys. Lett.* **75**, 3545 (1999).
- [15] S. DePanfilis, A.C. Melissinos, B.E. Moskowitz, J.T. Rogers Y.K. Semertzidis, W.U. Wuensch, H.J. Halama, A.G. Prodell, W.B. Fowler and F.A. Nesrick, *Phys. Rev. Lett.* **59**, 839 (1987); W.U. Wuensch, S. DePanfilis-Wuensch, Y.K. Semertzidis, J.T. Rogers, A.C. Melissinos, H.J. Halama, B.E. Moskowitz, A.G. Prodell, W.B. Fowler, and F.A. Nezrick, *Phys. Rev. D* **40**, 3153 (1989).
- [16] C. Hagmann, P. Sikivie, N.S. Sullivan and D.B. Tanner, *Phys. Rev. D* **42**, 1297 (1990).

Preliminary Results from the Yale Microwave Cavity Experiment

A. J. Martin¹, O. K. Baker¹, J. L. Hirshfield¹, Y. Jiang¹, S. Kazakov¹, M. A. LaPointe¹, A. Malagon¹, S. Shchelkunov¹, P. L. Slocum¹, A. Szymkowiak¹

¹Physics Department, Yale University, New Haven, CT, USA

DOI: http://dx.doi.org/10.3204/DESY-PROC-2011-04/martin_andrew

We present the first preliminary measurements from the Yale Microwave Cavity Experiment from a search for galactic halo axion like particles at about 34 GHz. The experiment can be run in two modes, a single cavity search or a two cavity search. We give estimated sensitivities for axions and axion like particles in this experimental setup.

1 Introduction

Many of the extensions of the standard model predict the presence of new particles which can have small masses. For example, the axion [1] and other axion-like particles (ALPS) have been postulated to account for broken symmetries and should behave as weakly interacting sub-eV particles (WISPs) (see e.g. [2]). In addition there are *hidden sector* particles with very low masses that arise from supersymmetry which only rarely interact with standard model particles [3, 4]. The discovery of a new low mass particle could be a solution to the cosmological dark matter problem.

Many of the searches for new sub-eV particles have relied on their coupling to low energy photons. Many of these experiments have taken the form of a *light shining through walls* (LSW) experiment (e.g. [5, 6, 7, 8]) and resonant cavity searches for galactic halo axions [9]. These experiments have placed limits on the photon coupling constants, predominantly below 1 meV.

In this work we discuss early results from an LSW experiment designed to use two resonant cavities at 34 GHz, one driven by the high power magnicon source at Yale [10, 11].

2 Experiment

The apparatus will consist of two side by side copper cavities operating in TE₀₁₁ mode inside the bore of a 7 T magnet. One cavity will be coupled to the magnicon, a 34.29 GHz microwave source. This cavity is a right cylinder which will be thermally tuned to the magnicon's frequency.

The second cavity is also a right cylinder whose frequency is tuned via a plunger assembly which will vary the length of the cavity. This cavity is located inside a cryostat and is cooled to liquid helium temperatures. The Q of the cavity has been seen as high as 14,000.

The electronics chain consists of a triple heterodyne receiver which mixes the central frequency of 34.29 GHz down to 0 Hz [12]. The first amplification is done by a cryogenically cooled

HEMT amplifier located in the cryostat just above the signal cavity separated by approximately 12 cm of WR28 waveguide. The remaining amplifiers, the mixers, and filters are all operated at room temperature inside a shielded room. The output of the final video amplifiers goes into an Infinium oscilloscope to digitize the waveform and then transferred to a computer for analysis.

3 Sensitivity Estimates

To calculate the sensitivity of this experiment we start with the ideal total power Dickie Radiometer equation [13] $\sigma_T = \frac{T_{sys}}{\sqrt{\Delta\nu_{RF}\tau}}$, where $\Delta\nu_{RF}$ is the measurement bandwidth of 1 MHz and τ is the integration time in seconds. For system noise temperature of 32 K and 1 s integration time a 5σ signal corresponds to a minimum detectable power of $P_{sig} = 2 \times 10^{-18}$ W.

For a galactic halo ALP search the expected signal power P_a is given by [14]

$$P_{sig} = g^2 V B_0^2 \rho_a C_{lmn} Q$$

where g is the coupling strength of the ALP to two photons, V is the volume of the cavity, B_0 is the external field strength, ρ_a is the local ALP density, and Q is the quality factor of the cavity. For a scalar ALP, the form factor C_{lmn} is the overlap integral between B_0 and the magnetic field of the TE₀₁₁ mode of the cavity

$$C_{lmn} \equiv \int_V d^3x \hat{\mathbf{B}}_0 \cdot \mathbf{B}_{cav} \approx 6 \times 10^{-7}$$

where B_{cav} is normalized using $\int_V d^3x (E_{cav}^2 + B_{cav}^2) = 1$. Taking ρ_a to be $10^{13}/\text{cm}^3$ at 0.1 meV [15] gives $P_{sig} = 2.8 \times 10^{-5}$ W GeV² g^2 . Using P_{sig} from above gives $g \gtrsim 2 \times 10^{-7}$ GeV⁻¹.

For the LSW experiment looking for ALPS we have two cavities with quality factors Q and Q' . The probability for a photon to convert to an ALP in the first cavity and the ALP to convert back to a photon in the second cavity is given by [2]

$$P_{trans} = \left(\frac{gB}{\omega_0}\right)^4 Q Q' |G|^2$$

where ω_0 is the energy of the incident photon and G is the dimensionless geometry factor for scalar ALPs. For the case where ω_0 is equal to the ALP mass, G is defined by [2]

$$G \equiv \omega_0^2 \int_{V'} \int_V d^3\mathbf{x} d^3\mathbf{x}' \frac{(E_1^2 - B_1^2)(E_2^2 - B_2^2)}{4\pi|\mathbf{x} - \mathbf{x}'|} \approx \omega_0^2 \int_{V'} \int_V d^3\mathbf{x} d^3\mathbf{x}' \frac{(\hat{\mathbf{B}}_0 \cdot \mathbf{B}_1)(\hat{\mathbf{B}}_0 \cdot \mathbf{B}_2)}{4\pi|\mathbf{x} - \mathbf{x}'|}$$

where $E_1, E_2, B_1,$ and B_2 are the electric and magnetic fields associated with the TE₀₁₁ mode of cavities 1 and 2 and are normalized as before. For our apparatus G is approximately 7×10^{-9} . Using 1 MW as the magnicon's input power, the expected output power is $P_{sig} = P_{mag} P_{trans} = 5 \times 10^{-8}$ W GeV⁴ g^4 . Using the minimum detectable power in 1 s of integration time yields a sensitivity of $g \gtrsim 2 \times 10^{-3}$ GeV⁻¹.

For the HSP case the probability for a photon to convert to an HSP, pass through the shielding, and reconvert back to a photon in the second cavity is given by [2]

$$P_{trans} = \chi^4 Q Q' \frac{m_{\gamma'}^8}{\omega_0^8} |G_{HSP}|^2.$$

For the case where $\omega_0 = m_{\gamma'}$, G_{HSP} is given by

$$G_{HSP} \equiv \omega_0^2 \int_{V'} \int_V d^3\mathbf{x} d^3\mathbf{x}' \frac{A(\mathbf{x}')A(\mathbf{x})}{4\pi|\mathbf{x} - \mathbf{x}'|},$$

where $A(\mathbf{x})$ and $A(\mathbf{x}')$ are the vector potentials in the two cavities. For our cavities and spacing G_{HSP} integrates to 0.02. Taking the magnicon's power to be 1 MW, the signal power is given by $P_{sig} = P_{mag}P_{trans} = 2.4 \times 10^{10} \text{W}\chi^4$. Using P_{sig} as before gives a sensitivity of $\chi \gtrsim 8 \times 10^{-8}$.

4 Measurements

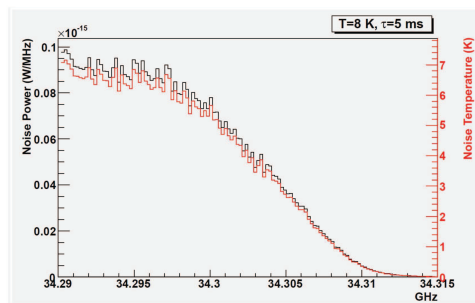


Figure 1: Noise power (top line) and noise temperature (bottom line) of the signal cavity.

We have taken data with a 50Ω terminator at the input to the HEMT. The result is shown in Fig. 1 where the time domain data has been Fourier transformed and converted to temperature. For this run the temperature of the HEMT was 7 K which agrees very well with the temperature given in the analysis. The rolloff as a function of frequency is due to the bandpass filters used in the receiver.

We have taken our first set of data runs looking for scalar ALPS with the cavity tuned to frequencies between 34.2775 and 34.3025 GHz with a step size of 2.5 MHz. For these runs the temperature of the cavity was 4.5 ± 0.5 K and the static magnetic field strength was 7 T.

The raw time domain data was Fourier transformed and then the power versus frequency spectrum is calculated. The left side of Fig. 2 show an example of the raw power spectrum when the cavity is tuned to 34.285 GHz. Note that the narrow spike seen at 34.3 GHz is an image of the 10 MHz master oscillator in the waveform after the final mixer. A baseline spectra is generated by the same procedure with the cavity has been tuned outside the bandpass of the receiver. The right side of Fig. 2 is the result of subtracting the baseline spectra from the raw spectra. The dip seen in this plot is related to the temperature difference between the cavity and the HEMT amplifier. The spike at 34.3 GHz was essentially eliminated by this procedure.

5 Outlook

These data have shown us that our receiver is working well and we have used it to take data using it for the scalar halo ALP search. We expect to be able to extend our data taking to the LSW type experiments soon. We are looking at ways to construct a similar sized signal cavity

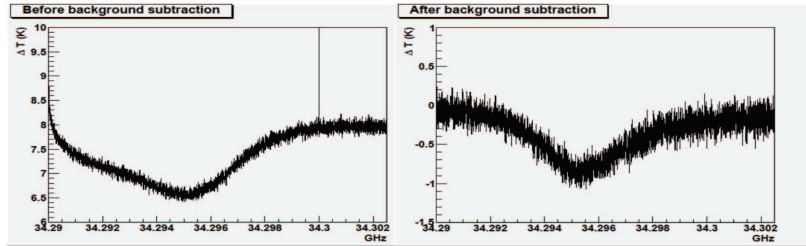


Figure 2: Raw data with cavity tuned to 34.285 GHz before background subtraction on left and after on right.

which will operate in TM_{010} mode which will enable us to improve our search capability for scalar ALPs and make searches for pseudoscalar ALPS possible.

Acknowledgements

This work was supported by the U. S. Office of Naval Research. The authors would also like to thank W. Guinon, J. Jaeckel, and S. Weinreb for many helpful discussions about this work.

References

- [1] R. D. Peccei, H. R. Quinn, “Constraints Imposed by CP Conservation in the Presence of Instantons,” *Phys. Rev.* **D16** (1977) 1791-1797.
- [2] J. Jaeckel, A. Ringwald, “The Low-Energy Frontier of Particle Physics,” *Ann. Rev. Nucl. Part. Sci.* **60** (2010) 405-437. [arXiv:1002.0329 [hep-ph]].
- [3] M. Ahlers, H. Gies, J. Jaeckel, J. Redondo, A. Ringwald, “Laser experiments explore the hidden sector,” *Phys. Rev.* **D77** (2008) 095001. [arXiv:0711.4991 [hep-ph]].
- [4] J. Jaeckel, A. Ringwald, “A Cavity Experiment to Search for Hidden Sector Photons,” *Phys. Lett.* **B659** (2008) 509-514. [arXiv:0707.2063 [hep-ph]].
- [5] A. Afanasev, O. K. Baker, K. B. Beard, G. Biallas, J. Boyce, M. Minarni, R. Ramdon, M. Shinn *et al.*, “New Experimental Limit on Photon Hidden-Sector Paraphoton Mixing,” *Phys. Lett.* **B679** (2009) 317-320. [arXiv:0810.4189 [hep-ex]].
- [6] A. Afanasev, O. K. Baker, K. B. Beard, G. Biallas, J. Boyce, M. Minarni, R. Ramdon, M. Shinn *et al.*, “New Experimental limit on Optical Photon Coupling to Neutral, Scalar Bosons,” *Phys. Rev. Lett.* **101** (2008) 120401. [arXiv:0806.2631 [hep-ex]].
- [7] K. Van Bibber, N. R. Dagdeviren, S. E. Koonin, A. Kerman, H. N. Nelson, “Proposed experiment to produce and detect light pseudoscalars,” *Phys. Rev. Lett.* **59** (1987) 759-762.
- [8] K. Ehret *et al.* [ALPS Collaboration], “Resonant laser power build-up in ALPS: A ‘Light-shining-through-walls’ experiment,” *Nucl. Instrum. Meth.* **A612** (2009) 83-96. [arXiv:0905.415 [physics.ins-det]].
- [9] P. Sikivie, “Of Axions, Domain Walls and the Early Universe,” *Phys. Rev. Lett.* **48** (1982) 1156-1159.
- [10] O. A. Nezhevenko, “Gyrocons and Magnicons: Microwave Generators with Circular Deflection of the Electron Beam,” *IEEE Trans. Plasma Sci.* **22** (1994) 756-772.
- [11] O. A. Nezhevenko, M. A. LaPointe, V. P. Yakovlev, J. L. Hirshfield, “Commissioning of the 34 GHz, 45 MW Pulsed Magnicon,” *IEEE Trans. Plasma Sci.* **32** (2004) 994-1001.
- [12] P. L. Slocum *et al.*, “Measurements in search for 0.1-meV axion-like particles and hidden sector photons using copper resonant cavities,” DESY-PROC-2010-03;

PRELIMINARY RESULTS FROM THE YALE MICROWAVE CAVITY EXPERIMENT

- [13] R. H. Dicke, “The Measurement of Thermal Radiation at Microwave Frequencies ” *Rev. Sci. Instrum.* **17** (1946) 268-275.
- [14] S. J. Asztalos *et al.* [The ADMX Collaboration], “A SQUID-based microwave cavity search for dark-matter axions,” *Phys. Rev. Lett.* **104** (2010) 041301. [arXiv:0910.5914 [astro-ph.CO]].
- [15] E. I. Gates, G. Gyuk, M. S. Turner, “The Local halo density,” *Astrophys. J.* **449** (1995) L123-L126. [arXiv:astro-ph/9505039 [astro-ph]].

Cold Dark Matter from the Hidden Sector

Paola Arias^{1,2}

¹*Deutsches Elektronen-Synchrotron (DESY), Hamburg, Germany*

²*Facultad de Física, Pontificia Universidad Católica de Chile, Casilla 306, Santiago 22, Chile*

DOI: http://dx.doi.org/10.3204/DESY-PROC-2011-04/arias_paola

Weakly interacting slim particles (WISPs) such as hidden photons (HP) and axion-like particles (ALPs) have been proposed as cold dark matter candidates. They might be produced non-thermally via the misalignment mechanism, similarly to cold axions. In this talk we review the main processes of thermalisation of HP and we compute the parameter space that may survive as cold dark matter population until today. Our findings are quite encouraging for experimental searches in the laboratory in the near future.

1 Introduction

WISPy cold dark matter (CDM) is not so surprising after all, since WISPs fulfill one of the prime conditions that one may ask to cold dark matter: a very weak coupling to Standard Model (SM) particles. A good example is the axion, produced non-thermally by the misalignment mechanism [1, 2, 3]. However, it has been proposed recently [4] that also cold dark matter comprised of light hidden Abelian gauge bosons - known as paraphotons or hidden photon (HP) - might be produced by this mechanism. As a matter of fact, the misalignment mechanism is quite general and can generate CDM out of any light boson field that satisfy some general conditions [5]. In the second part of the manuscript we discuss detection techniques and present constraints.

2 WISPy cold dark matter and the misalignment mechanism

The misalignment mechanism was originally conceived for the non-thermal production of axions. During the QCD phase transition era the initial angle of the axion field starts to realign with the true QCD vacuum. The energy in the field then behaves like dark matter. Such a mechanism can also produce a population of a different boson field provided its mass is smaller than the characteristic time of the universe ($t_0 \sim H$), $m t_0 \ll 1$. When $m t_0 \sim 1$ is reached the field is able to respond to the existence of its mass, readjusting the state to a different minimum of the potential. Once the minimum is reached, certain overshoot is expected, causing the oscillation of the field around it. The smaller the mass of the field, the later it will begin to oscillate, allowing for bigger dark matter abundances. Therefore, the misalignment mechanism could naturally give rise to a population of WISPy CDM, provided it does not thermalise until today.

For instance, let us consider the case of the hidden photon, which occur naturally in many SM extensions based on field and string theory [6]. Assuming the universe underwent a period of

inflation at a value of the Hubble expansion parameter (H) larger than the HP mass, $m_{\gamma'} \ll H$, where $m_{\gamma'}$ is the HP mass, the equation of motion for the spatial components in an expanding Universe reads [4],

$$\ddot{B}^i + 3H\dot{B}^i + m_{\gamma'}^2 B^i = 0. \quad (1)$$

Details can be found in [5]. The equation undergoes two different regimes: $H \gg m_{\gamma'}$, the field gets essentially frozen and cannot respond to the mass term. At a later time, t_{initial} , at which $H(t_{\text{initial}}) \sim m_{\gamma'}$ the damping becomes undercritical and the field can roll down the potential and start to oscillate. The residual damping due to the expansion factor reduces the amplitude of the oscillations, such that the energy density of the HP field scales as $\frac{1}{2}m_{\gamma'}^2 (B^i)^2 \sim a^{-3}$, which is exactly the behavior expected for non-relativistic matter. The dark matter density of the HP field today depends on the initial *misalignment*, B_{initial}^i , of the field therefore to achieve the correct dark matter density requires a fine-tuning.

3 Cosmological constraints on hidden photons

In order to ensure that the boson field produced by the misalignment mechanism survives until today one needs to check whether there is some process that could thermalise it. It is generally assumed that the SM particles are uncharged under the HP and the only interaction between the visible and hidden sector is through kinetic mixing between photons and HPs [7]

$$\mathcal{L} = -\frac{1}{4}F_{\mu\nu}F^{\mu\nu} - \frac{1}{4}B_{\mu\nu}B^{\mu\nu} + \frac{m_{\gamma'}^2}{2}B_\mu B^\mu - \frac{\chi}{2}F_{\mu\nu}B^{\mu\nu} + J^\mu A_\mu, \quad (2)$$

where the A_μ and B_μ correspond to photon and hidden photon field, respectively. The mixing between both is parametrised by the kinetic mixing term χ and we have included the coupling between electrically charged matter described by the current J_μ , and photons. Nevertheless, once a change of basis of the type $A_\mu \rightarrow \tilde{A}_\mu - \chi\tilde{B}_\mu$, $B_\mu \rightarrow \tilde{B}_\mu$ to remove the kinetic mixing, one can see that ordinary matter also couples to the massive hidden photon state. Thus, the HP couples to charged matter with a strength χ . However, in the early universe the plasma effects modify the effective kinetic mixing dramatically (details can be seen in [8, 9, 10, 11]). The effective mixing parameter shows a resonance at the effective photon mass m_γ ,

$$\chi^2 \rightarrow \chi_{\text{eff}}^2 = \frac{\chi^2 m_{\gamma'}^4}{(m_\gamma^2 - m_{\gamma'}^2)^2 + (\omega\Gamma_0)^2}, \quad (3)$$

where m_γ is the photon mass in a plasma and $\omega\Gamma_0$ is a damping coefficient associated with absorption part of the refractive index of the medium. Examining the possible processes that could thermalise the condensate, the Compton evaporation $\gamma' + e \rightarrow \gamma + e$ may be a dominant process, as discussed in [4]. A close estimate of the condition $\Gamma/H < 1$, where Γ is the interaction rate of Compton evaporation,

$$\Gamma = \int d^3p \sigma(p) v(p) f_e(p), \quad (4)$$

and the Hubble expansion rate, $H = 1.66 g_*^{1/2} T^2/M_P$, shows that an important contribution to the ratio Γ/H comes from the resonance condition $m_\gamma \sim m_{\gamma'}$, associated with a resonance

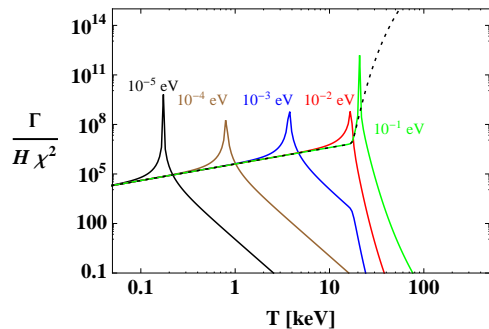


Figure 1: $\Gamma / (\chi^2 H)$ for different hidden photon masses. The effects near the resonance clearly dominates. The corresponding approximation from reference [4] is shown as a dotted line.

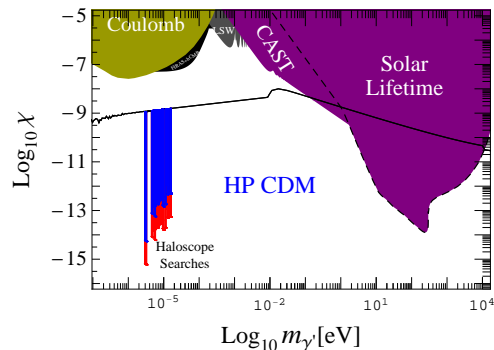


Figure 2: The region under the black curve corresponds to where the HP CDM condensate does not thermalise.

temperature, T_{res} . The result, for different HP masses, is plotted in Fig. 1. As expected the decay rate is heavily enhanced at T_{res} , corresponding to $m_\gamma = m_{\gamma'}$, and rapidly drops at higher temperatures. These effects have not been taking into account in Ref. [4] which neglected the plasma effects. Performing a more careful computation at the resonance temperatures we can obtain the maximal $\chi(m_{\gamma'})$ at which is possible to keep the condensate alive, displayed in Fig. 2. This result is quite encouraging: hidden photons in this parameter range are not only predicted in popular string compactifications [12], but are also within reach of the next generation of pure laboratory experiments based on light-shining-through walls [13].

4 Microwave cavity searches

Microwave cavity experiments looking for relic axions could also be used to constrain and search for the hypothetical cold HP condensate that we have been discussing so far. To start with, let us assume the energy density in the hidden photons is equal to the dark matter density, therefore, $\rho_{DM} = m_{\gamma'}^2 / 2 |\mathbf{B}|^2$. To simplify things, we will consider two possible scenarios: the direction of the HP field is (essentially) unaffected by structure formation and all HPs point in the same direction (at least for a suitably big region of space). Or, the direction of HPs behave like a gas of particles with the vector pointing in random directions. In the first scenario the HP direction is characterized by a fixed vector \hat{n} , whereas in the second case we have to average the final result over all directions for \hat{n} . With this understood, let us write for the hidden photon field, $\mathbf{B}(\mathbf{x}) = \hat{n} \frac{\sqrt{2\rho_0}}{m_{\gamma'}}$, with ρ_0 the dark matter density on earth.

In the microwave cavity, the power emission is related to the energy stored inside, U , and the quality factor of the cavity, Q , as $\mathcal{P}_{\text{out}} = \kappa \omega_0 U / Q$, where κ is the coupling of the cavity to the detector. Evaluating at resonance ($\omega_0 = m_{\gamma'}$) we find [5]

$$\mathcal{P}_{\text{out}} = \kappa \chi^2 m_{\gamma'} \rho Q V \mathcal{G}, \quad (5)$$

where the geometric factor \mathcal{G} is defined as

$$\mathcal{G} = \frac{|\int dV \mathbf{A}^{*cav}(\mathbf{x}) \cdot \hat{\mathbf{n}}|^2}{V \int d^3 \mathbf{x} |\mathbf{A}^{cav}(\mathbf{x})|^2}. \quad (6)$$

In a cavity $\mathbf{E} = \omega \mathbf{A}$. This geometry factor has exactly the same form as in the axion case (cf. [14]) but with the direction $\hat{\mathbf{n}}$ replacing the direction of the external magnetic field \mathbf{B}_{magnet} in the axion case. It is interesting that already now the negative searches for CDM axions of past microwave cavity experiments can be turned, via Eq. (5), into new exclusion regions for HPs, cf. the region "Haloscope Searches" in Fig. 2.

5 Conclusions

We have argued that the misalignment mechanism is a very powerful tool to produce a condensate of practically any light boson field in the early universe. In particular, in this letter we have focused on hidden photons. Our results show that the parameter space where the CDM population may have survived until today is accessible to future laboratory experiments, such as light-shining-through-walls experiments, helioscope experiments, and microwave cavity searches (haloscopes). All the above applies also to an axion-like particle (ALP) which can be considered to be a (pseudo-)scalar field ϕ enjoying a periodic shift symmetry - a common feature occurring in string compactifications. A generic ALP may have its mass arising from some hidden interactions, such as string instanton effects or explicit symmetry breaking. In some cases, the mass of the ALP can also vary in time, for instance due to thermal corrections. The results of these investigations will appear in a near future [5].

6 Acknowledgments

This talk is based on work in progress with Davide Cadamuro, Mark Goodsell, Joerg Jaeckel, Javier Redondo and Andreas Ringwald. P. A. acknowledges the valuable support of the Alexander von Humboldt Foundation.

References

- [1] J. Preskill, M. B. Wise and F. Wilczek, Phys. Lett. B **120** (1983) 127.
- [2] L. F. Abbott and P. Sikivie, Phys. Lett. B **120** (1983) 133.
- [3] M. Dine and W. Fischler, Phys. Lett. B **120** (1983) 137.
- [4] A. E. Nelson and J. Scholtz, arXiv:1105.2812 [hep-ph].
- [5] P. Arias, D. Cadamuro, M. D. Goodsell, J. Jaeckel, J. Redondo and A. Ringwald, work in progress.
- [6] M. Goodsell and A. Ringwald, Fortsch. Phys. **58** (2010) 716
- [7] B. Holdom, Phys. Lett. B **166** (1986) 196
- [8] J. Redondo, JCAP **0807** (2008) 008.
- [9] J. Jaeckel, J. Redondo and A. Ringwald, Phys. Rev. Lett. **101** (2008) 131801.
- [10] A. Mirizzi, J. Redondo and G. Sigl, JCAP **0903** (2009) 026.
- [11] J. Redondo and M. Postma, JCAP **0902** (2009) 005.
- [12] M. Cicoli, M. Goodsell, J. Jaeckel and A. Ringwald, JHEP **1107** (2011) 114.
- [13] J. Redondo and A. Ringwald, Contemp. Phys. **52** (2011) 211.
- [14] S. J. Asztalos *et al.*, Phys. Rev. D **64** (2001) 092003.

Dark Forces and Dark Matter in a Hidden Sector

Sarah Andreas

Deutsches Elektronen-Synchrotron (DESY), Hamburg, Germany

DOI: http://dx.doi.org/10.3204/DESY-PROC-2011-04/andreas_sarah

Hidden sectors in connection with GeV-scale dark forces and dark matter are not only a common feature of physics beyond the Standard Model such as string theory and SUSY but are also phenomenologically of great interest regarding recent astrophysical observations. The hidden photon in particular is also searched for and constrained by laboratory experiments, the current status of which will be presented here. Furthermore, several models of hidden sectors containing in addition a dark matter particle will be examined regarding their consistency with the dark matter relic abundance and direct detection experiments.

1 Motivation

Hidden sectors are often predicted in string theories and contained in various supersymmetric models as the source of SUSY breaking. As the hidden sector (HS) is not charged under the Standard model (SM) gauge groups and vice versa the two sectors are not directly connected and only interact via messenger particles. An example for a messenger is the hidden photon γ' which is a frequent feature of SM extensions as extra hidden U(1) symmetries for example often remain in the breaking of larger gauge groups or appear in string compactifications.

On the other hand there are several observations in indirect and direct dark matter detection experiments like PAMELA, Fermi, DAMA and CoGeNT which favour dark matter (DM) models with light messenger particles. Such a messenger, despite mediating the DM scattering on nuclei, most importantly ensures that the DM annihilation is at the same time leptophilic and greatly enhanced by the Sommerfeld effect.

A GeV-scale mass for the hidden photon can be obtained quite naturally both through the Stückelberg and the Higgs mechanism. The former, being the simplest mechanism to give mass to abelian gauge bosons, can give for example in certain string compactifications with D7-branes a mass to the hidden photon according to $m_{\gamma'} \gtrsim M_S^2/M_{\text{Pl}}$, which depends on the volume of the extra dimension, i.e. the string-scale M_S , and the Planck scale M_{Pl} [1, 2]. For intermediate string-scales $M_S \sim 10^9 - 10^{10}$ GeV, which are preferred by the axion decay constant and SUSY breaking scales, this leads to $m_{\gamma'} \sim$ GeV-scale. In the case of the Higgs mechanism where the symmetry breaking is transferred by the kinetic mixing from the visible to the hidden sector the hidden photon mass can be estimated by $m_{\gamma'} \simeq \sqrt{g_Y g_h c_{2\beta}} v \sqrt{\chi}$ [3, 4]. Assuming that the kinetic mixing χ is generated supersymmetrically at high scales, without light fields charged under both U(1)s, it is of the order of a loop factor [1] and we impose the following relation with the hidden gauge coupling g_h

$$\chi = \frac{g_Y g_h}{16\pi^2} \kappa \quad (1)$$

where κ is an $\mathcal{O}(1)$ factor leading typically to $\chi \sim 10^{-3} - 10^{-4}$ and thus $m_{\gamma'} \sim$ GeV-scale.

2 Hidden Photon: Constraints and future experiments

We consider the most simple hidden sector containing only an extra U(1) symmetry and the corresponding hidden photon γ' which kinetically mixes with the ordinary photon. The most general Lagrangian for such a scenario, including a mass-term $m_{\gamma'}$ for the hidden photon and the kinetic mixing between γ and γ' parameterized by χ , is given by

$$\mathcal{L} = -\frac{1}{4}F_{\mu\nu}F^{\mu\nu} - \frac{1}{4}X_{\mu\nu}X^{\mu\nu} - \frac{\chi}{2}X_{\mu\nu}F^{\mu\nu} + \frac{m_{\gamma'}^2}{2}X_\mu X^\mu + g_Y j_{\text{em}}^\mu A_\mu, \quad (2)$$

where $F_{\mu\nu}$ is the field strength of the ordinary electromagnetic field A_μ and $X_{\mu\nu}$ the field strength of the hidden U(1) field X_μ . The hidden photon can be constrained by and searched for in experiments through its coupling to SM fermions which is possible due to the kinetic mixing with the photon. SM precision measurements (SM PM) [5], the muon and electron anomalous magnetic moment (a_μ, a_e) [6] and a reinterpretation of the BaBar search for the $\Upsilon(3S)$ decay to a pseudoscalar in the process $e^+e^- \rightarrow \gamma\mu^+\mu^-s$ [7] exclude large values of kinetic mixing as shown in grey in the left plot of Fig. 1. Fixed-target experiments where γ' can be produced in

Bremsstrahlung off e^-/p -beams place additional constraints from the non-observation of the decay $\gamma' \rightarrow e^+e^-$. Limits from past e^- -beam dump searches that have been studied in [8] are shown in the left plot of Fig. 1 as grey areas. The same graph also contains as coloured lines the new limits set by currently running (MAMI [9], KLOE-2 [10], APEX [11]) and reanalyzed older experiments (Serpukhov [12], Orsay [13]). Experiments are closing in on the remaining region of the parameter space and more is to be tested in the (near) future by presently operating or planned fixed-target experiments at JLab (APEX [7], HPS [14], DarkLight [15, 16]), Mainz (MAMI, MESA [17]) and DESY (HIPS [18]). The expected sensitivities of those experiments are shown as coloured lines in the right plot of Fig. 1.

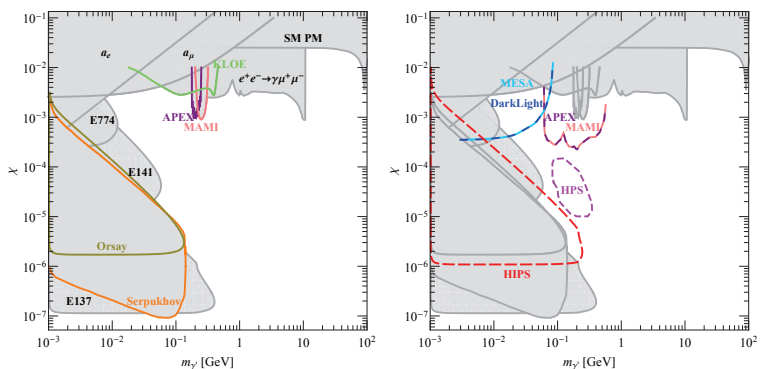


Figure 1: Hidden photon parameter space with past and new exclusion regions (*left*) as well as projected sensitivities (*right*). Experiments are closing in on the remaining region of the parameter space and more is to be tested in the (near) future by presently operating or planned fixed-target experiments at JLab (APEX [7], HPS [14], DarkLight [15, 16]), Mainz (MAMI, MESA [17]) and DESY (HIPS [18]). The expected sensitivities of those experiments are shown as coloured lines in the right plot of Fig. 1.

3 Hidden Dark Matter

The results of this section are based on an analysis that has been presented in detail in [19].

Hidden Sector toy model: Dirac fermion dark matter

The simplest possible extension of the hidden sector studied in the previous section is the addition of a Dirac fermion as dark matter candidate (cf. [20, 21, 22, 23]). As the hidden photon mediates both the DM annihilation and the DM scattering on nuclei it is essential for the determination of the DM relic abundance and direct detection rate respectively.

Using relation (1) with $\kappa = 0.1$ we find that for a DM mass of 6 GeV the correct relic abundance can be obtained on the dark green stripe in Fig. 2 while in the light green area the contribution to the total DM density is only subdominant. The spin-independent (SI) scattering on nuclei of the Dirac fermion DM can explain the CoGeNT [24] signal in the purple band (90% CL lighter 99% CL darker purple). The plotted cross section σ_{SI} has been rescaled by the relic abundance for subdominant DM and fits the one found in [25] to be compatible with CoGeNT for a Standard Halo Model. Constraints from CDMS [26] and XENON [27] are not shown as they do not apply to DM masses as light as 6 GeV. The excluded grey areas and coloured lines for sensitivities of future experiments are the same as in Fig. 1. A scan over the DM mass allows to fill the complete parameter space as shown in Fig. 3 on the left for $\kappa = 1$ where dark green corresponds to the correct relic abundance, light green to subdominant and purple to CoGeNT allowed points (all points are compatible with other direct detection limits). The effects of varying the DM mass, the parameter κ and the details of the halo model have been studied in more detail in [19].

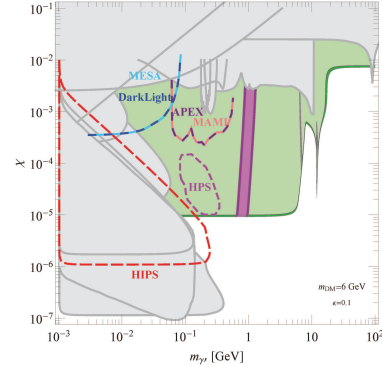


Figure 2: Toy model HS with relic abundance (green) and CoGeNT region (purple) for the Dirac fermion DM.

Supersymmetric hidden sector: Majorana and Dirac fermion dark matter

As a more sophisticated and better motivated model, we consider three chiral superfields S, H_+, H_- with H_+ and H_- charged under the hidden $U(1)$. Taking the superpotential $W \supset \lambda_S S H_+ H_-$ and the dimensionless coupling λ_S this is the simplest anomaly-free model possible without adding dimensionful supersymmetric quantities. While we assume the MSSM in the visible sector, the DM phenomenology of the HS depends on the details of the SUSY breaking. If the breaking of the hidden gauge symmetry is via the effective Fayet-Iliopoulos

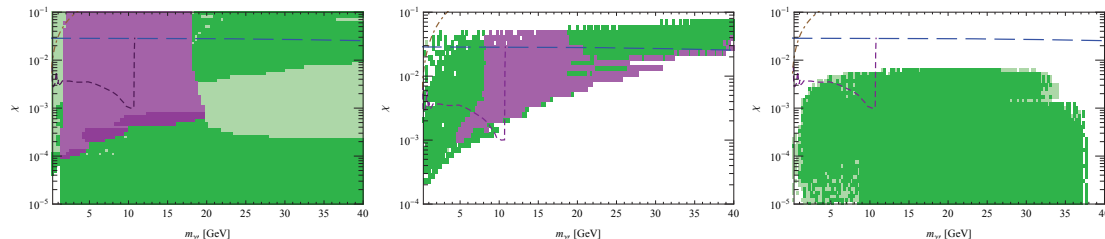


Figure 3: Scatter plots for the toy model (*left*) and the SUSY HS with visible sector induced breaking (*middle*) as well as radiative breaking domination (*right*). Lines are constraints from EWPT (long dashed), BaBar (short dashed) and muon $g-2$ (dash-dotted) similar to Fig. 1.

term induced in the HS by the kinetic mixing with the visible Higgs D-term we find that the DM can be either a Dirac or a Majorana fermion. The former has similar prospects for SI scattering as in the toy model as shown in the middle plot of Fig. 3 where the parameter κ has been scanned over in the range $0.1 \leq \kappa \leq 10$. The axial couplings of the latter lead to dominantly spin-dependent (SD) scattering which is partly constrained by experiments but without any chance of explaining any of the signals in SI direct detection experiments. In the case where the hidden gauge symmetry breaking is induced by the Yukawa coupling λ_S , we find only a Majorana fermion as lightest particle in the spectrum. As before this only shows in SD direct

detection experiments, hence the missing purple colour for CoGeNT in the right plot of Fig. 3.

4 Conclusions

Hidden sectors are motivated by various aspects from top-down (string theory, SUSY) and bottom-up (DM) and have a potentially rich content like dark forces and dark matter which despite their weak coupling can be phenomenologically interesting. We reviewed past constraints on hidden photons as dark force and showed the reach of future experiments. A simple toy model for a HS with DM is found to be consistent with relic abundance and direct detection and additionally provides the correct cross section for explaining CoGeNT. The better-motivated supersymmetric hidden sectors show some similarities with the toy model but have a more complicated phenomenology where spin-dependent scattering must also be taken into account. Nevertheless, they also give viable models for DM with interesting signatures in experiments.

Acknowledgments

This work was done in collaboration with Mark Goodsell and Andreas Ringwald.

References

- [1] M. Goodsell, J. Jaeckel, J. Redondo, A. Ringwald, JHEP **0911** (2009) 027. [arXiv:0909.0515].
- [2] M. Cicoli, M. Goodsell, J. Jaeckel, A. Ringwald, JHEP **1107** (2011) 114. [arXiv:1103.3705].
- [3] M. Baumgart, C. Cheung, J.T. Ruderman, L.-T. Wang, I. Yavin, JHEP **0904** (2009) 014. [arXiv:0901.0283].
- [4] D. E. Morrissey, D. Poland, K. M. Zurek, JHEP **0907** (2009) 050. [arXiv:0904.2567].
- [5] A. Hook, E. Izaguirre, J. G. Wacker, [arXiv:1006.0973].
- [6] M. Pospelov, Phys. Rev. **D80** (2009) 095002. [arXiv:0811.1030].
- [7] R. Essig, P. Schuster, N. Toro, B. Wojtsekhowski, JHEP **1102** (2011) 009. [arXiv:1001.2557].
- [8] J. D. Bjorken, R. Essig, P. Schuster, N. Toro, Phys. Rev. **D80** (2009) 075018. [arXiv:0906.0580].
- [9] H. Merkel *et al.* [A1 Collaboration], Phys. Rev. Lett. **106** (2011) 251802. [arXiv:1101.4091].
- [10] F. Archilli *et al.*, [KLOE-2 Collaboration], [arXiv:1107.2531] and [arXiv:1110.0411].
- [11] S. Abrahamyan *et al.* [APEX Collaboration], [arXiv:1108.2750].
- [12] J. Blumlein, J. Brunner, Phys. Lett. **B701** (2011) 155-159. [arXiv:1104.2747].
- [13] S. Andreas, J. Jacobsohn,, C. Niebuhr A. Ringwald, *work in preparation*.
- [14] T. Maruyama, talk given at the SLAC - Dark Forces Workshop, 2009.
- [15] M. Freytsis, G. Ovanessian and J. Thaler, JHEP **1001** (2010) 111 [arXiv:0909.2862].
- [16] J. Thaler and P. Fisher, talk given at the SLAC - Dark Forces Workshop, 2009.
- [17] A. Denig, talk given at the JLab Workshop - Searching for a New Gauge Boson at JLab, 2010.
- [18] S. Andreas, A. Ringwald, [arXiv:1008.4519].
- [19] S. Andreas, M. D. Goodsell, A. Ringwald, [arXiv:1109.2869].
- [20] D. Feldman, B. Kors, P. Nath, Phys. Rev. **D75** (2007) 023503. [hep-ph/0610133].
- [21] M. Pospelov, A. Ritz and M. B. Voloshin, Phys. Lett. B **662** (2008) 53 [arXiv:0711.4866].
- [22] E. J. Chun, J. C. Park and S. Scopel, JHEP **1102** (2011) 100 [arXiv:1011.3300].
- [23] Y. Mambrini, JCAP **1009** (2010) 022 [arXiv:1006.3318].
- [24] C. E. Aalseth *et al.* [CoGeNT Collaboration], Phys. Rev. Lett. **106** (2011) 131301. [arXiv:1002.4703].
- [25] C. Arina, J. Hamann, Y. Y. Y. Wong, JCAP **1109** (2011) 022. [arXiv:1105.5121].
- [26] Z. Ahmed *et al.* [CDMS-II Collaboration], Phys. Rev. Lett. **106** (2011) 131302. [arXiv:1011.2482].
- [27] E. Aprile *et al.* [XENON100 Collaboration], [arXiv:1104.2549].

Microwave Hidden Sector Photons at UWA

Rhys G. Povey¹, John G. Hartnett¹, Michael E. Tobar¹

¹University of Western Australia (UWA), Perth, Australia

DOI: http://dx.doi.org/10.3204/DESY-PROC-2011-04/povey_rhys

In these proceedings we present the latest progress on our microwave cavity light shining through a wall hidden sector photon experiment, as well as introduce a new method of hidden sector photon detection. Our new experiment uses a high Q superconducting Niobium emitter cavity and moderate Q room temperature copper detector cavity separated by ample shielding. The projected sensitivity of our setup to the kinetic mixing factor is $\chi \sim 1.8 \times 10^{-8}$ at a hidden sector photon mass of $52.1 \mu\text{eV}$. A new technique for detecting hidden sector photons using a threshold crossing is also presented.

1 Introduction

Many extensions to the standard model of particle physics predict an extra hidden U(1) gauge symmetry [1, 2]. Within this hidden sector of particles the only interaction to standard model matter is through kinetic mixing between the hidden sector photon γ' and ordinary photon γ [3, 4]. The possibly massive hidden sector photon belongs to a class of hypothetical particles known as WISPs (Weakly Interacting Slim/Sub-eV Particles) [5] and is characterized by its unknown mass $m_{\gamma'}$ and the hidden sector kinetic mixing parameter χ .

A range of different experiments using the light shining through a wall (LSW) phenomenon [3, 6] and photon regeneration technique have been conducted to search for hidden sector photons. Within the laboratory [7–11] the majority of experiments have been carried out with lasers [12–22], however microwaves are now also being used [23, 24]. Since 2009 UWA has been actively involved in microwave cavity experiments searching for hidden sector photons.

2 Microwave cavity LSW experiment

After completing a prototype experiment work has now begun on a microwave cavity light shining through a wall experiment that will provide new limits on the hidden sector photon. The basic premise of the experiment [11] is to have two microwave cavities of the same resonance frequency separated by an impenetrable wall. An on resonance microwave signal is then used to excite the emitter cavity, whilst a detector is operated on the detector cavity. With enough shielding between the cavities standard photons are unable to directly excite the detector cavity. The presence of a hidden sector however would allow photons to oscillate into hidden sector photons, travel through the wall, and regenerate into photons inside the detector cavity. The

MICROWAVE HIDDEN SECTOR PHOTONS AT UWA

probability of this transmission taking place is

$$\begin{aligned} \mathbb{P}_{\text{trans}} &= \frac{P_{\text{det}}}{P_{\text{emit}}} = \chi^4 Q_{\text{emit}} Q_{\text{det}} \left(\frac{m_{\gamma'} c^2}{\hbar \omega_{\gamma'}} \right)^8 |\mathcal{G}|^2 \\ &= \chi^4 Q_{\text{emit}} Q_{\text{det}} \left(1 - \frac{k_{\gamma'}^2}{k_{\gamma}^2} \right)^4 |\mathcal{G}|^2 \end{aligned}$$

where P s are the powers in and out of the emitter and detector cavities respectively, Q s are the cavity quality factors, ω_{γ} is the angular (and cavity resonance) frequency of the photons, k_{γ} is the photon wavenumber, $k_{\gamma'}$ is the hidden sector photon wavenumber and \mathcal{G} is

$$\mathcal{G} \left(\frac{k_{\gamma'}}{k_{\gamma}} \right) = k_{\gamma}^2 \int_{V_{\text{emit}}} \int_{V_{\text{det}}} \frac{e^{i k_{\gamma'} |\mathbf{x}-\mathbf{y}|}}{4\pi |\mathbf{x}-\mathbf{y}|} A_{\text{emit}}^j(\mathbf{y}) A_{\text{det}}^j(\mathbf{x}) d^3\mathbf{x} d^3\mathbf{y}$$

where A is the gauge field vector within the cavity.

The new experiment being set up at UWA will use a superconducting Niobium cavity in a cryo-cooler with a $Q \sim 10^8$ as the emitter cavity and a room temperature copper cavity in a vacuum chamber with a $Q \sim 10^4$ as the detector cavity. Having the two cavities in separate chambers provides a great deal of shielding and significantly reduces microwave leakage. The lower quality factor detector cavity means it has a wider resonance bandwidth and is easier to match with the emitter cavity. A loop oscillator will be used on the emitter cavity to ensure it is always driven on the cavity resonance. The detector cavity output will be mixed down by an offset frequency inside the vacuum chamber to allow for a spectrum analyzer measurement and to ensure the exterior circuit is unaffected by microwave leakage. A schematic of the full setup is given in Fig. 1

Both cavities have a radius $R \approx 20.91$ mm and length $L \approx 39.65$ mm which using the TM_{020} mode have a resonance frequency of 12.595 GHz. The mode was chosen as the most sensitive whilst also compatible with our microwave components operating in the X-band range of microwave frequencies. Given these conditions we obtain a peak $|\mathcal{G}| \approx 0.28$ and $\mathcal{F}^2 \approx 37000$. The projected limit on χ , compared with other microwave experiments, is given in Fig. 2.

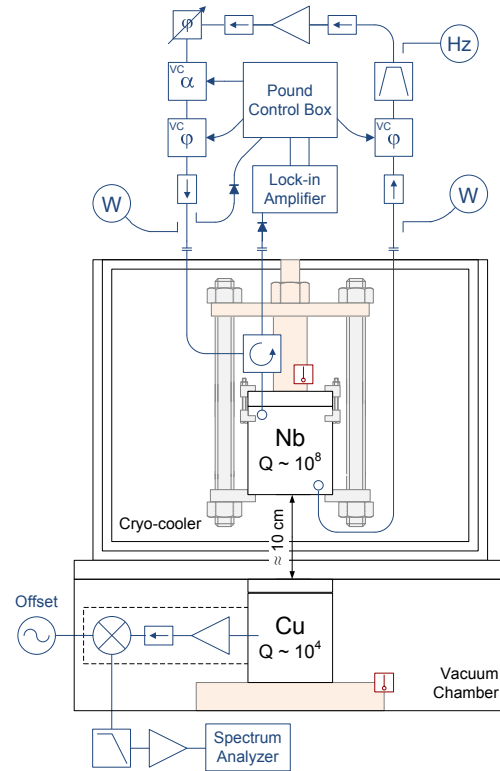


Figure 1: Diagram of the new UWA microwave cavity light shining through a wall experiment.

3 Hidden sector photon threshold crossing

Here we give a brief introduction to a new experimental method of searching for hidden sector photons using microwave cavities. In this approach we use only one microwave cavity, i.e. no photon regeneration, and hence are not faced with the difficulties of microwave leakage and resonance matching two cavities. The drawback is a narrow hidden sector photon mass search range but this can be useful for testing and refining a positive signal from another experiment.

For a photon to oscillate into a hidden sector photon it must have an energy greater than the rest mass energy of the hidden sector photon. This gives us a hidden sector photon threshold frequency, whereby only photons of greater frequency can mix into hidden sector photons. If a microwave cavity is driven on resonance and slowly tuned over this threshold frequency there will be a sudden drop in circulating power as photons oscillate into hidden sector photons and escape. Thus we are able to search for hidden sector photons at particular frequencies, and hence of particular masses, by looking for this drop in circulating power.

To model this effect we calculate a hidden sector photon quality factor, $Q_{\gamma'} = \omega_{\gamma'} \times$ time average stored energy in cavity / power loss to hidden sector photons. We calculate this by obtaining the stress-energy-momentum tensor and then determining the stored energy in the cavity from photons and the energy flow out of the cavity from hidden sector photons. The description of the hidden sector photon field [11], however, includes an unsolvable integral that requires us to take a Taylor series approximation. The hidden sector photon quality factor is optimized by the TM_{010} mode and at a 0th order approximation comes out to be

$$\frac{1}{Q_{\gamma'}} \approx \frac{2\chi^2 L}{3} \left(\frac{c}{\omega_{\gamma'}}\right)^4 \left(\frac{c}{\hbar} m_{\gamma'}\right)^4 \sqrt{\left(\frac{\omega_{\gamma'}}{c}\right)^2 - \left(\frac{c}{\hbar} m_{\gamma'}\right)^2}$$

where L is the cavity length. Plots showing the hidden sector quality factor with the predicted effect are given in Fig. 3. When the threshold is crossed there is a sudden spike in $1/Q_{\gamma'}$.

The hidden sector photon quality factor can be related to the unloaded quality factor and couplings to the cavity. These in turn are related to the incident, reflected and transmitted power levels which can be measured in an experiment. Tuning the cavity can be carried out by temperature or tuning rods and to keep it excited on resonance a loop oscillator can be used. Using state-of-the-art equipment limits of $\chi < 10^{-10}$, well below current limits, may be achievable.

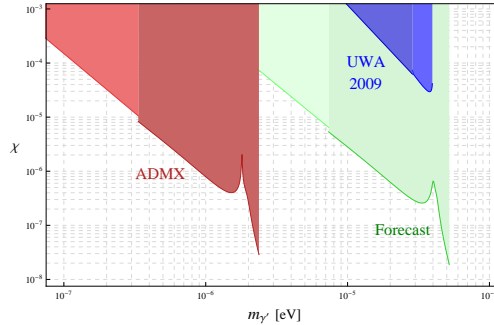


Figure 2: Plot of the predicted hidden sector photon limit from the new experiment against limits established by other microwave experiments.

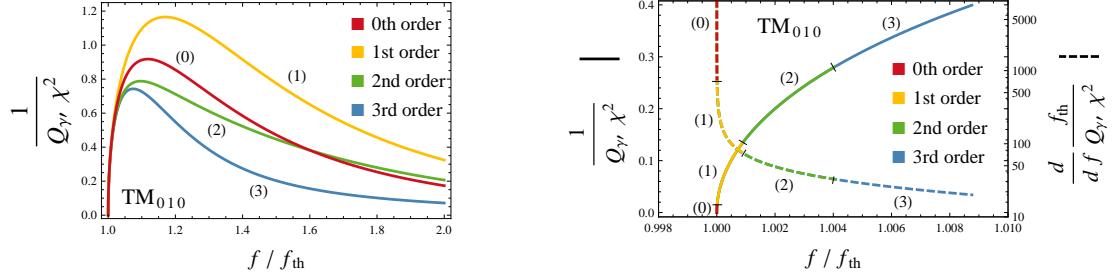


Figure 3: Plots of the 0th, 1st, 2nd and 3rd order approximations of $1/Q_{\gamma'}$ (solid line) and its derivative (dashed line) against frequency / threshold frequency for the TM_{010} mode in a cylindrical cavity of unity aspect ratio ($L = 2R$) with tuning performed by changing the size of the cavity whilst maintaining the aspect ratio.

References

- [1] S. A. Abel, M. D. Goodsell, J. Jaeckel, V. V. Khoze, and A. Ringwald, *JHEP* **07**, 124 (2008), arXiv:0803.1449.
- [2] M. Goodsell, J. Jaeckel, J. Redondo, and A. Ringwald, *JHEP* **11**, 027 (2009), arXiv:0909.0515.
- [3] L. B. Okun, *Sov. Phys. JETP* **56**, 502 (1982).
- [4] B. Holdom, *Phys. Lett. B* **166**, 196 (1986).
- [5] J. Jaeckel and A. Ringwald, *Annual Review of Nuclear and Particle Science* **60**, 405 (2010).
- [6] J. Redondo and A. Ringwald, (2010), arXiv:1011.3741.
- [7] K. Van Bibber, N. R. Dagdeviren, S. E. Koonin, A. K. Kerman, and H. N. Nelson, *Phys. Rev. Lett.* **59**, 759 (1987).
- [8] F. Hoogeveen and T. Ziegenhagen, *Nucl. Phys. B* **358**, 3 (1991).
- [9] P. Sikivie, D. B. Tanner, and K. van Bibber, *Phys. Rev. Lett.* **98**, 172002 (2007), arXiv:hep-ph/0701198.
- [10] G. Mueller, P. Sikivie, D. B. Tanner, and K. van Bibber, *Phys. Rev. D* **80**, 072004 (2009), arXiv:0907.5387.
- [11] J. Jaeckel and A. Ringwald, *Phys. Lett. B* **659**, 509 (2008), arXiv:0707.2063.
- [12] BFRT, R. Cameron *et al.*, *Phys. Rev. D* **47**, 3707 (1993).
- [13] BFRT, G. Ruoso *et al.*, *Z. Phys. C* **56**, 505 (1992).
- [14] BMV, C. Robilliard *et al.*, *Phys. Rev. Lett.* **99**, 190403 (2007), arXiv:0707.1296.
- [15] M. Ahlers, H. Gies, J. Jaeckel, J. Redondo, and A. Ringwald, *Phys. Rev. D* **76**, 115005 (2007), arXiv:0706.2836.
- [16] GammeV, A. S. Chou *et al.*, *Phys. Rev. Lett.* **100**, 080402 (2008), arXiv:0710.3783.
- [17] M. Ahlers, H. Gies, J. Jaeckel, J. Redondo, and A. Ringwald, *Phys. Rev. D* **77**, 095001 (2008), arXiv:0711.4991.
- [18] LIPSS, A. Afanasev *et al.*, *Phys. Rev. Lett.* **101**, 120401 (2008), arXiv:0806.2631.
- [19] BMV, M. Fouché *et al.*, *Phys. Rev. D* **78**, 032013 (2008), arXiv:0808.2800.
- [20] LIPSS, A. Afanasev *et al.*, *Phys. Lett. B* **679**, 317 (2009), arXiv:0810.4189.
- [21] ALPS, K. Ehret *et al.*, *Nucl. Instrum. Meth. Phys. Res. A* **612**, 83 (2009), arXiv:0905.4159.
- [22] ALPS, K. Ehret *et al.*, *Phys. Lett. B* **689**, 149 (2010), arXiv:1004.1313.
- [23] R. G. Povey, J. G. Hartnett, and M. E. Tobar, *Phys. Rev. D* **82**, 052003 (2010), arXiv:1003.0964v2.
- [24] ADMX, A. Wagner *et al.*, *Phys. Rev. Lett.* **105**, 171801 (2010), arXiv:1007.3766.

GammeV: Laser Experiments at Fermilab for WISPs and Other Effects

William Wester*

Fermilab, MS209, Batavia IL, USA

presented on behalf of the GammeV and GammeV-CHASE Collaborations

DOI: http://dx.doi.org/10.3204/DESY-PROC-2011-04/wester_william

The GammeV and GammeV-CHASE experiments have searched for Weakly Interacting Slim Particles (WISPs) and have published exclusion plots for axion-like particles and chameleons that couple to photons. R&D continues in long baseline optical cavities that might be required for an axion photon resonant regeneration experiment or a search for holographic noise.

1 Introduction

Physics beyond the Standard Model might include Weakly Interacting Slim Particles (WISPs) that address questions such as what is the nature of dark matter or even shed insight into the underlying nature of dark energy. WISPs are a general class of particles that include axions, axion-like particles, hidden sector photons, milli-charged particles, chameleons, etc. The GammeV (**G**amma to **m**illi-**e**V) experiment originated in 2007 in order to test a positive anomalous axion-like particle interpretation of the PVLAS experiment which was not evident in subsequent data [1, 2]. The experiment was also motivated as it was realized that the milli-eV scale appears naturally in a see-saw between the electroweak and Planck scales, neutrino mass differences, the dark energy density, and the possible mass for certain dark matter candidates. GammeV excluded both a scalar and pseudoscalar axion-like particle interpretation of the anomalous PVLAS result setting a limit of around $3.1 \times 10^{-7} \text{ GeV}^{-1}$ on the coupling to photons for low mass scalar axion-like particles.

Further work by the GammeV team has focused on a reconfiguration of the apparatus to be sensitive to possible chameleon particles. Chameleons are scalar (or pseudoscalar) particles that couple to the stress energy tensor in a potential such that their properties depend on their environment. In particular, a chameleon acquires an effective mass which increases with local matter density, ρ . For a certain class of such potentials, the chameleon field has properties that might explain dark energy [3]. GammeV set the first limits on the coupling of chameleons to photons. A dedicated follow-up experiment, GammeV-CHASE, (**CH**ameleon **A**fterglow **SE**arch), has also been performed and sets limits on both photon and some model dependent matter couplings as a function of an effective chameleon mass.

*This work is supported by the U.S. Department of Energy under Contract No. DE-AC02-07CH11359

2 Experimental setup

The GammeV and GammeV-CHASE apparatus are shown in Fig. 1. Both experiments were conducted at the Fermilab Magnet Test Facility that allowed for high field operation of Tevatron magnets. Both experiments used a 3W pulsed Nd:YAG laser frequency doubled to 532 nm shown into the bore of a Tevatron dipole magnet operating at 5 T. The GammeV experiment used a light shining through a wall (LSW) [4] configuration where a photon propagating in a magnetic field could oscillate into an axion-like particle, traverse an opaque barrier, and have a small probability for reconverting back into a detectable photon. Two novel aspects were employed in order to increase sensitivity over the region of interest. A “plunger” was constructed so that the wall could be placed either in the middle or toward one end of the magnet in order to remove regions of insensitivity of mass where the oscillation probability vanishes. The second aspect utilized time correlated single photon counting techniques in order to reject noise from an already relatively low-noise photomultiplier tube (PMT). An *a priori* 10 ns wide search window was established using a calibration run where laser photons were attenuated by approximately 19 orders of magnitude (i.e. no wall) and allowed to be recorded by the PMT.

For GammeV-CHASE, a “particle trapped in a jar” afterglow technique was employed [5, 6]. The configuration improved many different experimental aspects from the first look by GammeV to extend sensitivity. Laser photons converting into chameleons would remain trapped in the vacuum system until possibly reconverting back into photons that could leave the vacuum system through an optical window and hit the PMT. Similar to the plunger, GammeV-CHASE divided the magnetic field region into three separate regions providing sensitivity to different effective chameleon masses. A small residual ~ 1 Hz rate of photons from an ion pump and a long-lived luminescence of orange photons similar to known phosphorescence of vacuum grease [7] provided calibration of the experiment’s sensitivity.

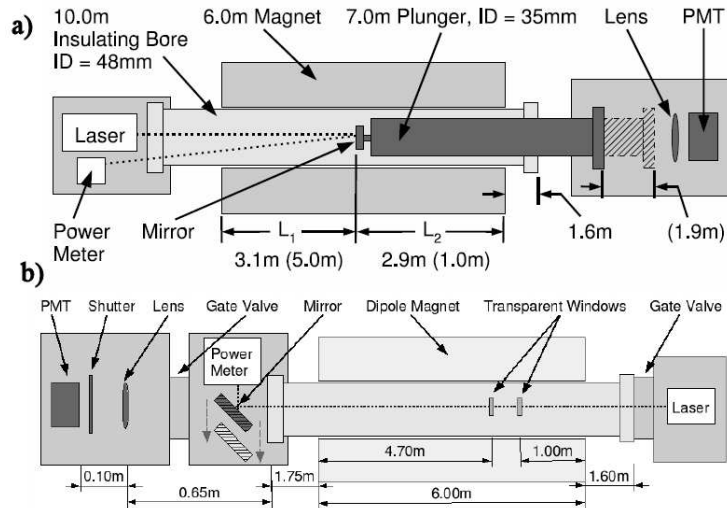


Figure 1: (a) Schematic diagram of the (a) GammeV experimental apparatus and (b) GammeV-CHASE experimental apparatus. The laser, spare Tevatron magnet, phototubes, and data acquisition electronics were used by both experiments.

3 Results

Both GammeV and GammeV-CHASE observed no significant WISP signal above background [8], [5], [10], [11]. Fig. 2 shows the exclusion regions of the coupling to photons versus the (effective) mass for axion-like particles (3σ) and chameleons (95% C.L.). For GammeV, data was recorded in two polarizations for two configurations of the position of the wall with each of these runs consisting of approximately 20 hours of magnet time. The non-observation of a signal has also been reported by other experiments worldwide [9]. For GammeV-CHASE, multiple runs were recorded with 10 hours to reach the smallest couplings of photons to chameleons. Shorter runs were recorded at reduced magnetic field to cover larger couplings of photons to chameleons.

The reach of the GammeV and GammeV-CHASE essentially was an energy scale of a 3×1000 TeV and 3×10000 TeV respectively. These high scales are made accessible by the intense photon beam (incident photons were a few $\times 10^{23}$) from which a small regenerated photon signal could be identified above background.

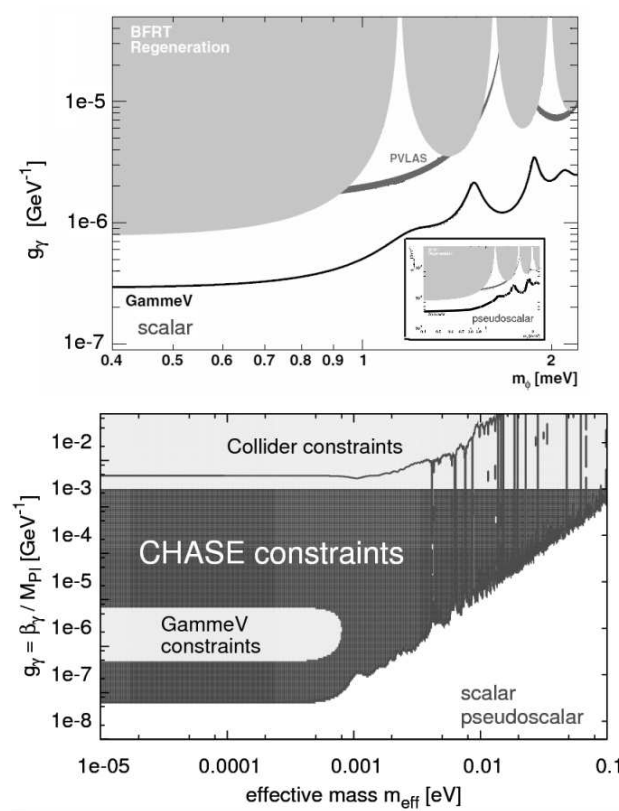


Figure 2: Published exclusion regions of photon coupling versus effective mass obtained (a) by GammeV for scalar and pseudoscalar (inset) axion-like particles at 3σ and (b) by GammeV and GammeV-CHASE for chameleon particles at 95% C.L. where the GammeV and GammeV-CHASE regions are valid for $\eta > 0.8$ and 0.1 respectively when expressing $m_{eff} > \rho^\eta$.

4 Future Plans

The future plans include extending the GammeV region of sensitivity from a few $\times 10^{-7}$ GeV $^{-1}$ to possibly the 10^{-12} GeV $^{-1}$ level. Such an effort has been called REAPR [12], **R**esonantly **E**nhanced **A**xion-**P**hoton **R**egeneration.” There is on-going R&D on long baseline optical cavities in conjunction with the Holometer [13] experiment.

There are ideas of extending the search region for chameleons as well as hidden sector photons. Before an experiment is proposed, careful consideration will be given to the increase in sensitivity compared with other experimental results and the motivation for and effort that it would take to obtain that sensitivity.

5 Conclusions

A research program at Fermilab has obtained published results for axion-like particle and chameleon searches. Next generation experiments have started or are undergoing R&D. The possibility that WISPs or other phenomenon might be observable using relatively inexpensive experimental optical set-ups allows for searches of physics beyond the Standard Model.

References

- [1] E. Zavattini *et al.* [PVLAS Collaboration], Phys. Rev. Lett. **96**, 110406 (2006) [arXiv:hep-ex/0507107].
- [2] E. Zavattini *et al.* [PVLAS Collaboration], Phys. Rev. D **77**, 032006 (2008) [arXiv:0706.3419 [hep-ex]].
- [3] J. Khoury, A. Weltman, Phys. Rev. **D69**, 044026 (2004). [astro-ph/0309411].
- [4] K. Van Bibber, N. R. Dagdeviren, S. E. Koonin, A. Kerman and H. N. Nelson, Phys. Rev. Lett. **59**, 759 (1987).
- [5] A. S. Chou *et al.* [GammeV Collaboration], Phys. Rev. Lett. **102**, 030402 (2009). [arXiv:0806.2438 [hep-ex]].
- [6] M. Ahlers, A. Lindner, A. Ringwald, L. Schrempp, C. Weniger, Phys. Rev. **D77**, 015018 (2008). [arXiv:0710.1555 [hep-ph]].
- [7] D.W. Cooke and B.L. Bennett, “Long-lived luminescence from commonly used Apiezon compounds”, Journal of Luminescence, Volume 65, 283 (1995).
- [8] A. S. .. Chou *et al.* [GammeV (T-969) Collaboration], Phys. Rev. Lett. **100**, 080402 (2008) [arXiv:0710.3783 [hep-ex]].
- [9] M. Fouche *et al.* [BMV Collaboration], Phys. Rev. D **78**, 032013 (2008) [arXiv:0808.2800 [hep-ex]]. K. Ehret *et al.* [ALPS Collaboration], Phys. Lett. B **689**, 149 (2010). A. Afanasev *et al.* [LIPSS Collaboration], Phys. Rev. Lett. **101**, 120401 (2008) [arXiv:0806.2631 [hep-ex]]. P. Pognat *et al.* [OSQAR Collaboration], Phys. Rev. D **78**, 092003 (2008) [arXiv:0712.3362 [hep-ex]].
- [10] A. Upadhye, J. H. Steffen and A. Weltman, Phys. Rev. D **81**, 015013 (2010) [arXiv:0911.3906 [hep-ph]].
- [11] J. H. Steffen *et al.*, Phys. Rev. Lett. **105**, 261803 (2010) [arXiv:1010.0988 [astro-ph.CO]].
- [12] G. Mueller, P. Sikivie, D. B. Tanner and K. van Bibber, Phys. Rev. D **80**, 072004 (2009) [arXiv:0907.5387 [hep-ph]].
- [13] C. J. Hogan, arXiv:0905.4803 [gr-qc]. See also: www.fnal.gov/directorate/program.planning/Nov2009PACPublic/holometer-proposal-2009.pdf.

Status of ALPS-II at DESY

Jan Eike von Seggern (DESY) for the ALPS collaboration

Deutsches Elektronen-Synchrotron (DESY), Hamburg, Germany

DOI: http://dx.doi.org/10.3204/DESY-PROC-2011-04/von_seggern_jan_eike

The light-shining-through-a-wall (LSW) experiment ALPS at DESY provides the current best lab-based bounds for WISP couplings. Based on this success, preparations for ALPS-II have started. The aim is to increase the sensitivity by three orders of magnitude to probe parameter regions with astrophysical hints for the existence of WISPs from white dwarf energy loss and the TeV transparency of the intergalactic medium. To reach this sensitivity, ALPS-II will be considerably longer, making use of 2×12 HERA dipole magnets. The laser power in the WISP-production region will be increased and a second optical cavity in the regeneration region will be constructed. Additionally, a very low-noise transition-edge photo-detector is in development. In a pre-experiment, it will be possible to probe the hidden-photon interpretation of the WMAP-7 excess in sterile neutrinos.

1 Introduction

The solution of the strong CP-problem of [1] postulated the axion, giving rise to a new class of particles called *weakly-interacting slim particles* (WISPs). Among these are axions, axion-like particles (ALPs) and hidden photons (HPs). While axions and ALPs couple to photons via a two-photon vertex, hidden photons mix kinematically with ordinary photons. WISPs are appealing because they can explain observations from astrophysics (*e.g.* TeV transparency of the universe, anomalous cooling of white dwarfs [2, 3]) and cosmology (*e.g.* Dark Matter, hCMB [4, 5]).

To detect WISPs via their interaction with photons one can use the principle of light-shining-through-a-wall (LSW): One points a strong light source on an opaque wall. While most photons will be absorbed or reflected by the wall, some photons can convert to WISPs before the wall and these can then easily traverse the wall. Behind the wall a fraction of these WISPs can re-convert to photons and can be detected by a low-noise photon detector. In the case of axions and ALPs a strong magnetic field is necessary. Fig. 1 shows schematic set-ups for this kind of experiments.

The probability for a $\text{WISP} \rightarrow \gamma$ or $\gamma \rightarrow \text{WISP}$ conversion is given by [6]

$$\mathcal{P}_{\gamma \leftrightarrow a} = g_a^2 (BL)^2 \sin^2 \left(\frac{M^2 L}{4\omega} \right) / \left(\frac{M^2 L}{4\omega} \right) \quad \text{and} \quad \mathcal{P}_{\gamma \leftrightarrow \gamma'} \simeq \chi^2 \frac{m_{\gamma'}^4}{M^4} \sin^2 \left(\frac{M^2 L}{4\omega} \right)$$

for axions and ALPs and HPs, respectively, with $M^2 = m_{a,\gamma'}^2 + 2\omega(n-1)$, g_a and χ being the respective couplings, B the magnetic field strength, L the length of the baseline, n the index of refraction of the medium and ω the photon energy.

Hence, for an experiment conducted in vacuum that measured N_{meas} photons after shining N_{in} photons on the wall using a detector with efficiency ε and production and regeneration

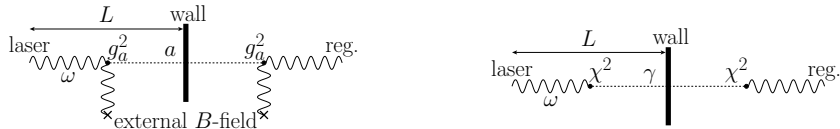


Figure 1: Schematic set-up of a light-shining-through-a-wall experiment searching for axions and ALPs (left) and hidden photons (right). The right-hand side of the wall is the production side, the left-hand side the regeneration side.

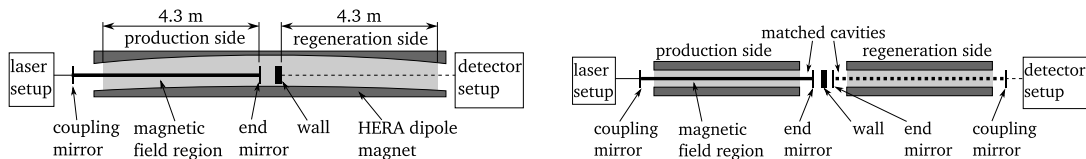


Figure 2: *Left*: Schematic set-up of ALPS-I. The production cavity is indicated by the coupling and end mirrors. The region of the magnetic field of the HERA dipole magnet is marked by the gray area. The length of the production cavity in the magnetic field and the length of the regeneration part in the magnetic field were both $L = 4.3$ m. For more details see Fig. 1 of [8]. *Right*: Schematic set-up of an improved LSW experiment utilizing an optical cavity in the regeneration side. The power build-up in the two cavities is indicated by the stronger strokes.

regions of same length L a naïve estimate of the coupling can be given in the limit of small masses for ALPs and HPs, respectively, by

$$g_a = \frac{1}{BL} \left(\frac{N_{\text{meas}}}{\varepsilon \cdot N_{\text{in}}} \right)^{1/4}, \quad \chi \propto \frac{1}{m_{\gamma'}^2} \left(\frac{N_{\text{meas}}}{\varepsilon \cdot N_{\text{in}}} \right)^{1/4}. \quad (1)$$

2 ALPS-I

The LSW experiment ALPS at DESY used a superconducting HERA dipole magnet allowing for a magnetic field of $B = 5$ T with a length of $L = 4.3$ m in both parts of the experiment [7]. It finished data taking in 2009 [8]. It used a green laser of ~ 4 W coupled into an optical resonator with a power build-up of up to 300 on the production side of the wall. This allowed for a continuously circulating power of up to 1.2 kW corresponding to 3.2×10^{21} photons/s. A commercial, liquid-cooled CCD device was used as detector. The left panel of Fig. 2 shows a schematic view of the set-up. The high photon-flux in the production cavity and the low background of the CCD rendered ALPS the most sensitive lab-based LSW experiment.

3 ALPS-II

In late 2010 work has begun to build a successor of ALPS-I. Increasing the sensitivity of an LSW experiment can be achieved by increasing the size of the experiment, improving the detection efficiency, increasing the power of the light source, and for axions and ALPs by using stronger magnets, where Eqs. 1 show that the length and magnetic field have the strongest effect. Since a stronger magnetic field could only be achieved by constructing new superconducting magnets,

	λ/nm	$P_{\text{prod}}/\text{kW}$	PB_{reg}	magn. set-up	L/m	eff.	noise/ h^{-1}	rel. gain
ALPS-I	532	1.2	1	0.5 + 0.5	4.3	0.96	32	1
step 1	1064 (1.2)	150 (3.3)	40 000 (14)	–	10 (–)	0.02 (0.38)	32 (1)	21
step 2	1064 (1.2)	150 (3.3)	40 000 (14)	–	130 (–)	1.0 (1.0)	0.3 (1.8)	101
step 3	1064 (1.2)	150 (3.3)	40 000 (14)	12 + 12	105 (24)	1.0 (1.0)	0.3 (1.8)	2500
fall back	1064 (1.2)	150 (3.3)	40 000 (14)	4 + 4	35 (8.1)	1.0 (1.0)	0.3 (1.8)	822

Table 1: The experimental parameters for the different steps for ALPS-II. The last column shows the expected improvement in sensitivity compared to ALPS-I. The individual influence on the sensitivity of each parameter is given in parentheses. For step 1 and 2 the influence on the HP-sensitivity is given, for step 3 and the fall-back set-up the influence of the ALP-sensitivity.

the work for ALPS-II concentrates on the first three components. Further increase of sensitivity can be achieved by a second optical cavity in the regeneration part as shown in the right panel of Fig. 2 [9]. This increases the probability for an ALP or HP to convert back to a photon proportional to the power build-up of the cavity.

Laser and cavities The period of continuous operations during ALPS-I measurements was limited by the durability of the mirrors of the production cavity. We hope to improve this by using an infrared laser with $\lambda = 1064$ nm. This will allow for a higher continuously circulating power of approximately 150 kW with a much increased durability of the cavity mirrors as is known from gravitational wave experiments [10].

For the regeneration cavity an approximate power build-up of 40 000 for IR light is planned. The matching of the alignment and resonance frequency of the regeneration cavity eigenmode to that of the production cavity will be achieved by a green reference beam, which will be produced from the IR beam by second-harmonic generation and will be split from regenerated IR photons in the optical detector set-up [11].

Magnet string The HERA dipole magnets have a curved beam pipe with a free aperture of 35 mm. Without modifications, this allows to use 2×4 HERA dipoles. For longer set-ups the power build-up decreases due to clipping of the laser beam resulting in a reduced overall sensitivity. Since the length of the experiment has the strongest influence, a method to straighten the beam pipes is developed. First tests showed that a free aperture of 50 mm can be achieved, allowing for lengths of $L = 130$ m (2×12 HERA dipoles).

Detector Switching from green to infrared light complicates the detection of single photons, especially when using a silicon-based CCD as was used in ALPS-I, because the photon energy is of the order of the Si band gap. This results in a much lower quantum efficiency of $\sim 2\%$.¹ But since the background of the CCD camera is known to be low and the efficiency influences the limit only by the fourth root, it is prepared to be used as fall-back detector.

¹For comparison, the quantum efficiency for green light in ALPS-I was 96 %.

As prime detector a transition-edge-sensor device (TES) is developed in cooperation with the BaRBE project [12]. This should result in a detector with almost zero intrinsic noise and a (limited) energy resolution. By coating the TES a quantum efficiency close to 100 % should be possible.

Realization The above improvements will be realized stepwise: In the first step, a 2×10 m long, HP-only experiment will be built, which will serve as proof-of-concept for the matching of the production and regeneration cavities and will eventually use the TES as detector. Second, this set-up will be enlarged to 2×130 m to prove that cavities of this length can be controlled, and finally this set-up will be equipped with 2×12 HERA dipoles for an ALP search.

The experimental parameters of the different steps are shown in Tab. 1 together with the resulting improvements on the sensitivity compared to ALPS-I. The parameter space of the hCMB interpretation of the WMAP-7 data of [5] should easily be reached with the 2×10 m HP-search set-up.

4 Conclusion

ALPS-I is the most sensitive lab-based LSW experiment up to now. The preparations for ALPS-II have begun at DESY. The experiment will be conducted in three steps. The first pre-experiment will serve as proof-of-concept for the matching of the production and regeneration cavities and reach the parameter region of the hCMB. The final set-up will be installed by 2017 and will improve the sensitivity by three orders of magnitude compared to ALPS-I.

References

- [1] R. D. Peccei and H. R. Quinn, “CP Conservation in the Presence of Instantons,” *Phys. Rev. Lett.* **38**, 1440 (1977).
- [2] M. Meyer, “Indications for a highly transparent universe at very high energies,” Contribution to this workshop (2011).
- [3] J. Isern, “White dwarfs as physical laboratories: the axion case,” Contribution to this workshop (2011).
- [4] M. Drees and G. Gerbier, “Dark matter” in K. Nakamura *et al.* [Particle Data Group Collaboration], “Review of particle physics,” *J. Phys. G G* **37**, 075021 (2010).
- [5] J. Jaeckel, J. Redondo and A. Ringwald, “Signatures of a hidden cosmic microwave background,” *Phys. Rev. Lett.* **101**, 131801 (2008) [arXiv:0804.4157 [astro-ph]].
- [6] J. Redondo and A. Ringwald, “Light shining through walls,” *Contemp. Phys.* **52**, 211 (2011) [arXiv:1011.3741 [hep-ph]].
- [7] K. Ehret *et al.* [ALPS Collaboration], “Resonant laser power build-up in ALPS: A ‘Light-shining-through-walls’ experiment,” *Nucl. Instrum. Meth. A* **612**, 83 (2009) [arXiv:0905.4159 [physics.ins-det]].
- [8] K. Ehret *et al.* [ALPS Collaboration], “New ALPS Results on Hidden-Sector Lightweights,” *Phys. Lett. B* **689**, 149 (2010) [arXiv:1004.1313 [hep-ex]].
- [9] P. Sikivie, D. B. Tanner and K. van Bibber, “Resonantly enhanced axion-photon regeneration,” *Phys. Rev. Lett.* **98**, 172002 (2007) [hep-ph/0701198 [HEP-PH]].
- [10] LIGO Laboratory/LIGO Scientific Collaboration, “Advanced LIGO reference design,” LIGO-060056-08-M (2007) <http://www.ligo.caltech.edu/docs/M/M060056-08/M060056-08.pdf>
- [11] T. Meier, “High-Power CW Green Lasers for Optical Metrology and Their Joint Benefit in Particle Physics Experiments,” Thesis (2011), Chapter 4.
- [12] G. Cantatore, “The BaRBE project and the perspectives of TES sensors in WISP searches,” Contribution to this workshop (2011).

Status report of the CERN light shining through the wall experiment with microwave axions and related aspects

*M. Betz*¹, *F. Caspers*¹, *M. Gasior*¹, *M. Thumm*²

¹European Organization for Nuclear Research (CERN), Geneva, Switzerland

²Karlsruhe institute of technology (KIT), Germany

DOI: http://dx.doi.org/10.3204/DESY-PROC-2011-04/betz_michael

One way to proof or exclude the existence of axion like particles is a microwave light shining through the wall experiment. In this publication we will emphasize on the engineering aspects of such a setup, currently under development at CERN. One critical point, to achieve meaningful results, is the electromagnetic shielding between axion-emitter and receiver cavity, which needs to be in the order of 300 dB to improve over existing experimental bounds. The RF leakage or electromagnetic crosstalk between both cavities must be well controlled and quantified during the complete duration of the experiment. A very narrow band (in the μHz range) homodyne detection method is used to reveal the axion signal from background thermal noise. The current status of the experiment is presented.

1 Motivation and introduction

The axion is a hypothetical elementary particle, which emerged originally from a proposal by Peccei and Quinn, intended to solve the strong CP problem [1]. The axion is neutral, only interacts very weakly with matter, has very low mass ($\approx 10^{-4}eV/c^2$), spin zero, and a natural decay constant (to 2 photons) in the order of 10^{17} years.

One way to detect axion like particles (ALPs) is to exploit their property of mixing with photons inside a static electric or magnetic field. In a simplified way, this provides “virtual photons”, forcing ALPs to decay into real photons which then can be detected conventionally [2]. All axion searches nowadays are based on this so called Primakoff effect.

A particular sensitive experiment is the light-shining-through-wall (LSW) setup, depicted in Fig. 1. The emitting part consists of a photon source (e.g., a microwave, laser or X-ray beam) and a strong magnet. By the Primakoff effect some photons convert to ALPs. A wall blocks the unconverted photons but not the ALPs, which traverse to the receiving part. There the reciprocal conversion takes place. The “reconverted” photons can be detected by conventional means and will have the same wavelength as the photons in the emitting part, considering that no energy is lost at any point. It shall be pointed out that a LSW experiment is also sensitive to hidden photons, which are a different kind of hypothetical particle [3]. The only necessary modification is not to use an external magnetic field.

The sensitivity of the experiment can be significantly increased by placing resonating structures in the emitting and detection part. Resonator cavities with particular low loss can be

constructed in the microwave regime. Q-factors $> 10^4$ can routinely be achieved with normal conducting cavities at room temperature. Q-factors of $\approx 10^{10}$ are technically feasible with superconducting cavities (however, this technology is not compatible with strong magnetic fields). Another advantage is that sensitive homodyne detection methods can be applied in the microwave range, further increasing sensitivity.

For the aforementioned reasons and because of the fact that the instruments, tools and facilities for building microwave cavities for particle accelerators already exist at CERN, a microwaves shining through the wall experiment will be setup in the course of the next 2 years.

2 Cavity design and construction

The operating frequency of the emitting cavity determines the energy of the photons inside ($E_{\text{ph}} = h \cdot f$). If the Primakoff effect takes place, the energy of the photon is converted to mass and kinetic energy ($\beta = v/c$) of the ALP as shown in Equ. 1. Therefore, as a first approximation, the choice of frequency determines an upper limit on ALP mass (m_a). As a rule of thumb $m_a = 4.14 \mu\text{eV}/c^2$ corresponds to $f = 1$ GHz.

$$E_{\text{ph}} = hf = E_{\text{ALP}} = m_a c^2 \left(1 + \frac{1}{2}\beta^2\right) \quad (1)$$

For the first experimental phase, operating at room temperature, testing the electromagnetic (EM) shielding and achieving a leak tight setup is of primary importance. For this phase, the TE_{011} mode will be used, as it has the highest Q-factor compared to other modes. Hidden photon search without a magnet is possible, however, this mode is not sensitive to ALPs in a magnetic field as its geometric overlap integral [4, 5] is zero. ALPs will be searched in the second phase of the experiment with the fundamental TM_{010} mode at 1.75 GHz. Higher order modes can be used for ALPs search as well, however certain requirements regarding the magnet and cavity design need to be fulfilled [6, 7].

The shape of the cavity used in this test setup is a classical pillbox with bevelled edges. The bevelling helps to separate the degeneracy of the TM_{111} and the TE_{011} mode.

To minimize losses, the surface of the brass cavities is coated with a $10 \mu\text{m}$ thick layer of silver. A $< 0.2 \mu\text{m}$ thick layer of gold prevents oxidation. The skin depth in silver at 3 GHz at room temperature is $\approx 1 \mu\text{m}$, so most of the surface current flows in the silver layer with low losses [8].

Power is transferred towards and out of the cavity by an inductive coupling loop. By adjusting the angle of the loop's cross section, the cavity impedance can be matched to a 50Ω system, providing maximum power transfer.

To compensate manufacturing tolerances, both cavities are equipped with a fine threaded tuning bolt, directly perturbing the cavity volume. The 20 mm diameter bolt provides ≈ 10 MHz adjustment range of the resonant frequency. For the time being, no sweep over the ALP mass during an experimental run is foreseen. Once the cavities have reached thermal equilibrium, their resonant frequency is sufficiently stable and no manual adjustment of the tune is needed during an experimental run. The resonant frequency of the emitting cavity is continuously monitored by means of its reflected power. The tune of the (room temperature) receiving cavity is determined from the recorded data by means of evaluating the spectral noise power density.

3 EMI shielding concept

There are three categories of perturbation which may disguise the useful signal from converted ALPs and which need to be mitigated:

- Environmental interference such as signals from cellphones, WIFI devices, radio stations, etc.
- Direct microwave leakage from the emitting cavity (no photon-ALP-photon conversion).
- Thermal noise, which is the random movement of charge carriers in a conductor at non-zero temperature.

The first two points can be diminished by electromagnetic shielding, enclosing the receiving cavity and the signal processing electronics. To minimize the third point, the receiving cavity and the first amplifier need to be cooled to cryogenic temperatures.

We require the screening attenuation of a shielding enclosure to be ≈ 100 dB (that means unwanted signals are attenuated by a factor of 10^{10} in power). Stacking several enclosures (the cavity and cryostat walls count as shielding too) we can reach a total screening attenuation of 300 dB, which is needed to achieve the desired sensitivity and realize reliable detection of an ALP signal with $P_{\text{signal}} \approx -230\text{dBm}$.

As the detection cavity and first amplifier will need to be placed in a strong magnetic field inside a cryogenic environment (in the second planning phase), the experiment is split into two parts, equipped with two separate shielding enclosures. The cryogenic part (Fig. 1, middle) contains the receiving cavity and first amplifier. The room temperature part (Fig. 1 right) contains the signal processing electronics. Both are connected by an analog optical link with > 3 GHz bandwidth. An optical fibre guides the noise like signal from the detection cavity to the measurement instruments, unaffected by ambient EM interference and without comprising the performance of the EM shielding enclosures.

Power is provided to the instruments in the shielding enclosures by a custom made feed-trough filter, blocking EMI signals from the outside. The filter consists of several L and C elements in a π - or T-type configuration [8]. An example for a L element is a tight fitting wire inside a ferrite tube, which represents a lossy inductor at microwave frequencies. An example of a C element is a commercial ceramic feed-trough terminal filter, which represents a low impedance short circuit at microwave frequencies.

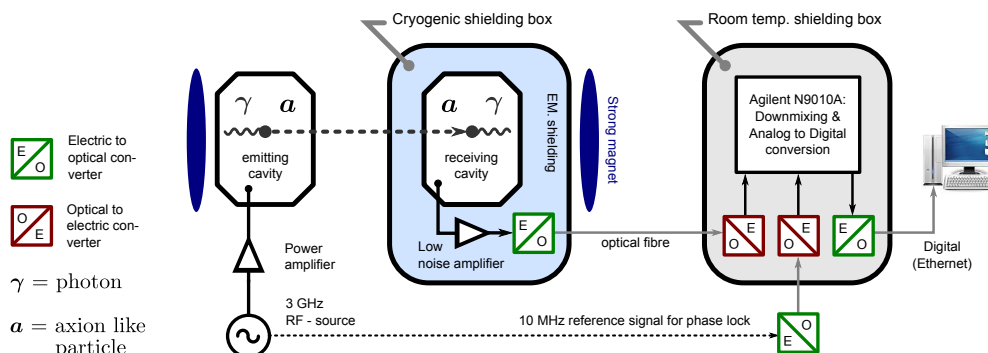


Figure 1: Overview of the light shining through the wall experiment in the microwave range.

Some of the practical measures which have been applied to improve robustness against EMI include: placing EM absorbing material between shielding layers, incorporating RF-gaskets on removable lids, applying conductive caulking material at material joints, etc.

4 Online shielding diagnostics

If there is a signal observed on the detection side of the experiment, it either originates from converted ALPs or from direct EM coupling as a consequence of microwave leakage. We need reliable ways to distinguish the two cases. One possibility is to use a slowly time varying (e.g., 1 cycle per hour) magnetic field. We would be able to detect the amplitude modulation sidebands only for an ALP signal but not for electromagnetic leakage. Another way is to look for small phase differences. Opposed to photons, ALPs have a non-zero rest mass and thus do not travel with the speed of light. Therefore we expect a small phase offset between the two signals.

Another, more robust and generally applicable way is to monitor and record the level of EM leakage during the experimental run. This can be done by emitting low power (in the μW range) probe signals in the laboratory space and between the shielding layers. Monitoring the strength of a signal after transversing one shielding layer gives information about its effective screening performance. Observing a probe signal with a level higher than a certain threshold indicates an EM leak and serves as a veto, rendering a positive result on ALP detection invalid. Each probe signal is emitted on a slightly different (phase locked) frequency so they can be identified and do not interfere with the detection of ALPs. The probe signals are guided inside the shielding layers by analog fibre-optic links.

5 Signal processing

A conceptual signal processing chain, which might be used for a cryogenic LSW setup, is depicted in Fig. 2. The smallest signal power at the coupling antenna of the cavity, determined by the specified sensitivity of the experiment is $P_{\text{signal}} = -230 \text{ dBm}$, corresponding to one 3 GHz photon every 3 minutes.

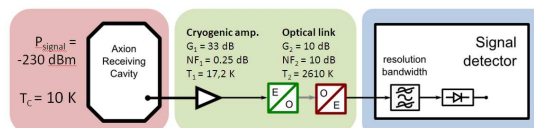


Figure 2: Analog signal processing chain.

$$F_n = 10^{\text{NF}_n/10} \quad F_{\text{equ}} = F_1 + \frac{F_2 - 1}{G_1} \quad T_n = 290\text{K} \cdot (F_n - 1) \quad (2)$$

The first amplifier in immediate vicinity to the cavity will be a cryogenic HEMT low noise amplifier, for which rather pessimistic gain and noise temperature values have been assumed in this example. While a typical analog optical link has a noise temperature¹ of 2610 K, its influence on the overall system is low. The equivalent noise temperature is determined by Friis formula (Equ 2) $T_{\text{equ}} = 18.5 \text{ K}$. The overall system noise temperature is $T'_{\text{noise}} = T_C + T_{\text{equ}} = 28.5 \text{ K}$ or in terms of power density at the detector (taking amplifier gain into account) $P'_{\text{noise}} = -141 \text{ dBm} / \text{Hz}$. The signal power at the detector is $P'_{\text{signal}} = -187 \text{ dBm}$. To upraise the signal from the noise, narrow band filtering is necessary.

¹We use the generally accepted Rayleigh-Jeans noise equation $P = kTB$, which is an approximation valid for $hf \ll kT$ (h is Planks constant, f the frequency, k Boltzmanns constant, and T the temperature) [9].

The filtering can be done by a commercial Fast Fourier Transform (FFT) type analyzer with the assumption that the photon to ALPs conversion and its reciprocal do not change the spectral properties of the signal and that it is defined with the spectral resolution of the original RF source. This allows to use very narrow resolution bandwidths ($B_{\text{res}} \leq 25 \mu\text{Hz}$), scaling down the noise power in one bin by $P_{\text{bin}} = P'_{\text{noise}} \cdot B_{\text{res}}$, nonetheless the signal power in this bin stays constant. To achieve the desired sensitivity with the previous assumptions and a signal to noise ratio of 1 we would need $B_{\text{res}} = 25 \mu\text{Hz}$ which demands a minimum length of the time trace of $T = 1/B_{\text{res}} = 11$ hours.

The RF-source and signal analyzer need to operate on the same frequency (within B_{res}) during the experimental run, otherwise the signal power will smear out over several bins in the spectrum and the signal to noise ratio will degrade. While absolute frequency drifts are unavoidable, phase-locking RF-source and signal analyzer to a common frequency reference allows to achieve a good relative frequency stability. This has been explained in [10] and has been successfully demonstrated with resolution bandwidths down to $10 \mu\text{Hz}$.

6 Results of the first measurement-run

A first measurement-run over 6 h, searching for hidden photons without an external magnetic field at room temperature has been accomplished in Nov. 2011. The non observation of a signal in the recorded data indicates a new preliminary exclusion limit with a sensitivity to the kinetic mixing parameter down to $\chi = 5 \cdot 10^{-8}$ at a hidden photon mass of $12.23 \mu\text{eV}/c^2$. This is a slight improvement over the Coulomb and FIRAS experiments, which also have produced exclusion limits in this energy range [3]. The new (preliminary) limit is depicted in Fig. 3, the technical parameters are summarized in Table 1. It shall be pointed out, that for the preliminary results, a rather pessimistic assumption for the hidden photon geometric factor of $|G| = 0.01$ has been used. The cavities were operated on the TE_{011} mode and placed next to each other, separated by a distance of 150 mm. For this configuration, we expect the actual value of $|G|$ to be significantly higher than the assumed one.

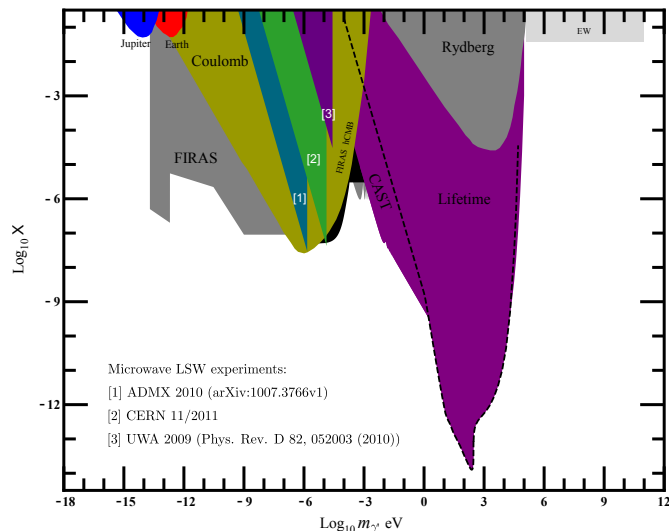


Figure 3: Preliminary exclusion limit for hidden photons as a result of the non observation of a signal in the measurement-run from the 11/2011 at CERN (labeled as [2]), compared to the result of other experiments. The collection of experimental data has been taken from [3], where it is also explained in detail.

Table 1: Technical param. for the hidden photon measurement run from Nov. 2011 at CERN.

f_{em}	2.9571 GHz	Operating frequency	Q_{em}	23416	Q-factor of emitting cav.
P_{em}	49 W	Power to emitting cav.	Q_{det}	23620	Q-factor of detector cav.
P_{det}	$1.74 \cdot 10^{-23}$ W	Detectable sign. power	$ G $	0.01	Geometric factor

7 Conclusion and Outlook

Mitigating electromagnetic interference is a critical point for sensitive light shining through the wall experiments in the microwave range. We propose a shielding concept, involving several metal shells and signal transmission over optical fibre. The injection of probe signals between the shielding layers allows to quantify the overall screening attenuation in real time. This allows to make sure that a hypothetical detected signal does not originate from environmental interference.

To receive very weak signals we proposed a narrow band detection scheme. A commercial signal analyser can be operated as homodyne detector by phase locking it to the RF-source driving the emitting cavity. Signals with a power level in the order of $P_{signal} \approx -230$ dBm can still be detected.

The first measurement-run on 11/2011 produced new exclusion limits for hidden photons, it showed that the aforementioned concepts are practical and also necessary for a sensitive LSW experiment in the microwave range.

8 Acknowledgments

The authors would like to thank R. Jones and the BE department management for encouragement. Thanks to K. Zioutas and the organizers of the Patras Workshop for a very enjoyable and inspiring conference. Supported by the Wolfgang-Gentner-Programme of the Bundesministerium für Bildung und Forschung (BMBF).

References

- [1] R. D. Peccei, H. R. Quinn; *CP Conservation in the Presence of Pseudoparticles* Phys. Rev. Lett. 38 no. 25 p. 1440, June 1977
- [2] G. Raffelt, L. Stodolsky; "Mixing of the photon with low-mass particles" Phys. Rev. D 37 no. 5; 1988
- [3] F. Caspers, J. Jäckel, A. Ringwald; Feasibility, engineering aspects and physics reach of microwave cavity experiments searching for hidden photons and axions JINST 4 P11013 (Nov. 2009)
- [4] F. Hoogeveen; Terrestrial axion production and detection using RF cavities CERN-TH-6500-92. Jun 1992. 10 pp. Phys.Lett. B288 (1992) 195-200
- [5] J. Jäckel, A. Ringwald; A Cavity Experiment to Search for Hidden Sector Photons, Phys.Lett. B659 509-514
- [6] M. Betz, F. Caspers, K. Zioutas; Directional Microwave Antenna Structures for the Detection of Dark Matter Axions; CERN-ATS-Note-2011-066 TECH
- [7] O. Baker, M. Betz, F. Caspers, J. Jaeckel, A. Lindner, A. Ringwald, et al.; Prospects for Searching Axion-like Particle Dark Matter with Dipole, Toroidal and Wiggler Magnets DCPT/11/110; DESY 11-163; IPPP/11/55
- [8] K. H. Gonschorek, H. Singer; Elektro- Magnetische Verträglichkeit , B. G. Teubner, 1992
- [9] A.Kerr, J. Randa; Thermal Noise and Noise Measurements A 2010 Update, IEEE Microwave Magazine, vol. 11, no. 6, pp.40-52, Oct. 2010
- [10] F. Caspers, S. Federmann, D. Seebacher; Demonstration of 10^{-22} W Signal Detection Methods in the Microwave Range at Ambient Temperature CERN-BE-Note-2009-026

Minicharged particles in light-shining-through-wall-experiments and the photon polarization tensor

Babette Döbrich^{1,2}, Holger Gies^{1,2} and Felix Karbstein^{1,2}

¹Theoretisch-Physikalisches Institut, Friedrich-Schiller-Universität Jena, Max-Wien-Platz 1, D-07743 Jena, Germany

² Helmholtz Institut Jena, Helmholtzweg 4, D-07743 Jena, Germany

DOI: http://dx.doi.org/10.3204/DESY-PROC-2011-04/karbstein_doebrich

A first theoretical feasibility study for a novel “light-shining-through-wall” scenario in the presence of an external magnetic field is performed. In contrast to standard scenarios, the barrier is not traversed by means of weakly interacting on-shell particles, but by virtual minicharged particle-antiparticle states. The study of this process heavily relies on the knowledge of the photon polarization tensor in the non-perturbative regime, and in particular requires its full momentum dependence, thereby rendering conventional approximations inapplicable. A first study and its results are presented and discussed in this contribution.

1 LSW with virtual particles - a motivation

“Light-shining-through-wall” (LSW) experiments are a versatile means in the search for numerous theoretically well-motivated “weakly interacting slim particles” (WISPs) that are proposed to exist beyond the standard model of particle physics. In standard LSW scenarios the barrier is ‘tunneled’ by *real*, i.e., on-shell WISPs. Their paradigm is the LSW scenario with axions or, more generally, axion-like particles (ALPs). LSW with axion-like particles is possible if the laser probe photons are converted into real ALPs in front of the wall and reconverted into photons behind that wall.

Intriguingly, LSW setups, although originally aimed at the detection of axions, are also sensitive to other WISPs, in particular to hidden photons and minicharged particles (MCPs); see [1, 2] and references therein for an overview and recent experimental results. For example, if MCPs and hidden photons exist, “light-shining-through-wall” is also possible by means of a real hidden photon: Photons can be converted into hidden photons through an intermediate MCP loop within an external magnetic field. Similar to the LSW scenario with ALPs, the hidden photons are then assumed to traverse the barrier unhindered and can thereafter be reconverted into photons [3]. Note however that this LSW scenario can only provide combined bounds on the fractional charge of the minicharged particles and the hidden-photon coupling.

A different LSW scenario for MCPs proposed recently in [5], is the ‘tunneling’ of a barrier through generally *virtual* particle-antiparticle intermediate states, cf. Fig. 1. This scenario, also referred to as “tunneling of the third kind”, is interesting from an experimental point of view since it could provide for *direct* bounds on the fractional charge of the MCPs, without any reference to the coupling strength of hidden photons. It has however been shown, that

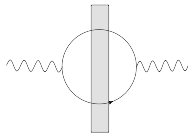


Figure 1: LSW scenario with virtual minicharged particles, also referred to as ‘tunneling of the 3rd kind’, cf. [5]. A spontaneous oscillation into a minicharged particle-antiparticle pair which traverses a light blocking barrier freely, enables the photon to effectively “shine through a wall”.

- in the absence of an external field - bounds derived from this LSW scenario are typically less restrictive than current laboratory limits for minicharged particles [5]. In this note, we briefly discuss the same scenario in the presence of a constant external magnetic field. We limit the discussion to fermionic minicharged particles. From the viewpoint of theory, tackling this problem in an external field is far more involved than the corresponding problem in the absence of a field. In particular, it turns out that new insights into the polarization tensor in external magnetic fields, which enters the computation of the photon-to-photon transition probability, are necessary. More detailed considerations and results are forthcoming [4].

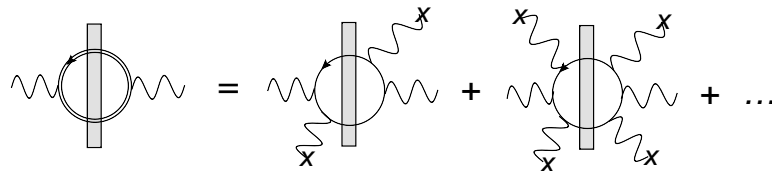


Figure 2: Same scenario as in Fig. 1, but now in the presence of an external magnetic field. The dressed propagator of the minicharged particles, accounting for all possible insertions of the external field, is represented by the double solid line. As argued in the main text, to make experimentally relevant predictions, a computational restriction to the lowest order perturbative corrections in the external field is insufficient.

Let us briefly introduce the basic equations which are needed to compute the transition probability for the tunneling scenario depicted in Fig. 2. The wall is assumed to be perpendicular to the propagation direction of the photons. A detailed presentation for the zero-field case can be found in [5]. The essential point to note here, is that the dressed particle-antiparticle loop traversing the wall in Fig. 2 corresponds to the one-loop photon polarization tensor in an external magnetic field, $\Pi^{\mu\nu}(x, x'|B)$, with the quantum loop run by minicharged particles. Hence, we start with the effective field theory describing photon propagation in a constant external magnetic field of strength $B = |\vec{B}|$, given by the following Lagrangian,

$$\mathcal{L}[A] = -\frac{1}{4}F_{\mu\nu}(x)F^{\mu\nu}(x) - \frac{1}{2} \int_{x'} A_\mu(x)\Pi^{\mu\nu}(x, x'|B)A_\nu(x'), \tag{1}$$

where $F_{\mu\nu}$ denotes the field strength tensor of the classical, macroscopic photon field A_μ . As the minicharged particles traverse the wall unhindered, translational invariance is maintained on the level of the polarization tensor at one-loop order, as long as the B field is homogeneous in the relevant space-time region, implying $\Pi^{\mu\nu}(x, x'|B) = \Pi^{\mu\nu}(x - x'|B)$.

Hence, upon a variation of Eq. (1) and a transformation to momentum space, the following equation of motion is obtained

$$(k^2 g^{\mu\nu} - k^\mu k^\nu + \Pi^{\mu\nu}(k)) A_\nu(k) = 0 . \tag{2}$$

We use a metric with signature $(-, +, +, +)$, i.e., $k^2 = \vec{k}^2 - \omega^2$.

In a next step, we impose reflecting boundary conditions at the wall for the incoming photons and determine the fluctuation induced current behind the wall with absorbing boundary conditions. The detector is assumed to be positioned asymptotically far from the back side of the wall. The photon-to-photon transition probability depends on the polarization mode of the photons. In the presence of an external field there are three independent polarization modes, henceforth labeled by an index $p = 1, 2, 3$. As the vacuum speed of light in external fields deviates from its zero-field value, and the vacuum exhibits medium-like properties, the occurrence of three (instead of two in the absence of an external field) independent polarization modes is not surprising.

Defining projectors $P_p^{\mu\nu}$ onto these modes, as done explicitly in Sect. 2 below, the photon-to-photon transition probability for photons polarized in the mode p , is given by

$$P_p^{\gamma \rightarrow \gamma} = \left| \int_d^\infty dx' \frac{e^{-i\omega x'}}{2\omega} \int_{-\infty}^0 dx'' P_p^{\mu\nu} \Pi_{\nu\mu}(x' - x'') \sin(\omega x'') \right|^2, \quad (3)$$

with ω denoting the photon frequency, and d the thickness of the wall.

2 The photon polarization tensor and its approximations

Let us now briefly introduce the photon polarization tensor in the presence of an external field. We stick to its representation in the propertime formalism [6] at one-loop level. The corresponding expression is known for arbitrary homogeneous, externally set electromagnetic field configurations in terms of a double parameter integral [7, 8]. Here we limit ourselves to the special case of a purely magnetic field [9]. This naturally suggests a decomposition of the photon four-momentum k^μ in components parallel and perpendicular to the magnetic field vector \vec{B} . Without loss of generality \vec{B} is assumed to point in \vec{e}_1 -direction, and the following decomposition is adopted,

$$k^\mu = k_\parallel^\mu + k_\perp^\mu, \quad k_\parallel^\mu = (\omega, k^1, 0, 0), \quad k_\perp^\mu = (0, 0, k^2, k^3). \quad (4)$$

In the same manner, tensors can be decomposed, e.g., $g^{\mu\nu} = g_\parallel^{\mu\nu} + g_\perp^{\mu\nu}$. It is then convenient to introduce the following projection operators onto photon polarization modes,

$$P_1^{\mu\nu} = g_\parallel^{\mu\nu} - \frac{k_\parallel^\mu k_\parallel^\nu}{k_\parallel^2}, \quad \text{and} \quad P_2^{\mu\nu} = g_\perp^{\mu\nu} - \frac{k_\perp^\mu k_\perp^\nu}{k_\perp^2}. \quad (5)$$

Defining a third projector as follows,

$$P_3^{\mu\nu} = g^{\mu\nu} - \frac{k^\mu k^\nu}{k^2} - P_1^{\mu\nu} - P_2^{\mu\nu}, \quad (6)$$

the three projectors $P_p^{\mu\nu}$ obviously span the transverse subspace. Whereas two of these polarization modes can be continuously related to the photon polarization modes in the absence of an external magnetic field, the third mode manifests itself in the presence of the external field only.

Note that $P_1^{\mu\nu}$ and $P_2^{\mu\nu}$ have an intuitive interpretation, given that $\vec{k} \not\parallel \vec{B}$. Namely, they project onto photon modes polarized parallel and perpendicular to the plane spanned by the

two vectors, \vec{k} and \vec{B} . For $\vec{k} \nparallel \vec{B}$ these are the polarization modes, that can be continuously related to those in the zero-field limit. Remarkably, for the special alignment of $\vec{k} \parallel \vec{B}$, the situation is different. Here, the modes 2 and 3 can be continuously related to the two zero-field polarization modes.

With the help of Eqs. (5) and (6), the photon polarization tensor in a purely magnetic field can be decomposed as follows [7],

$$\Pi^{\mu\nu}(k) = \Pi_1(k) P_1^{\mu\nu} + \Pi_2(k) P_2^{\mu\nu} + \Pi_3(k) P_3^{\mu\nu}, \quad (7)$$

where the scalar functions Π_p are the components of the polarization tensor in the respective subspaces. The coupling of the MCPs to photons is ϵe , with ϵ referring to a dimensionless fractional coupling, and m denotes the mass of the MCPs. Specifying $\epsilon \equiv 1$ and identifying m with the electron mass, the photon polarization tensor of standard quantum electrodynamics is retained. The general structure of the scalar components is

$$\Pi_p(k) = (\epsilon e)^2 \int_0^\infty \frac{ds}{s} \int_{-1}^{+1} \frac{d\nu}{2} e^{-i\Phi_0(k,\nu,z)s} f_p(k,\nu,z), \quad (8)$$

with the dependence on the magnetic field encoded in the variable $z \equiv \epsilon e B s$. Here, the parameter s denotes the proptime, and the parameter ν governs the momentum distribution within the loop. The explicit expressions for the functions f_p can be found in [7], and the phase factor in the argument of the exponential function reads

$$\Phi_0 = m^2 + \frac{1-\nu^2}{4} k_\parallel^2 + \frac{\cos \nu z - \cos z}{2z \sin z} k_\perp^2. \quad (9)$$

In particular due to the complicated functional dependence on s in Eq. (9), the proptime integral in general cannot be performed analytically, and is also hard to tackle numerically. Hence, basically all explicit insights into the photon polarization tensor in the presence of a constant magnetic field can be traced back to three well-established approximations:

- a perturbative expansion in the number of external field insertions (cf. Fig. 2), which can be associated with the limit $\frac{\epsilon e B}{m^2} \ll 1$,
- a quasi-classical approximation [10] developed in the seminal works of Tsai and Erber [11, 12], derived “on-the-light-cone”, i.e., for $k^2 = 0$, and restricted to $\frac{k_\perp^2}{\epsilon e B} \gg 1$ only [4], and
- the restriction to the lowest Landau level, or equivalently a “large- z ” expansion [13, 14], valid in the limit where $\frac{\epsilon e B}{m^2} \gg 1$, and commonly utilized below pair-creation threshold, $\omega^2 < 4m^2$.

Concerning MCPs, neither their fractional charge ϵe , nor their mass m is restricted *a priori*, which means that in principle arbitrary values for the ratio $\frac{\epsilon e B}{m^2}$ are possible. Given that the zero-field bounds, and therewith also these for $\frac{\epsilon e B}{m^2} \ll 1$, fall into a parameter regime in the ϵ - m plane already excluded by means of other laboratory experiments, we subsequently aim at gaining insights into the parameter regime where $\frac{\epsilon e B}{m^2} \gg 1$. As the full momentum dependence is essential for the virtual tunneling process, none of the approximations listed above is applicable here.

However, reconsidering Eqs. (8) and (9), a significant simplification can be expected in the special situation where $\vec{k} \parallel \vec{B}$, which implies that $k_{\perp}^2 \equiv 0$. In this limit the z -dependence in Eq. (9) drops out, and the proptime integration can even be performed analytically [4]; see also [15, 16]. Combining the “large- z ” expansion with an analytic continuation in B , we recently devised a strategy to surpass the pair creation threshold [4], indicating that the 1-component of the polarization tensor in the limit $\vec{k} \parallel \vec{B}$ indeed results in the maximum transition probability, achievable in the tunneling process with virtual MCPs in the regime where $\frac{\epsilon e B}{m^2} \gg 1$. This can be traced back to the fact that the lowest Landau level is unscreened only for this component.

Note, that the situation is somewhat subtle, as in the strict limit $\vec{k} \parallel \vec{B}$, exactly this component corresponds to the polarization mode that cannot be continuously related to any of the two polarization modes in the absence of an external field. The question if and how this particular mode can be excited is disputed in the literature [15, 16]. However, as discussed above, it turns out that for any non-vanishing angle between \vec{k} and \vec{B} , the 1-mode can be continuously related to one of the photon polarization modes in the absence of an external field, but as a function of the angle between \vec{k} and \vec{B} receives an exponential suppression as compared to its maximum in the asymptotic limit $\sphericalangle(\vec{k}, \vec{B}) \rightarrow 0$.

3 Transition probability for LSW with virtual MCPs

Hence, in order to estimate the maximum achievable photon to photon transition probability in the regime where $\frac{\epsilon e B}{m^2} \gg 1$, we subsequently exclusively focus on the 1-component of the photon polarization tensor and limit ourselves to the special alignment $\vec{k} \parallel \vec{B}$. Let us emphasize that this is an essential difference to conventional LSW setups, where the magnetic field is applied perpendicular to the propagation direction of the photons.

We then find that the maximum achievable photon transition probability (cf. Eq. (3)) in the limits $md \ll 1$ and $m \ll \omega$ is well approximated by the following simple formula,

$$P_{\max}^{\gamma \rightarrow \gamma} \simeq \left(\frac{\epsilon^2 e^2}{24\pi^2} \right)^2 \left(\frac{\epsilon e B}{m^2} \right)^2. \quad (10)$$

To understand the elementary dependencies of this transition probability, it is useful to consider the fluctuations of the MCPs in position space where their associated space-time trajectories have an intrinsic length scale of the order of the Compton wavelength $\sim 1/m$. For $md \ll 1$, this size of the fluctuations exceeds the thickness of the wall. Thus, the transition probability becomes d -independent. In the limit $m/\omega \ll 1$, also the dependence on the probe photon wavelength drops out as the large Compton wavelength of the virtual fluctuations dominates all other length scales. Note, however that in an actual experiment, the smallest testable minicharged mass is limited by the extent and the scale of homogeneity of the external magnetic field.

As outlined above, the transition rate as given in Eq. (10) is the maximal transition rate, which can only asymptotically be reached in an experiment. In practice, it is therefore necessary to choose a finite but preferably very small angle between the propagation direction of the photons and the external magnetic field. This introduces an exponential suppression factor in Eq. (10) (cf. Sect. 2), which reduces the transition probability as a function of the photon incidence angle $\sphericalangle(\vec{k}, \vec{B})$ and the ratio $\frac{\epsilon e B}{m^2}$. However, for experimentally feasible photon incidence angles, this additional suppression does not result in any severe reduction of the testable parameter space for minicharged particles [4].

4 Towards a new test of MCPs

We have performed a first theoretical feasibility study for a novel “light-shining-through-wall” scenario in the presence of an external magnetic field. In this scenario, the barrier is traversed by means of virtual particle-antiparticle states, rather than by on-shell particles. We argued that the evaluation of the corresponding photon-to-photon transition probability requires profound knowledge of the photon polarization tensor in the presence of external fields, and in particular requires to keep its full momentum dependence. As established approximations for the photon polarization tensor are inappropriate here, we focused on a special alignment of the photon propagation direction and the external magnetic field. Based on the insights obtained in this limit, we devised a strategy that allows for a solid estimate of the transition probability beyond this special alignment also. Further details of this investigation are forthcoming [4].

Building on the in-depth experience with LSW setups in the experimental community, we hope that these considerations can soon lead to a novel experiment that puts the existence of minicharged particles to the test.

B.D. and H.G. acknowledge support by the DFG under grants SFB-TR18 and GI 328/4-1 (Heisenberg program) as well as GRK-1523. We thank N. Neitz for collaboration on the presented topics, and J. Jaeckel and A. Lindner for interesting discussions and helpful correspondence.

References

- [1] J. Redondo, A. Ringwald, *Contemporary Physics* **52**, 3 (2011) [arXiv:1011.3741 [hep-ph]].
- [2] K. Ehret *et al.*, *Phys. Lett. B* **689**, 149 (2010) [arXiv:1004.1313 [hep-ex]].
- [3] M. Ahlers, H. Gies, J. Jaeckel *et al.*, *Phys. Rev.* **D76**, 115005 (2007) [arXiv:0706.2836 [hep-ph]].
- [4] B. Döbrich, H. Gies, N. Neitz and F. Karbstein, in preparation (2011)
- [5] H. Gies and J. Jaeckel, *JHEP* **0908**, 063 (2009) [arXiv:0904.0609 [hep-ph]].
- [6] J. S. Schwinger, *Phys. Rev.* **82**, 664 (1951).
- [7] W. Dittrich and H. Gies, *Springer Tracts Mod. Phys.* **166**, 1 (2000).
- [8] I. A. Batalin and A. E. Shabad, *Sov. Phys. JETP* **33**, 483 (1971).
- [9] L. F. Urrutia, *Phys. Rev. D* **17**, 1977 (1978).
- [10] V. N. Baier, V. M. Katkov, *Phys. Lett.* **A374**, 2201-2206 (2010). [arXiv:0912.5250 [hep-ph]].
- [11] W. y. Tsai and T. Erber, *Phys. Rev. D* **10**, 492 (1974).
- [12] W. y. Tsai and T. Erber, *Phys. Rev. D* **12**, 1132 (1975).
- [13] A. E. Shabad, *Annals Phys.* **90**, 166 (1975).
- [14] A. E. Shabad, arXiv:hep-th/0307214.
- [15] R. A. Cover, G. Kalman, *Phys. Rev. Lett.* **33**, 1113-1116 (1974).
- [16] W. Y. Tsai and T. Erber, *Acta Phys. Austriaca* **45**, 245 (1976).

Notes from the 5th Axion Strategy Meeting

Giovanni Cantatore

Università and INFN Trieste, Trieste, Italy

DOI: http://dx.doi.org/10.3204/DESY-PROC-2011-04/cantatore_giovanni

This note contains a brief summary of the informal discussions which took place during the *5th Axion Strategy Meeting* held on the last day of the 7th Patras Workshop.

1 Introduction

The ending day of the 7th Patras Workshop was marked by the *5th Axion Strategy Meeting (ASM)*, which continued a series of informal round tables started in January 2009 at CERN. The second ASM was held in Durham, also in 2009, at the end of the 5th Patras Workshop, while the third Axion Strategy Meeting took place during the "Axions 2010" conference held in January 2010 in Florida. Finally, the 4th ASM was hosted in the 2010 6th Patras Workshop in Zurich. The 5th Axion Strategy Meeting came after a one year interval, which was agreed upon as a more meaningful time span between meetings.

The originally formulated "mission statement" of the strategy meeting was to "provide a round table environment for the community of physicists, both theorists and experimentalists, working in axion, and more generally in WISP physics, to freely float ideas and informally discuss them in order to discern the global trend of the field and identify interesting and promising directions for future developments."

This format has proved valid and fruitful in the course of the series. The 5th ASM was widely attended and the discussion was more than lively, touching all the fundamental themes of the field, seeing also the active participation of the younger attendants to the 7th Patras Workshop.

2 Notes from the discussion

It has become clear in occasion of the 5th ASM that the "Axion Strategy" title no longer completely covers the spirit of the discussion, since in recent times the field of interest has widened considerably to include objects such as hidden photons (paraphotons) and chameleons, giving full meaning to the WISP acronym. For these and other particles, research is moving beyond theoretical formulations and initial "parasitical" searches on to well-aimed experimental detection efforts. This was widely recognized as a very welcome development, both from a scientific point of view and from the point of view of the never ending search for funds.

The 5th ASM was also marked by the participation of several researchers working in the WIMP field, who stayed on after attending the Patras Workshop sessions. This is a clear signal that the central problem of identifying all the unknown constituents of the universe is starting to be seen more and more as a unitary scientific quest having several complementary aspects.

One of the recurring themes of past strategy meetings was the perception of the need to form a more closely tied community of physicists working in the WISP field. This goal appeared closer during the meeting. Here the discussion evidenced the ties between existing experimental groups, as in the case of the ALPS-CAST contacts or of the forming group in the US centered on the Fermilab facilities, and the coagulation of large scale international collaborations to start future advanced projects, as in the case of the next generation axion helioscope. This trend in the WISP community follows the successful ones in the WIMP community, where, for instance, a data sharing program has been started between the CDMS and EDELWEISS experiments, and in the gravity wave community, where a large "world observatory" has been formed by coordinating data taking and by sharing data between VIRGO and LIGO.

There was unanimous agreement that Konstantin Zioutas must be specially thanked for his successful efforts in bringing the WISP community together, both physically and intellectually.

Almost all active experiments and all future ones plan to search for chameleons or hidden photons, or both. ADMX, for instance, intends to search for chameleon interactions. There are also ideas to look for hidden photons with microwave cavities, while the SHIPS collaboration in Hamburg will soon start directly searching for hidden photons emitted by the sun. In addition, other WISPs, such as Mini Charged Particles, could be produced and detected with a light-shining-through-a-wall (LSW) scheme. The search for axions, however, particularly for the QCD axion, is still the mainstream of the WISP field. In fact axions are also very often searched for "parasitically" in WIMP and neutrino experiments.

From a theoretical point of view, it was pointed out that axions are still Dark Matter candidates even in the case of a "nightmare scenario" at LHC, where nothing is found after the available energy range is explored. The axion case is also reinforced by Pierre Sikivie's opinion that the bulk of DM is made up of axions. This view sparked a discussion on whether galactic axions form Bose-Einstein condensates and caustics, resulting in an impact on observatory-type searches. Astrophysics proved again a source of surprises: many comments centered on the so-called "White Dwarf" data, based on the observation of cooling rates, which point at an axion coupling to electrons of $g \approx 2.24 \cdot 10^{-13} \text{ GeV}^{-1}$ with a mass $\approx 8 \text{ meV}$. This mass value would interestingly place QCD axions right within "the gap" in the axion-photon-coupling vs. mass plane, where no present experiment has yet access.

Regarding detection techniques, the main avenue of approach remains as always the axion coupling to photons, thus the stress is placed more than ever on low background single photon detection at all the energies of interest, such as eV scale for LSW experiments, or keV scale for observatories such as CAST. The other interesting technique also unfolding in the WISP field is cryogenics, both as a way to access the superconducting regime, as in cavity experiments, and as a direct way to minimize detector background.

As a final note, it must be pointed out that the *CAST barrier*, that is the experimental bound set by CAST in the axion-like particles parameter space, is still the standard towards which present and projected experimental performances are compared.

3 Conclusions

The series of informal, round table style, Axion Strategy Meetings continued successfully in Mykonos with the 5th ASM having rising attendance and intense discussions. The present meeting, while touching all the main subjects in WISP research, above all gave all present a real sense of a community sharing ambitious scientific goals and the strong will to attain them.

If a personal view is allowed here, it is my opinion that this should be regarded as the most important outcome of the 5th Axion Strategy Meeting.

4 Acknowledgments

A heartfelt thank you goes to all colleagues who took the time and put in the effort to actively participate in the 5th Axion Strategy Meeting, making it a worthwhile addition to the 7th Patras Workshop.

Chapter 3

Solar Axions

CAST: Status and Latest Results

*T. Dafni*¹, *S. Aune*², *K. Barth*³, *A. Belov*⁴, *S. Borghi*^{22,3}, *H. Bräuninger*⁵, *G. Cantatore*⁶, *J. M. Carmona*¹, *S. A. Cetin*⁷, *J. I. Collar*⁸, *M. Davenport*³, *C. Eleftheriadis*⁹, *N. Elias*³, *C. Ezer*⁷, *G. Fanourakis*¹⁰, *E. Ferrer-Ribas*², *P. Friedrich*⁵, *J. Galán*¹, *J. A. García*¹, *A. Gardikiotis*¹², *E. N. Gazis*¹³, *T. Gerasis*¹⁰, *I. Giomataris*², *S. Gninenko*⁴, *H. Gómez*¹, *E. Gruber*¹¹, *T. Guthörl*¹¹, *R. Hartmann*^{23,14}, *F. Haug*³, *M. D. Hasinoff*¹⁵, *D. H. H. Hoffmann*¹⁶, *F. J. Iguaz*^{2,1}, *I. G. Irastorza*¹, *J. Jacoby*¹⁷, *K. Jakovčić*¹⁸, *M. Karuza*⁶, *K. Königsmann*¹¹, *R. Kotthaus*¹⁹, *M. Krčmar*¹⁸, *M. Kuster*^{24,5,16}, *B. Lakić*¹⁸, *J. M. Laurent*³, *A. Liolios*⁹, *A. Ljubičić*¹⁸, *V. Lozza*⁶, *G. Lutz*^{23,14}, *G. Luzón*¹, *J. Morales*^{1*}, *T. Niinikoski*^{25,3}, *A. Nordt*^{3,5,16}, *T. Papaevangelou*², *M. J. Pivovarov*²⁰, *G. Raffelt*¹⁹, *T. Rashba*²¹, *H. Riege*¹⁶, *A. Rodríguez*¹, *M. Rosu*¹⁶, *J. Ruz*^{1,3}, *I. Savvidis*⁹, *P. S. Silva*³, *S. K. Solanki*²¹, *L. Stewart*³, *A. Tomás*¹, *M. Tsagri*^{3,12}, *K. van Bibber*^{26,20}, *T. Vafeiadis*^{3,9,12}, *J. Villar*¹, *J. K. Vogel*^{20,11}, *S. C. Yildiz*⁷ and *K. Zioutas*^{3,12}

¹Instituto de Física Nuclear y Altas Energías, Universidad de Zaragoza, Zaragoza, Spain

²IRFU, Centre d'Études Nucléaires de Saclay (CEA-Saclay), Gif-sur-Yvette, France

³European Organization for Nuclear Research (CERN), Genève, Switzerland

⁴Institute for Nuclear Research (INR), Russian Academy of Sciences, Moscow, Russia

⁵Max-Planck-Institut für Extraterrestrische Physik, Garching, Germany

⁶Instituto Nazionale di Fisica Nucleare (INFN), Sezione di Trieste and Università di Trieste, Trieste, Italy

⁷Dogus University, Istanbul, Turkey

⁸Enrico Fermi Institute and KICP, University of Chicago, Chicago, IL, USA

⁹Aristotle University of Thessaloniki, Thessaloniki, Greece

¹⁰National Center for Scientific Research "Demokritos", Athens, Greece

¹¹Albert-Ludwigs-Universität Freiburg, Freiburg, Germany

¹²Physics Department, University of Patras, Patras, Greece

¹³National Technical University of Athens, Athens, Greece

¹⁴MPI Halbleiterlabor, München, Germany

¹⁵Department of Physics and Astronomy, University of British Columbia, Vancouver, Canada

¹⁶Technische Universität Darmstadt, IKP, Darmstadt, Germany

¹⁷Johann Wolfgang Goethe-Universität, Institut für Angewandte Physik, Frankfurt am Main, Germany

¹⁸Rudjer Bošković Institute, Zagreb, Croatia

¹⁹Max-Planck-Institut für Physik (Werner-Heisenberg-Institut), München, Germany

²⁰Lawrence Livermore National Laboratory, Livermore, CA, USA

²¹Max-Planck-Institut für Sonnensystemforschung, Katlenburg-Lindau, Germany

²²Department of Physics and Astronomy, University of Glasgow, Glasgow, UK

²³PNSensor GmbH, München, Germany

²⁴European XFEL GmbH, Notkestrasse 85, 22607 Hamburg, Germany

²⁵Excellence Cluster Universe, Technische Universität München, Garching, Germany

²⁶Naval Postgraduate School, Monterey, CA, USA

DOI: <http://dx.doi.org/10.3204/DESY-PROC-2011-04/dafni.theopisti>

In July 2011, CAST finished the data-taking of its nominal programme, having scanned axion masses up to $\sim 1.18 \text{ eV}/c^2$. Here we present the first results of the data taken in 2008, first year of the last data-taking campaign when ^3He was used inside the magnet bores. No excess of signal over background has been recorded, and an upper limit has been set to the axion-to-photon coupling to $2.3 \times 10^{-10} \text{ GeV}^{-1}$ for axion masses between 0.39 and 0.64 eV. CAST remains the most sensitive axion helioscope and for the first time crosses the benchmark line of the KSVZ model at the upper end of the spectrum.

1 Introduction

The CERN Axion Solar Telescope (CAST) is looking for axions and axion-like particles since 2003. The axions are hypothetical particles arising in models which may explain the CP problem of strong interactions and can be Dark Matter candidates. With the help of a decommissioned LHC dipole magnet hopes to convert axions produced by the Primakoff process in the solar core into detectable x-ray photons. These photons would carry the energy and the momentum of the original axion. CAST is the most sensitive axion helioscope built so far. Its sensitivity is based on three points, a powerful magnet, an x-ray focusing device and low-background detectors. The magnet employed in CAST is an LHC dipole prototype, which can reach 9 T along the 9 m of its length. With the help of a moving platform, it is aligned with the center of the sun for 90 min twice a day. A total of four detectors are connected at the two ends of the magnet, two looking at sunrise and two at sunset.

CAST has been taking data since 2003. During 2003 and 2004 the experiment operated with vacuum in the magnet bores (CAST phase I) and set the best experimental limit on the axion-photon coupling constant in the range of axion masses up to $0.02 \text{ eV}/c^2$ [1, 2]. For CAST, above this mass the sensitivity is degraded due to coherence loss. The experimental setup was upgraded in 2005 in order to extend the sensitivity to higher axion masses. For this purpose, the experiment has to operate with the magnet bores filled with a buffer gas whose density has to be increased in appropriate steps to cover equally a range of higher axion masses. During 2005 and 2006, ^4He was used as a buffer gas and the experiment scanned the range of axion masses from $0.02 \text{ eV}/c^2$ to $0.39 \text{ eV}/c^2$ and set the most restrictive limit on the axion-photon coupling constant for this range of masses [3]. Furthermore, for the first time the theoretically favoured region of masses has been probed. Due to the condensation of ^4He at high pressures (aprox. 14 mbar at 1.8 K, the operating temperature of the CAST magnet), the system had to be thoroughly upgraded to use ^3He as a buffer gas. In parallel, CAST has been looking into other related searches, such as high energy axions [4], 14.4 keV axions from M1 transitions in the sun [5] and low energy axions in the visible [6].

2 Upgrades and latest results

After the ^4He data-taking, several upgrades were necessary in order to prepare for data taking with ^3He . The most important of these was the design and installation of a sophisticated ^3He gas system. As mentioned above, in order to scan over a range of axion masses, CAST fills the cold bores with gas in incremental steps. It is essential to know and reproduce the exact gas density inside the bores but also to ensure that the density remains homogeneous along the bores. To achieve the desired gas density, the amount of gas introduced into the cold bores

*Deceased.

needs to be accurately calculated, with the help of several temperature and pressure sensors, strategically placed in the magnet and the gas system. A lot of effort has been invested from the collaboration in order to perform extensive simulations for a most detailed model of the system under the different configurations and the calculations of the gas density, which have to be performed through computational fluid dynamic (CFD) simulations. The achieved agreement between the simulated and measured parameters allow us to believe that despite the variations in the value of the temperature and gas density, this latter remains homogeneous along the magnet.

During the ^3He data taking, the CAST x-ray detectors were upgraded as well. The number of Micromegas detectors was increased from one to three, when the Time Projection Chamber (TPC) with a multi-wire proportional readout [7] that had covered both bores of the sunset end of the magnet was replaced. The two sunset microbulks use the shielding that was already in place for the TPC detector, while the sunrise detector counts with a dedicated shielding since the latest upgrade [8, 9, 10]. The microbulk detectors belong to the latest generation of Micromegas and the ones installed in CAST have obtained background levels down to 5×10^{-6} counts $\text{keV}^{-1} \text{cm}^{-2} \text{s}^{-1}$ in the energy range of interest, already one order of magnitude better than the previous ones [11]. On the other hand, the x-ray mirror telescope with a pn-CCD chip [12] covering the other bore of the sunrise side remained unchanged.

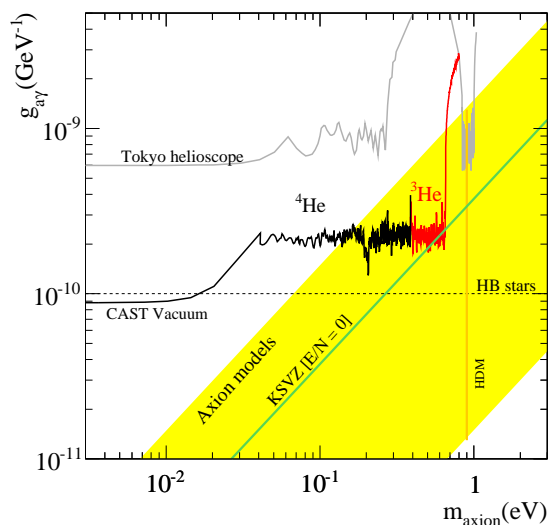


Figure 1: The CAST exclusion plot after the different phases of the experiment: in vacuum [1, 2], ^4He [3] and ^3He [13] phase. The limit achieved in the ^3He CAST phase for axion mass range between 0.39 eV and 0.64 eV. The results from the Tokyo helioscope [14, 15, 16], horizontal branch (HB) stars [17], and the hot dark matter (HDM) bound [18] are also shown. The yellow band represents typical theoretical models with. The green solid line corresponds to $E/N = 0$ (KSVZ model).

Here we present the results obtained from the data-taking in 2008, the first year of operation with ^3He . The axion mass range scanned was between 0.39 eV and 0.64 eV. The data analysis performed is similar to the results obtained with ^4He gas. The differences are mainly due to the overall reduction of background rates achieved by CAST detectors with respect to the ones of the ^4He phase, as well as the reduced ^3He density setting exposure time of the overall data taking period. Figure 1 presents these results: CAST has extended the last exclusion plot towards higher axion masses, probing further inside the theoretically favoured region and excluding the axion-photon coupling down to $2.3 \times 10^{-10} \text{GeV}^{-1}$ for axion masses between 0.39 and 0.64 eV [13], the exact value depending on the pressure setting. It is the first time that the limit given by the KSVZ model is crossed.

2.1 The next steps

Currently, the collaboration is analysing the remaining of the data, from the campaigns of 2009 through the summer of 2011. In parallel, there are preparations in course regarding the short- and long-term future of the experiment. Given the latest upgrades of the system, the first idea would be to repeat the measurements with ^4He in the magnet bores. Focusing on the detectors which now obtain rather low backgrounds, one can expect an improvement on the limits already set by CAST which will lower the sensitivity in the range of most interest and will probably probe the KSVZ line at lower masses. As a second step, the vacuum-phase of CAST could be revisited. Work is also done towards lowering the detector thresholds; in this way, when the system will be back to vacuum operation, other studies could be foreseen, regarding paraphotons [19] and solar chameleons [20]. A feasibility study of a new generation axion helioscope is ongoing [21]. This initiative includes the construction of a new toroidal magnet with much larger magnetic volume, together with exhaustive use of x-ray optics and low background detectors. A sensitivity of more than one order of magnitude in the axion-to-photon coupling beyond CAST seems feasible.

3 Conclusions

CAST presents the first results of the data taken when using ^3He as buffer gas inside the magnet bores. The axion-to-photon coupling has been excluded to $2.3 \times 10^{-10} \text{ GeV}^{-1}$ for axion masses between 0.39 and 0.64 eV. The remaining of the data taken, which have reached axion masses up to 1.18 eV are being analysed. Short term prospects include revising some ^4He and vacuum configurations, given the improved performance of the detectors. For the longer term, studies of a new generation axion helioscope are ongoing

4 Acknowledgments

We thank CERN for hosting the experiment and for the technical support. We acknowledge support from NSERC (Canada), MSES (Croatia) under the grant number 098-0982887-2872, CEA (France), BMBF (Germany) under the grant numbers 05 CC2EEA/9 and 05 CC1RD1/0 and DFG (Germany) under grant numbers HO 1400/7-1 and EXC-153, the Virtuelles Institut für Dunkle Materie und Neutrinos –VIDMAN (Germany), GSRT (Greece), RFFR (Russia), the Spanish Ministry of Science and Innovation (MICINN) under grants FPA2007-62833 and FPA2008-03456, Turkish Atomic Energy Authority (TAEK), NSF (USA) under Award number 0239812, US Department of Energy, NASA under the grant number NAG5-10842. Part of this work was performed under the auspices of the US Department of Energy by Lawrence Livermore National Laboratory under Contract DE-AC52-07NA27344. We acknowledge the helpful discussions within the network on direct dark matter detection of the ILIAS integrating activity (Contract number: RII3-CT-2003-506222).

References

- [1] K. Zioutas *et al.* [CAST Collaboration], “First Results from the CERN Axion Solar Telescope,” *Phys. Rev. Lett.* **94** 121301 (2005).
- [2] S. Adriamonte *et al.* [CAST Collaboration], “An improved limit on the axion-photon coupling from the CAST experiment,” *J. Cosmol. Astropart. Phys.* JCAP04(2007)01.

CAST: STATUS AND LATEST RESULTS

- [3] E. Arik *et al.* [CAST Collaboration], “Probing eV-scale axions with CAST,” J. Cosmol. Astropart. Phys. JCAP 02(2009)008.
- [4] S. Adriamonte *et al.* [CAST Collaboration], “Search for solar axion emission from ${}^7\text{Li}$ and $\text{D}(p,\gamma){}^3\text{He}$ nuclear decays with the CAST γ -ray calorimeter,” J. Cosmol. Astropart. Phys. JCAP03(2010)032.
- [5] S. Adriamonte *et al.* [CAST Collaboration], “Search for 14.4 keV solar axions emitted in the M1-transition of ${}^{57}\text{Fe}$ nuclei with CAST,” J. Cosmol. Astropart. Phys. JCAP12(2009)002.
- [6] G. Cantatore for the CAST collaboration, “Search for low Energy solar Axions with CAST,” [arXiv:0809.4581 [hep-ex]].
- [7] D. Autiero *et al.*, “The CAST time projection chamber,” New J. Phys. **9**, 171 (2007).
- [8] S. Adriamonte *et al.*, “Development and performance of Microbulk Micromegas detectors,” J. Instrum. JINST 5, P02001 (2010).
- [9] J. Galan *et al.*, “MICROMEGAS detectors in the CAST experiment,” J. Instrum. JINST 5, P01009 (2010).
- [10] S. Aune *et al.*, “New Micromegas detectors in the CAST experiment,” Nucl. Instrum. Meth. A **604**, 15 (2009).
- [11] P. Abbon *et al.*, “The Micromegas detector of the CAST experiment,” New J. Phys. **9**, 170 (2007).
- [12] M. Kuster *et al.*, “The x-ray telescope of CAST,” New J. Phys. **9**, 169 (2007).
- [13] S. Aune *et al.* [CAST Collaboration], “CAST search for sub-eV mass solar axions with ${}^3\text{He}$ buffer gas,” [arXiv:1106.3919 [hep-ex]].
- [14] S. Moriyama *et al.*, “Direct search for solar axions by using strong magnetic field and X-ray detectors,” Phys. Lett. B **434**, 147 (1998).
- [15] Y. Inoue *et al.*, “Search for sub-electronvolt solar axions using coherent conversion of axions into photons in magnetic field and gas helium,” Phys. Lett. B **536**, 18 (2002).
- [16] Y. Inoue *et al.*, “Search for solar axions with mass around 1 eV using coherent conversion of axions into photons,” Phys. Lett. B **668**, 93 (2008).
- [17] G. G. Raffelt, “Astrophysical Axion Bounds”, Lect. Notes Phys. **741**, 51 (2008).
- [18] S. Hannestad, A. Mirizzi, G. G. Raffelt and Y. Y. Y. Wong, “Neutrino and axion hot dark matter bounds after WMAP-7,” J. Cosmol. Astropart. Phys. JCAP08(2010)001.
- [19] S. Troitsky, proceedings of this conference.
- [20] P. Brax, A. Lindner and K. Zioutas, “Chameleon foreCAST,” [arXiv:1110.2583v2 [hep-ph]].
- [21] I. G. Irastorza *et al.*, “Towards a new generation axion helioscope,” J. Cosmol. Astropart. Phys. JCAP06(2011)013.

The International Axion Observatory (IAXO)

I. G. Irastorza¹, F. T. Avignone², G. Cantatore³, S. Caspi⁴, J. M. Carmona¹, T. Dafni¹, M. Davenport⁵, A. Dudarev⁵, G. Fanourakis⁶, E. Ferrer-Ribas⁷, J. Galán^{1,7}, J. A. García¹, T. Gerialis⁶, I. Giomataris⁷, S. Gninenko¹⁴, H. Gómez¹, D. H. H. Hoffmann⁸, F. J. Iguaz⁷, K. Jakovčić⁹, M. Krčmar⁹, B. Lakić⁹, G. Luzón¹, A. Lindner¹¹, M. Pivovarov¹⁰, T. Papaevangelou⁷, G. Raffelt¹², J. Redondo¹², A. Rodríguez¹, S. Russenschuck⁵, J. Ruz⁵, I. Shilon^{5,13}, H. Ten Kate⁵, A. Tomás¹, S. Troitsky¹⁴, K. van Bibber¹⁵, J. A. Villar¹, J. Vogel¹⁰, L. Walckiers⁵, K. Zioutas¹⁶

¹Laboratorio de Física Nuclear y Astropartículas, Universidad de Zaragoza, Zaragoza, Spain

²Department of Physics and Astronomy, University of South Carolina, Columbia, SC, USA

³Instituto Nazionale di Fisica Nucleare (INFN), Sezione di Trieste and Università di Trieste, Trieste, Italy

⁴Lawrence Berkeley National Laboratory, Berkeley, CA 94720, USA

⁵CERN, Geneva, Switzerland

⁶National Center for Scientific Research Demokritos, Athens, Greece

⁷IRFU, Centre d'Études Nucléaires de Saclay (CEA-Saclay), Gif-sur-Yvette, France

⁸Technische Universität Darmstadt, IKP, Darmstadt, Germany

⁹Rudjer Bošković Institute, Zagreb, Croatia

¹⁰Lawrence Livermore National Laboratory, Livermore, CA, USA

¹¹DESY, Hamburg, Germany

¹²Max-Planck-Institut für Physik, Munich, Germany

¹³Physics Department, Ben-Gurion University of the Negev, Beer-Sheva 84105, Israel

¹⁴Institute for Nuclear Research (INR), Russian Academy of Sciences, Moscow, Russia

¹⁵Naval Postgraduate School, Monterey, CA, USA

¹⁶University of Patras, Patras, Greece

DOI: http://dx.doi.org/10.3204/DESY-PROC-2011-04/irastorza_igor

The International Axion Observatory (IAXO) is a new generation axion helioscope aiming at a sensitivity to the axion-photon coupling of $g_{a\gamma} \gtrsim \text{few} \times 10^{-12} \text{ GeV}^{-1}$, i.e. 1–1.5 orders of magnitude beyond the one currently achieved by CAST. The project relies on improvements in magnetic field volume together with extensive use of x-ray focusing optics and low background detectors, innovations already successfully tested in CAST. Additional physics cases of IAXO could include the detection of electron-coupled axions invoked to explain the white dwarf cooling, relic axions, and a large variety of more generic axion-like particles (ALPs) and other novel excitations at the low-energy frontier of elementary particle physics. This contribution is a summary of our recent paper [1].

1 Introduction

The Peccei-Quinn (PQ) mechanism of dynamical symmetry restoration [2, 3] stands out as the most compelling solution of the strong CP problem. Central to the PQ mechanism is the axion [4, 5], the Nambu-Goldstone boson of a new spontaneously broken symmetry $U(1)_{\text{PQ}}$.

The properties of axions allow them to be produced in the early universe as coherent field oscillations and as such to provide all or part of the cold dark matter [6, 7].

It is still possible to find these “invisible axions” in realistic search experiments and in this way test a fundamental aspect of QCD. The generic $a\gamma\gamma$ vertex allows for axion-photon conversion in external electric or magnetic fields in analogy to the Primakoff effect for neutral pions. As shown in 1983 by Pierre Sikivie, the smallness of the axion mass allows this conversion to take place coherently over macroscopic distances, compensating for the smallness of the interaction strength [8]. Especially promising is to use the Sun as a source for axions produced in its interior by the Primakoff effect. Directing a strong dipole magnet toward the Sun allows one to search for keV-range x-rays produced by axion-photon conversion, a process best visualized as a particle oscillation phenomenon [9] in analogy to neutrino flavor oscillations. Three such helioscopes have been built, in Brookhaven [10], Tokyo [11] and at CERN [12]. The CERN Axion Solar Telescope (CAST) has just finished a 8-year long data taking period, having strongly improved on previous experiments and even surpassed astrophysical limits in some range of parameters, although axions have not been found.

We have shown [1] that large improvements in magnetic field volume, x-ray focusing optics and detector backgrounds with respect to CAST are possible. Based on these improvements, and on the experience gathered within CAST, we propose the International Axion Observatory (IAXO), a new generation axion helioscope. IAXO could search for axions that are 1–1.5 orders of magnitude more weakly interacting than those allowed by current CAST constraints. It appears conceivable to surpass the SN 1987A constraint on the axion mass, $m_a \lesssim 10\text{--}20$ meV, test the white-dwarf (WD) cooling hypothesis [13], and explore a substantial part of uncharted axion territory experimentally. Moreover, IAXO would explore other more generic models of weakly interacting sub-eV particles (WISPs) [15], in particular some ALPs models that have been invoked in the context of several unexplained astrophysical observations. Equipped with microwave cavities, this setup could also aim at detecting relic axions [16].

2 Experimental setup and expected sensitivity

IAXO will follow the basic conceptual layout of an enhanced axion helioscope seen in figure 1, which shows a toroidal design for the magnet, together with X-ray optics and detectors attached to each of the magnet bores. The improvements anticipated for each of the experimental parameters of the helioscope were quantified in [1], organized in four scenarios (IAXO 1 to 4) ranging from most conservative to most optimistic values (see table 1 of [1]). These values are justified by several considerations on the magnet, x-ray optics and detectors, that are briefly outlined in the following, but we refer to [1] for a detailed discussion.

The magnet parameters are the ones contributing mostly to the helioscope’s figure of merit. The CAST success has relied, to a large extent, on the availability of the first class LHC test magnet which was recycled to become part of the CAST helioscope. While going beyond CAST magnet’s B or L is difficult, the improvement may come however in the cross section area, which in the case of the CAST magnet is only 3×10^{-3} m². Substantially larger cross sections can be achieved, although one needs a different magnet configuration. It is an essential part of our proposal that a new magnet must be designed and built specifically for this application, if one aims at a substantial step forward in sensitivity. A toroidal configuration for the IAXO magnet is being studied with a total cross section area A of up to few m², while keeping the product of BL close to levels achieved for CAST.

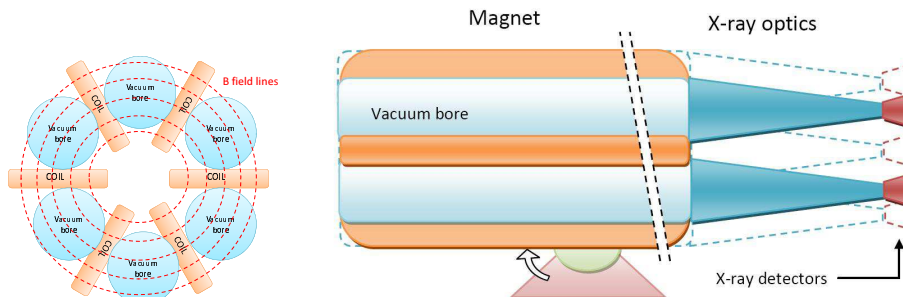


Figure 1: Possible conceptual arrangement for IAXO. On the left we show the cross section of the IAXO toroidal magnet, in this example with six coils and bores. On the right the longitudinal section with the magnet, the optics attached to each magnet bore and the x-ray detectors.

Another area for improvement will be the x-ray optics. Although CAST has proven the concept, only one of the four CAST magnet bores is equipped with optics. The use of focusing power in the entire magnet cross section A is implicit in the figures of merit defined in [1], and therefore the improvement obtained by enlarging A comes in part because a correspondingly large optic is coupled to the magnet. Here the challenge is not so much achieving exquisite focusing or near-unity reflectivity but the availability of cost-effective x-ray optics of the required size. IAXO's optics specifications can be met by a dedicated fabrication effort based on segmented glass substrate optics like the ones of HEFT or NuSTAR [14].

Finally, CAST has enjoyed the sustained development of its detectors towards lower backgrounds during its lifetime. The latest generation of Micromegas detectors in CAST are achieving backgrounds of $\sim 5 \times 10^{-6}$ counts $\text{keV}^{-1} \text{cm}^{-2} \text{s}^{-1}$. This value is already a factor 20 better than the backgrounds recorded during the first data-taking periods of CAST. Prospects for reducing this level to 10^{-7} counts $\text{keV}^{-1} \text{cm}^{-2} \text{s}^{-1}$ or even lower appear feasible.

The computed sensitivities of each of the four IAXO scenarios are represented by the family of blue lines in figure 2, both for hadronic axions (left) and non-hadronic ones (right). They include two data taking campaigns for each of the scenarios: one three years long performed without buffer gas (analogous to CAST I), and another three years long period with varying amounts of ^4He gas inside the magnet bore (analogous to CAST II, although without the need to use ^3He). In general, IAXO sensitivity lines go well beyond current CAST sensitivity for hadronic axions and progressively penetrate into the decade 10^{-11} – 10^{-12} GeV^{-1} , with the best one approaching 10^{-12} GeV^{-1} . They are sensitive to realistic QCD axion models at the 10 meV scale and exclude a good fraction of them above this. For non-hadronic axions, IAXO sensitivity lines penetrate in the DFSZ model region, approaching or even surpassing the red-giant constraints. Most relevantly, the IAXO 3 and IAXO 4 scenarios start probing the region of parameter space highlighted by the cooling of WDs.

References

- [1] I. Irastorza *et al.*, *Towards a new generation axion helioscope*, *JCAP* **1106** (2011) 013 [arXiv:1103.5334].
- [2] R. D. Peccei and H. R. Quinn, *Constraints imposed by CP conservation in the presence of instantons*, *Phys. Rev.* **D16** (1977) 1791.

THE INTERNATIONAL AXION OBSERVATORY (IAXO)

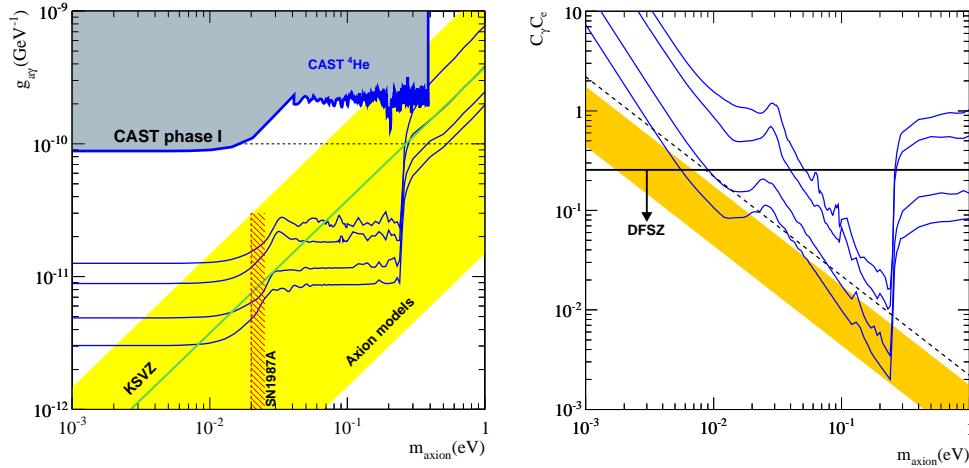


Figure 2: LEFT: The parameter space for hadronic axions and ALPs. The CAST limit, some other limits, and the range of PQ models (yellow band) are also shown. The blue lines indicate the sensitivity of the four scenarios discussed in the text. RIGHT: The expected sensitivity regions of the same four scenarios in the parameter space of non-hadronic axions with both electron and photon coupling. The orange band represents the region motivated by WD cooling, and the dashed line along the diagonal the red giants bound on the electron coupling. See [1] for details.

- [3] R. D. Peccei and H. R. Quinn, *CP Conservation in the presence of instantons*, *Phys. Rev. Lett.* **38** (1977) 1440.
- [4] S. Weinberg, *A New Light Boson?*, *Phys. Rev. Lett.* **40** (1978) 223.
- [5] F. Wilczek, *Problem of strong P and T invariance in the presence of instantons*, *Phys. Rev. Lett.* **40** (1978) 279.
- [6] P. Sikivie, *Axion cosmology*, *Lect. Notes Phys.* **741** (2008) 19 [[astro-ph/0610440](#)].
- [7] O. Wantz and E. P. S. Shellard, *Axion cosmology revisited*, *Phys. Rev.* **D82** (2010) 123508 [[arXiv:0910.1066](#)].
- [8] P. Sikivie, *Experimental tests of the “invisible” axion*, *Phys. Rev. Lett.* **51** (1983) 1415.
- [9] G. Raffelt and L. Stodolsky, *Mixing of the photon with low mass particles*, *Phys. Rev.* **D37** (1988) 1237.
- [10] D. M. Lazarus *et al.*, *A Search for solar axions*, *Phys. Rev. Lett.* **69** (1992) 2333.
- [11] S. Moriyama *et al.*, *Direct search for solar axions by using strong magnetic field and X-ray detectors*, *Phys. Lett.* **B434** (1998) 147 [[hep-ex/9805026](#)].
- [12] K. Zioutas *et al.*, *A decommissioned LHC model magnet as an axion telescope*, *Nucl. Instrum. Meth.* **A425** (1999) 480 [[astro-ph/9801176](#)].
- [13] J. Isern, E. Garcia-Berro, L. Althaus, and A. Corsico, *Axions and the pulsation periods of variable white dwarfs revisited*, *Astron. Astrophys.* **512** (2010) A86 [[arXiv:1001.5248](#)].
- [14] J. E. Koglin *et al.*, *Hard x-ray optics: from HEFT to NuSTAR*, *Proc SPIE* (2004) 856.
- [15] J. Jaeckel and A. Ringwald, *The Low-Energy Frontier of Particle Physics*, *Ann. Rev. Nucl. Part. Sci.* **60** (2010) 405 [[arXiv:1002.0329](#) [[hep-ph](#)]].
- [16] O. K. Baker *et al.*, [arXiv:1110.2180](#) [[physics.ins-det](#)].

Solar paraphotons

Sergey Troitsky

Institute for Nuclear Research of the Russian Academy of Sciences,
60th October Anniversary Prospect 7A, 117312, Moscow, Russia

DOI: http://dx.doi.org/10.3204/DESY-PROC-2011-04/troitsky_sergey

I revisit the question of production of paraphotons, or hidden photons, in the Sun and suggest that a simultaneous observations of solar flares by conventional instruments and by axion helioscopes may provide a discovery channel for paraphotons.

1 Introduction

Hidden sectors, which interact very weakly with the observable world, are a usual ingredient of theories extending the Standard Model and aimed at the explanation of its parameters and their hierarchies. Commonly, the interaction between the observable and hidden sectors is mediated by a very heavy particle and appears in the effective lagrangian, which describes the physics at the experimentally testable energies, through non-renormalizable terms with couplings suppressed by inverse powers of the mediator mass. It has been understood long ago, however, that there generally exist renormalizable interactions between two sectors, so-called portals, whose strength is not suppressed by the mediator mass. Unless protected by some symmetries, these interactions may be strong enough to allow tests of the hidden sector even for the mediator masses of order the Planck scale. The Standard Model fields allow for three kinds of such interactions: (i) the quartic coupling of the Higgs scalar with some hidden scalar field (so-called Higgs portal), (ii) the Yukawa coupling with neutrino, Higgs and a hidden fermion, and (iii) the kinetic mixing term between the Standard-Model and hidden $U(1)$ gauge fields. Here, we concentrate on the latter case, first discussed in Ref. [1] where the gauge boson of the additional $U(1)$ group was called a paraphoton. The kinetic mixing term, which mixes the field strength of a hidden $U(1)$ gauge field with that of the electromagnetic (or hypercharge) $U(1)$, is allowed by Lorenz and gauge invariance and is renormalizable. Even if absent at the tree level, it should be therefore generated by loop corrections unless a particular symmetry prohibits it [2]. There is no lack of theoretical models which have sufficient freedom to justify observable paraphotons with almost arbitrary parameters allowed by experimental constraints. Some part of the paraphoton parameter space (which for our purposes consists of the paraphoton mass m and the kinetic-mixing coupling χ but in general includes also the gauge coupling of the hidden $U(1)$), however, have special phenomenological importance because these values have been invoked for models explaining either experimental anomalies or the origin of the Standard-Model parameters. We emphasize three particularly interesting regions.

(1) Mimicking extra neutrinos in the CMB. Recent cosmological results suggest that the effective number N_{eff} of light neutrino species is larger than three: the WMAP7 data [3] gives $N_{\text{eff}} = 4.34_{-0.88}^{+0.86}$, in agreement with somewhat less precise SDSS Data Release 7 [4] and Atacama

Cosmology Project [5]. It has been suggested that paraphotons with mass m in the range $(10^{-5} \div 10^{-2})$ eV may mimic extra neutrino species, the change in N_{eff} determined [6] by the mixing χ . For the WMAP7 values quoted above, $\chi = (1.1 \div 2.4) \times 10^{-6}$.

(2) String compactifications with TeV-scale gravity. Some of popular approaches to the gauge hierarchy problem in the Standard Model imply lowering the fundamental gravitational scale down to the values of order electroweak scale or slightly higher. This is usually achieved in models with extra space dimensions, in particular, in string models. Paraphotons are generic by-product in these compactification models. In a certain class of the latter, the fundamental string scale is related [7] to the kinetic-mixing parameter χ . The string scale is bounded from below by the early LHC results to be larger than a few TeV; its values within $(5 \div 1000)$ TeV would correspond to $\chi \sim (10^{-12} \div 10^{-10})$ for a wide range of possible paraphoton masses.

(3) ‘‘Unified’’ or ‘‘secluded’’ dark matter and hidden SM Higgs. These approaches attempt to explain the anomalies observed by DAMA, PAMELA and INTEGRAL, as well as possible non-observation of a light (~ 100 GeV) Higgs boson with unusual decay channels. Though quite different, all these scenarios point to $\chi \sim (10^{-4} \div 10^{-3})$ and paraphoton mass in the GeV range.

For different values of the parameters m and χ , various experimental techniques have been implemented to search for a potential signal of paraphotons. None was found, resulting in severe limits on the parameter space, see e.g. Ref. [8] for a review.

In the Sun, paraphotons may be produced from solar thermal photons by means of the kinetic mixing, see e.g. Refs. [9, 10, 11, 12]. The oscillation probability for the most general case will be presented elsewhere [12]; here we will be interested in two limiting cases important for the Sun, namely the case of optically thick emission region (the solar interior) and that of transparent emission region (solar outer atmosphere and solar flares).

2 Contribution of the optically thick Sun

The Sun has a rather sharp boundary where the density, and hence the transparency, changes by many orders of magnitude. It has been shown (see, e.g., Ref. [10]) that for paraphotons of keV energies, the contribution of the optically thick interior dominates. The total flux of paraphotons in this case is given by [10]

$$\frac{d\Phi}{d\omega} = \frac{3 \times 10^{24}}{\text{cm}^2 \cdot \text{s} \cdot \text{eV}} \left(\frac{\chi}{10^{-5}} \right)^2 \left(\frac{m}{\text{eV}} \right)^4 f_1(\omega, m),$$

where

$$f_1(\omega, m) = 1 \text{ eV} \times \omega^2 \int_0^1 d\xi \xi^2 \frac{\Gamma(\xi R_\odot)}{e^{\omega/T(\xi R_\odot)} - 1} \frac{1}{(\omega_p^2(\xi R_\odot) - m_1^2)^2 + \omega^2 \Gamma(\xi R_\odot)^2}.$$

m and ω are the paraphoton mass and energy, ω_p is the usual plasma frequency, χ is the mixing coupling, ξ is the radial coordinate measured in the units of the solar radius, R_\odot , while T and Γ determine the temperature and the inverse mean free path of a photon with energy ω , calculated at a given point in the Sun, respectively. The plasma frequency in the Sun varies roughly from 0.1 eV to 300 eV and for m within this range, the integral is saturated by a contribution of a rather thin resonance slice, the paraphotosphere; otherwise, high-temperature inner parts dominate (see Fig. 1, left panel). The right panel of Fig. 1 gives approximate exclusion limits on

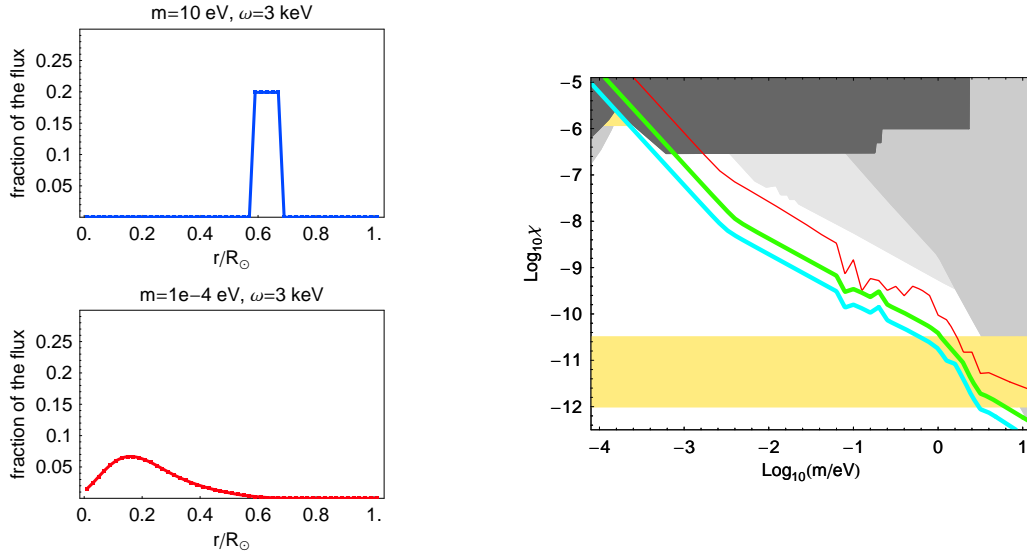


Figure 1: *Left*: Normalized contributions of various parts of the Sun to the total paraphoton flux. Upper panel: no resonance, the central part dominates. Lower panel: resonance, a thin slice dominates. *Right*: Paraphoton parameters. Dark gray: laboratory exclusion; light gray: astrophysical exclusion; very light gray: CAST exclusion from Ref. [10]. Very light gray (yellow online): theoretically favoured regions (see the Introduction). It is expected that future X-ray helioscopes will exclude the space above lines (top to bottom, the planned CAST upgrade and two options for the next-generation axion helioscope IAXO [13]).

the plane of paraphoton parameters (mass and coupling) expected for future X-ray helioscopes, together with current experimental bounds.

3 Solar flares

We assume that a flare happens in a small region with constant temperature and electron density and its emission is thermal. Then the ratio of the paraphoton flux from the flare to the photon flux at the same energy is approximately $P/(1 - P)$, where P is the probability of the conversion at the emission point. The duration of the flare is $\sim 10^3$ s and normally, since $P \ll 1$, only a tiny number of paraphotons reach the detector during this time. The situation changes drastically if the density of plasma in the flare happens to be such that the resonance takes place. Then $P \approx 1/2$ and a large number of photons were converted to paraphotons. It is easy to demonstrate that for a detector with area S and background noise n , the 95% CL exclusion limit on the mixing parameter χ for one particular resonant mass may be determined by

$$\chi \gtrsim 8 \times 10^{-7} \left(\frac{F_{\text{obs}}}{10^5 \text{ cm}^{-2} \text{ s}^{-1} \text{ eV}^{-1}} \right)^{-1/2} \left(\frac{t}{1 \text{ s}} \right)^{-1/4} \left(\frac{n}{10^{-3} \text{ Hz}} \right)^{1/4} \left(\frac{S}{10 \text{ cm}^2} \right)^{-1/2} \left(\frac{\omega}{\text{keV}} \right)^{-1/2},$$

where F_{obs} is the flux of solar *photons* with energy ω detected from the flare. In this formula, t is the period of time when the flare keeps resonant conditions, that is the plasma frequency does not change more than the resonance width. We note that while a flare looks as a rapid process at a particular wavelength, the change in appearance is related mostly to change in the temperature and not in the density (see e.g. discussion in Ref. [14] and particular numbers in Ref. [15]), so that $t \gtrsim 1$ s is a typical value. However, in practice this approach can hardly be used to constrain χ because one does not know the conditions in the flare with the required precision.

Instead, I suggest that the observation of flares with helioscopes may be a discovery channel for paraphotons. Indeed, the resonant conversion of photons to paraphotons in the flare manifests itself not only by appearance of paraphotons but also by a $\sim 1/2$ drop in the regular *photon* flux. The study of light curves with excellent time resolution is possible with various instruments (e.g., SOXS, SPHINX etc.). One may search them for temporal coincidences between events in helioscopes and drops in the flare lightcurves; the background is almost zero and even a single coincident event may serve as a strong evidence for paraphotons.

4 Acknowledgements

I acknowledge collaboration with Dmitry Gorbunov, Martyn Davenport and Konstantin Zioutas at various stages of this work. I am indebted to the organizers of the Mykonos workshop for the invitation to this very interesting meeting and to many participants of the meeting, notably to Javier Redondo, for illuminating discussions. This work was supported in part by the grants RFBR 10-02-01406, 11-02-01528 and FASI 02.740.11.0244, by the grant of the President of the Russian Federation NS-5525.2010.2 and by the Dynasty foundation.

References

- [1] L. B. Okun, Sov. Phys. JETP **56** (1982) 502 [Zh. Eksp. Teor. Fiz. **83** (1982) 892].
- [2] K. R. Dienes, C. F. Kolda and J. March-Russell, Nucl. Phys. B **492**, 104 (1997).
- [3] E. Komatsu *et al.* [WMAP Collaboration], Astrophys. J. Suppl. **192** (2011) 18.
- [4] J. Hamann *et al.*, JCAP **1007** (2010) 022.
- [5] J. Dunkley *et al.*, Astrophys. J. **739** (2011) 52.
- [6] J. Jaeckel, J. Redondo, A. Ringwald, Phys. Rev. Lett. **101** (2008) 131801. [arXiv:0804.4157 [astro-ph]].
- [7] M. Goodsell *et al.*, JHEP **0911** (2009) 027.
- [8] J. Jaeckel and A. Ringwald, Ann. Rev. Nucl. Part. Sci. **60** (2010) 405.
- [9] V. Popov, Turk. J. Phys. **23** (1999) 943; V.V. Popov and O.V. Vasil'ev, Europhys. Lett. **15** (1991) 7.
- [10] J. Redondo, JCAP **0807** (2008) 008; S. N. Gninenko and J. Redondo, Phys. Lett. B **664**, 180 (2008)

- [11] D. Cadamuro and J. Redondo, arXiv:1010.4689 [hep-ph]; J. Redondo, talk at the 7th Patras Workshop, Mykonos, 2011.
- [12] D. Gorbunov *et al.*, to appear.
- [13] I. G. Irastorza JCAP **1106** (2011) 013.
- [14] M. Aschwanden, *Physics of the solar corona*, Springer, 2006.
- [15] E. P. Kontar, I. G. Hannah, N. H. Bian, *Astrophys. J.* **730** (2011) L22.

Search for 5.5 MeV Solar Axions Produced in a $p(d, {}^3\text{He})\text{A}$ Reaction with Borexino Detector

A. Derbin*, V. Muratova* on behalf of Borexino Collaboration:

G. Bellini, J. Benziger, D. Bick, G. Bonfini, D. Bravo, M. Buizza Avanzini, B. Caccianiga, L. Cadonati, F. Calaprice, C. Carraro, P. Cavalcante, A. Chavarria, D. D'Angelo, S. Davini, A. Etenko, K. Fomenko, D. Franco, C. Galbiati, S. Gazzana, C. Ghiano, M. Giammarchi, M. Goeger-Neff, A. Goretti, L. Grandi, E. Guardincerri, S. Hardy, Al. Ianni, An. Ianni, A. Kayunov, V. Kobayev, D. Korablev, G. Korga, Y. Koshio, D. Kryn, M. Laubenstein, T. Lewke, E. Litvinovich, B. Loer, F. Lombardi, P. Lombardi, L. Ludhova, I. Machulin, S. Manecki, W. Maneschg, G. Manuzio, Q. Meindl, E. Meroni, L. Miramonti, M. Misiaszek, D. Montanari, P. Mosteiro, L. Oberauer, M. Obolensky, F. Ortica, K. Otis, M. Pallavicini, L. Papp, L. Perasso, S. Perasso, A. Pocar, S. Raghavan, G. Ranucci, A. Razeto, A. Re, A. Romani, A. Sabelnikov, R. Saldanha, C. Salvo, S. Schönert, H. Simgen, M. Skorokhvatov, O. Smirnov, A. Sotnikov, S. Sukhotin, Y. Suvorov, R. Tartaglia, G. Testera, D. Vignaud, R.B. Vogelaar, F. von Feilitzsch, J. Winter, M. Wojcik, A. Wright, M. Wurm, J. Xu, O. Zaimidoroga, S. Zavatarelli, and G. Zuzel

*St. Petersburg Nuclear Physics Institute, 188300, Gatchina, Russia

DOI: http://dx.doi.org/10.3204/DESY-PROC-2011-04/derbin_alexander

A search for 5.5-MeV solar axions produced in the $p + d \rightarrow {}^3\text{He} + \gamma(5.5\text{MeV})$ reaction was performed using the Borexino detector. Model independent limits on axion-electron (g_{Ae}), axion-photon ($g_{A\gamma}$), and isovector axion-nucleon (g_{3AN}) couplings are obtained: $|g_{Ae} \times g_{3AN}| \leq 5.5 \times 10^{-13}$ and $|g_{A\gamma} \times g_{3AN}| \leq 4.6 \times 10^{-11} \text{GeV}^{-1}$ at $m_A < 1 \text{MeV}$ (90% c.l.). These limits are 2-4 orders of magnitude stronger than those obtained in previous laboratory-based experiments using nuclear reactors and accelerators.

The Sun potentially represents an efficient and intense source of axions. The most intense flux of high energy axions is expected from the formation of the ${}^3\text{He}$ nucleus [1]-[3]:



According to the Standard Solar Model (SSM), 99.7% of all deuterium is produced from the fusion of two protons, $p + p \rightarrow d + e^+ + \nu_e$, while the remaining 0.3% is due to the $p + p + e^- \rightarrow d + \nu_e$ reaction. The expected solar axion flux can thus be expressed in terms of the pp -neutrino flux. The proton capture from the S state corresponds to an isovector transition, and the ratio between the probability of a nuclear transition with axion production (ω_A), and the probability of a magnetic transition (ω_γ) depends only on g_{3AN} : [4]-[6]:

$$\frac{\omega_A}{\omega_\gamma} = \frac{\chi}{2\pi\alpha} \left[\frac{g_{3AN}}{\mu_3} \right]^2 \left(\frac{p_A}{p_\gamma} \right)^3 = 0.54 (g_{3AN})^2 \left(\frac{p_A}{p_\gamma} \right)^3. \quad (2)$$

The expected solar axion flux on the Earth's surface is then

$$\Phi_{A0} = \Phi_{\nu pp} (\omega_A / \omega_\gamma) = 3.23 \times 10^{10} (g_{3AN})^2 (p_A / p_\gamma)^3 = 2.44 \times 10^{-5} m_A^2 (p_A / p_\gamma)^3,$$

where $\Phi_{\nu pp} = 6.0 \times 10^{10} \text{cm}^{-2} \text{s}^{-1}$ is the pp solar neutrino flux and m_A is the axion mass in eV units.

An axion can scatter an electron to produce a photon in the Compton-like process $A + e \rightarrow \gamma + e$. For axions with fixed g_{Ae} the phase space contribution to the cross section is approximately independent of m_A for $m_A < 2 \text{ MeV}$ and the integral cross section is $\sigma_{CC} \approx g_{Ae}^2 \times 4.3 \times 10^{-25} \text{cm}^2$. The dimensionless coupling constant g_{Ae} is associated with the electron mass m , so that $g_{Ae} = C_e m / f_A$, where C_e is a model dependent factor of the order of unity. The hadronic axion has no tree-level couplings to the electron, but there is an induced axion-electron coupling at one-loop level [7].

The other process associated with axion-electron coupling is the axio-electric effect $A + e + Z \rightarrow e + Z$ (the analogue of the photo-electric effect). In this process the axion disappears and an electron is emitted from an atom with an energy equal to the energy of the absorbed axion minus the electron binding energy [8]. The cross section has a Z^5 dependence and for carbon atoms the cross section is low $\sigma_{ae} \approx g_{Ae}^2 \cdot 1.3 \cdot 10^{-29} \text{cm}^2/\text{electron}$ for $m_A < 1 \text{ MeV}$. However, the axio-electric effect is a potential signature for axions with detectors having high Z active mass [3].

For axions with a mass above $2m_e$, the main decay mode is the decay into an electron-positron pair: $A \rightarrow e^+ + e^-$. The condition that time of flight is less than lifetime - $\tau_f < 0.1\tau_{e^+e^-}$ (in this case, 90% of all axions reach the Earth) limits the sensitivity of solar axion experiments to $g_{Ae} < (10^{-12} - 10^{-11})$ [3].

If the axion mass is less than $2m_e$, $A \rightarrow e^+ + e^-$ decay is forbidden, but the axion can decay into two γ quanta. The probability of the decay, which depends on the axion-photon coupling constant $g_{A\gamma}$ and the axion mass, is given by the expression: $\tau_{2\gamma} = 64\pi / g_{A\gamma}^2 m_A^3$. The flux of axions reaching the detector is given by $\Phi_A = \exp(-\tau_f / \tau_{2\gamma}) \Phi_{A0}$.

Another process depending on $g_{A\gamma}$ coupling is the Primakoff photo-production on carbon nuclei $A + {}^{12}\text{C} \rightarrow \gamma + {}^{12}\text{C}$. The integral inverse Primakoff conversion cross section is proportional Z^2 : $\sigma_{PC} \approx g_{A\gamma}^2 Z^2 \alpha$ [6]. Because the cross section depends on the $g_{A\gamma}$ coupling, the decrease in the axion flux due to $A \rightarrow 2\gamma$ decays during their flight from the Sun should be taken into account.

Borexino is a real-time detector for solar neutrino spectroscopy located at the Gran Sasso Underground Laboratory. The main features of the Borexino detector and its components have been thoroughly described in ([9]-[11] and refs therein). The Monte Carlo method has been used to simulate the Borexino response $S(E)$ to electrons and γ -quanta produced by axion interactions. The MC simulations are based on the GEANT4 code, taking into account the effect of ionization quenching and non-linearity induced by the energy dependence on the event position.

Figure 1 shows the observed Borexino energy spectrum in the (3.0 – 8.5) MeV range in which the axion peaks might appear. The obtained upper limits on the number of counts in the peak ($S_{CC}^{lim} \leq 0.013 \text{ c}/(100 \text{ t day})$ at 90% c.l.) are very low, e.g. $\sim 10^4$ times lower than expected number of events from pp - neutrino (135 $\text{c}/(100 \text{ t day})$).

The upper limits on the number of events with energy 5.5 MeV constrain the product of axion flux Φ_A and the interaction cross section $\sigma_{A-e,p,C}$ via relation: $S_{events} = \Phi_A \sigma_{A-e,p,C} N_{e,p,C} T \varepsilon \leq S^{lim}$. Here $N_{e,p,C}$ is the number of electrons, protons and carbon nuclei in the IV, T is the

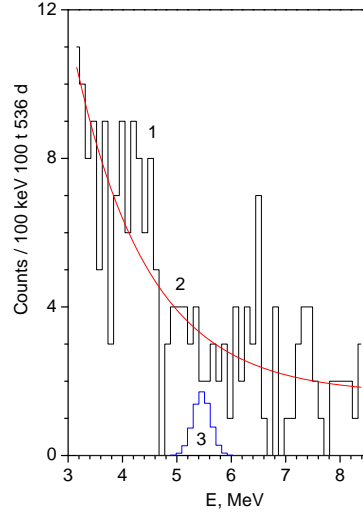


Figure 1: The fitted Borexino spectrum in the (3.2 – 8.4) MeV range. Curve 3 is the detector response function for Compton axion-photon conversion at the 90% c.l. upper limit ($S=6.9$ events).

measurement time and ε is the detection efficiency. The individual rate limits are:

$$\Phi_A \sigma_{A-electron} \leq 4.5 \times 10^{-39} \text{s}^{-1} \quad (3)$$

$$\Phi_A \sigma_{A-proton} \leq 2.5 \times 10^{-38} \text{s}^{-1} \quad (4)$$

$$\Phi_A \sigma_{A-carbon} \leq 3.3 \times 10^{-38} \text{s}^{-1} \quad (5)$$

For comparison the standard solar neutrino capture rate is $\text{SNU} = 10^{-36} \text{s}^{-1} \text{atom}^{-1}$.

The axion flux Φ_A is proportional to the constant $(g_{3AN})^2$, and the cross section σ_{CC} is proportional to the constant g_{Ae}^2 . The S_{CC} value depends, then, on the product of $g_{Ae}^2 \times (g_{3AN})^2$. The range of excluded $|g_{Ae} \times g_{3AN}|$ values is shown in Fig.2 (line 2). At $(p_A/p_\gamma)^3 \approx 1$ or $m_A < 1\text{MeV}$ the limit is:

$$|g_{Ae} \times g_{3AN}| \leq 5.5 \times 10^{-13} (90\% \text{c.l.}). \quad (6)$$

These constraints are completely model-independent and valid for any pseudoscalar particle. Within the hadronic (KSVZ) axion model, one can obtain a constraint on the g_{Ae} constant, depending on the axion mass (Fig.2. line 1). For $(p_A/p_\gamma)^3 \approx 1$ the limit on g_{Ae} and m_A is:

$$|g_{Ae} \times m_A| \leq 2.0 \times 10^{-5}, \quad (7)$$

where m_A is given in eV units (90% c.l.).

The analysis of $A \rightarrow 2\gamma$ decay and Primakoff photoproduction is more complicated because axions can decay during their flight from the Sun. The exponential dependence of the axion

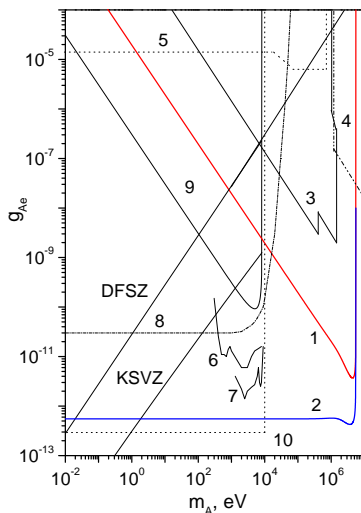


Figure 2: The limits on the g_{Ae} coupling constant obtained by 1- present work, 2 - present work for $|g_{Ae} \times g_{3AN}|$, 3- reactor and solar experiments, 4- beam dump experiments, 5- ortho-positronium decay, 6- CoGeNT, 7- CDMS, 8- solar axion luminosity, 9-resonance absorption [12], 10- read giant. The excluded values are located above the corresponding lines.

flux on $g_{a\gamma}$ and m_A must be taken into account. In the assumption that $\beta \approx 1$ the number of decays in the FV depends on g_{3AN}^2 , $g_{A\gamma}^2$ and m_A^4 . The limit derived at 90% C.L., is

$$|g_{A\gamma} \times g_{3AN}| \times m_A^2 \leq 3.3 \times 10^{-2}. \quad (8)$$

The number of expected events due to inverse Primakoff conversion is $S_{PC} = \Phi_A \sigma_{PC} N_C T \varepsilon_{PC}$, where σ_{PC} is the Primakoff conversion cross sections. Under the assumption that $\Phi_A \approx \Phi_{A0}$ one can obtain the restriction ($g_{A\gamma}$ is in GeV^{-1} units):

$$|g_{A\gamma} \times g_{3AN}| \leq 4.6 \times 10^{-11} (90\%c.l.), \quad (9)$$

This limit is 25 times stronger than the one obtained by CAST [14], which searches for conversion of 5.5 MeV axions in a laboratory magnetic field In the KSVZ model the constraint on $g_{A\gamma}$ and m_A is given by the relation:

$$|g_{A\gamma}| \times m_A \leq 1.7 \times 10^{-3} \quad (10)$$

For $m_A=1$ MeV, this corresponds to $g_{A\gamma} \leq 1.2 \times 10^{-3}$. The region of excluded values of $g_{A\gamma}$ and m_A are shown in Fig.3, line 1b; under the assumption that $g_{A\gamma}$ depends on m_A as in the KSVZ model we exclude axions with masses between (1.5 - 73) keV. Our results from the inverse Primakoff process exclude a new region of $g_{A\gamma}$ values at $m_A \sim 10$ keV.

A search for 5.5 MeV solar axions emitted in the $p(d, {}^3\text{He})\gamma$ reaction has been performed with the Borexino detector. The Compton conversion of axions into photons, the decay of axions

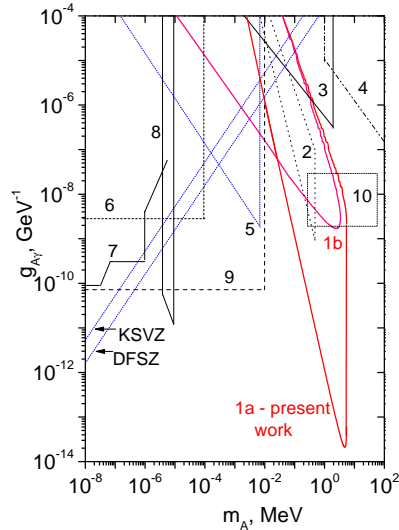


Figure 3: The limits on $g_{A\gamma}$ obtained by 1- present work (a - $A \rightarrow 2\gamma$, b - PC, areas of excluded values are located inside contour), 2 - CTF [1], 3- reactor experiments, 4- beam dump experiments, 5- resonant absorption [13], 6- solar axions conversion in crystals, 7- CAST, 8- telescopes, 9- HB Stars, 10- expectation region from heavy axion models.

into two photons, and inverse Primakoff conversion on nuclei were studied. The signature of all these reactions is a 5.5 MeV peak in the energy spectrum of Borexino. No statistically significant indications of axion interactions were found. New, model independent, upper limits on the axion coupling constants to electrons, photons and nucleons were obtained.

References

- [1] G. Bellini et al., (Borexino coll.) *Europ. Phys. J. C*54, 61 (2008).
- [2] G. Bellini et al., (Borexino coll.) submitted to *Phys. Rev. D*(2011).
- [3] A.V. Derbin, A.S. Kayunov, and V.N. Muratova, *Bull. Rus. Acad. Sci. Phys.* 74, 805 (2010), arXiv:1007.3387
- [4] W.C. Haxton and K.Y. Lee, *Phys. Rev. Lett.* 66, 2557 (1991).
- [5] T.W. Donnelly et al., *Phys. Rev. D*18, 1607 (1978).
- [6] F.T. Avignone III et al., *Phys. Rev. D*37, 618 (1988).
- [7] M. Srednicki, *Nucl. Phys. B*260, 689 (1985).
- [8] A.R. Zhitnitskii and Yu.I. Skovpen, *Yad. Fiz.* 29, 995 (1979).
- [9] G. Alimonti et al. (Borexino Coll.), *Nucl. Instr. and Meth. A*600, 58 (2009).
- [10] G. Bellini et al. (Borexino Coll.), *Phys. Rev. C*81, 034317,(2010).
- [11] G. Bellini et al. (Borexino Coll.), *Phys. Rev. D*82, 033006,(2010).
- [12] A.V. Derbin et al., *Phys. Rev. D*83, 023505 (2011).
- [13] A.V. Derbin et al., *Phys. Lett. B*678, 181 (2009).
- [14] S. Andriamonje et al., (CAST Coll.), *JCAP* 1003:032 (2010). arXiv:0904.2103

A Search for the Resonant Absorption of Solar Axions by Atomic Nuclei

A. Derbin¹, A.Kayunov¹, V. Muratova¹, D. Semenov¹, E. Unzhakov¹

¹Petersburg Nuclear Physics Institute (PNPI), Gatchina, Russia

DOI: http://dx.doi.org/10.3204/DESY-PROC-2011-04/unzhakov_evgeniy

A search for resonant absorption of solar axions by ⁵⁷Fe and ¹⁶⁹Tm targets was performed. The Si(Li) detector placed inside a low-background setup was used to detect the γ -quanta appearing from the de-excitation of the low-lying nuclear levels of ⁵⁷Fe and ¹⁶⁹Tm (14.4 keV and 8.41 keV correspondingly): $A + N_{target} \rightarrow N_{target}^* + \gamma$. The obtained data allowed us to set the new upper limits on the axion mass value: $m_A \leq 145$ eV at 95% c.l.

1 Introduction

A natural solution of the strong CP-problem is based on the introduction of the global chiral symmetry $U(1)_{PQ}$ that was proposed by Peccei and Quinn in 1997. The spontaneous breaking of this new symmetry at the energy scale f_a should lead to the generation of a new neutral zero-spin pseudoscalar particle - axion. Theory describes the interaction of axions with ordinary matter (nucleons, leptons and photons) in terms of effective coupling constants: g_{AN} , g_{Ae} , $g_{A\gamma}$ correspondingly. The axion mass m_A and the values of these constants appear to be inversely proportional to the $U(1)_{PQ}$ symmetry breaking scale f_A . After the first hypothesis of $f_A \approx 250$ GeV (electro-weak scale) was experimentally excluded, two types of new theoretical models were introduced. They removed the restrictions on the f_A value, allowing it to go up to the Planck mass, therefore significantly suppressing the interaction of axions with ordinary matter and shifting the expected axion mass to the lighter region.

2 Solar axion flux

If axions do exist, then stars (including the Sun) should be intense sources of these particles. There are several possible mechanisms that could stand behind the production of solar axions.

Firstly, the Primakoff conversion of photons in the electromagnetic field of plasma can efficiently produce axions ($\gamma + \vec{B} \rightarrow A$). The resulting axion flux has an average energy of 4 keV and can be detected by inverse Primakoff conversion in laboratory magnetic fields or by the coherent conversion to photons in crystal detectors. These experiments are sensitive to $g_{A\gamma}$ constant. The flux of Primakoff axions is parameterized by the following expression [1]:

$$\frac{d\Phi_A}{dE_A} = (g_{A\gamma})^2 \cdot 3.82 \cdot 10^{30} \frac{E_A^3}{\exp(E_A/1.103) - 1}$$

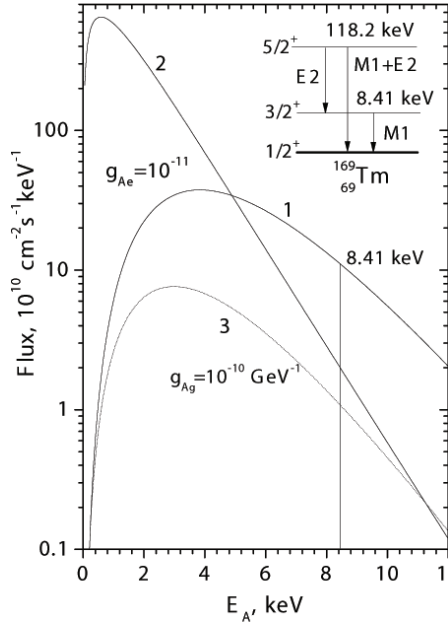


Figure 1: **1, 2** - Compton process and the bremsstrahlung axion spectra, correspondingly. **3** - Primakoff axion spectrum. The level scheme of ^{169}Tm nucleus is shown in the inset.

produced by $p(d,^3\text{He})A$ reaction was made in [3].

Also, axions could be produced as a result of the Compton process ($\gamma + e^- \rightarrow e^- + A$) and bremsstrahlung ($e^- + Z \rightarrow Z + e^- + A$) in the hot solar plasma. The cross sections of these reactions depend on the axion-electron coupling constant g_{Ae} . The expected spectrum of such axions is calculated using the theoretical predictions for the Compton cross section and the axion bremsstrahlung produced by the electron-nucleus collisions. The axion flux is determined by radial temperature distribution $T(r)$ and densities of electrons $N_e(r)$ and nuclei $N_{Z,A}(r)$. The resulting corresponding parameterizations of Compton and bremsstrahlung axions are [4]:

$$\frac{d\Phi_A}{dE_A} = g_{Ae}^2 \cdot 1.33 \cdot 10^{33} E_A^{2.98} e^{-0.774E_A}$$

$$\frac{d\Phi_A}{dE_A} = g_{Ae}^2 \cdot 4.14 \cdot 10^{35} E_A^{0.89} e^{-0.7E_A - 1.26\sqrt{E_A}}$$

The total flux of solar axions produced by various processes is shown in Fig. 1. In our work we used ^{169}Tm target for resonant absorption of bremsstrahlung, Compton and Primakoff axions and ^{57}Fe for the absorption of 14.4 keV monochromatic axions. Therefore, these experiments were sensitive to g_{Ae} , $g_{A\gamma}$ and g_{AN} values correspondingly.

The second mechanism is based on the possibility of thermal excitation of low-lying nuclear energy levels ($N^* \rightarrow N + A$). The most intense monochromatic axion flux is connected with $M1$ -transition of ^{57}Fe nucleus. The energy of the first excited nuclear level $3/2^-$ is equal to 14.413 keV, and the admixture of $E2$ -transition is $\delta^2 = 0.22\%$. The axion flux depends on the level energy $E_\gamma = 14.413$ keV, temperature T , nuclear level lifetime $\tau_\gamma = 1.34 \mu\text{s}$, the abundance of the ^{57}Fe isotope on the Sun N and the axion/photon emission branching ratio ω_A/ω_γ [2]:

$$\Phi_A \sim \frac{N}{\tau_\gamma} \frac{2 \exp(-E_\gamma/kT)}{1 + 2 \exp(-E_\gamma/kT)} \frac{\omega_A}{\omega_\gamma}$$

Monochromatic 14.4 keV axions produced by the $M1$ -type nuclear transition of ^{57}Fe nucleus can be observed in the inverse reaction of the resonant absorption and registration of the following γ -rays emitted by the de-excitation of ^{57}Fe target nuclei. The probability of emission and subsequent absorption of the axion in a $M1$ -type transition is determined only by the axion-nucleon coupling g_{AN} .

Nuclear reactions of the solar cycle could be another source of axions. An attempt to detect heavy 5.5 MeV monochromatic solar axions pro-

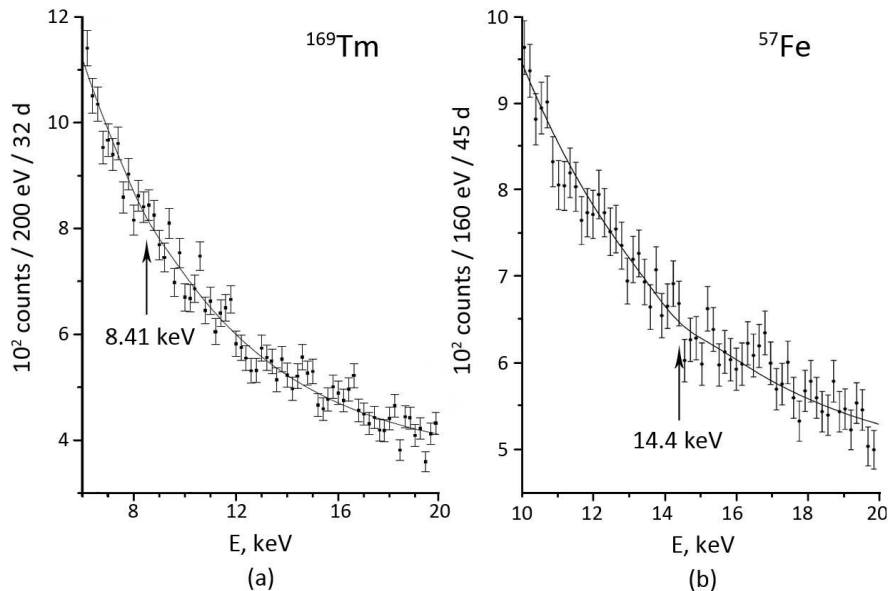


Figure 2: The Si(Li) detector energy spectra of ^{169}Tm (a) and ^{57}Fe (b) targets, measured in the anticoincidence with the veto signal. Solid line shows the fitting results for corresponding regions.

3 Experimental setup

In order to observe 8.41 keV and 14.4 keV γ -rays we used the planar Si(Li) detector with a sensitive area diameter $d = 66$ mm and thickness of 5 mm. The detector was mounted on 5 cm thick copper plate that protected the detector from the external radiation. The detector and the holder were placed in a vacuum cryostat and cooled to the temperature of the liquid nitrogen. The corresponding target was uniformly deposited on a Plexiglas substrate 70 mm in diameter at the distance of 1.5 mm from the detector surface. External passive shielding composed of copper, iron and lead layers was adjusted to the cryostat and suppressed the external radioactivity background by a factor of about 500.

The experimental setup was located on the ground surface. The events produced by cosmic rays and fast neutrons were registered by the active shielding consisting of five plastic scintillators $50 \times 50 \times 12$ cm in size. The rate of $50 \mu\text{s}$ veto signals was 600 counts/s that lead to $\approx 3\%$ of the dead time. The Si(Li) detector was sectionalized into nine separate subregions in order to reduce the capacities of individual sections and, therefore, increase the overall energy resolution. Every section was equipped with a charge-sensitive preamplifier with resistive feedback, a shaping amplifier and a 12-step ADC. Eighteen 4096-channel spectra (in coincidence and anticoincidence with the veto signal) were collected.

Though the detector amplifications were actually the same, the energy calibrations were performed for each section individually. Standard ^{57}Co and ^{241}Am calibration sources were used. The total energy resolution for a 14.4 keV γ -ray line was equal to $\sigma = 0.63$ keV. The high energy resolution and accurate knowledge of energy scale are of great importance for our experiment, because the energies of thulium characteristic x-rays are close to 8.41 keV.

The sensitive volume and area of the (Si)Li detector were measured via the x-ray and γ -lines of a standard ^{241}Am source. The detection efficiency was estimated by the MC simulation that included the self-absorption of γ -rays by the target. Total detection efficiency for the 8.41 γ -rays turned out to be $\epsilon \approx 6\%$.

4 Results

The measurements were carried out during 45 days of live time with ^{57}Fe target and during 32 days of live time with ^{169}Tm target. The detailed energy spectra of the regions where axion peak was expected are presented in Fig. 2. There were no statistically significant peaks in the given regions, therefore, we used the standard method of χ^2 profiling in order to determine the upper limits on the number of events inside the axion peak. The result of the fit corresponding to the minimum of χ^2 is shown by a solid line in Fig. 2. The value of χ^2 was determined for different fixed values of axion peak intensity S_A while the other parameter were left unrestricted. The obtained probability function $P(\chi^2(S))$ was normalized to unity for $S \geq 0$.

Ultimately, the expected number of the axion peak γ -quanta would be proportional to the number of target nuclei N_{target} , time of measurement T , γ -ray detection efficiency ϵ and the internal conversion ratio of the corresponding nuclear transition η .

The obtained results allowed us to set the following upper limits on the values of coupling constants and axion mass: $|g_{AN}^0 + g_{AN}^3| \leq 3.0 \times 10^{-6}$ and $m_A \leq 145$ eV for ^{57}Fe measurements; $g_{Ae} \times |g_{AN}^0 + g_{AN}^3| \leq 2.1 \times 10^{-14}$ and $g_{Ae} \times m_A \leq 3.2 \times 10^{-7}$ eV in case of Compton and bremsstrahlung axion absorption by ^{169}Tm ; $g_{A\gamma} \times m_A \leq 1.36 \times 10^{-5}$ and $m_A \leq 169$ eV in case of Primakoff axion absorption by ^{169}Tm . All the limits are given at 95 % c.l.

For more details on the calculation of the axion absorption rates, model parameter dependencies and result comparison see [1], [2] and [4].

References

- [1] A. Derbin, S. Bakhlanov, A. Egorov, I. Mitropolsky, V. Muratova, D. Semenov, E. Unzhakov, "Search for Solar Axions Produced by Primakoff Conversion Using Resonant Absorption by ^{169}Tm Nuclei," Phys. Lett. B **678**, 181-185 (2009) [arXiv:0904.3443 [hep-ex]].
- [2] A. Derbin, A. Egorov, I. Mitropolsky, V. Muratova, D. Semenov, E. Unzhakov, "Search for Resonant Absorption of Solar Axions Emitted in M1 Transition in ^{57}Fe Nuclei," Eur. Phys. J. C **62**, 755-760 (2009) [arXiv:0906.0256 [hep-ex]].
- [3] A. Derbin, A. Kauynov, V. Muratova, Search for 5.5 MeV solar axions produced in $p(d,^3\text{He})A$ reaction," Bull. Rus. Acad. Sci. Phys. **74**, 805 (2010) [arXiv:1007.3387v1 [hep-ex]].
- [4] A. Derbin, A. Kauynov, V. Muratova, D. Semenov, E. Unzhakov, "Constraints on the axion-electron coupling for solar axions produced by Compton process and bremsstrahlung," Phys. Rev. D **83**, 023505 (2011) [arXiv:1101.229 [hep-ex]].

Solar Chameleons: Production and Detection

Philippe Brax

Institut de Physique Theorique, CEA, IPhT, CNRS, URA 2306, F-91191Gif/Yvette Cedex, France

DOI: <http://dx.doi.org/10.3204/DESY-PROC-2011-04/brax-philippe>

Chameleon fields evade gravitational tests in the solar system and the laboratory while playing the role of quintessence on cosmological scales. They could be produced in magnetised regions of the inner sun, e.g. around the tachocline. Once produced, they can be backconverted into X-ray photons in the sun's atmosphere or reach helioscope detectors on earth where the spectrum of photons is typically peaked in the sub-keV region. Dedicated laboratory shining-through-a-wall experiments using powerful X-ray lasers could be used to test the existence of chameleons.

1 Introduction

Quintessence models used to analyse the acceleration of the expansion of the Universe suffer from the presence of an ultra-light scalar field of mass of order $H_0 \sim 10^{-43}$ GeV which would lead to the existence of a fifth force and strong violations of the equivalence principle. Unless the quintessence field is almost decoupled from ordinary matter, this fact would rule out most dark energy models. Fortunately, it turns out that on small scales compared to the size of the Universe, typically in the solar system or the laboratory, screening mechanisms can be at play. We will focus on the chameleon mechanism whereby a scalar field develops an environmentally dependent mass which can become large enough in dense regions to induce a Yukawa suppression of the fifth force between massive bodies.

Chameleons[1] can also couple to photons and could therefore be produced in magnetised regions by the Primakoff effect. This could well occur in the sun where strong magnetic fields are understood to be present around the tachocline at $0.7 R_\odot$ with a strength $B = 20 - 50$ T.

Chameleon production could be either resonant or non-resonant. The resonant case is restricted to very small regions where the spatially varying mass of the chameleon is equal to the plasma frequency in the sun, and is therefore depleted compared to the non-resonant production which takes place in large magnetised zones. Such solar chameleons mostly escape the sun unscathed reaching the earth where they are energetic enough to penetrate into helioscope pipes where they could regenerate X-ray photons. A small fraction of the solar chameleons can also regenerate photons in the weak magnetic field of the quiet sun's atmosphere, hence contributing to the solar X-ray spectrum. If X-ray photons were observed with helioscopes, an experimental signature of the existence of chameleon particles could be attained using powerful X-ray lasers shining into two magnetised pipes separated by a X-ray thick barrier.

Indeed chameleons would be created in the vacuum pipe, cross the barrier and regenerate X-rays in the second pipe downstream. This would not be the case anymore when the pipe is

SOLAR CHAMELEONS: PRODUCTION AND DETECTION

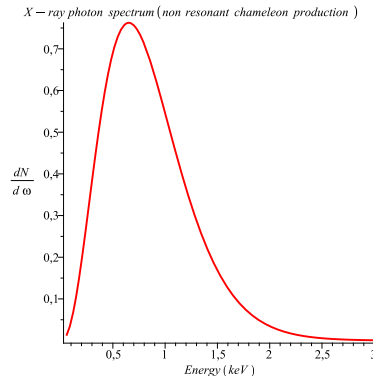


Figure 1: The spectrum of back-converted photons from solar chameleons giving the number of counts per hour and per keV predicted to be seen in a magnetic helioscope like CAST in vacuum as a function of the reconverted photon energy.

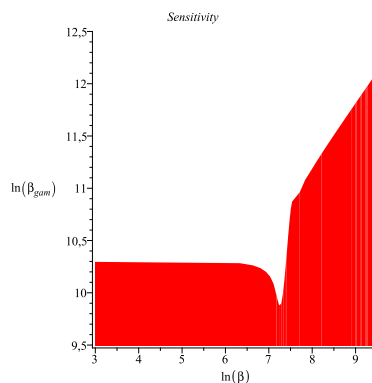


Figure 2: The sensitivity region at the 2σ level above the red region for a magnetic helioscope like CAST in vacuum at a temperature of 1.8K and for the photon coupling $\log \beta_\gamma$ as a function of the matter coupling $\log \beta$.

filled with a gas at moderate pressure, a clear demonstration of the density dependence of the chameleon mass.

2 Solar Chameleons

Chameleons are dark energy candidates. Chameleon models depend on the shape of the dark energy potential $V(\phi)$ and the coupling to matter β . Chameleons have an effective potential which becomes matter density dependent $V_{\text{eff}}(\phi) = V(\phi) + e^{\beta\phi/m_{\text{Pl}}}\rho$ where ϕ is the chameleon field and ρ the non-relativistic matter density. The effective potential has always a matter dependent minimum and fluctuations around the vacuum expectation values at the minimum can be seen as chameleon particles which couple to matter. The density-dependent minimum

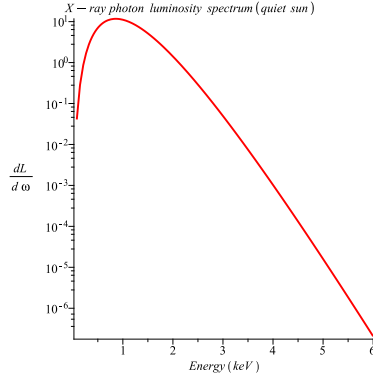


Figure 3: The X-ray luminosity spectrum from back-converted chameleons leaving the quiet sun as a function of the photon energy in keV in $\text{erg} \cdot \text{keV}^{-1} \cdot \text{s}^{-1} \cdot \text{cm}^{-2}$. The photons are backconverted at altitudes larger than 5000 km with a magnetic field of 1 Gauss and a density of order $10^{-16} \text{g} \cdot \text{cm}^{-3}$. We have used $B_{\text{out}} L_{\text{out}} \approx 10^4 \text{ T} \cdot \text{m}$ to determine the length of the magnetic region.

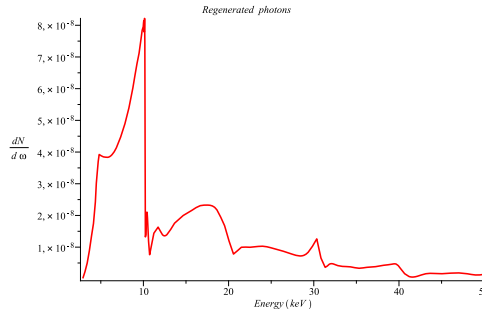


Figure 4: An example of photon flux in $\text{s}^{-1} \cdot \text{keV}^{-1}$ as a function of the photon energy in keV for the regenerated photons as predicted to be seen by a chameleon through wall experiment using two magnetic pipes on both sides of a thick barrier. The coupling to matter is $\beta = 10^6$ while the coupling to photons $\beta_\gamma = 10^{10.32}$ implies a corresponding 2σ result obtained in 300 days with a detection sensitivity of $10^{-6} \text{s}^{-1} \cdot \text{cm}^{-2}$. For magnetic pipes of 3 times the CAST pipe length, a 5σ result would only take 6 days.

is such that the mass of the scalar field becomes also density dependent. We will focus on inverse power law models defined by $V(\phi) = \Lambda^4 + \frac{\Lambda^{4+n}}{\phi^n} + \dots$ where we have neglected higher inverse powers of the chameleon field. We will choose $\Lambda = 2.4 \cdot 10^{-12} \text{GeV}$ to accommodate the acceleration of expansion rate of the universe on large scales. The potential has a minimum located at $\phi_{\text{min}} = \left(\frac{n m_{\text{Pl}} \Lambda^{4+n}}{\beta \rho}\right)^{1/(n+1)}$ where ρ is the total non-relativistic matter density. The chameleon rest mass at the minimum is $m^2 \approx \beta \frac{\rho}{m_{\text{Pl}} \phi_{\text{min}}^{n+1}}$. Chameleons also couple to photons in a way akin to the axion coupling $S_{EM} = - \int d^4x \sqrt{-g} \frac{e^{\phi/M_\gamma}}{4} F^2$ where g is the determinant of the metric $g_{\mu\nu}$ and $F^2 = F_{\mu\nu} F^{\mu\nu}$ where $F_{\mu\nu}$ is the photon field strength. The chameleon

parameter space depends on the discrete index n and two continuous parameters $\beta = \frac{m_{\text{Pl}}}{M_m}$, the coupling to matter, and M_γ the suppression scale of the coupling to photons. It is also convenient to introduce the photon coupling parameter $\beta_\gamma = \frac{m_{\text{Pl}}}{M_\gamma}$.

Chameleons can be produced during the propagation of photons inside the macroscopic magnetic fields of the sun. The mixing of photons and chameleons depends on $k^2(\omega) = \omega^2 - m_{\text{eff}}^2 \left(\frac{\cos \theta + 1}{2 \cos 2\theta} \right)$ where the effective mass is $m_{\text{eff}}^2 = m^2 - \frac{B^2}{M_\gamma^2} - \omega_{\text{pl}}^2$ and ω is the initial frequency of the incoming photons. This depends on the mixing angle which is given by $\tan 2\theta = \frac{2\omega B}{M_\gamma m_{\text{eff}}^2}$ and the plasma frequency which is $\omega_{\text{pl}}^2 = \frac{4\pi\alpha n_e}{m_e}$ where α is the fine structure constant. Electro-neutrality implies that, in the sun, $n_e = \frac{\rho m}{m_p}$, where m_p is the proton mass. When $\theta \ll 1$: as is the case in most helioscope pipes and also inside the sun, we have $\theta = \frac{\omega B}{M_\gamma m_{\text{eff}}^2}$. Chameleon production in a magnetised region of size L is obtained from the transition probability $P_{\text{chameleon}}(\omega) = \sin^2(2\theta) \sin^2\left(\frac{\Delta}{\cos 2\theta}\right)$ where $\Delta = m_{\text{eff}}^2 L / 4\omega$. It is important to notice that chameleon production is only possible when $\omega^2 \geq m_{\text{eff}}^2$ for small values of θ . We focus on a conservative assumption, where a constant magnetic field is present in a small shell of size $0.01 R_\odot$ around the tachocline about $0.7 R_\odot$ with $B = 30\text{T}$. Chameleons are non-resonantly produced in this magnetised region and would lead to the X-ray spectrum in a CAST-like experiment shown in Fig. 1. The couplings $\beta = 10^6$ and $\beta_\gamma = 10^{10.29}$ are chosen according to the sensitivity diagram shown in Fig. 2 at the 2σ level for a detection rate of one count per hour. The photon coupling is (almost) saturating the solar excess luminosity bound for exotic particle production $\beta_\gamma \leq 10^{10.32}$ and is below the CHASE bound $\beta_\gamma \leq 10^{11}$. Some of the escaping chameleons can regenerate photons in the quiet sun's atmosphere. The corresponding spectrum is shown in Fig.3, contributing to the solar X-ray spectrum and maybe providing a possible mechanism to tackle the corona problem. Finally, powerful X-ray lasers could be used to test the existence of (sub-) keV chameleons. Indeed, chameleons could be produced in a magnetised vacuum pipe and cross a X-ray thick barrier while regenerating X-rays downstream. This would not be the case anymore when a gas at moderate pressure is injected into the pipes. Indeed, the mass of chameleons would increase and reduce the photon to chameleon conversion probability. For a spectrum with a flux of 10^{19} X-rays photons per second, we have given the regenerated X-ray spectrum in Fig. 4. For long pipes (multiple CAST pipes), a few days of observations could be enough to detect keV chameleons.

References

- [1] see P. Brax, A. Lindner, K. Zioutas, [arXiv:1110.2583 [hep-ph]], and references therein.

Solar flares as harbinger of new physics

K. Zioutas¹, M. Tsagri^{2*}, Y. Semertzidis³, T. Papaevangelou⁴, E. Georgiopoulou¹, A. Gardikiotis¹ and T. Dafni⁵

¹Physics Department, University of Patras, Patras, Greece

²European Organization for Nuclear Research (CERN), Genève, Switzerland

³Brookhaven National Laboratory, NY, USA

⁴IRFU, Centre d'Études Nucléaires de Saclay (CEA-Saclay), Gif-sur-Yvette, France

⁵Instituto de Física Nuclear y Altas Energías, Universidad de Zaragoza, Zaragoza, Spain

DOI: http://dx.doi.org/10.3204/DESY-PROC-2011-04/zioutas_konstantin

The trigger mechanism of the energy release of solar flares is still unknown. This work provides additional evidence on the involvement of exotic particles like axions and/or other WISPs. The axion scenario suggests a dynamical behaviour behind white-light (WL) solar flares, which results to the measured spectral shape, and, the timing between visible-UV light and soft X-rays. Similarly, axions converted some 1000 km inside the photosphere with a rest mass of ~ 17 meV fit the unexpected soft X-ray emission from the quietest Sun in 2009, i.e., the manifestation of the solar corona problem. Chameleons behave similarly, but they couple to photons enhanced in vacuum, i.e., in the magnetized empty outer space, since their coherent conversion length stretches with better vacuum.

1 Introduction

The solar coronal heating mechanism remains an unsolved problem since 1939, being therefore one of the prominent challenges in solar physics and astrophysics. In addition, the so called White-Light (WL) solar flares were observed for the first time in 1859, but their trigger remains elusive. In this work we provide additional evidence that the working principle of CAST can be at work at the Sun, where outstreaming solar axions can convert to the otherwise unexpectedly measured X-rays [1]. If CAST's working principle has been fine tuned by nature at the Sun, then the most promising places to look out for similar effects, should be preferentially above Active Regions (ARs), i.e., sunspots. Note that these regions are also the birth places of flares, while the corona above non-flaring/quiet ARs is hotter than the rest of the quiet Corona. The temperature reaches ~ 10 MK and the unexpectedly emitted photons have a characteristic spectral shape (power law) that resembles down-comptonized hard X-rays appearing otherwise unexpectedly [1]. Indeed, the “*Sun's intense X-ray emission is a remarkable and fascinating...mystery*” [2]. The idea of the down-comptonization underneath magnetized solar surface has been presented in [1]. Below, we update some of the conclusions in [1], following recent X-ray measurements with SPHINX in the ~ 1 –5 keV.

*Part of the PhD thesis.

2 The new observational evidence

2.1 The X-ray emission from the quietest Sun in 2009

The X-ray mission SPHINX has established a basal level of solar X-ray emission even during the most quiet solar minimum without flares or sunspots in 2009. The estimated quiet solar X-ray luminosity is $L_x \approx 6.7 \times 10^{20}$ erg/s $\approx 1.5 \times 10^{-13} L_\odot$ [3]. This fraction of the total solar luminosity is about 10 times below the numerical example given in Footnotes 9 and 14 of [1], and in consequence fits even better the scenario that axions escape from the solar hot core with a rest mass of about 17 meV and do convert to X-rays near the magnetized solar surface. In addition, the spectral shape follows a perfect power-law as it is shown in Figure 1, pointing at a depth of 1000 km below the surface as the initiation place of the following down-comptonization. The spectral agreement between observation (SPHINX) and simulation extends over 3-4 orders of magnitude (see Figure 1). The soft X-ray component below ~ 2.5 keV could be explained in general with light axions or other particles with similar couplings [1]. An alternative scenario is that with the solar chameleons [6, 7]. In fact, X-ray photons from regenerated outstreaming chameleons could emerge in the outer solar magnetic fields, resembling that of the 2-3 MK quiet Sun X-ray emission (see Figure 1). If the rest of the spectrum above 2.5 keV is real [4], such a second component might come, in principle, from regenerated axions in the upper photosphere / lower atmosphere, with suppressed down-comptonization. Furthermore, other exotica like radiatively decaying massive particles [5] could also be at the origin.

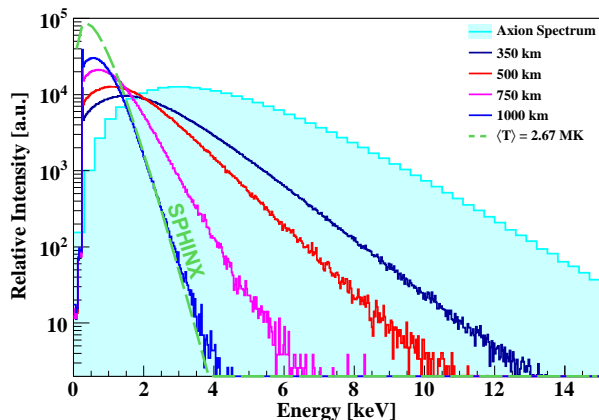


Figure 1: The shadowed histogram gives the expected converted solar axion spectrum. Four degraded spectra due to multiple Compton scattering from 4 different depths into the photosphere are also shown. The spectrum measured by the SPHINX mission (green dashed line) during the extremely quiet Sun in 2009 [4] agrees with that of the axion or axion-like scenario, assuming the conversion place is 1000 km underneath the photosphere [1].

2.2 The White-Light flares: analog spectrum and time correlations

Figure 2 shows the quiet Sun analog spectrum (in blue) [8] along with a few points (stars in red) of the white-light (WL) emission during a flare. One notes at the high-energy end the one flare-related point, which is far above that expected from the ~ 9000 K WL flare black-body emission. Thus, comparing with the quiet Sun spectral distribution with its striking photon excess at the high energy end ($> 10^{15}$ Hz), which reflects the solar corona problem, it seems that a flare develops its own and relatively more intense “corona”. This flare related “corona” is even better seen in Figure 2 of ref. [9], where the EUV intensity resembles also a flare’s

intense “corona”, being far above that of a black body WL flare distribution of $\sim 10^4$ K. The appearance of a flare “corona” fits our axion or axion-like picture, since it is widely accepted that a flare is magnetic in origin, though with several open questions remaining, like: where, when and how electrons are accelerated [10]? In the axion scenario an intervening magnetic field is just the catalyst, which transforms outstreaming axions or other particles like chameleons [6, 7] to photons near and/or far from the Sun. As it was noticed in [11, 12], the magnetic field is a viable flare forecasting tool, while what powers/triggers a solar eruption is not known. But, “*it might be possible that an unknown mechanism produces the black body white-light flare spectrum near 9000 K*” [11, 12](Figure 2). Moreover, the total energy radiated by flares exceeds by $\sim 100\times$ the flare soft X-ray energy emission, with a major contribution in the visible and near-UV. Then, the required axion conversion efficiency is not unnaturally large.

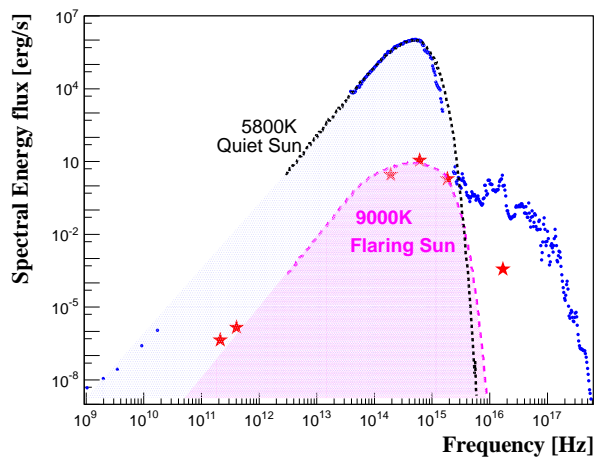


Figure 2: The continuum flare spectrum (red stars), with the dashed line representing a blackbody at ~ 9000 K. For comparison, it is also given the spectrum of the quiet Sun (blue points). The overall spectrum of the quiet Sun has a near blackbody shape at visible and near-IR. Excesses over a fitted blackbody appear at EUV and far-IR and beyond. The striking EUV excess of the quiet Sun is the manifestation of the solar corona problem. Courtesy H.S. Hudson [8].

As it is shown in Figure 3, the visible light (TSI) appears first and *later* takes place the soft X-ray emission. The axion scenario [1] for the WL flares is this: the energy deposition from converted axions streaming out of the inner Sun occurs at some deep photospheric layer. This gives rise to local ionization and thermalization, once a sufficiently strong magnetic field is combined with the appropriate density (which fits an axion rest mass of about 17 meV [1]), maximizing thus the coherence length for the axion-to-photon conversion to happen efficiently. The so heated-up environment does not thermalize completely to ~ 6000 K, and photons are escaping from the photosphere being a little hotter (~ 9000 K). In addition, thanks to the horizontal magnetic field component, an outwards moving compressed front is possible, which pushes the resonant axion-conversion place ($\rho \approx m_{axion}$) upwards. This results in a decreasing column density above the actual conversion place. With time, the newly back-converted hard X-rays 1) do propagate in an ionized environment, and 2) suffer a more and more limited down-comptonization until they leave the Sun as soft X-rays [1].

In other words, the sequence of events, is this: first starts the energy deposition by axion conversion in a relatively deep photospheric layer; this gives rise to the ambient ionization associated with a rather incomplete thermalization of about 10^4 K with the escaping WL. The initial hard X-rays make their way outwards in a random walk, once the ambient plasma is complete, which allows multiple Compton scatterings to occur. Following this reasoning, the soft X-ray emission can come only later, and this is what has been observed recently, only (!)

when analyzing many flares [11, 12]. An estimate of this time delay is interesting: the outward propagation speed of any energy deposition [13], e.g., by converted axions or other exotica, is about 1 km/s; this determines the compression time of the moving heated layer by some 500 km upwards inside the photosphere, which takes some 10 minutes. Interestingly, this order of magnitude estimate fits the observed delay of ~ 5 minutes (see Figure 3). In summary:

- a. the WL can come from not completely thermalized ~ 4 keV photons from converted axions (inverse Primakoff effect) at large photospheric depths, and
- b. this additional radiation pressure combined with the magnetic field in sub-photospheric layers [14] pushes the ionized axion conversion place upwards; the decreasing depth of the axion conversion layer (relative to that of the WL source origin), allows the X-rays to undergo a limited down-comptonization before escaping as soft X-rays with a characteristic power-law spectral shape, and this occurs 5 minutes later, matching also observation.

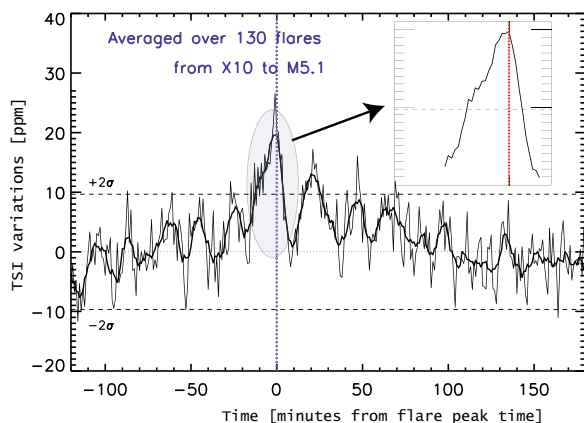


Figure 3: The excess time distribution of the Total Solar Irradiance (TSI) emission of 130 flares relative to the soft X-ray peak (= zero time) [11, 12]. X-rays come about 5 minutes later than the extra light emitted during flares. Courtesy M. Kretzschmar.

Thus, a chain of processes observed during WL flares fit the axion scenario. However, this does not exclude synergism with conventional physics reactions and/or the involvement of other WISPs; axions [1] and chameleons [6, 7] are rather two generic examples, which can be at work underneath and above the solar surface, respectively. Most probably, the conventionally mysterious multifaceted Sun cannot be understood only by a single global reaction mechanism.

3 Discussion

Outstreaming solar axions with a rest mass of ~ 17 meV can explain solar X-ray activity being enhanced above the magnetized photosphere [1]. Here we have elaborated the underlying processes, following the recent findings of WL flares. Following the same reasoning, the quiet and the flaring Sun appear as two extreme cases. Assuming that the same chain of processes happens in both cases, the photosphere dynamics determines the spectral outcome. Because, the initial axion conversion layer (i.e., the origin of the WL) can move with the compressed hot front at less deep layers upwards, being thus shielded with a decreased column density above

(i.e., the origin of the X-ray emission). This defines also the degree of the down-comptonization of the escaping radiation, –as it was pointed out in Figure 10 of [1]– the solar magnetic fields appear deeper in the quiet Sun than in the ARs, and therefore the quiet Sun is less X-ray active as a decreasing number of X-rays can reach the surface from deeper layers. This fits the fact that the solar corona above non-flaring ARs is hotter than that of the near quiet Sun (~ 10 MK *vs.* ~ 2 MK) [1].

As a second example of potential exotic particle involvement we mention solar chameleons with an energy of about 600 eV, which can be created near the strongly magnetized tachocline [7]. Since their conversion efficiency is maximum in vacuum, the magnetized solar outer space appears as their favourable place to get back-converted to soft X-rays by the inverse Primakoff effect. For example, the strong dipole magnetic field component between Sun and Earth ($\mathbf{BL} \approx 10^5$ Tm) is of relevance only for particles like chameleons. Similar or even stronger fields appear in Corona Mass Ejections ($\mathbf{BL} \approx 10^6$ Tm), since the magnetic field strength is up to 200 Gauss [15]. Then, the Sun, its near and/or far transverse magnetic field components as seen from an orbiting observatory, being sensitive up to 10 keV, resemble an Earth bound axion helioscope like CAST or Sumico. Such a “natural” helioscope might have occasionally a built-in axion or chameleon parameter fine tuning, which man made equipment did not yet have the time to reach.

4 Acknowledgments

We are thankful to Klaus Galsgaard, Manolis Georgoulis and Angelos Vourlidas for interesting discussions and suggestions. We also thank Hugh Hudson for allowing us to use Figure 2, and, Matthieu Kretzschmar for kindly generating for us Figure 3.

References

- [1] K. Zioutas, M. Tsagri, Y. Semertzidis, T. Papaevangelou, T. Dafni and V. Anastassopoulos, *New J. Phys.* **11** 105020 (2009)
- [2] S. Tsuneta, *AAPPS Bulletin*, 19(#3) 11 (June 2009)
- [3] S. Gburek et al., *Solar System Research* **45** 182 (2011) [see also *Eos Trans. AGU*, **91**(8), 73 (2010)]
- [4] S. Gburek et al., *Solar System Research* **45** 189 (2011); see also the contribution to these proceedings.
- [5] L. Di Lella and K. Zioutas, *Astropart. Phys.* **19**, 145 (2003)
- [6] P. Brax and K. Zioutas, *Phys. Rev. D* **82** 043007 (2010) [arXiv:1004.1846v1 [astro-ph.SR]]
- [7] P. Brax, A. Lindner and K. Zioutas, *Phys. Rev. D* (2012) *in press*, [arXiv:1110.2583v2 [hep-ph]]
- [8] H. S. Hudson, *Space Sci. Rev.* **158** 5 (2011)
- [9] H. S. Hudson, *RHESSI Nugget #145* (2011)
- [10] G. D. Fleishman, E. P. Kontar, G. M. Nita and D. E. Gary, *Astrophys. J. Lett.* **731** L19 (2011)
- [11] M. Kretzschmar, *Astron. & Astrophys.* **530** A84 (2011) [arXiv:1103.3125v2 [astro-ph.SR]]
- [12] M. Kretzschmar et al., *Nat. Phys.* **6** 690 (2010)
- [13] M. Georgoulis and A. Vourlidas, private communication (May 2011)
- [14] C. J. Schrijver, *Adv. Space Res.* **43** 739 (2009)
- [15] N. Mittal and U. Narain, *J. Atm. Sol.-Ter. Phys.* **72** 643 (2010)

The SphinX Spectrometer for solar soft X-rays

Szymon Gburek, Janusz Sylwester

Space Research Center, Polish Academy of Sciences, Wroclaw, Poland

DOI: http://dx.doi.org/10.3204/DESY-PROC-2011-04/gburek_szymon

Solar Photometer in X-rays (SphinX) was an instrument designed to observe the Sun in the energy range 1.2 - 15.0 keV. SphinX was incorporated within the Russian TESIS X and EUV telescope complex aboard the *CORONAS-Photon* satellite which was launched on January 30, 2009 at 13:30 UT from the Plesetsk Cosmodrome in northern Russia. Since February 2009, SphinX was measuring solar X-ray radiation nearly continuously till the end of the mission in early December 2009. The principle of SphinX operation is explained. Information on SphinX data archive and the calibration is presented together with general recommendations for the data use.

1 Introduction

SphinX was a fast and sensitive spectrophotometer for observations of solar soft X-ray radiation in the energy range 1.2-15.0 keV with an energy resolution of 0.4 keV and a time resolution down to fraction of a second. SphinX initiated the measurements on February 20, 2009 about three weeks after the satellite launch. Since that time the instrument observed the Sun nearly continuously and collected measurements with a telemetry rate up to 150 MB/day till the end of active satellite operation i.e. 29 November, 2009.

For measurements of solar X-ray flux SphinX used four pure, 500 μm thick, silicon crystals placed inside XR-100CR detectors. The detectors were manufactured by US Amptek company. Each detector had 12.5 μm thick beryllium entrance window. Three of the detectors (called D1, D2 and D3) formed the main SphinX measurement block and were exposed directly to solar X-rays. The detector D1 operated with its nominal effective area (19.63 mm^2). Over the detectors D2 and D3 there were apertures placed in order to limit their sensitivity. The detector D1 with the highest effective area was designed to measure low intensity solar photon fluxes. Pileup and saturation in detector D1 would take place even for moderate solar flux. The aperture of the second detector D2 (0.495 mm^2) was chosen so that it gave good signal/noise ratio (S/N) measurements during moderate solar fluxes for which pileup in D1 could become a problem. The third detector D3 with the smallest aperture (0.01008 mm^2) could measure substantial signal for strong solar flux when pileup in detector D2 would appear (detector D1 would be completely saturated at such high flux values). The aperture of D3 detector was so small that it would not saturate even for the strongest solar flares. Thus, using this three detector block, it was possible to observe solar fluxes from the very small X-ray activity level to the strongest ever observed flares. The fourth detector D4 was in a special SphinX fluorescence measurement channel which was designed to measure X-ray fluorescence emission excited by solar radiation in narrow selected energy bands.

SphinX observed the Sun in the deepest in almost a century solar activity minimum. Thus much of the instrument broad measurement capabilities were unexploited. Due to low solar flux during the mission, detectors D3 and D4 measured the noise only. Detector D2 provided some useful signal but its measurements were always accompanied with simultaneous measurements from D1 detector with much better signal to noise ratio. Thus for flux and spectral variability analysis it is sufficient to use D1 measurements only.

The operation of SphinX consisted of two phases. In the first short lasting phase SphinX team was changing the instrument operation modes and on-board software in order to fix the optimum instrument operation conditions and data collection strategy. This optimum strategy was activated on April 6, 2009 and from that time the second phase of the mission lasted with no further instrument settings.

More information on SphinX, its data reduction and dissemination can be found in [1] and [2].

2 SphinX data

During its operation SphinX measured in the event counting mode and spectral mode.

In the event counting mode every single output pulse from the detector electronic system was processed. Output pulse was produced by electronics when an X-ray photon hit the detector crystal. The pulse amplitude was proportional to the photon energy. When pulse event was detected its amplitude was attributed to corresponding energy channel by the PHA electronics and the time of arrival was recorded. Next the event time and energy were stored by the SphinX onboard computer into telemetry memory frames each of eight kB in size. A single frame could store information for several thousands of events.

From the analysis of SphinX calibration data it was found that the optimum number of energy channels for flight SphinX operations is 256. In this way the energy bin width was few times smaller than FWHM. Thus all SphinX multichannel analyzers had 256 energy bins covering the useful energy range 1.2 - 15.0 keV. (Nominal energy range is 0 - 15 keV but due to amplifier detection threshold and filter transmissions useful range extends from 1.2 keV onwards.) Individual event arrival times were determined with the 1 μ s accuracy.

In the spectral mode, the events, detected in a given detector electronics system, were collected in a selected number of energy bins and stored as histograms in the telemetry frame together with the exposure times. Only 256-channel and ancillary, 4-band spectra (so called basic mode observations) were recorded during the mission.

The most versatile SphinX observing mode is the event counting mode. Indeed all the other observation modes, including the basic mode, can be reconstructed from the event data. The spectral mode was however useful for a fast onboard computer processing which was intended to serve the instrument quickly and autonomously in selected pre-programmed ways depending on the results of online analysis of the flux rates determined based on the basic mode records.

The eight kB memory frames containing SphinX events and spectra were packed by the onboard computer and send to telemetry with the cadence of usually one second. Sometimes the cadence was set to five or eight seconds in order to save on global telemetry quota. Together with SphinX events and spectra, an additional information on start/end times for each frame and housekeeping data were also send to telemetry. The data received from telemetry at the ground station were sent via internet to Solar Physics Division of Space Research Centre Polish Academy of Sciences (SRC-PAS) for further processing. These data were decompressed and separated into binary files containing typically several thousands of telemetry frames and

covering a couple of hours of the observing time.

The data in binary files were successively reduced to level-0 format. In the level-0 format SphinX event counting and spectral mode observations are stored as arrays using Interactive Data Language (IDL) native file format.

Analysis and interpretation of level-0 data is possible but necessitates a full knowledge of all instrumental effects which are embedded in the data.

In 2010, the SphinX data from the second phase of the mission were reduced to level-1 format. Reduction of data from the first mission phase is more difficult due to many changes of the instrument software and settings in that time and therefore cannot be performed automatically. However level-1 data for the first mission phase can be obtained from SRC-PAS on request.

3 SphinX data format, access and calibration Information

SphinX team recommends level-1 data for the external users. Level-1 data are of scientific grade and can be used without further knowledge of the instrument related issues.

On-line access to SphinX level-1 data is possible via internet catalogue available on dedicated SphinX server at the site http://156.17.94.1/sphinx_l1_catalogue/SphinX_cat_main.html

This catalogue comes with legend and description of the content. From level-1 catalogue it is also possible to download SphinX calibration FITS file and useful IDL software developed at SRC-PAS for data processing.

SphinX level-1 data are stored as event lists in Flexible Image Transport System (FITS) files. Well documented and standardized Office of Guest Investigator Programs (OGIP) FITS format was used for preparation of SphinX level-1 FITS files. A description of the OGIP FITS format also can be found on the level-1 catalogue website.

In the level-1 FITS files all kinds of SphinX events are stored. A special flag is associated with each particular event with description of its origin. These flags can be used to select events according to user specific needs. For instance, one can use flag to filter out events caused by X-ray photons. These can be used next for construction of the higher level data products (lightcurves or spectra) and together with the calibration information used for scientific analysis of the observations.

Data from X-ray tests of SphinX performed in Palermo at the XACT facility (2007) and at Bessy II synchrotron in Berlin (2008) were finally processed in 2010 in order to prepare all necessary calibration information for the SphinX data reduction and analysis. The calibration information is stored in a single OGIP FITS file - SphinX response FITS file. This FITS is named *SPHINX_RSP_256_nom_D1.fits* and contains detector response matrix (DRM) and tables for conversion of SphinX channels to energy. SphinX response FITS file also can be downloaded from the instrument level-1 catalogue page.

4 Application of SphinX data

SphinX had no spatial resolution over the solar disk and therefore observed the Sun as a star. Thus the data analysis focuses mainly on properties of spectra and lightcurves constructed from detector events. The data were collected during the deepest ever solar minimum observed in X-rays. There were no other instruments observing at that time with so high energy and temporal resolution as SphinX had and sensitivity covering similar energy range. Thus SphinX measurements give a unique reference point - the measurements of the lowest level of solar

activity in X-rays. Hence SphinX data allow for analysis of previously unknown quiet Sun X-ray flux, observations of soft X-ray emission associated with emerging active regions, investigations of small flare energetics and studies of the statistical properties of coronal activity. An example of the SphinX spectrum for a very low solar activity level measured by SphinX in the time interval 2009-09-11 10:35:00 - 2009-09-12 23:20:00 is shown in Figure 1.

An interesting feature of SphinX spectra obtained during very low activity times is that they cannot be fully explained using isothermal model only. There is an excess of the spectral signal over the isothermal best fit to data as is seen in Figure 1. The data and fit begin to diverge there at 2.5 keV. For the quiet Sun conditions the discrepancy of data and the isothermal fit is small because the signal has low statistical significance between 3 keV and 4 keV where it deeps into the level of orbital background arising from energetic particles. The contribution of the particle background is still under investigation. Longer integration time intervals for spectra accumulation are necessary in order to determine the properties of SphinX emission and background seen above 3keV.

The excess of spectral signal over the isothermal fit becomes much more pronounced for increased levels of solar activity. Explanation to the SphinX spectral shape in general necessitates more temperature components in the fit model. One possible additional contribution to be taken into account is the spectrum due to envisaged axion interaction with magnetic field. This contribution would be particularly important for higher solar activity intervals.

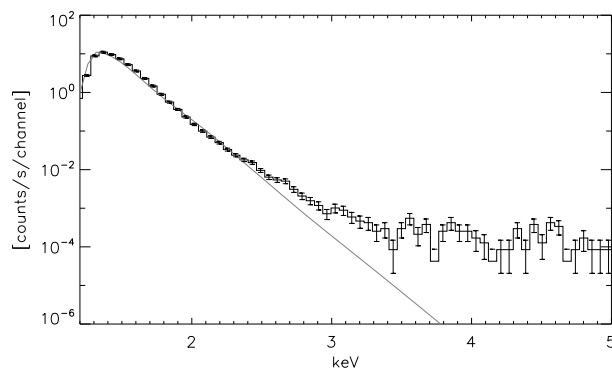


Figure 1: The SphinX solar X-ray spectrum measured for a very low activity period. The best isothermal model fit folded with DRM is shown in dashed line

5 Acknowledgments

The Polish Ministry of Education and Science grant no. N203 381736 is acknowledged for financial support of the SphinX project. The research leading to these results has received funding from the European Commission's Seventh Framework Programme (FP7/2007-2013) under the grant agreement SOTERIA (project n 218816, www.soteria-space.eu).

References

- [1] S. Gburek *et al.*, "Soft X-ray variability over the present minimum of solar activity as observed by SphinX", *Solar System Research*, Volume 45, Issue 2, pp.182-187 DOI: 10.1134/S0038094611020055, (2011).
- [2] S. Gburek *et al.*, "SphinX soft X-ray spectrophotometer: Science objectives, design and performance", *Solar System Research*, Volume 45, Issue 3, pp.189-199, DOI: 10.1134/S0038094611020067, (2011).

Solar Hidden Photon Search

Matthias Schwarz¹, Axel Lindner², Javier Redondo³, Andreas Ringwald², Günter Wiedemann¹

¹Hamburger Sternwarte, Gojenbergsweg 112, D-21029 Hamburg, Germany

²Deutsches Elektronen-Synchrotron DESY, Notkestraße 85, D-22607 Hamburg, Germany

³Max-Planck-Institut für Physik, Föhringer Ring 6, D-80805 München, Germany

DOI: http://dx.doi.org/10.3204/DESY-PROC-2011-04/schwarz_matthias

The Solar Hidden Photon Search (SHIPS) is a joint astroparticle project of the Hamburger Sternwarte and DESY. The main target is to detect the solar emission of a new species of particles, so called Hidden Photons (HPs). Due to kinetic mixing, photons and HPs can convert into each other as they propagate. A small number of solar HPs – originating from photon \rightarrow HP oscillations in the interior of the Sun – can be converted into photons in a long vacuum pipe pointing to the Sun – the SHIPS helioscope.

1 Introduction

Hidden Photons (HPs) are the gauge bosons of a hypothetical hidden local U(1) symmetry. Such symmetries arise in popular extensions of the Standard Model, especially in those based on string theory [1]. Known particles have no direct interaction with HPs (hence the latter are hidden), but still HPs may have a tiny residual interaction with them, as very massive particles with both electric and hidden charge can generate kinetic mixing with the standard photon [2]. In this case, the natural value of the kinetic mixing angle χ is that of a quantum correction, $\chi \sim ee_h/(16\pi^2)$. Since the hidden gauge coupling e_h can be very small and because of possible cancellations between different mediator contributions, there is no clear minimum for χ : values in the 10^{-16} – 10^{-3} range have been predicted in the literature [3, 4, 5, 6, 7]. The very feeble interaction makes HPs promising candidates for the dark sector that current cosmology and astrophysics are revealing. They have been proposed as Dark Matter (DM) [8, 9, 10, 11] and as mediating Dark Forces between DM particles [12, 13]. Moreover, if their mass is in the meV and their kinetic mixing in the micro range, their cosmological relic abundance could also provide the right amount of extra dark radiation [14] favored by recent CMB observations [15, 16, 17].

The kinetic mixing term induces flavor oscillations between photons and HPs [18]. After a propagation length L , a HP has a probability to convert into a photon (or viceversa) given by

$$P(\gamma' \leftrightarrow \gamma) = \frac{\sin^2 2\chi}{(\cos 2\chi + f)^2 + \sin^2 2\chi} \sin^2 \left(\frac{m_{\gamma'}^2 L \sqrt{(\cos 2\chi + f)^2 + \sin^2 2\chi}}{4\omega} \right), \quad (1)$$

where $m_{\gamma'}$ is the HP mass, setting the oscillation length $\propto 4\omega/m_{\gamma'}^2$, with ω the photon frequency, and $f = 2\omega^2 \Delta n/m_{\gamma'}^2$, encodes medium effects via $\Delta n = n - 1$, with n the photon index of refraction in the medium.

This oscillation mechanism enables us to search for HPs even if χ is tiny. One of the most powerful means to search for HPs is to measure the flux of HPs from the Sun [19, 20]. These HPs originate from oscillations of photons from the outer layers of the Sun’s interior and their flux predictions are covered by one of us in another article in these proceedings [21]. The enhanced luminosity from the solar surface produces a ring-like structure in the signal on Earth that can be used to optimize the signal-to-noise [22]. Therefore, imaging detectors might be very advantageous for searching for HPs.

In this article we report on the status of the Solar Hidden Photon Search (SHIPS), a search for the reconversion of solar HPs into detectable photons in a long light-tight vacuum tube tracking the Sun. SHIPS is an offspring of the ongoing ALPS (Any Light Particle Search) project [23, 24] at DESY in Hamburg.

2 Experimental setup

SHIPS is a helioscope-type experiment very much like SUMICO [25] at Tokyo University or the CERN Axion Solar Telescope (CAST) [26]. There is however an important difference: unlike these other helioscopes, SHIPS does not exploit a magnet. In fact, a background electromagnetic field is not needed for solar HP search, since HP-photon oscillations happen already in vacuum. This is in contrast to axion \leftrightarrow photon oscillations, which occur only in electromagnetic fields.

The expected number of photons originating from the reconversion of solar HPs in the vacuum tube is proportional to the HP flux ($\Phi_{\gamma'}$) the collecting area (A), the tube’s length (L), measuring time (T), and the oscillation probability (1),

$$N_{\gamma} = AT \int \frac{d\Phi_{\gamma'}}{d\omega} P(\gamma' \rightarrow \gamma) d\omega. \quad (2)$$

The oscillation probability can be enormously suppressed if $f \gg 1$, i.e. if the index of refraction is large. Therefore, the gas density has to be kept under a certain minimum given by the HP mass. To obtain optimal results, the collecting area and tube length should be as large as possible.

The current Telescope for Solar Hidden Photon Search TSHIPS consists of a 430 cm long stainless steel tube with a diameter of 25 cm combined from the tubes of two prototype vacuum vessels and a detector compartment (see Fig. 1). The upper tube is a lightweight vault structure developed for this project. TSHIPS is mounted on the Oskar Lühning Telescope (OLT) located at the Hamburger Sternwarte in Hamburg-Bergedorf and can thus be remotely controlled. It



Figure 1: The helioscope TSHIPS attached to the equatorial mount of the Oskar Lühning Telescope at the Hamburger Sternwarte.

SOLAR HIDDEN PHOTON SEARCH

will be run in a pressure range of 10^{-6} mbar or lower. A membrane pump creates a pre-vacuum of 10^{-2} mbar. A turbopump, directly attached to TSHIPS, establishes the required minimal pressure of less than 10^{-4} mbar in the helioscope volume of more than 260 liters within minutes.

Regenerated electromagnetic photons propagate along the same trajectories as their HP progenitors. This enables us to observe a source like our sun in the ‘light’ of HPs. The optical system is placed inside the detector compartment. The principal item is a Fresnel lens with a focal length of about 20 cm. This device ensures a high transitivity and image quality in the optical and near infrared band, where the solar flux of sub-eV mass HPs dominates as they are created deep in the solar photosphere. Initially available ultra-low-noise detectors are two photomultiplier tubes (PMTs) and a low-noise CCD camera, all cooled to minimize dark current. The frequency range of the detectors is chosen to be optical and near infrared. TSHIPS is currently mounted with a PMT featuring a dark current of approximately 2.8 Hz at ambient temperature. This makes single photons detectable. The other available PMT has even a lower dark current of 0.5 Hz.

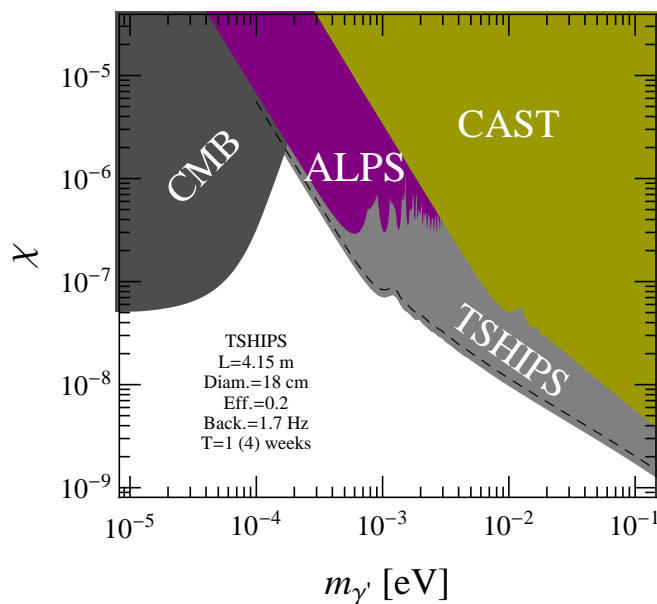


Figure 2: Current exclusion regions for hidden photons with kinetic mixing angle χ and mass $m_{\gamma'}$, in particular from the light-shining-through-a-wall experiment ALPS and from the helioscope experiment CAST, together with the projected sensitivity of TSHIPS (gray region).

3 Present status and outlook

The first measurements and results on HPs are expected within the next weeks. We estimated the dark current noise to be $\gamma_{dc} \simeq 1.7$ Hz. The significance of an HP flux discovery scales as $S = 2(\sqrt{N_\gamma + \gamma_{dc}T} - \sqrt{\gamma_{dc}T}) \sim N_\gamma/\sqrt{\gamma_{dc}T}$. Figure 2 shows the expected $S < 3$ exclusion limit (similar to 95% C.L.) achievable in 1 and 4 weeks of Sun tracking. Assuming a hypothetical

flux of solar HPs producing one photon every 100 seconds on TSHIPS, a discovery would be achievable during a data taking period of less than 2 days. The physical values of HP mass and coupling parameter could then be estimated by tuning experimental parameters in Eq. (2) such as the refractive index or the oscillation length.

Phase II planning has started for a much wider (diameter of 125 cm) and longer (13 m) helioscope. This massive tube will be put on a separate large alt az mount for long term operation and will probably be installed on the DESY premises. Detector development is ongoing in conjunction with other astronomical programs.

References

- [1] M. Goodsell and A. Ringwald, *Fortsch. Phys.* **58**, 716 (2010) [arXiv:1002.1840 [hep-th]].
- [2] B. Holdom, *Phys. Lett. B* **166**, 196 (1986).
- [3] K. R. Dienes, C. F. Kolda and J. March-Russell, *Nucl. Phys. B* **492**, 104 (1997) [arXiv:hep-ph/9610479].
- [4] S. A. Abel, M. D. Goodsell, J. Jaeckel, V. V. Khoze and A. Ringwald, *JHEP* **0807**, 124 (2008) [arXiv:0803.1449 [hep-ph]].
- [5] M. Goodsell, J. Jaeckel, J. Redondo and A. Ringwald, *JHEP* **0911**, 027 (2009) [arXiv:0909.0515 [hep-ph]].
- [6] M. Cicoli, M. Goodsell, J. Jaeckel and A. Ringwald, *JHEP* **1107**, 114 (2011) [arXiv:1103.3705 [hep-th]].
- [7] M. Goodsell, S. Ramos-Sanchez, A. Ringwald, [arXiv:1110.6901 [hep-th]].
- [8] J. Redondo and M. Postma, *JCAP* **0902**, 005 (2009) [arXiv:0811.0326 [hep-ph]].
- [9] M. Pospelov, A. Ritz and M. B. Voloshin, *Phys. Rev. D* **78**, 115012 (2008) [arXiv:0807.3279 [hep-ph]].
- [10] A. E. Nelson and J. Scholtz, *Phys. Rev. D* **84**, 103501 (2011) [arXiv:1105.2812 [hep-ph]].
- [11] P. Arias, *these proceedings*.
- [12] N. Arkani-Hamed, D. P. Finkbeiner, T. R. Slatyer and N. Weiner, *Phys. Rev. D* **79**, 015014 (2009) [arXiv:0810.0713 [hep-ph]].
- [13] S. Andreas, *these proceedings*, arXiv:1110.2636 [hep-ph].
- [14] J. Jaeckel, J. Redondo and A. Ringwald, *Phys. Rev. Lett.* **101**, 131801 (2008) [arXiv:0804.4157 [astro-ph]].
- [15] E. Komatsu *et al.* [WMAP Collaboration], *Astrophys. J. Suppl.* **192**, 18 (2011) [arXiv:1001.4538 [astro-ph.CO]].
- [16] J. Dunkley, R. Hlozek, J. Sievers, V. Acquaviva, P. A. R. Ade, P. Aguirre, M. Amiri and J. W. Appel *et al.*, *Astrophys. J.* **739**, 52 (2011) [arXiv:1009.0866 [astro-ph.CO]].
- [17] R. Keisler, C. L. Reichardt, K. A. Aird, B. A. Benson, L. E. Bleem, J. E. Carlstrom, C. L. Chang, H. M. Cho *et al.*, [arXiv:1105.3182 [astro-ph.CO]].
- [18] L. B. Okun, *Sov. Phys. JETP* **56**, 502 (1982) [*Zh. Eksp. Teor. Fiz.* **83**, 892 (1982)].
- [19] J. Redondo, *JCAP* **0807**, 008 (2008) [arXiv:0801.1527 [hep-ph]].
- [20] S. N. Gninenko and J. Redondo, *Phys. Lett. B* **664**, 180 (2008) [arXiv:0804.3736 [hep-ex]].
- [21] J. Redondo, *these proceedings*.
- [22] D. Cadamuro and J. Redondo, arXiv:1010.4689 [hep-ph].
- [23] K. Ehret *et al.* [ALPS Collaboration], *Nucl. Instrum. Meth. A* **612**, 83 (2009) [arXiv:0905.4159 [physics.ins-det]].
- [24] K. Ehret, M. Frede, S. Ghazaryan, M. Hildebrandt, E. -A. Knabbe, D. Kracht, A. Lindner and J. List *et al.*, *Phys. Lett. B* **689**, 149 (2010) [arXiv:1004.1313 [hep-ex]].
- [25] S. Moriyama, M. Minowa, T. Namba, Y. Inoue, Y. Takasu and A. Yamamoto, *Phys. Lett. B* **434**, 147 (1998) [hep-ex/9805026].
- [26] E. Arik *et al.* [CAST Collaboration], *JCAP* **0902**, 008 (2009) [arXiv:0810.4482 [hep-ex]].

The Sun in Hidden Photons

Javier Redondo

Max Planck-Institute für Physik, Föhringer Ring 6, D-80805 München, Germany

DOI: http://dx.doi.org/10.3204/DESY-PROC-2011-04/redondo_javier

We present some aspects and first results of the emission of sub-eV mass hidden photons from the Sun. The contribution from a resonant region below the photosphere can be quite significant, raising previous estimates. This is relevant for the Telescope for Hidden Photon Search, TSHIPS I, currently targeting at meV-mass hidden photons with $\mathcal{O}(10^{-6})$ kinetic mixing with the photon. These particles could account for the large effective number of neutrinos pointed at by the cosmic microwave background and other large-scale structure probes, and are motivated in some scenarios of string theory.

Paraphotons were first discussed by L. Okun as means to study the limits of our knowledge on electrodynamics [1]. The basic idea is that the photon (the interaction state that couples to electric charge) might not be a propagation eigenstate if there is a new species of vector boson that mixes with it. Okun parametrized the precision achieved in many observables in electrodynamics by means of the mixing angle, χ , and the mass, $m_{\gamma'}$ of the non-zero mass eigenstate, which he called paraphoton. Interestingly, he found that the most astonishing constraints on the mixing angle do not come from virtual effects as Lamb-shifts or deviations of Coulomb's law, but from the real emission of paraphotons from the Sun, although this depends strongly on $m_{\gamma'}$. In following works, the solar constraints were refined and also the idea of detecting the flux of paraphotons from the Sun with an helioscope was considered experimentally [2]. In these studies it was already realized that aiming at the low-energy part of the HP solar spectrum was more advantageous than focusing in the X-ray regime.

Some years later, theoretical advances put these ideas in a different context. It was realized that similar particles arise in extensions of the standard model as gauge bosons of hidden U(1) symmetries, i.e. symmetries under which fields of the standard model are left unchanged. The paraphoton was re-baptized as “hidden photon” (HP) in this context. Despite the hidden nature of these particles at tree-level, the key ingredient, the mixing with the photon can happen at one-loop level via radiative corrections. These corrections mix the photon and HP field strengths, $F_{\mu\nu}$ and $F'_{\mu\nu}$ resp., contributing to the kinetic mixing operator [3],

$$\mathcal{L}_{mix} = -\frac{1}{4}\chi F_{\mu\nu}F'^{\mu\nu}, \quad (1)$$

which being a renormalizable operator, it is only logarithmically sensitive to the energy-scale at which mixing is generated. This means that irrespectively of the high-energy physics completion of the SM that connects with the hidden sector, one can expect mixings of the order of a radiative correction $\chi \sim 10^{-3}$ [3]. These relatively large couplings are already excluded by a number of experiments and observations in the HP mass range $10^{-14} \sim 10^{10}$ eV [4]. But models in which the hidden and/or the electromagnetic U(1) are embedded in a non-abelian group, on in which the hidden gauge coupling is small—such as in the LARGE volume scenarios of Type-IIb string

theory— predict necessarily smaller mixings [5]. Values down to $\chi \sim 10^{-12}$ arise naturally in string theory, see [6] for a review.

More importantly, hidden photons have been motivated by recent observations. In cosmology they can account for the cold dark matter of the universe either via the misalignment mechanism—in much the same fashion as axions (see [7, 8] and the contribution of P. Arias to these proceedings)— or through their resonant production in the early universe [9] (for $m_{\gamma'} \sim 100$ keV, $\chi \sim 10^{-12}$). The resonant production of $m_{\gamma'} \sim$ meV HPs with $\chi \sim 10^{-6}$ happens after BBN and before structure formation. The creation of HPs and depletion of photons implies a sizable number of extra effective neutrinos ΔN_{eff} (a measure of the amount of dark radiation) imprinted in the CMB [10], just as recent cosmological probes are suggesting [11]. This last region of parameter space is the primary goal of the first Telescope for Solar Hidden Photon Search, TSHIPS I (see the contribution of M. Schwartz to these proceedings). In order to interpret its results it is crucial to have a reliable estimate of the solar HP flux in the visible region, where the telescope sensitivity is optimized.

The solar HP flux comes from oscillations of the photons of the solar interior into HPs, which then escape unimpeded, see [12] for a detailed theoretical study. In an inhomogenous medium, the oscillation probability can be estimated in a perturbative fashion through an integral over the putative photon trajectory inside the Sun, $r = r(s)$, as

$$P(\gamma \rightarrow \gamma') = \left| \chi \frac{m_{\gamma'}^2}{2\omega} \int_0^\infty e^{i\Phi(s) - \tau(s)} ds \right|^2 \quad (2)$$

where ω is the photon energy and

$$\Phi(s) = \int_0^s \frac{m_\gamma^2(r(s')) - m_{\gamma'}^2}{2\omega} ds' \quad ; \quad \tau(s) = \int_0^s \frac{\Gamma(r(s'))}{2} ds'. \quad (3)$$

Here $M^2 = m_\gamma^2 - i\omega\Gamma$ is the effective photon mass in the medium, generally complex and depending on the solar radial coordinate r . If it does not change appreciably in an absorption length, $\Gamma|d \log |M^2|/dr|^{-1} \ll 1$, we can approximate $M^2(r) \simeq M^2(r_0)$ to obtain

$$P(\gamma \rightarrow \gamma') = \frac{\chi^2 m_{\gamma'}^4}{(m^2(r_0) - m_{\gamma'}^2)^2 + (\omega\Gamma(r_0))^2}. \quad (4)$$

The differential HP flux results from integrating over the solar interior the photon emission rate times the conversion probability, which can be written and parametrized as

$$\frac{d\Phi_{\gamma'}}{d\omega} = \int_0^{R_\odot} \frac{r^2 dr}{D_{\text{Sun}}^2} \frac{\Gamma}{e^{\omega/T} - 1} \frac{\omega^2}{\pi^2} P(\gamma \rightarrow \gamma') \equiv \chi^2 \left(\frac{m_{\gamma'}}{\text{eV}} \right)^4 \int_0^{R_\odot} dr F(r, \omega, m_{\gamma'})$$

where $T = T(r)$ is the temperature and $D_{\text{Sun}} \simeq 1.5 \times 10^8$ km. A model of photon refraction and absorption of the solar interior $M^2(r)$ is needed. Refraction is determined by forward scattering off the ambient electrons, either free or bound in atoms, while absorption happens through a number of reactions involving electrons, mainly inverse bremsstrahlung and Thomson scattering. The required quantities depend on the position inside of the Sun via T , the density of electrons (n_e) and the solar composition, which are available from solar models. The calculations shown here use data from [13], which offers great detail in the outer layers of the Sun.

THE SUN IN HIDDEN PHOTONS

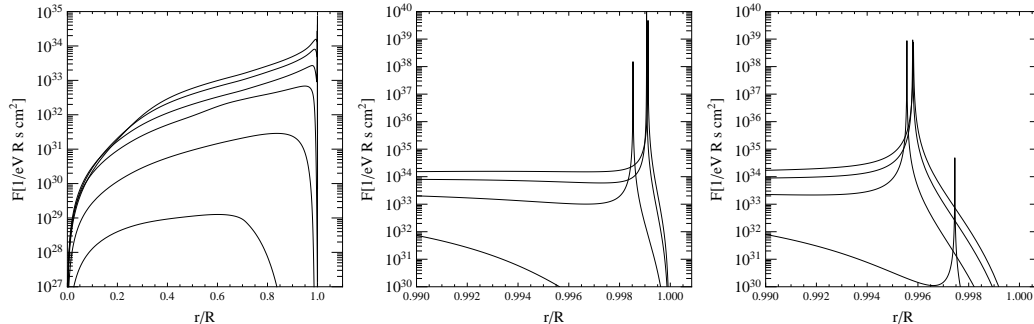


Figure 1: The flux function $F(r, \omega, m_{\gamma'})$ for $m_{\gamma'} = 0$ (LEFT and CENTER) and $m_{\gamma'} = 0.1$ eV (RIGHT). The curves show different HP energies $\omega = 2, 3, 6, 14, 10^2$ and 10^3 eV (top to bottom). In the last plots the two highest energies are not visible.

Before discussing our numerical results, it is possible to obtain a bit of analytical insight. For the low mass HPs of interest, the flux function F does not depend on $m_{\gamma'}$ in the solar interior $F(r, \omega, m_{\gamma'}) \simeq F(r, \omega, 0)$. In this region, $m_{\gamma'}^2$ is determined by the electron density and mass (m_e) through the plasma frequency, $m_{\gamma'}^2 = \omega_p^2 \propto n_e/m_e$, while the absorption coefficient is dominated by electron-proton bremsstrahlung, which gives $\Gamma \propto n_e n_p (1 - e^{-\omega/T}) / (m_e^{3/2} T^{1/2} \omega^3)$ where n_p is the proton density. Using Eq. 4 with $n_p \simeq n_e$ and $\omega\Gamma \ll m_{\gamma'}^2$ we find

$$F(r, \omega) \propto r^2 e^{-\omega/T} / (\omega \sqrt{T}). \quad (5)$$

This shows that the flux of low mass HPs from the solar interior is not suppressed by the larger electron density, as previously stated. It is however suppressed by the temperature and the volume factor r^2 such that the solar external shells and low HP energies do indeed dominate. The energy emission is more evenly distributed, as the integral over energies of F is $\propto r^2 \sqrt{T}$, which is relatively constant inside the Sun. A plot of $F(r, \omega, 0)$ is shown in Fig. 1 (LEFT). In this figure we also see sharp peaks close to the solar surface, which we have magnified in Fig. 1 (CENTER). These peaks arise from resonances where $m_{\gamma'}^2 = 0$ because the positive contribution from free electrons is cancelled by a negative contribution arising from electrons bounded in Hydrogen atoms oscillating below their resonant energy. In the Sun, the most important resonance is the Ly- α transition at $\omega_{12} \simeq 10.2$ eV. Other resonances play a role only for HP energies very close to them.

For nonzero HP mass, the resonant condition becomes $m_{\gamma'}^2 - m_{\gamma'}^2 = 0$ and the regions of

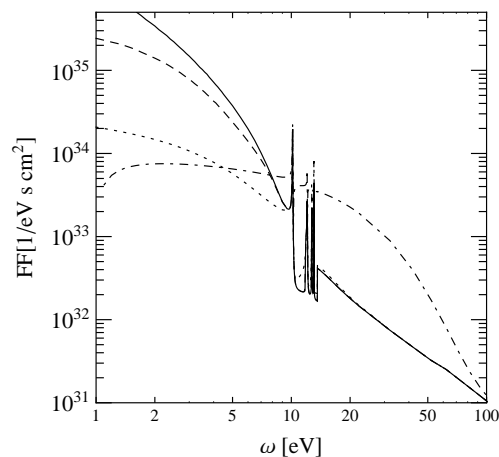


Figure 2: The Sun-integrated HP flux function $\int_0^{R_\odot} dr F(\omega, m_{\gamma'})$ as a function of the HP energy, for $m_{\gamma'} = 0, 0.01, 0.1$ and 1 eV, resp. solid, dashed, dotted and dot-dashed.

resonant conversion move deeper into the Sun as m_γ^2 grows more positive inside the Sun where the density and the ionization fraction are larger, see [14]. In Fig. 1 (RIGHT) we show how the peak structure of F moves inwards in the $m_\gamma = 0.1$ eV case with respect to the massless limit.

At low energies, the resonant photon \leftrightarrow HP conversion contributes significantly to the total HP flux or dominates it completely. In Fig. 2 we show the Sun-integrated emission for different HP masses as a function of energy. The results are significantly larger than the conservative estimate used in [15], based upon an uncomplete solar model and neglecting bound electrons. In this calculation we have only taken into account the resonant transitions of Hydrogen and assumed the validity of Eq. 4. The contribution of Helium and metals is likely to be irrelevant for the low energy HP flux ($\omega \sim \mathcal{O}(\text{eV})$) since they are much less abundant than Hydrogen. Also, their strongest resonant transitions happen at frequencies higher than ω_{12} and their contributions to m_γ^2 are inversely proportional to the resonant frequency squared. The assumption of Eq. 4 breaks necessarily down when approaching the solar surface. However, most of the low energy emission comes from the resonance which happens at a finite depth even in the $m_\gamma = 0$ case so Eq. 4 provides a good estimate in most of the cases. We plan to refine these estimates and arguments in a further publication.

Acknowledgments

I am very thankful to Davide Cadamuro, Jörg Jaeckel, Georg Raffelt, Andreas Ringwald, Pat Scott and Sergey Troitsky for discussions around the topic presented here and to the organizers of the 7th Patras meeting for a wondrous time in a much inspiring atmosphere.

References

- [1] L. B. Okun, Sov. Phys. JETP **56** (1982) 502 [Zh. Eksp. Teor. Fiz. **83** (1982) 892].
- [2] V. V. Popov and O. V. Vasil'ev, Europhys. Lett. **15** (1991) 7; V. Popov, Turkish Journal of Physics **23** (1999) 943 .
- [3] B. Holdom, Phys. Lett. B **166** (1986) 196.
- [4] J. Jaeckel and A. Ringwald, Ann. Rev. Nucl. Part. Sci. **60** (2010) 405 .
- [5] M. Goodsell, J. Jaeckel, J. Redondo and A. Ringwald, JHEP **0911** (2009) 027; M. Cicoli, M. Goodsell, J. Jaeckel and A. Ringwald, JHEP **1107** (2011) 114.
- [6] M. Goodsell and A. Ringwald, Fortsch. Phys. **58** (2010) 716 .
- [7] A. E. Nelson and J. Scholtz, Phys. Rev. D **84** (2011) 103501 .
- [8] P. Arias, D. Cadamuro, M. Goodsell, J. Jaeckel, J. Redondo and A. Ringwald, DESY 11-226; MPP-2011-140; IPPP/11/80; DCPT/11/160.
- [9] J. Redondo and M. Postma, JCAP **0902** (2009) 005; M. Pospelov, A. Ritz and M. B. Voloshin, Phys. Rev. D **78** (2008) 115012.
- [10] J. Jaeckel, J. Redondo and A. Ringwald, Phys. Rev. Lett. **101** (2008) 131801;
- [11] E. Komatsu *et al.* [WMAP, Astrophys. J. Suppl. **192** (2011) 18 ; J. Dunkley *et al.* , Astrophys. J. **739** (2011) 52 ; R. Keisler *et al.*, Astrophys. J. **743** (2011) 28 .
- [12] J. Redondo, JCAP **0807** (2008) 008 ;
- [13] S. Turck-Chieze *et al.*, Astrophys. J. **555** (2001) L69.
- [14] D. Cadamuro and J. Redondo, arXiv:1010.4689 [hep-ph].
- [15] S. N. Gninenko and J. Redondo, Phys. Lett. B **664** (2008) 180 .

Chapter 4

Cosmological Implications and Constraints

Cosmological constraints on thermal relic axions and axion-like particles

Davide Cadamuro¹, Javier Redondo¹

¹Max-Planck-Institut für Physik, Munich, Germany

DOI: http://dx.doi.org/10.3204/DESY-PROC-2011-04/cadamuro_davide

Cosmological precision data can be used to set very strict constraints on Axions and Axion-like particles (ALPs) produced thermally in the big bang. We briefly review the known bounds and propose two new constraints for Axions and ALPs decaying in the early universe, based upon the concomitant dilution of baryon and neutrino densities, using WMAP7 and other cosmological data.

1 Cosmology of decaying axions and ALPs

The axion is a pseudo-Goldstone boson arising from the spontaneous breaking of the global axial Peccei-Quinn $U(1)$ symmetry proposed to solve the strong CP problem [1]. The effective lagrangian relevant for this work includes only their coupling to photons

$$\mathcal{L}_{\text{eff}}^a = \frac{1}{2} \partial^\mu a \partial_\mu a - \frac{1}{2} m_a^2 a^2 - a \frac{g_{a\gamma}}{4} F^{\mu\nu} \tilde{F}_{\mu\nu}. \quad (1)$$

Considering couplings to electrons and other leptons changes only slightly our conclusions. The mass and the photon coupling are calculable in chiral perturbation theory as [1],

$$m_a = \frac{f_\pi m_\pi}{f_a} \frac{\sqrt{m_u m_d}}{m_u + m_d} \simeq 6 \text{ eV} \left(\frac{10^6 \text{ GeV}}{f_a} \right) \quad (2)$$

$$g_{a\gamma} = \frac{\alpha}{2\pi f_a} \left(\frac{E}{N} - \frac{2}{3} \frac{m_u + 4m_d}{m_d + m_u} \right) \equiv \frac{1.9 \alpha \delta}{2\pi f_a}. \quad (3)$$

and are related to each other via δ , a free $\mathcal{O}(1)$ parameter. The two-photon coupling allows the decay $a \rightarrow \gamma\gamma$, at the rate

$$\Gamma_{a\gamma\gamma} = \frac{g_{a\gamma}^2 m_a^3}{64\pi}. \quad (4)$$

The two photon coupling allows to axions thermalize in the early universe via the Primakoff process $q^\pm + \gamma \leftrightarrow q^\pm + a$. However, at some temperature axions decouple. Additional axion interactions with pions or electrons can lower the decoupling temperature, but are not relevant for this discussion. This thermal axion population behaves as hot dark matter, which is currently disfavoured, implying the constraint $m_a < 0.7 \text{ eV}$ [2].

The axion lifetime $\tau = \Gamma_{a\gamma\gamma}^{-1} \sim 10^{24} \text{ s} (\text{eV}/m_a)^5 \delta^{-2}$ becomes shorter than the age of the universe if the mass exceeds $\sim 20 \text{ eV}$ and the above bound loses his meaning. We have therefore explored the possibility that, above a certain mass, the axion could disappear from the universe without leaving any observable trace [3]. Still, the decay of axions would affect

BBN, the neutrino temperature and the CMB. The exquisite precision of cosmological data sets permits to constrain the axion parameters. All in all, we found that axions are allowed by cosmology to have $m_a > 300$ keV [3].

These cosmological limits become even more interesting in the case of axion-like particles (ALPs): pseudo-scalars having similar properties of the axion except the relation between the mass and the photon coupling, which are now free to span the whole parameter space [4]. In a recent paper [5], we have extended to ALPs the axion cosmological bounds we found in [3]. The summary of the constraints we found is in Fig. 2, together with some other relevant cosmological and astrophysical bounds.

The most interesting bounds arise because of the entropy released during the decay. As the decay products are photons (and in some axion models also electrons), *this entropy is shared only among the species in thermal equilibrium with the electromagnetic radiation*. If axions or ALPs decay when inverse reactions are efficient, $\gamma\gamma \rightarrow a$, they do it in local thermal equilibrium (LTE). This is the case if ALPs decay when the temperature exceeds greatly their mass. The raise in entropy follows from entropy conservation by counting the relevant relativistic degrees of freedom g_{*S} before and after the disappearance, like one usually does for the e^\pm annihilation. For instance, if axions or ALPs decay affects only photons, the photon entropy is increased by a factor $(2 + 1)/2 = 3/2$.

The other extreme possibility is that the temperature is smaller than the mass when axions or ALPs decay, which implies far out-of-equilibrium decay. In this case the energy density in scalars can even dominate the universe expansion thrusting in a huge amount of entropy. In this case, one finds [6]

$$\frac{S_f}{S_i} \sim \frac{m_a R}{\sqrt{m_{\text{Pl}} \Gamma_{a\gamma\gamma}}} \quad (5)$$

where R is the number of ALPs per photon before the decay. Solving the Boltzmann equations we exactly calculated the entropy emitted during the decay and how this influences the thermodynamics of the other species.

2 Number of effective neutrinos

If axions or ALPs decay after the decoupling of neutrinos, the latter can not be heated by the radiation released and the final ratio T_ν/T_γ would be lower than the standard value $(4/11)^{1/3}$. The number of effective neutrinos is defined as

$$N_{\text{eff}} = \frac{8}{7} \left(\frac{11}{4} \right)^{4/3} \frac{\rho_\nu}{\rho_\gamma} \quad (6)$$

to measure the neutrino energy density. From WMAP7, the 7th release of the SDSS and the measurement of H_0 by the HST, we obtained the following limits on N_{eff} [3]

$$N_{\text{eff}} > \begin{cases} 2.70 & \text{at 68\% C.L.} \\ 2.39 & \text{at 95\% C.L.} \\ 2.11 & \text{at 99\% C.L.} \end{cases} \quad (7)$$

assuming a prior $N_{\text{eff}} < 3$ because we assume only 3 standard neutrinos and in the ALP decay scenario sketched the ALP decay can only increase ρ_γ , i.e. lower N_{eff} . We plot our results in Fig. 2 in the ALP mass and lifetime plane. Axion models with $\delta = 1$ lie along the steep line labelled KSVZ.

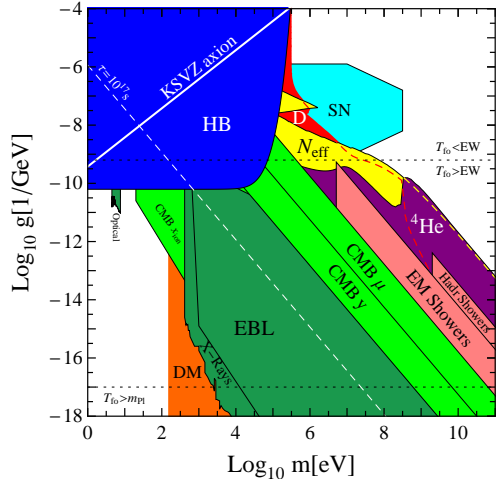


Figure 1: Summary of ALP bounds in the mass-coupling plane. The ALP relic density exceeds the observed value in the region labelled DM; EBL, Optical and X-Rays regions are excluded by the non observation of photons from relic ALP decay; The black-body spectrum of CMB would be unacceptably distorted by ALP decays in the regions labelled CMB. N_{eff} , D, Showers and He are described in the text; SN and HB are astrophysical bounds. See [5] for details.

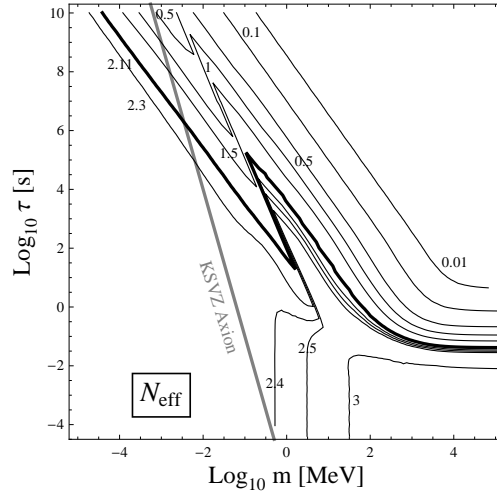


Figure 2: Isocontours of N_{eff} , as a function of the ALP mass m and the lifetime τ . The excluded region lies above the thick black line. LTE decay (lower-left corner) produces no bound for N_{eff} . In the upper-right corner the decay is out-of-equilibrium and during ALP domination: ν s are almost washed out. Decreasing τ the bound becomes less severe: it completely disappears τ shorter than the ν freeze-out [5]. For the KSVZ axion $m_a \gtrsim 3$ keV is allowed at 99% C.L.. [3].

3 Primordial Nucleosynthesis

The photons emitted in ALP decays decrease the baryon to photon ratio η_B , which is well measured from CMB to be $\eta_B^{\text{CMB}} = 6.23 \times 10^{-10}$. This value agrees with what inferred from standard BBN. If a relic population decays before the CMB release but after BBN it means BBN happened with a higher η_B , i.e. $\sim (S_f/S_i)\eta_B^{\text{CMB}}$. The LTE value $S_f/S_i = 3/2$ is enough to create a disagreement between BBN simulations and the observation of primordial elements. ALPs with longer lifetimes decay increasingly out-of-equilibrium and rise the tension, unless a decrease in R compensates the growth of $(\Gamma_{a\gamma\gamma})^{-1/2}$, c.f. Eq. (5) (the sharp features of our results correspond to the large decrease in R when ALPs decouple around the QCD phase transition). Deuterium is the most affected nucleus in a high η_B BBN, where it can be more efficiently processed into heavier elements: it is the best observable to test S_f/S_i . Values of $D/H < 2.2 \times 10^{-5}$ are presently excluded at 99% C.L., which allows only axions with mass larger than 300 keV [3]. The results for the ALP case are plotted in Figs. 3. Higher mass ALPs initiate EM and hadronic showers, which dissociate nuclei. Also ALPs decays produce charged pions, whose presence alters the neutron/proton equilibrium. In general, they enhance n_n/n_p , which can even reach values ~ 1 . This translates into high He and D/H yields [5]. The N_{eff} , D and He limits are presently the most constraining ones for shorter ALP lifetimes.

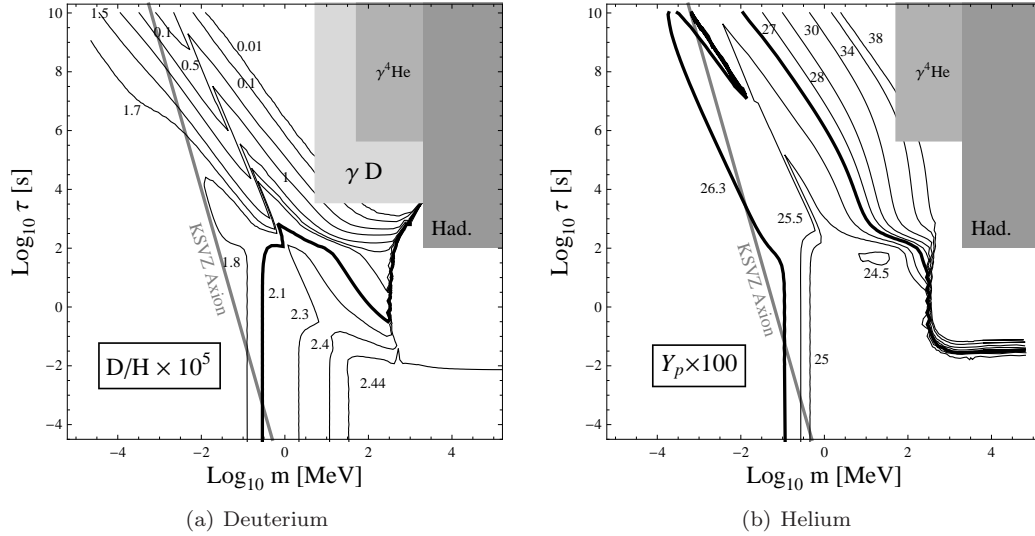


Figure 3: Deuterium to proton abundances ratio (left) and helium mass fraction (right) from BBN in the decaying ALP cosmology, as in Fig. 2. The LTE decay (lower-left corner) case is enough to exclude masses below 300 keV at 99% C.L. because of D underproduction, also for the KSVZ axion [3]. Massive ALPs dissociate nuclei through EM and hadronic cascades and are excluded in the grey regions. BBN happens in a low N_{eff} universe for $\tau < 100$ s, which generally translates into helium overproduction. For shorter lifetimes ($\tau \sim 0.1 - 100$ s) the decay produces charged pions that enhance the neutron-to-proton ratio at BBN, resulting in a high D/H and He mass fraction [5].

References

- [1] R. Peccei, Lect. Notes Phys. **741** (2008) 3-17; J. E. Kim, Phys. Rept. **150** (1987) 1-177.
- [2] S. Hannestad, A. Mirizzi, G. G. Raffelt and Y. Y. Y. Wong, JCAP **1008** (2010) 001
- [3] D. Cadamuro, S. Hannestad, G. Raffelt, J. Redondo, JCAP **1102** (2011) 003.
- [4] E. Massó and R. Toldrà, Phys. Rev. D **52** (1995) 1755; E. Massó and R. Toldrà, Phys. Rev. D **55** (1997) 7967.
- [5] D. Cadamuro, J. Redondo, [arXiv:1110.2895].
- [6] E. W. Kolb, M. S. Turner, “The Early universe”, Front. Phys. **69** (1990).

How a cold axion background influences photons

Domènec Espriu, Albert Renau

Departament d'Estructura i Constituents de la Matèria and Institut de Ciències del Cosmos (ICCUB), Universitat de Barcelona, Martí i Franquès 1, 08028 Barcelona, Catalonia, Spain

DOI: http://dx.doi.org/10.3204/DESY-PROC-2011-04/espriu_domènec

A cold relic axion condensate resulting from vacuum misalignment in the early universe oscillates with a frequency $\sim m_a$, where m_a is the axion mass. We summarize how the properties of photons propagating in such a medium are modified. Although the effects are small due to the magnitude of the axion-photon coupling, some consequences are striking.

1 Introduction

Cold relic axions resulting from vacuum misalignment in the early universe is a valid candidate for dark matter [1]. In this model, a coherent spatially constant axion field (it may be a Peccei-Quinn axion [2] or a similar field) acquires a mass m_a once instanton effects set in to find itself, in general, not in the minimum of the potential. In late times, the axion field oscillates,

$$a(t) = a_0 \cos m_a t, \quad (1)$$

and the energy density stored in these oscillations is $\rho \simeq a_0^2 m_a^2$, contributing to the energy budget.

Axions affect photons in a universal way, described by $\mathcal{L}_{a\gamma\gamma}$

$$\mathcal{L}_{a\gamma\gamma} = g_{a\gamma\gamma} \frac{\alpha}{2\pi} \frac{a}{f_a} F_{\mu\nu} \tilde{F}^{\mu\nu}.$$

Popular models such as DFSZ and KSVZ [3] all give $g_{a\gamma\gamma} \simeq 1$. Using (1) this becomes

$$\mathcal{L}_{a\gamma\gamma} = -g_{a\gamma\gamma} \frac{\alpha a_0}{\pi f_a} \cos(m_a t) \epsilon^{ijk} A_i F_{jk}.$$

Note that the above term is Lorentz non-invariant.

A natural question is whether and how the presence of this axion background could be detected thus making the cold axion hypothesis plausible. Three possible effects are proposed: (1) Cold axions influence cosmic ray propagation and induce photon Bremsstrahlung; (2) Cold axions induce an additional rotation in the polarization plane of light (on top of the familiar one [4]); and (3) Some photon wave-lengths are forbidden in a universe filled with cold axions.

In this talk we shall concentrate mostly on points (2) and (3). Point (1) has been discussed in detail in [5]. In order to determine the properties of photons in such a medium we need to solve the equation of motion in momentum space

$$[g^{\lambda\nu} (k^2 - m_\gamma^2) + i \epsilon^{\lambda\nu\alpha\beta} \eta_\alpha k_\beta] \tilde{A}_\lambda(k) = 0. \quad (2)$$

where $\eta_\alpha \sim \partial_\alpha a = \delta_\alpha^0 \dot{a}$. Two complex and space-like chiral polarization vectors $\varepsilon_\pm^\mu(k)$ can be defined (see [6]).

Let us now assume that we are dealing with photons of momenta $|\mathbf{k}| \gg m_a$. Then it makes sense to treat in (2) the axion background adiabatically with $\eta_\alpha = (\eta_0, 0, 0, 0)$ where η_0 can be taken as approximately constant, and $\eta_0 = 2g_{a\gamma\gamma} \frac{\alpha}{\pi} \frac{a_0 m_a}{f_a}$. The two polarization vectors are solutions of the vector field equations if and only if

$$k_\pm^\mu = (\omega_{\mathbf{k}\pm}, \mathbf{k}) \quad \omega_{\mathbf{k}\pm} = \sqrt{\mathbf{k}^2 + m_\gamma^2 \pm \eta_0 |\mathbf{k}|}. \quad (3)$$

The astrophysical and observational bounds indicate that $\eta_0 < 10^{-20} \text{eV}$. The situation when $|\mathbf{k}| \leq m_a$ will be discussed later.

2 Bremsstrahlung

The process $p(\mathbf{p}) \rightarrow p(\mathbf{p}-\mathbf{k})\gamma(\mathbf{k})$ (or $e \rightarrow e\gamma$) is possible in a Lorentz-violating theory. The cold axion background provides the necessary source of Lorentz non-invariance. Cosmic rays can lose energy due to the radiation of photons while preserving momentum and energy conservation thanks to eq. (3). The differential decay width for the process is [5]

$$d\Gamma(Q) = \frac{\alpha}{2} \frac{|\mathbf{k}|}{|\mathbf{p}|} \frac{1}{E\omega_{\mathbf{k}}} (-p \cdot k + |\mathbf{p}|^2 \sin^2 \theta) d|\mathbf{k}|,$$

and in the relevant limit $E \ll m_p^2/|\eta_0|$ we have

$$\frac{dE}{dx} = -\frac{\alpha\eta_0^2 E^2}{4m_p^2}, \quad E(x) = \frac{E(0)}{1 + \frac{\alpha\eta_0^2}{4m_p^2} E(0)x}.$$

From the likely detection of extragalactic cosmic rays we can get a model independent bound $\eta_0 < 10^{-15} \text{eV} \Rightarrow f_a > 100 \text{GeV}$ (i.e. exclude weak scale axions in a completely model independent way).

However the total amount of energy loss for a cosmic ray is very low. It is therefore more meaningful to look for the radiated photons. Those emitted from electrons have a spectrum which is different from the overwhelming galactic synchrotron radiation background. Several hypothetical ways of detecting this radiation are discussed in [5].

3 Exotic rotation of the polarization plane

In order to find the effect of axions on the photon propagator one has to consider:

- A constant magnetic field (well known result). For simplicity we shall assume $\mathbf{k} \cdot \vec{B} = 0$.
- The cold axion background (new).

The photon propagator for $\mathbf{k} \cdot \vec{B} = 0$ is ($\vec{b} \equiv \frac{2g_{a\gamma\gamma}\alpha}{\pi f_a} \vec{B}$)

$$\mathcal{D}_{\mu\nu}(k) \simeq \frac{-ig_{\mu\nu}}{k^2} + \frac{ik_0^2 b_\mu b_\nu}{k^2[k^2(k^2 - m^2) - k_0^2 \vec{b}^2]} - g_\mu^j g_\nu^l \frac{\eta_0 k_0^2 [b_j(\vec{b} \times \vec{k})_l - b_l(\vec{b} \times \vec{k})_j]}{k^4 [k^2(k^2 - m^2) - k_0^2 \vec{b}^2]}.$$

HOW A COLD AXION BACKGROUND INFLUENCES PHOTONS



Figure 1: Propagator in the cold axion background and the magnetic field

Then, for a photon plane wave initially with an electric field forming an angle β with \vec{B} , the plane of polarization rotates as

$$\tan 2\alpha(x) = \frac{[1 + 2f(x)] \sin 2\beta + 3\eta_0|x| \cos 2\beta}{4f(x) + [1 + 4f(x)] \cos 2\beta - 3\eta_0|x| \sin 2\beta}, \quad f(x) = \frac{\vec{b}^4}{16m^4} k_0^2 |x|^2,$$

and the expected value for the angle is

$$\bar{\alpha} = -\frac{1}{2} \frac{[1 + 2f(x)] \sin 2\beta + 3\eta_0|x| \cos 2\beta}{[1 + 4f(x)] \cos 2\beta - 3\eta_0|x| \sin 2\beta}.$$

The rotation survives even without magnetic field and the effect is independent of the frequency. Note that the previous results hold only for table-top experiments when the photon can approximately be considered an eigenstate of energy, i.e. for a period where the time-of-flight of the photon is smaller than $2\pi/m_a$. We have not considered the relevance of the effect when the latter condition is not fulfilled. It is clear, however, that then the effect of the cold axion background has to be proportional to η_0^2 instead of η_0 .

4 What if $|\mathbf{k}| \leq m_a$? Forbidden wavelengths

As mentioned in the introduction, $a(t)$ changes sign with a period $2\pi/m_a$ and this is now relevant. Let us approximate the sinusoidal variation by a triangle wave (see 2) and solve exactly for the propagating modes. The equation for $\hat{A}_\nu(t, \vec{k})$ is

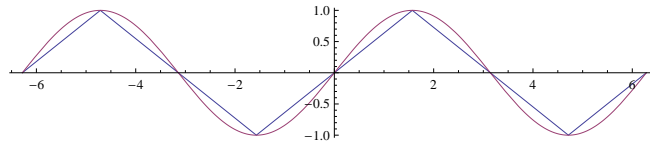


Figure 2: Triangle wave versus sine

$$\left[g^{\mu\nu} (\partial_t^2 + \vec{k}^2) - i\epsilon^{\mu\nu\alpha\beta} \eta_\alpha k_\beta \right] \hat{A}_\nu(t, \vec{k}) = 0. \quad \hat{A}_\nu(t, \vec{k}) = \sum_{\lambda=+,-} f_\lambda(t) \varepsilon_\nu(\vec{k}, \lambda).$$

We now write $f(t) = e^{-i\omega t} g(t)$ and demand that $g(t)$ have the same periodicity as $\eta(t) = \eta_0 \sin(m_a t)$. This requires

$$\cos(2\omega T) = \cos(\alpha T) \cos(\beta T) - \frac{\alpha^2 + \beta^2}{2\alpha\beta} \sin(\alpha T) \sin(\beta T), \quad T = \frac{\pi}{M_a}, \quad \alpha, \beta = \sqrt{k^2 \pm \eta_0 k}.$$

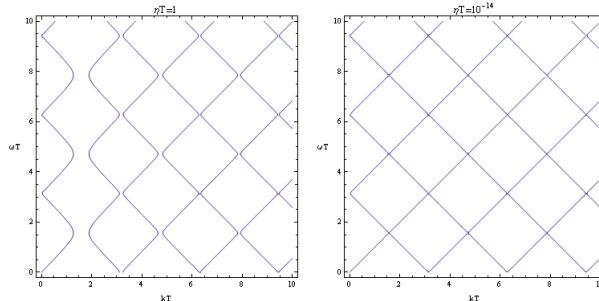


Figure 3: Forbidden wavenumbers

For $\eta_0 \equiv \eta_{\max} \ll m_a$ there is no relevant variation with respect to the decay rate computed assuming $|\mathbf{k}| \gg m_a$ is found, and this can be understood intuitively. However if η_0/m_a grows there is a surprise; some values of $|\mathbf{k}|$ admit no solution for ω . We arrive then at the striking conclusion that in a universe filled with cold axions oscillating with a period $2\pi/m_a$ some wavelengths are forbidden by a mechanism that is similar to the one preventing some energies from existing in a semiconductor. Of course the width of the forbidden bands is very narrow (proportional to η_0), hence difficult to detect. Further details can be found in [7]

Acknowledgments

It is a pleasure to thank K. Zioutas and the rest of organizers of Patras 2011 for an enjoyable conference and encouragement. We acknowledge financial support from projects FPA2010-20807, 2009SGR502 and Consolider CPAN.

References

- [1] L. Abbott and P. Sikivie, Phys. Lett. 120B, 133 (1983); M. Kuster, G. Raffelt and B. Beltran (eds), Lecture Notes in Physics 741 (2008).
- [2] R.D. Peccei, H.R. Quinn, Phys. Rev. Lett. 38 (1977) 1440; S. Weinberg, Phys. Rev. Lett. 40 (1978) 223; F. Wilzcek, Phys. Rev. Lett. 40 (1978) 279.
- [3] M. Dine, W. Fischler and M. Srednicki, Phys. Lett. B, 104, 199 (1981); A.R. Zhitnitsky, Sov. J. Nucl. Phys. 31, 260 (1980); J. E. Kim, Phys. Rev. Lett. 43, 103 (1979); M. A. Shifman, A. I. Vainshtein and V. I. Zakharov, Nucl. Phys. B 166, 493 (1980).
- [4] G. Raffelt and L. Stodolsky, Phys. Rev. D 37, 1237 (1988).
- [5] A. Andrianov, D. Espriu, F. Mescia and A. Renau, Phys. Lett. B 684 (2010) 101; D. Espriu, F. Mescia, A. Renau, JCAP 1108 (2011) 002.
- [6] A.A. Andrianov, D. Espriu, P. Giacconi and R. Soldati, JHEP 0909:057,2009.
- [7] D. Espriu and A. Renau, arXiv:1106.1662 [hep-ph] (to appear in Phys. Rev. D).

New constraints on very light pseudoscalars

A. Payez¹, J.R. Cudell¹, D. Hutsemékers¹

¹IFPA group, AGO Dept., University of Liège, Liège, Belgium

DOI: http://dx.doi.org/10.3204/DESY-PROC-2011-04/payez_alexandre

Nearly massless axion-like particles are of interest for astrophysical observations, and some constraints on their parameter space do exist in the literature. Here, we propose to put new constraints on these particles using polarisation and, in particular, the polarisation differences observed between different quasar classes.

There is quite a number of puzzling phenomena in astrophysics that could be clarified with the existence of very light scalar or pseudoscalar particles, commonly referred to as *axion-like particles* (a.k.a. ALPs). One of the main reasons is that these hypothetical particles can have a coupling to photons inside external magnetic fields, as in the axion case [1], and can lead to observable signatures in every measurable property of light: its intensity, its spectrum, or its polarisation. In this work, we want to present polarimetry as a tool to search for (or, at least, to constrain) the existence of such nearly massless particles.

To illustrate this, we use the sample of 355 high-quality polarisation measurements which confirmed the existence of large-scale correlations of (linear) polarisation position angles of visible light from quasars in some regions of the sky [2]. It was thought that these large-scale alignments could be naturally explained by ALP-photon mixing, as their phenomenology predicts the creation of linear (p_{lin}) and circular (p_{circ}) polarisations. However, the recent observation of vanishing circular polarisation [3] is a problem for this hypothesis; see [4] and references therein.

As ALPs cannot explain the alignments, these data can be exploited to constraint axion-like-particle parameters. We are going to consider objects located behind the Virgo supercluster, as we have information on p_{lin} and p_{circ} in this region. One can then consider ALP-photon mixing in the magnetic field of that supercluster, and check for which parameters the generated polarisation would match (or in this case contradict) the observations. We use the following:

- For the type of quasars we are discussing, which have linear polarisations at the 1%-level, it is known [5] that objects with broad absorption lines (BAL quasars) are typically more polarised than other radio-quiet quasars in the continuum: $\langle p_{\text{lin}}^{\text{BAL}} - p_{\text{lin}}^{\text{non-BAL}} \rangle \lesssim 2\%$. This feature still holds in the sample considered; the expected distributions of polarisation are thus preserved [6]. Therefore, while we do not have access to the initial polarisations, we know that the linear polarisation generated by ALP-photon mixing on the way towards us cannot be larger than 2%, otherwise we would not see the difference between the two quasar distributions anymore.
- Even though we know that quasars are intrinsically linearly polarised, we do not want to make assumptions on the initial distribution of polarisations. Therefore, to avoid any overestimation of the final (observed) polarisation, we start from unpolarised light beams.

ALP phenomenology tells us that we are going to underestimate the linear, but also the circular polarisation. This, in turn, will give us conservative constraints.

- As reported in [3], out of the 21 p_{circ} measurements of quasars, all have null circular polarisation, except two highly linearly polarised blazars which might be intrinsically circularly polarised. As we want to be conservative, we use a 3σ level bound for p_{circ} and require that the circular polarisation produced by ALP-photon mixing is within these bounds. Also, as we only have data for objects with $p_{\text{lin}} \geq 0.6\%$, we will only apply the p_{circ} constraint if the linear polarisation is such.

For cluster and supercluster magnetic fields [7], the morphology discussed in the literature is often a “patchy” one. More precisely, one can assume a cell-like composition, such that the magnetic field is constant in each cell¹ but its direction changes from cell to cell. Here, we allow for 3-dimensional rotations [4], so that when the field picks up a longitudinal component (most of the time), this leads to (much) lower values of the mixing, as only the transverse part of the magnetic field is relevant for ALPs. In the end, taking a slice of the magnetic field projected in the transverse plane, we get something similar to what is depicted in Fig 1.

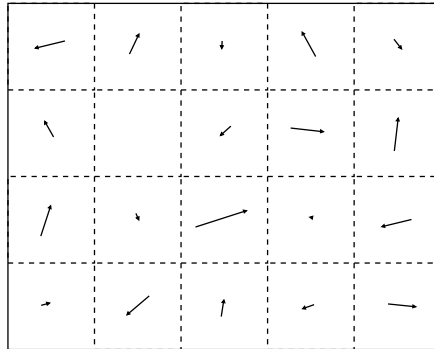


Figure 1: Sketch of the assumed cellular morphology for the transverse magnetic field in superclusters.

With such a configuration, when looking at objects located in different directions, we effectively look at different fields. As the exact structure of the magnetic field inside the Virgo supercluster is poorly known, we assume that the fields are sufficiently irregular so that, for photons coming from different objects, the encountered fields essentially correspond to random ones (with possibly some additional correlations at the supercluster scale).

Our constraints are obtained iteratively for each point in the ALP parameters space (mass m , and coupling to photons g). Each time, we first generate a random configuration for the magnetic field and, for an initially unpolarised light beam, calculate the linear and circular polarisations after propagation. We then change the magnetic field configuration and repeat, always comparing the results to our conservative constraints. With the number of successes over the number of trials, we eventually obtain a probability for the couple (m, g) . This probability

¹Here, for the sake of simplicity, we will not consider fluctuations; this is done in [8].

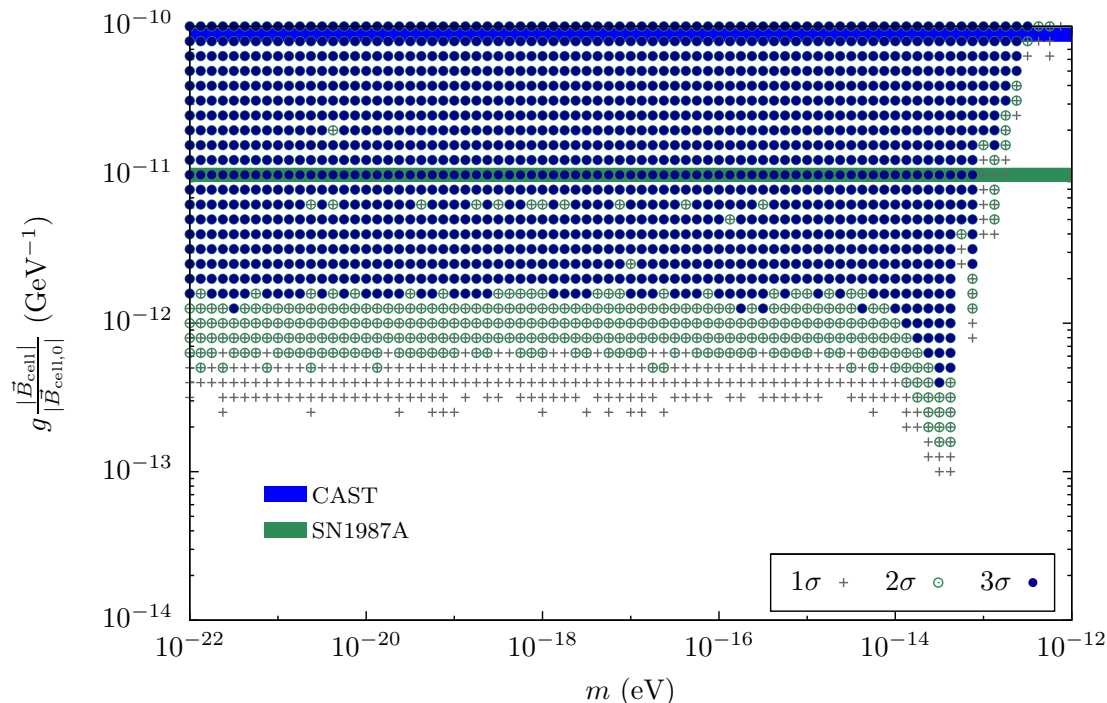


Figure 2: Exclusion plot for the monochromatic case ($\lambda = 250$ nm) ; parameters are excluded at 1, 2 or 3σ CL. Here, $|\vec{B}_{\text{cell},0}| = 2 \mu\text{G}$ and the electron density is $n_e = 10^{-6} \text{ cm}^{-3}$. Also shown are the constraints, by CAST ($g \lesssim 8.8 \cdot 10^{-11} \text{ GeV}^{-1}$), and derived from SN 1987A ($g \lesssim 10^{-11} \text{ GeV}^{-1}$), for low-mass ALPs.

effectively measures how likely it is that the mass and coupling of the ALP do not contradict the observations if we do not assume anything special about the magnetic field. Note that in the following “excluded at 2σ ” means that the probability is 5% or lower (probability of 95% not to be compatible with the data), and similarly for 1σ and 3σ .

Now, strictly speaking, the observations have been made in a given bandwidth, and the constraints must be applied taking this into account. Indeed, as explained in [4], one usually expects a smaller amount of polarisation from axion-photon mixing compared to the simpler monochromatic case. This will be presented elsewhere [8]; here, we stick to the mean value of the wavelengths observed (namely, 250 nm)² because it illustrates what constraints we would have if the same observations were performed in a very narrow band with the same statistics. These constraints are thus slightly more stringent in this case, as more polarisation is produced.

The result is seen in Fig. 2: for low-mass axion-like particles, we can obtain new constraints at the 2σ -level down to values below $g \approx 10^{-12} \text{ GeV}^{-1}$. For reference, the current best limits, by CAST [9], and derived from SN 1987A [10], are shown and are confirmed for nearly massless ALPs. For the magnetic field [7], we have used a hundred 100 kpc cells with a field strength

²Note that, over the supercluster scale, the effect of cosmological redshift on the wavelength is negligible: even though λ was shorter at the emission, it does not change over the last 10 Mpc we are interested in.

of $2 \mu\text{G}$; one can also find slightly lower values in the literature for superclusters (down to $\approx 0.3 \mu\text{G}$), but then typically over larger coherence lengths (up to the supercluster size). The exact value of the magnetic field strength one uses is not really an issue however, as the equations for the mixing always involve the coupling and the magnetic field strength together: as in this case there is only one scale (set by the modulus of the total magnetic field of each cell $|\vec{B}_{\text{cell}}|$), Fig. 2 can be rescaled straightforwardly for any other value of $|\vec{B}_{\text{cell}}|$ if our best knowledge of it changes. Note that the region near $m = 10^{-14}$ eV is more significantly excluded as the mixing is stronger for masses close to the plasma frequency.

We have verified the stability of our constraints against changes of a factor two up and down for the sizes and numbers of cells, or for the electron density, against the effect of an additional background field of $0.3 \mu\text{G}$ (in which case, one cannot rescale anymore), the influence of fluctuations of the magnetic field strength and of the electron density, and of the average over the observed bandwidth.

To conclude, we have illustrated that polarimetry is a tool that can be used to probe the ALP parameter space. Using quasar polarisation data and sticking to a conservative approach to avoid any overestimation of the polarisation, we have shown that new constraints can be put on very light axion-like particles. While the constraints are proven to be robust, the only drawback is associated with the uncertainties about the magnetic field of the supercluster. This technique could be applied to observations of polarisation for objects located behind clusters of galaxies, for instance, for which we have a much better knowledge of the magnetic field structure, and to higher-energy data, for instance in X-Ray polarimetry with tools like the GEMS satellite, which is to be launched in 2014 and which will definitely help the search for signals of low-mass ALPs.

References

- [1] G. Raffelt and L. Stodolsky, “Mixing of the Photon with Low Mass Particles,” *Phys. Rev. D* **37** (1988) 1237.
- [2] D. Hutsemékers, R. Cabanac, H. Lamy and D. Sluse, “Mapping extreme-scale alignments of quasar polarization vectors,” *Astron. Astrophys.* **441** (2005) 915 [arXiv:0507274 [astro-ph]].
- [3] D. Hutsemékers, B. Borguet, D. Sluse, R. Cabanac and H. Lamy, “Optical circular polarization in quasars,” *Astron. Astrophys.* **520** (2010) L7 [arXiv:1009.4049 [astro-ph]].
- [4] A. Payez, J.R. Cudell and D. Hutsemékers, “Can axionlike particles explain the alignments of the polarizations of light from quasars?,” *Phys. Rev. D* **84** (2011) 085029 [arXiv:1107.2013 [astro-ph]].
- [5] D. Hutsemékers, H. Lamy and M. Remy, “Polarization properties of a sample of broad absorption line and gravitationally lensed quasars,” *Astron. Astrophys.* **340** (1998) 371; G.D. Schmidt and D.C. Hines, “The Polarization of Broad Absorption Line QSOs,” *Astron. J.* **512** (1999) 125; H. Lamy and D. Hutsemékers, “Polarization properties of broad absorption line QSOs: New statistical clues,” *Astron. Astrophys.* **427** (2004) 107 [arXiv:0408476 [astro-ph]].
- [6] D. Hutsemékers and H. Lamy, “Confirmation of the existence of coherent orientations of quasar polarization vectors on cosmological scales,” *Astron. Astrophys.* **367** (2001) 381. [arXiv:0012182 [astro-ph]].
- [7] See *e.g.* J.P. Vallée, “Magnetic fields in the galactic Universe, as observed in supershells, galaxies, intergalactic and cosmic realms,” *New Astron. Rev.* **55** (2011) 91; Y. Xu, P. P. Kronberg, S. Habib and Q. W. Dufton, “A Faraday Rotation Search for Magnetic Fields in Large Scale Structure,” *Astrophys. J.* **637** (2006) 19.
- [8] A. Payez *et al.*, in preparation.
- [9] S. Andriamonje *et al.* [CAST Collaboration], “An improved limit on the axion-photon coupling from the CAST experiment,” *JCAP* **0704** (2007) 010 [arXiv:0702006 [hep-ex]].
- [10] See G. G. Raffelt, “Astrophysical axion bounds,” *Lect. Notes Phys.* **741** (2008) 51 [arXiv:0611350 [hep-ph]] and references therein.

Indications for a suppression of pair production at very high energies

Manuel Meyer¹ and Dieter Horns¹

¹Institut für Experimentalphysik, University of Hamburg, Luruper Chaussee 149, 22767 Hamburg, Germany

DOI: http://dx.doi.org/10.3204/DESY-PROC-2011-04/meyer_manuel

The transparency of the universe for very high energy (VHE) photons is limited due to pair-production with low energy photons of the extra galactic background light (EBL) in the ultra-violet to infrared wavelength band. Here, we use 58 energy spectra from VHE emitting active galactic nuclei (AGN) from redshift 0.004 to 0.536 to search for signatures of deviations from the minimum expected opacity. A statistical study of the individual measurements reveals indications for an overcorrection of AGN spectra with current EBL models. Axion like particles are discussed as a possible explanation of the result.

1 Introduction

The opacity of the universe for very high energy (VHE, energy $E \gtrsim 100$ GeV) photons arises through the interaction with background radiation fields, $\gamma_{\text{VHE}} + \gamma_{\text{bkg}} \rightarrow e^+ + e^-$. The photon flux dN_{int}/dE of a cosmological source with redshift z corrected for absorption is commonly expressed as

$$\frac{dN_{\text{int}}}{dE} = \frac{dN_{\text{obs}}}{dE} \times \exp[\tau_{\gamma\gamma}(E, z)], \quad (1)$$

where the observed spectrum is denoted as dN_{obs}/dE . The optical depth $\tau_{\gamma\gamma}$ is a threefold integral over the cross section for pair production multiplied with the number density of background photons over the cosmological distance, the cosine of the angle between the photon momenta, and the energy of the background photons. The cross section for pair production strongly peaks at a wavelength $\lambda = 1.24(E/\text{TeV})$ m which makes the extragalactic background light (EBL) the dominant radiation field responsible for the attenuation of VHE photon fluxes. The EBL ranges from the ultra-violet / optical to the far infrared wavelength band and originates mainly from starlight integrated over all epochs and starlight that has been reprocessed by dust in galaxies [1]. These two contributions lead to two peaks in the spectral energy distribution (SED) of the EBL: the first at around 1 m for the emitted starlight and at around 100 m for the re-emitted dust component. Direct measurements of the EBL are challenging due to the contamination with foreground emission such as the zodiacal light [2] and, therefore, a number of models have been published in the past that forecast the EBL density [3, 4, 5, for some recent examples].

In grand unified theories that aim to combine the standard model of particle physics with gravity, effects can occur that alter the opacity of the universe. This is for example the case in certain quantum gravity theories that predict the breakdown of Lorentz invariance [6, 7] or in

the presence of particles like axions or axion like particles (ALPs) [8, 9, 10, 11, 12]. In the case of Lorentz invariance violation (LIV), an energy dependent time delay of photons is predicted as well as a shift of the threshold energy for pair production. The latter effect alters $\tau_{\gamma\gamma}$ at a fixed energy. On the other hand, in ALP scenarios, photons can convert into ALPs in magnetic fields that pervade the source, the Milky Way and presumably in the intergalactic medium. The effect of photon-ALPs oscillation is twofold. Fluxes of photons for which the universe appears optically thin, i.e. whose energies and source distances translate into small values of $\tau_{\gamma\gamma}$, are additionally dimmed as the photons convert to ALPs which are not detected on earth. With increasing $\tau_{\gamma\gamma}$, the photon-ALP conversion probability increases so the probability is higher that ALPs convert back into photons. Consequently, the attenuation is decreased as ALPs are not subject to pair production. As a result, the applied correction for fluxes of photons for which the universe is optically thick will be too large and a hardening of the intrinsic spectra is expected.

In this article we statistically investigate 58 VHE spectra from 25 sources obtained with the imaging air Cherenkov telescopes CAT, HEGRA, H.E.S.S., MAGIC, VERITAS and WHIPPLE for a systematic effect in the transition from the optical thin to optical thick regime. This guarantees that the results derived here are independent from source physics as $\tau_{\gamma\gamma}$ is a nontrivial combination of the energy of the γ -ray photon and the distance of the source. The observed spectra are corrected for the EBL absorption with Eq. 1 and using the lower limit EBL model by [4]. This lower limit model predicts the guaranteed level of EBL density which is just in agreement with the 1σ downward fluctuation of the galaxy number counts obtained with *Spitzer* [13] and gives the lowest possible absorption.

The considered sources are all active galactic nuclei (AGN) with known redshift¹. It follows from Eq. 1 and from the ignorance of the exact shape of the SED of the EBL that it is impossible to measure the intrinsic source spectrum directly. The measured photon indices² vary between ~ 1.4 and ~ 4 which makes it difficult to infer some generic intrinsic spectrum valid for all blazars. Furthermore, the source sample might suffer from observational bias, i.e. only certain sources are detected at large redshifts.

These difficulties stress the necessity that the statistical test introduced here is independent of any assumptions of the intrinsic VHE spectra and / or their distance alone.

2 A statistical test to search for an overcorrection of VHE spectra

As a compromise between number of spectra and the strength of the expected effect, we define optical thick as $\tau_{\gamma\gamma} \geq 2$ and optical thin as $\tau_{\gamma\gamma} < 2$. This value of the optical depth also ensures that the dimming due to pair production is not confused with the dimming of the initial flux because of photon-ALPs conversion. The latter can reduce the initial photon flux by maximally 1/3 [8] which already occurs for $\tau_{\gamma\gamma} \approx 0.4$.

The statistical test is devised as follows. For a given VHE spectrum the data points are determined that correspond to an optical depth $\tau_{\gamma\gamma} < 1$. These points are then fitted with a power law using a χ^2 -minimization algorithm. If the resulting p -value of the fit is less than

¹Sources for which the redshift is under discussion (e.g. 3C 66A, PG 1553+113 and S 50716+714) are not included in the analysis.

²Most observed VHE spectra are adequately described by power laws of the form $dN/dE \propto E^{-\Gamma}$, where Γ is called the photon index, see also Table 1.

Table 1: Analytical functions used to fit the data points of the spectra. The smoothing parameter f of the broken power law is fixed to 4 and the energy normalization E_0 is set to 1 TeV.

Function Name	$dN/dE(E)$	Fit parameters
Power law	$N_0(E/E_0)^{-\Gamma}$	N_0, Γ
Logarithmic parabola	$N_0(E/E_0)^{-(\Gamma+\beta \ln(E/E_0))}$	N_0, Γ, β
Broken power law	$N_0(E/E_0)^{-\Gamma_1} [1 + (E/E_{\text{break}})^f]^{(\Gamma_1-\Gamma_2)/f}$	$N_0, \Gamma_1, \Gamma_2, E_{\text{break}}$

5% a logarithmic parabola is fitted instead and if the p -value still remains below 5% a broken power law is used. The analytic functions are summarized in Table 1.

The functions determined this way are extrapolated to all remaining data points. As an example, the procedure is shown in Fig. 1 for the spectrum of 1ES 1101-232 measured with H.E.S.S. [14]. The deviation of the i -th data point from the extrapolation is quantified by the ratio R_i ,

$$R_i = \frac{\varphi_i - f^{\text{ext}}(E_i)}{\varphi_i + f^{\text{ext}}(E_i)}. \quad (2)$$

Here, f^{ext} denotes the extrapolation of the analytic description of the data points with $\tau_{\gamma\gamma} < 1$ and φ_i is the shorthand notation for dN_i^{int}/dE_i . For our purposes to find an overcorrection of the observed spectra, the choice of analytical functions can be considered conservative as they show less curvature than e.g. a power law modified with an exponential cut-off. The extrapolation of such a function could lead to an overestimation of R for the highest energy bins. The ratios are calculated for all considered VHE spectra³ and two distributions of ratios are defined that correspond to optical thin and thick measurements, respectively,

$$\mathcal{S}_{\text{thin}} = \{R_i \mid 1 \leq \tau_{\gamma\gamma}(E_i, z) < 2\}, \quad (3)$$

$$\mathcal{S}_{\text{thick}} = \{R_i \mid \tau_{\gamma\gamma}(E_i, z) \geq 2\}. \quad (4)$$

These two distributions are compared with the Kolmogorov-Smirnov (KS) test [16, 17] under the null-hypothesis that the underlying probability distributions are equal.

3 Results

From the 58 spectra, only 28 (8) spectra have data points that correspond to an optical depth ≥ 1 (≥ 2). Figure 2 shows the result of the KS-test. The left panel displays the ratios R for each data point of every spectrum plotted against the optical depth. It can be seen that spectra of distant sources measured up to several hundreds of GeV along with spectra of sources close by and detected beyond tens of TeV contribute to the $\mathcal{S}_{\text{thick}}$ sample. A trend is visible that observations at large $\tau_{\gamma\gamma}$ tend to show higher values of R as well. This is confirmed in the right panel which depicts the corresponding cumulative distribution functions (CDFs). About 60% of the ratios in $\mathcal{S}_{\text{thin}}$ are below zero and not 50% as one would naively expect. The reason for this might be an intrinsic curvature of the spectra or an underestimation of the EBL density for $1 \leq \tau_{\gamma\gamma} < 2$ by the lower limit model. In the case of the extrapolation to values that correspond $\tau_{\gamma\gamma} \geq 2$, the CDF of $\mathcal{S}_{\text{thick}}$ shows a systematic increase towards higher values of

³For the entire VHE sample considered here, see [15] and references therein.

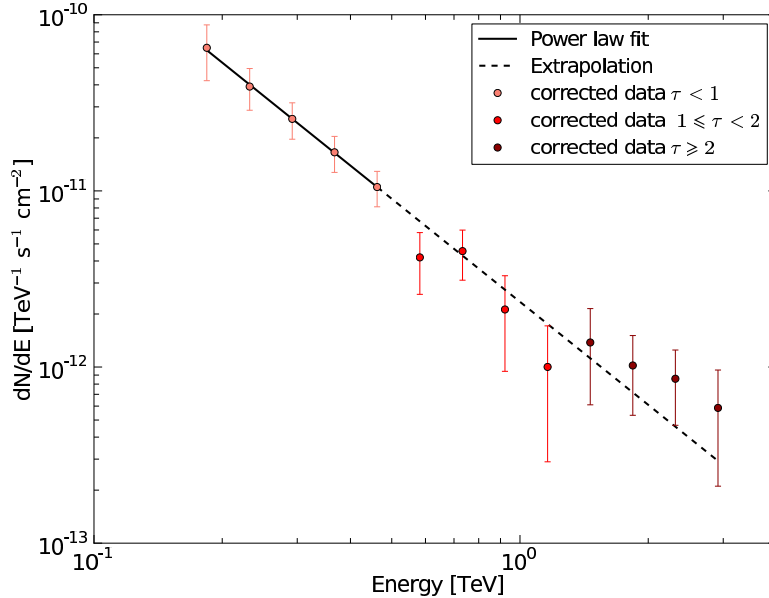


Figure 1: The spectrum of 1ES 1101-232 measured with H.E.S.S. [14] with 1σ statistical errors on the flux. The first five points correspond to a $\tau_{\gamma\gamma}$ value smaller than one and thus enter into the power-law fit. The fit itself is shown as a black solid line. The fit is extrapolated to all other points (dashed line) and the ratios R_i are calculated according to Eq. 2. The ratios of the red points enter $\mathcal{S}_{\text{thin}}$ while the ratios of the dark red points contribute to $\mathcal{S}_{\text{thick}}$, see Eq. 3 and 4.

R , indicating a hardening of the intrinsic spectra which can be taken as evidence that the correction is indeed too strong. The maximum distance D between the CDFs of $\mathcal{S}_{\text{thin}}$ and $\mathcal{S}_{\text{thick}}$ is found to be $D \approx 0.68$ for which the KS-test gives a probability of $Q_{KS} \approx 3.78 \times 10^{-5}$ that the underlying probability distributions are equal. This corresponds to a significance of 3.96σ (one-sided confidence interval) that they are different from each other. A cross check with galactic sources shows that this result cannot be explained by instrumental effects such as an overestimation of the flux in the highest energy bins [15].

4 Conclusion

In this article a new approach based on the Kolmogorov-Smirnov test is presented that searches for systematic changes in VHE spectra corrected for the EBL absorption in the transition from $\tau_{\gamma\gamma}(E, z) < 2$ (optically thin) to $\tau_{\gamma\gamma}(E, z) \geq 2$ (optically thick). The approach is independent of the exact shape of the intrinsic VHE spectra and, thus, the obtained results do not suffer from possible observational bias, e.g. only certain types of sources are detected at high redshifts. Furthermore, the test is designed to be independent of the statistical uncertainties of the individual flux measurements as they seem to be overestimated independent of the telescope that observed the source [15].

An indication with a significance of 3.96σ is found that optically thick measurements are over

INDICATIONS FOR A SUPPRESSION OF PAIR PRODUCTION AT VERY HIGH ENERGIES

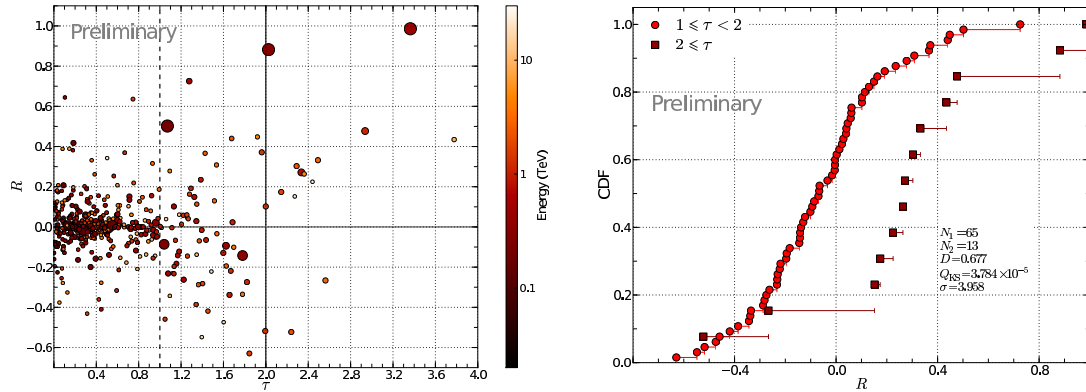


Figure 2: Result of the KS-test. Left Panel: The Ratios R plotted against the Optical depth $\tau_{\gamma\gamma}$. The size of the markers is proportional to the redshift while the color encodes the corresponding energy of each data point. Right panel: CDFs of $\mathcal{S}_{\text{thin}}$ and $\mathcal{S}_{\text{thick}}$.

corrected by a lower limit EBL model. If the significance of this result is confirmed and improved with future observations⁴ it demands for an explanation other than tuning the EBL density as the lower limit model already predicts a minimum attenuation that is in accordance with lower limit measurements of the EBL. The result is difficult to explain with source physics since many objects measured at different redshifts and energies enter the test. For instance, an upturn of the intrinsic spectra at multiple TeV energies caused by effects like second order inverse Compton scattering [18], comptonization of cosmic microwave background (CMB) photons [19], or interactions of ultra-high energy cosmic rays with the CMB [20, 21, 22] are not able to explain our findings. On the one hand, such features could possibly enter the ratios of $\mathcal{S}_{\text{thin}}$ and $\mathcal{S}_{\text{thick}}$ since they are distinguished by $\tau_{\gamma\gamma}$ and not by the energy E . On the other hand, distant sources like 3C 279 measured below 1 TeV also contribute to the result. One candidate for a way out might be given by photon-ALPs conversion as theory predicts a decrease of the attenuation for large values of the optical depth.

Acknowledgements

The authors would like to thank the organizers of the *7th Patras Workshop on Axions, WIMPs and WISPs 2011* for the opportunity to present their results. This work was made possible with the support of the state excellence cluster “Cosmic radiation fields and search for dark matter” at the university of Hamburg.

References

- [1] Hauser M G and Dwek E 2001 *Ann. Rev. Astron. Astrophys.* **39** 249–307 (*Preprint arXiv: astro-ph/0105539*)

⁴There are $\mathcal{O}(10)$ new detections of VHE emitting AGN announced, see e.g. <http://tevcat.uchicago.edu>

- [2] Hauser M G, Arendt R G, Kelsall T, Dwek E, Odegard N, Weiland J L, Freudenreich H T, Reach W T, Silverberg R F, Moseley S H, Pei Y C, Lubin P, Mather J C, Shafer R A, Smoot G F, Weiss R, Wilkinson D T and Wright E L 1998 *Astrophys. J.* **508** 25–43 (*Preprint arXiv:astro-ph/9806167*)
- [3] Franceschini A, Rodighiero G and Vaccari M 2008 *Astron. Astrophys.* **487** 837–852 (*Preprint 0805.1841*)
- [4] Kneiske T M and Dole H 2010 *Astron. Astrophys.* **515** A19+ (*Preprint 1001.2132*)
- [5] Domínguez A, Primack J R, Rosario D J *et al.* 2010 *Mon. Not. R. Astron. Soc.* 1665+ (*Preprint 1007.1459*)
- [6] Jacob U and Piran T 2008 *Phys. Rev. D* **78** 124010+ (*Preprint 0810.1318*)
- [7] Shao L and Ma B 2010 *Modern Physics Letters A* **25** 3251–3266 (*Preprint 1007.2269*)
- [8] Mirizzi A, Raffelt G G and Serpico P D 2007 *Phys. Rev. D* **76** 023001+ (*Preprint 0704.3044*)
- [9] Hochmuth K A and Sigl G 2007 *Phys. Rev. D* **76** 123011+ (*Preprint 0708.1144*)
- [10] Hooper D and Serpico P D 2007 *Physical Review Letters* **99** 231102+ (*Preprint 0706.3203*)
- [11] Sánchez-Conde M A, Paneque D, Bloom E, Prada F and Domínguez A 2009 *Phys. Rev. D* **79** 123511+ (*Preprint 0905.3270*)
- [12] Mirizzi A and Montanino D 2009 *JCAP* **12** 4+ (*Preprint 0911.0015*)
- [13] Fazio G G, Ashby M L N, Barmby P, Hora J L, Huang J S, Pahre M A, Wang Z, Willner S P, Arendt R G, Moseley S H, Brodwin M, Eisenhardt P, Stern D, Tollestrup E V and Wright E L 2004 *Astrophys. J., Suppl. Ser.* **154** 39–43 (*Preprint arXiv:astro-ph/0405595*)
- [14] Aharonian (for the HESS Collaboration) F *et al.* 2007 *Astron. Astrophys.* **470** 475–489 (*Preprint 0705.2946*)
- [15] Horns D and Meyer M 2011 *Indications for an pair-production anomaly from the propagation of VHE gamma-rays, submitted to JCAP*
- [16] Meyer M and Horns D 2010 *Proceedings of Cosmic Radiation Fields: Sources in the early Universe (CRF 2010). November 9-12, 2010. Desy, Germany. Editors: Martin Raue (chair), Tanja Kneiske, Dieter Horns, Dominik Elsaesser, and Peter Hauschildt. Published online at <http://pos.sissa.it/cgi-bin/reader/conf.cgi?confid=121>, p.11* ed M Raue, T Kneiske, D Horns, D Elsaesser, & P Hauschildt pp 11+
- [17] Press W H 2002 *Numerical recipes in C++ : the art of scientific computing*
- [18] Bloom S D and Marscher A P 1996 *Astrophys. J.* **461** 657+
- [19] Böttcher M, Dermer C D and Finke J D 2008 *Astrophys. J., Lett.* **679** L9–L12 (*Preprint 0804.3515*)

INDICATIONS FOR A SUPPRESSION OF PAIR PRODUCTION AT VERY HIGH ENERGIES

- [20] Essey W and Kusenko A 2010 *Astroparticle Physics* **33** 81–85 (*Preprint* 0905.1162)
- [21] Essey W, Kalashev O E, Kusenko A and Beacom J F 2010 *Physical Review Letters* **104** 141102–+ (*Preprint* 0912.3976)
- [22] Essey W, Kalashev O, Kusenko A and Beacom J F 2011 *Astrophys. J.* **731** 51–+ (*Preprint* 1011.6340)

White dwarfs as physics laboratories: the case of axions

J. Isern^{1,2}, *L. Althaus*^{3,4}, *S. Catalán*⁵, *A. Córscico*^{3,4}, *E. García-Berro*^{6,2}, *M. Salaris*⁷, *S. Torres*^{7,2}

¹Institut de Ciències de l'Espai ICE(CSIC/IEEC), Campus UAB, 08193 Bellaterra, Spain

²Institut d'Estudis Espacials de Catalunya (IEEC), Ed. Nexus, c/Gran Capità, 08034 Barcelona, Spain

³Facultad de Ciencias Astronómicas y Geofísicas, Universidad Nacional de La Plata, Argentina

⁴CONICET, Argentina

⁵Center for Astrophysics Research, University of Hertfordshire, College Lane, Hatfield AL10 9AB, UK

⁶Departament de Física Aplicada, Universitat Politècnica de Catalunya, c/Esteve Terrades 5, 08860 Castelldefels, Spain

⁷Astrophysics Research Institute, Liverpool John Moores University, 12 Quays House, Birkenhead, CH41 1LD, UK

DOI: http://dx.doi.org/10.3204/DESY-PROC-2011-04/iser_n.jordi

White dwarfs are almost completely degenerate objects that cannot obtain energy from thermonuclear sources, so their evolution is just a gravothermal cooling process. Recent improvements in the accuracy and precision of the luminosity function and in pulsational data of variable white dwarfs suggest that they are cooling faster than expected from conventional theory. In this contribution we show that the inclusion of an additional cooling term due to axions able to interact with electrons with a coupling constant $g_{ae} \sim (2 - 7) \times 10^{-13}$ allows to fit better the observations.

1 Introduction

During the cooling process, white dwarfs experience some phases of pulsational instability powered by the κ - and the convective-driven mechanisms [1]. Depending on the composition of the atmosphere, variable white dwarfs are known as DAV (atmospheres dominated by H) and DOV, DBV (atmospheres non dominated by H). These objects are experiencing g -mode non-radial pulsations, where the main restoring force is gravity. An important characteristic of these pulsations is that their period experiences a secular drift caused by the evolution of their temperature and radius. For a semi-qualitative purpose this drift can be well approximated by [2]: $d \ln \Pi / dt \simeq -a d \ln T / dt + b d \ln R / dt$, where a and b are constants of the order of unity that depend on the details of the model, and R and T are the stellar radius and the temperature at the region of period formation, respectively. This equation reflects the fact that, as the star cools down, the degeneracy of electrons increases, the buoyancy decreases and, as a consequence, the spectrum of pulsations gradually shifts to lower frequencies. At the same time, since the

star contracts, the radius decreases and the frequency tends to increase. In general, DAV and DBV stars are already so cool (and degenerate) that the radial term is negligible and the change of the period of pulsation can be directly related to the change in the core temperature of the star. Therefore, the measurement of such drifts provides an effective method to test the theory of white dwarf cooling. This, in turn, allows to obtain a simple relationship [3, 4] to estimate the influence of an additional sink of energy, axions for instance, on the period drift of variable white dwarfs:

$$(L_X/L_{\text{model}}) \approx (\dot{\Pi}_{\text{obs}}/\dot{\Pi}_{\text{model}}) - 1 \quad (1)$$

where the suffix “model” refers to those models built using standard physics and L_X is the extra luminosity.

Another way to test the theory of white dwarf cooling is based on their luminosity function. This function is defined as the number density of white dwarfs of a given luminosity per unit magnitude interval:

$$n(l) = \int_{M_i}^{M_u} \Phi(M) \Psi(t) \tau_{\text{cool}}(l, M) dM \quad (2)$$

where t satisfies the condition $t = T - t_{\text{cool}}(l, M) - t_{\text{PS}}(M)$ and $l = -\log(L/L_{\odot})$, M is the mass of the parent star (for convenience all white dwarfs are labeled with the mass of the main sequence progenitor), t_{cool} is the cooling time down to luminosity l , $\tau_{\text{cool}} = dt/dM_{\text{bol}}$ is the characteristic cooling time, M_s and M_i are the maximum and the minimum masses of the main sequence stars able to produce a white dwarf of luminosity l , t_{PS} is the lifetime of the progenitor of the white dwarf, and T is the age of the population under study. The remaining quantities, the initial mass function, $\Phi(M)$, and the star formation rate, $\Psi(t)$, are not known a priori and depend on the properties of the stellar population under study. In order to compare theory with observations and since the total density of white dwarfs is not well known yet, the computed luminosity function is usually normalized to the bin with the smallest error bar, traditionally the one with $l = 3$. An important property of Eq. (2) is that the bright branch of the luminosity function is only sensitive to the average characteristic cooling time of white dwarfs at the corresponding luminosity when this function is normalized.

$$n = \langle \tau_{\text{cool}} \rangle \int_{M_i}^{M_u} \phi(M) \psi(T - t_{\text{cool}} - t_{\text{ps}}) dM. \quad (3)$$

The reason [4, 5] is that the stellar population is dominated by low-mass stars and, since the lifetime of stars increases very sharply when the mass decreases, the lower limit of the integral in Eq. (3) is almost independent of the luminosity, so the value of the integral is absorbed by the normalization constant.

2 The case of G117–B15A and the luminosity function

The measurement of the secular drift of the period of pulsation has been performed in the case of G117–B15A [6], a member of the ZZ Ceti (DAV) stars. The most recent value obtained so far is [7]:

$$(d\Pi/dt)_{\text{obs}} = (4.89 \pm 0.53 \pm 1.56) \times 10^{-15} \text{ s/s} \quad (4)$$

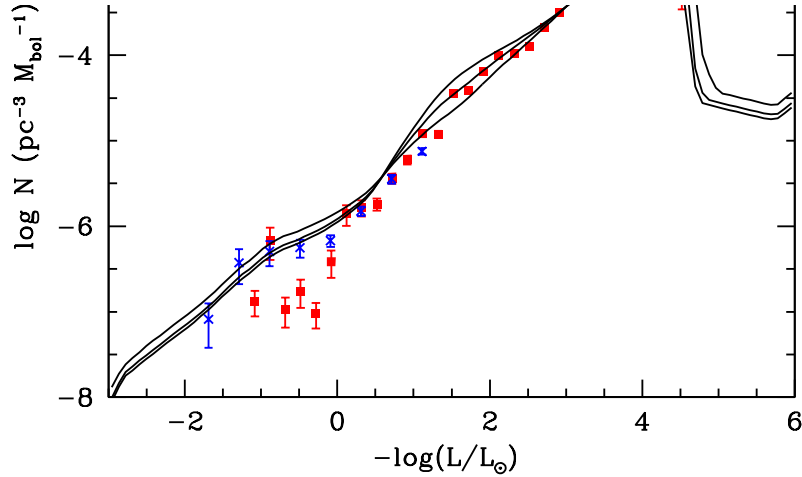


Figure 1: White dwarf luminosity function. The solid lines represent the models obtained with (up to down) $g_{aee}/10^{-13} = 0, 2.2, 4.5$ respectively.

with an estimated proper motion correction $\dot{\Pi} = -(7.0 \pm 0.2) \times 10^{-16}$ s/s. Theoretical predictions [8] indicate that this star should experience a secular drift of only $\dot{\Pi} = 1.2 \times 10^{-15}$ s/s. Similar values ($\dot{\Pi} = 1.92 \times 10^{-15}$ s/s or $\dot{\Pi} = 2.98 \times 10^{-15}$ s/s depending on the adopted mass of the envelope) have been independently obtained [9]. These results suggest that white dwarfs are cooling faster than expected (it is important to confirm this statement by measuring this drift in other stars). There are three possible reasons for this. i) An observational error. This measurement is difficult and it has been obtained by only one team on just one star. Although the measurement tends to stabilize, it suffered strong fluctuations in the past [10]. ii) A modelling error. Models have been noticeably improved during the last ten years and the two independent models computed up to now [8, 9] are in a qualitative agreement. iii) An additional sink of energy is responsible of the accelerated cooling rate [3].

Under the conditions of temperature and density in the interior of G117-B15A, the axion emission rate is dominated by electron bremsstrahlung (only the DFSZ axion model) that behaves as $\dot{\epsilon}_{ax} \propto g_{aee}^2 T_7^4$ erg/g/s, where T_7 is the temperature in units of 10^7 K and g_{aee} is the strength of the axion–electron Yukawa coupling [11]. Thus it is possible to include the axion emissivity in Eq. (1) and adjust g_{aee} to fit the observed values. The value that best fits the observations is in the range of $g_{aee} \sim (3 - 7) \times 10^{-13}$.

Figure 1 displays the white dwarf luminosity function, DA and non-DAs [12]. The values from the DR4 of the SDSS [13] (squares) were complemented at high luminosities with those obtained using the more recent DR7 [14] (crosses). It is important to notice that models without axions [15] predict an excess of white dwarfs in the region $\log(L/L_\odot) \sim -2$ as in the case of the pure-DA sample [4]. If axions are included, the best fit is obtained for $g_{aee} \sim (2 - 3) \times 10^{-13}$. The luminosity function at high luminosities is still poorly known from both the theoretical and observational point of views, but it is clear that will provide strong constraints.

3 Conclusions

There are two independent pieces of evidence, the luminosity function and the secular drift of DAV white dwarfs, that white dwarfs are cooling down more rapidly than expected. The introduction of an additional sink of energy linked to the interaction of electrons with a light boson (axion, ALP, ...) with an strength $g_{\text{aee}} \sim (2-7) \times 10^{-13}$ solves the problem satisfactorily. Naturally, the uncertainties that still remain, both observational and theoretical, still prevent to claim the existence of such interaction. A systematic analysis aimed to discard any possible conventional solution is under way.

Acknowledgments

This work has been supported by the MICINN grants AYA08-1839/ESP and AYA2008-04211-C02-01, by the ESF EUROCORES Program EuroGENESIS (MICINN grant EUI2009-04170), by SGR grants of the Generalitat de Catalunya and by the EU-FEDER funds.

References

- [1] L.G. Althaus, A.H. Córscico, J. Isern, & E. García-Berro, “Evolutionary and pulsational properties of white dwarfs”, *Astron. & Astrophys. Rev.*, **18**, 47 (2010)
- [2] D.E. Winget, C. J. Hansen, & H. M. Van Horn, “Do pulsating PG1159-035 stars put constraints on stellar evolution?”, *Nature*, **303**, 781 (1983)
- [3] J. Isern, M. Hernanz, & E. García-Berro, “Axion cooling of white dwarfs”, *Astrophys. J.*, **392**, L23 (1992)
- [4] J. Isern, & E. García-Berro, “White dwarfs as physics laboratories: the axion case”, *Mem. Soc. Astr. It.*, **79**, 545 (2008)
- [5] J. Isern, S. Catalán, E. García-Berro, & S. Torres, “Axions and the white dwarf luminosity function”, *J. Phys.: Conf. Ser.*, **172**, 012005 (2009)
- [6] S.O. Kepler *et al.*, “Measuring the evolution of the most stable optical clock G117-B15A”, *Astrophys. J.*, **634**, 1311 (2005)
- [7] S.O. Kepler, “White dwarf stars: Pulsations and Magnetism”, *Proc. of “The 61st Fujuhara Seminar: Progress in solar/stellar physics with helio and asteroseismology”*, in press (2011)
- [8] A. H. Córscico, L.G. Althaus, A.D. Romero, M.H. Miller Bertolami, E. García-Berro, & J. Isern, “Constraining the axion mass through the asteroseismology of the ZZ Ceti star G117-B15A”, *Proc. of “The 61st Fujuhara Seminar: Progress in solar/stellar physics with helio and asteroseismology”*, in press (2011)
- [9] A. Bischoff-Kim, M.H. Montgomery, & D.E. Winget, “Strong limits on the DFSZ axion mass with G117-B15A”, *Astrophys. J.*, **675**, 1512 (2008)
- [10] J. Isern, E. García-Berro, L.G. Althaus, & A.H. Córscico, “Axions and the pulsation periods of variable white dwarfs revisited”, *Astron. & Astrophys.*, **512**, A86 (2010)
- [11] M. Nakagawa, Y. Kohyama, & N. Itoh, “Axion bremsstrahlung in dense stars”, *Astrophys. J.*, **322**, 291 (1987)
- [12] J. Isern, E. García-Berro, M. Hernanz, & R. Mochkovitch, “The physics of white dwarfs”, *J. Phys. Cond. Matter*, **10**, 11263 (1998)
- [13] H.C. Harris *et al.*, “The white dwarf luminosity function from Sloan Digital Sky Survey Imaging data”, *Astron. J.*, **131**, 571 (2006)
- [14] J. Krzesinski, *et al.*, “A hot white dwarf luminosity function from the Sloan Digital Sky Survey”, *Astron. Astrophys.*, **508**, 339 (2009)
- [15] M. Salaris *et al.*, “A large stellar evolution database for population synthesis studies. VI. White dwarf cooling sequences”, *Astrophys. J.*, **716**, 1241 (2010)
- [16] J. Isern, E. García-Berro, S. Torres, & S. Catalán, “Axions and the cooling of white dwarf stars”, *Astrophys. J.*, **682**, L109 (2008)

Chapter 5

Accelerator Physics and other Topics

Z' from GUTs, CPs, Axions, and the μ Problem

Jihn E. Kim^{1,2}

¹Department of Physics and Astronomy, Seoul National University, Seoul 151-747, Korea

²GIST College, Gwangju Institute of Science and Technology, Gwangju 500-712, Korea

DOI: http://dx.doi.org/10.3204/DESY-PROC-2011-04/kim_jihn

We can think of a few interesting topics beyond the standard model(SM), “Are there a new $U(1)'$, axions, supersymmetry(SUSY), and string effects?” Here, I discuss my recent works related to $U(1)'$, the weak CP violation, and the μ related problems.

The most pending question beyond the standard model(BSM) is, “Is there a new $U(1)'$ at the TeV scale?” The SM is fitted to the vast electroweak data very successfully without a need for an extra neutral gauge boson(s). There already exist a vast references on the extra Z' [1]. A strongly motivated framework for extra Z' bosons is the grand unified theories(GUTs). The ranks of the $SO(10)$ and E_6 are greater than 4 and hence in those GUTs there can exist an extra Z' boson(s) at the TeV scale if the spontaneous symmetry breaking of the GUTs leaves them light. In Ref. [2], we have shown that it is improbable to have a TeV scale Z' if the GUT group is a subgroup of E_6 . This is a very simple remark since any generator corresponding to the $U(1)_{Z'}$ from E_6 belongs to the Cartan subalgebra of E_6 and is a linear combination of the diagonal E_6 generators. It is equivalent to considering the Cartan subalgebra of a rank 6 subgroup of E_6 . For this purpose, the $SU(6) \times SU(2)_h$ subgroup of E_6 is very convenient because the $SU(6) \times SU(2)_h$ quantum numbers can be read by representing $(\mathbf{15}, \mathbf{1})$ and $(\bar{\mathbf{6}}, \mathbf{2})$ like matrices. There can be a “No-go theorem” for $U(1)_{\text{Baryon number}}$. For $U(1)_X$ with $X \neq B$, there is a subtlety as shown below, but it is not likely that the mass of Z' is below 10 TeV. The LHC preliminary result with a light lightest SUSY particle(LSP) is consistent with this claim as reported at this Meeting [3]. On the contrary, if Z' is found below 10 TeV, our understanding of the SM from the subgroups of E_6 is not realized. In particular, the $SU(5)$, $SO(10)$, and $SU(3) \times SU(3) \times SU(3)$, $SU(6) \times SU(2)$, and flipped $SU(5)$ GUTs are not acceptable.

Let the baryon number generator be as commented in the subsequent paragraph.

$$B = aY + bY_6 + cX_3 + dR \quad (1)$$

where we included the global R charge also. But we will neglect R since it is broken by the supergravity effects. The notations in Eq. (1) are derived from $SU(6) \times SU(2)$. The generators F_3, F_8, T_3, Y , and Y_6 belong to the algebra of the vertical group $SU(6)$ and X_3 belongs to the algebra of the horizontal group $SU(2)$. The leptons and the Higgs doublets do not carry the baryon number. Their B charges according to Eqs. (1,3) are

$$e^c : a - \frac{b}{3} = 0, \quad (\nu_e, e) : -\frac{a}{2} + \frac{b}{6} + \frac{c}{2} = 0, \quad H_d : -\frac{a}{2} + \frac{b}{6} - \frac{c}{2} = 0, \quad H_u : \frac{a}{2} + \frac{2b}{3} = 0 \quad (2)$$

which cannot be satisfied simultaneously.

The SU(6) GUT model discussed in connection with the F-theory [4] has been known since early 1980s [5]. For the diagonal subgroups of E_6 , any U(1) generator can be a linear combination of the Cartan subgroup of E_6 . Therefore, we can prove a no-go possibility in terms of the Cartan subgroup of $SU(6) \times SU(2) \subset E_6$, where SU(6) will be called vertical and SU(2) will be called horizontal as shown below for $(\mathbf{15}, \mathbf{1})$ and $(\bar{\mathbf{6}}, \mathbf{2})$ of $SU(6) \times SU(2)_h$ for the first family,

$$\mathbf{15}_L \equiv (\mathbf{15}, \mathbf{1}) = \begin{pmatrix} 0 & u^c & -u^c & u & d & D \\ -u^c & 0 & u^c & u & d & D \\ u^c & -u^c & 0 & u & d & D \\ -u & -u & -u & 0 & e^c & H_u^+ \\ -d & -d & -d & -e^c & 0 & H_u^0 \\ -D & -D & -D & -H_u^+ & -H_u^0 & 0 \end{pmatrix}, \quad (3)$$

$$\bar{\mathbf{6}}_{2,1} \equiv (\bar{\mathbf{6}}, \mathbf{2}^\uparrow) = \begin{pmatrix} d^c \\ d^c \\ d^c \\ -\nu_e \\ e \\ N \end{pmatrix}, \quad \bar{\mathbf{6}}_{2,2} \equiv (\bar{\mathbf{6}}, \mathbf{2}^\downarrow) = \begin{pmatrix} D^c \\ D^c \\ D^c \\ -H_d^0 \\ H_d^- \\ N' \end{pmatrix}.$$

Equation (1) for B is equivalent to discussing a U(1) subgroup of E_6 . Thus, B cannot be a generator belonging to E_6 . On the other hand, three conditions except the H_u condition in Eq. (2) can be satisfied, which is called the *leptophobic* case. H_u carries a nonvanishing Y' and also N of Eq. (3) carries a nonvanishing Y' . Therefore, the singlet neutrino mass scale is the Z' mass scale. In this case, we consider Z' couplings both to B and L . We considered $SU(6) \times SU(2)$ for the Z_6 hexality and the $Z - Z'$ mass (with fine tuned coupling constants). In the latter case, of course we assumed the lepton coupling to Z' as phrased above as Z' couplings both to B and L . Then, the LEP2 precision experiment bound on the ρ parameter is crucial to constrain the model [2], but the leptophobic case in terms of kinetic mixing softens this condition.

Another issue going beyond the SM is to understand how the weak CP violation is realized at the high energy scale. CP violation observed in the K-meson and the B-meson systems is given by the Cabibbo-Kobayashi-Maskawa (CKM) matrix [6]. Recently, we presented an exact CKM matrix [7], replacing the approximate Wolfenstein form. It is worthwhile to write any convenient form if it is useful for obtaining some information on the high energy scale physics. The well-known facts about the CKM matrix are: (1) Det. V_{CKM} is better to be real, (2) the 3×3 V_{CKM} is complex to describe the weak CP violation, (3) any among the nine elements is zero, then there is no weak CP violation, (4) there is a good expansion parameter λ , (5) the product of the elements $V_{\text{CKM}(31)} \cdot V_{\text{CKM}(22)} \cdot V_{\text{CKM}(13)}$ is the barometer of weak CP violation, and (6) eventually, V_{CKM} will be derivable from the Yukawa texture. The fact (1) is related to the issue of $\text{Arg. Det. } M_q$ which hints a relation to the strong CP problem [8]. If $\text{Arg. Det. } M_q$ is not zero, then we remove this to define a good quark mass basis, using the PQ symmetry [9] or by some other mechanism [8]. But this reality condition is not absolutely necessary, but only a very convenient choice. As done with the expansion parameter λ , the expansion can be achieved in terms of the $V_{\text{CKM}(12)}$ angle θ_1 since θ_2 and θ_3 are known to be of order θ_1^2 . If the CKM matrix is expanded in terms of θ_1 instead of λ , it is easy to write an exact form. Now we

can write an exact CKM matrix, satisfying all the above requirements [7],

$$V_{\text{KS}} = \begin{pmatrix} c_1 & s_1 c_3 & s_1 s_3 \\ -c_2 s_1 & e^{-i\delta} s_2 s_3 + c_1 c_2 c_3 & -e^{-i\delta} s_2 c_3 + c_1 c_2 s_3 \\ -e^{i\delta} s_1 s_2 & -c_2 s_3 + c_1 s_2 c_3 e^{i\delta} & c_2 c_3 + c_1 s_2 s_3 e^{i\delta} \end{pmatrix} \quad (4)$$

where $s_i = \sin \theta_i$ and $c_i = \cos \theta_i$, and the parameters are determined as $\theta_1 = 13.0305^\circ \pm 0.0123^\circ = 0.227426 \pm (2.14 \times 10^{-4})$, $\theta_2 = 2.42338^\circ \pm 0.1705^\circ = 0.042296 \pm (2.976 \times 10^{-3})$, $\theta_3 = 1.54295^\circ \pm 0.1327^\circ = 0.027567 \pm (2.315 \times 10^{-3})$, and $\delta = 89.0^\circ \pm 4.4^\circ$. The determinant is real, but its six elements are complex with the following δ dependent parts, $V_{11}V_{22}V_{33} \rightarrow 2c_1c_2c_3s_2s_3 \cos \delta - c_1c_2c_3s_1^2s_2s_3e^{i\delta}$, $V_{11}V_{23}V_{32} \rightarrow 2c_1c_2c_3s_2s_3 \cos \delta - c_1c_2c_3s_1^2s_2s_3e^{i\delta}$, $V_{12}V_{23}V_{31} \rightarrow -c_1c_2c_3s_1^2s_2s_3e^{i\delta}$, $V_{12}V_{21}V_{33} \rightarrow -c_1c_2c_3s_1^2s_2s_3e^{i\delta}$, $V_{13}V_{21}V_{32} = -c_1c_2c_3s_1^2s_2s_3e^{i\delta}$, $V_{13}V_{22}V_{31} \rightarrow -c_1c_2c_3s_1^2s_2s_3e^{i\delta}$. Each of the six products has the same imaginary part. Therefore, the weak CP violation is unambiguously signaled by the product of the CKM matrix elements, e.g. the imaginary part of $V_{\text{CKM}(31)} \cdot V_{\text{CKM}(22)} \cdot V_{\text{CKM}(13)}$ is $-ic_1c_2c_3s_1^2s_2s_3 \sin \delta$. One more merit is that one can read the Jarlskog triangles directly from Eq. (4). For a Jarlskog triangle, three lines of the Jarlskog triangle are given by three elements obtained from two columns (or two rows) of Eq. (4). Three Jarlskog triangles for columns are presented in Ref. [7].

The CKM matrix does not fix a BSM. The chief reason is that the unitary matrices of the right-handed fields, R , are not completely fixed. One interesting choice is $R = L$. In Ref. [10], $R = L$ is used to determine the maximal CP phase through the Froggatt-Nielsen mechanism.

The good choice of the phases such that $\text{Det}.V_{\text{CKM}} = \text{real}$ is related to the PQ symmetry. The PQ symmetry needs heavy quarks [11] or two Higgs doublets [12]. Supersymmetry (SUSY) needs two Higgs doublets also, H_u and H_d . But, the PQ symmetry forbids the $\mu H_u H_d$ term in the superpotential W , which is the so-called μ problem [13]. This is a serious problem challenging a TeV scale electroweak symmetry breaking. We must achieve the $\text{SU}(2) \times \text{U}(1)$ breaking at a TeV scale. This μ problem has been expressed in several different objectives: (1) The doublet-triplet splitting problem in SUSY GUTs, (2) ‘‘Is there the PQ symmetry?’’, (3) ‘‘How large is the μ term?’’, (4) The B_μ problem in the GMSB, (5) ‘‘Why is there only one pair of Higgs doublets?’’, etc. To forbid a GUT scale μ , the PQ or R symmetries have been used, e.g. $W = \mu H_u H_d$ is forbidden if $X_{\text{PQ}}(H_u) = 1$ and $X_{\text{PQ}}(H_d) = 1$. Generating a TeV scale μ is another problem. There are two well-known method generating a TeV scale μ [13, 14]. At this PATRAS Workshop, the axion solution is of common interest, employing a nonrenormalizable term using singlet fields $S_{1,2}$, $W \sim (1/M_P)S_1S_2H_uH_d$, with $\langle S_{1,2} \rangle \approx 10^{10-12}$ GeV. This leads to the very light axion and axion cosmology. The axion cosmology restricts the axion decay constant below 10^{12} GeV, but it also depends on the initial misalignment angle θ_1 as recently calculated in [15], taking into account the overshoot factor and the anharmonic correction.

String compactification has been used to study the axion, the μ problem and R-parity. Since there is no exact global symmetry in string, the $\text{U}(1)_{\text{PQ}}$ and $\text{U}(1)_R$ symmetries (if needed) must be approximate. For the PQ symmetry, the coupling $c_{a\gamma\gamma}$ turns out to be small [16].

Finally, we comment on the realization of one Higgs doublet pair and an exact R-parity, by enlarging the electroweak group to $\text{SU}(3) \times \text{U}(1)$ at the GUT scale. It has been worked out in a \mathbb{Z}_{12-I} orbifold compactification [17]. Under $\text{SU}(3)_c \times \text{SU}(3)_W$, the left-handed three quark families appear as $3(\mathbf{3}_c, \mathbf{3}_W)$. To cancel $\text{SU}(3)_W$ anomaly, we must have nine $\mathbf{\bar{3}}_W$. Nine $\mathbf{\bar{3}}_W$'s split into three $\mathbf{\bar{3}}_W$'s, each constituting like (N, ν_e, e) . The remaining six contain H_u and H_d : $T_u = (S^+, H_u^+, H_u^0)$ and $T_d = (S^0, H_d^0, H_d^-)$. Now, we note that H_u and H_d coupling must come from a product of $\mathbf{\bar{3}}$'s. Note that it is not possible to write a term with two $\mathbf{\bar{3}}$'s. A

$SU(3)_W$ invariant coupling is possible by multiplying three $\bar{\mathbf{3}}$'s with antisymmetric combinations, $\epsilon_{IJK}\bar{\mathbf{3}}^I\bar{\mathbf{3}}^J\bar{\mathbf{3}}^K$. Therefore, in the flavor space the $H_u - H_d$ mass matrix is antisymmetric and hence its determinant is zero. It presents a bosonic flavor symmetry of Higgs doublets, and in effect one Higgs doublet pair must be light [17]. In fact, we realize this type of realization in an F-theory compactification [4]. We had this in the orbifold compactification. Of course, $SU(5)$ GUT cannot house $SU(3)_c \times SU(3)_W \times U(1)$. To have a hexality, we must extend to an $SU(6)$ GUT since the center of $SU(6)$ is \mathbb{Z}_6 . A hexality model, housing an exact R-parity, has been constructed in [4].

In conclusion, I presented three topics beyond the SM paying attention to my recent papers: There is no Z' below 10 TeV, otherwise our wisdom to the SM is in trouble, a useful suggestion for the CKM matrix, and a realization of one pair of Higgs doublets and an exact R-parity in the MSSM from a string compactification.

Acknowledgments

This work is supported in part by the National Research Foundation (NRF) grant funded by the Korean Government (MEST) (No. 2005-0093841).

References

- [1] For a review, see, P. Langacker, “The Physics of Heavy Z' Gauge Bosons ”, *Rev. Mod. Phys.* **81** (2009) 1199 [arXiv:0801.1345 [hep-ph]].
- [2] J. E. Kim and S. Shin, “ Z' from $SU(6) \times SU(2)_h$ GUT, W_{jj} Anomaly and Higgs Boson Mass Bound”, [arXiv:1104.5500[hep-ph]].
- [3] B. M. Demirköz *et al.*[ATLAS collaboration], talk presented at this 7th PATRAS Meeting.
- [4] K.-S. Choi and J. E. Kim, “Supersymmetric Three Family Chiral $SU(6)$ Grand Unification Model from F-theory”, *Phys. Rev.* **D 83**, 065016 (2011) [arXiv: 1012.0847[hep-ph]].
- [5] J. E. Kim, “Reason for $SU(6)$ Grand Unification”, *Phys. Lett.* **B 107** (1981) 69.
- [6] K. Nakamura *et al.* (Particle Data Group), *J. Phys. G* **37**, 075021 (2010).
- [7] J. E. Kim and M.-S. Seo, “Parametrization of the CKM Matrix”, *Phys. Rev.* **D 84**, 037303 (2011) [arXiv:1105.3304[hep-ph]].
- [8] For a review, see, J. E. Kim and G. Carosi, “Axions and the Strong CP Problem”, *Rev. Mod. Phys.* **82** (2010) 557 [arXiv: 0807.3125[hep-ph]].
- [9] R. D. Peccei and H. R. Quinn, “CP Conservation in the Presence of Instantons”, *Phys. Rev. Lett.* **38** (1977) 1440.
- [10] J. E. Kim, “The CKM Matrix with Maximal CP Violation from \mathbf{Z}_{12} symmetry”, *Phys. Lett.* **B 704** (2011) 360 [arXiv:1109.0995[hep-ph]].
- [11] J. E. Kim, “Weak Interaction Singlet and Strong CP Invariance”, *Phys. Rev. Lett.* **43** (1979) 103; M. A. Shifman, V. I. Vainstein, V. I. Zakharov, *Nucl. Phys.* **B 166** (1980) 4933.
- [12] M. Dine, W. Fischler and M. Srednicki, “A Simple Solution to the Strong CP Problem with a Harmless Axion”, *Phys. Lett.* **B 104** (1981) 199; A. P. Zhitnitskii, *Sov. J. Nucl. Phys.* **31**, 260 (1980).
- [13] J. E. Kim and H. P. Nilles, “The μ -Problem and the Strong CP Problem”, *Phys. Lett.* **B 138** (1984) 150.
- [14] G. Giudice and A. Masiero, “A Natural Solution to the μ Problem in Supergravity Theories”, *Phys. Lett.* **B 206** (1988) 480.
- [15] K.-J. Bae, J.-H. Huh and J. E. Kim, “Update of Axion CDM Energy Density”, *J. Cos. Astropart. Phys.* **09** (2008) 005.
- [16] K.-S. Choi, I.-W. Kim, and J. E. Kim, “String Compactification, QCD Axion and Axion-Photon-Photon Coupling”, *J. High Energy Phys.* **0703** (2007) 116 [arXiv:hep-ph/0612107].
- [17] J. E. Kim, *Phys. Lett.* **B 656** (2007) 207 [arXiv:0707.3292].

LHCb Physics, Performance, Prospects

Olaf Steinkamp, on behalf of the LHCb collaboration

Physik-Institut der Universität Zürich, Winterthurerstrasse 190, 8057 Zürich, Switzerland

DOI: http://dx.doi.org/10.3204/DESY-PROC-2011-04/steinkamp_olaf

The LHCb experiment at CERN's Large Hadron Collider (LHC) performs precision measurements of processes involving B mesons and other hadrons containing b or c quarks. Of particular interest are observables that exhibit high sensitivity to possible contributions from New Physics. LHCb has seen a rapid and very successful startup during the first year of physics at the LHC. About 37 pb^{-1} of pp collisions at a center of mass energy of 7 TeV were collected in 2010 and first competitive results from the analysis of these data were presented at the 2011 winter conferences. Analyses based on an almost ten times larger data set collected in spring 2011 are being prepared for the summer conferences. About 1 fb^{-1} are going to be collected by the end of 2011. These data will enable LHCb to perform sensitive searches for New Physics in many analyses.

1 The LHCb experiment

The main goal of the LHCb experiment [1] is to search for signatures of New Physics beyond the Standard Model of particle physics. LHCb does this by performing precision measurements of the mixing and decay of hadrons that contain a b or c quark. Of particular interest are processes that involve loop diagrams and that are suppressed in the Standard Model. Most New Physics models predict heavy, new particles that can appear in the loops and affect the magnitudes or phases of observables. The sensitivity to these possible contributions from New Physics is particularly large, if the predicted Standard Model value of the observable is small. A prominent example is the $B_s^0 - \bar{B}_s^0$ mixing phase, ϕ_s . In the Standard Model, $B_s^0 - \bar{B}_s^0$ mixing proceeds through box diagrams involving a double W^\pm exchange. The phase of this process is predicted to be close to zero with small uncertainty. The observation of a significantly larger mixing phase would be a clear hint for contributions from New Physics. A precise measurement of ϕ_s involves many of the key features of the LHCb experiment: large samples of reconstructed B_s^0 and \bar{B}_s^0 decays, an excellent decay time resolution to resolve the rapid $B_s^0 - \bar{B}_s^0$ flavour oscillations, and an efficient kaon identification for tagging the flavour of the B_s^0 meson at production.

The $b\bar{b}$ production cross section at the LHC is strongly peaked towards small polar angles with respect to the beam axis. The LHCb detector is therefore laid out as a forward spectrometer, as illustrated in Fig. 1. Excellent vertex and momentum resolution is provided by the vertex locator (VELO) and four tracking stations (TT, T1-T3) surrounding a dipole magnet with an integrated field of about 4 Tm. To achieve the best possible resolution on production and decay vertices and the decay length of the short-lived and rapidly oscillating B mesons, the VELO is installed inside the LHC vacuum vessel. Only a $300 \mu\text{m}$ thin aluminium foil separates the detectors from the LHC beams. During data taking, the detectors approach the beams to

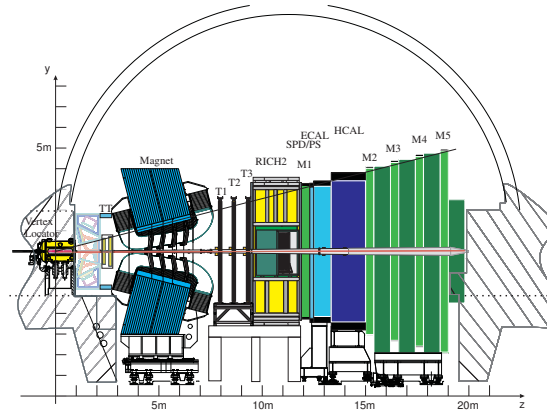


Figure 1: Vertical cross section through the LHCb detector. The LHC proton beams collide inside the Vertex Locator on the left.

as little as 8 mm. Excellent kaon/pion separation over a wide momentum range from 2 GeV/ c to above 100 GeV/ c is provided by two RICH detectors using a combination of three different radiators. The detector is completed by a calorimeter system (PRS, SPD, ECAL, HCAL) and a muon system (M1-M5). The calorimeter and muon systems provide the input for the first level trigger. This trigger level is implemented in hardware and searches for muon and hadron candidates with transverse momenta above a few GeV/ c . It reduces the event rate from the 40 MHz bunch crossing frequency of the LHC to about 1 MHz. The higher level triggers have access to the full detector information and are implemented in software running on a multi-processor computer farm. They make use of generic features of B decays, such as displaced decay vertices as well as large impact parameters and high transverse momenta of decay products to reduce the rate to about 30 kHz and then perform exclusive event selections for specific decay channels. Events are saved to disk at a rate of a few kHz. The flexibility of the trigger scheme proved very useful during the first year of LHC operation as it allowed to adjust selection criteria to the rapidly changing running conditions.

LHCb was designed to operate at an instantaneous luminosity of $2 \times 10^{32} \text{ cm}^{-2}\text{s}^{-1}$. Towards the end of the 2010 data taking period, this luminosity was reached although the number of proton bunches circulating in the LHC was still significantly smaller than nominal. This was made possible by operating the experiment at significantly higher number of proton-proton interactions per LHC bunch crossing than originally foreseen. Even under these harsher than foreseen running conditions, the LHCb experiment performed extremely well. Significantly more than 90% of all detector channels were fully operational and about 37 pb^{-1} of data were collected in 2010 with a data taking efficiency in excess of 90%. Key performance parameters, such as decay time and invariant mass resolutions were close to expectation from Monte Carlo simulations. Small remaining differences are attributed to the not yet perfect spatial alignment of the detector and calibration of the magnetic field strength. In 2011, the number of proton bunches in the LHC has been increased to half its nominal value and LHCb is operating at up to a factor of two higher instantaneous luminosity than originally foreseen.

2 Selected results from the 2010 data taking

The data collected in 2010 were successfully employed not only to verify the detector performance and commission analyses but also to produce first competitive physics results. An example of this is the first LHCb measurement of the $B_s^0 - \bar{B}_s^0$ oscillation frequency, Δm_s . This quantity has been previously measured at the Tevatron and the most precise result, $\Delta m_s = 17.77 \pm 0.10(\text{stat}) \pm 0.07(\text{syst}) \text{ ps}^{-1}$ [2], has been published by the CDF collaboration. For LHCb, the ability to resolve the rapid $B_s^0 - \bar{B}_s^0$ oscillations is a prerequisite for several key analyses, most notably the measurement of the $B_s^0 - \bar{B}_s^0$ mixing phase, ϕ_s , mentioned above. A first measurement of Δm_s has been performed using a sample of 1800 $B_s^0 \rightarrow D_s^\pm \pi^\mp$ and $B_s^0 \rightarrow D_s^\pm 3\pi$ decays collected in 2010. The measurement essentially requires three ingredients from each event: the decay time of the B_s^0 meson, its flavour at production, and its flavour at decay. The decay time is determined from the measured positions of the production and decay vertices and the reconstructed momentum of the B_s^0 meson. The flavour at decay is given by the charge of the D_s^\pm meson. The determination of the flavour at production relies on the fact that a b quark is usually produced in association with an \bar{b} quark and vice-versa. The flavour of the B_s^0 under investigation can therefore be implied by looking at flavour-specific signatures from the decay of the accompanying opposite-flavour b hadron. In particular, the charge of a decay lepton or kaon or the sum of charges of particles from the decay vertex of the accompanying b hadron are used. The preliminary result of this first LHCb measurement, $\Delta m_s = 17.63 \pm 0.11(\text{stat}) \pm 0.04(\text{syst}) \text{ ps}^{-1}$ [3], is compatible with the published CDF measurement and already has a comparable statistical error and a significantly smaller systematic error. This result reflects the excellent vertex and momentum resolution of the detector. A measurement of Δm_s with reduced statistical uncertainty, using a ten times larger data sample collected in spring 2011, will be shown at the summer conferences.

The particle identification capability of the experiment is illustrated by the observation of a clear signal for direct CP violation in $B^0 \rightarrow K^\pm \pi^\mp$ decays. Excellent kaon/pion separation is required, first to separate the $B^0 \rightarrow K^\pm \pi^\mp$ signal from other two-body B meson decays such as $B^0 \rightarrow \pi^+ \pi^-$ and $B_s^0 \rightarrow K^+ K^-$, and then to distinguish between $B^0 \rightarrow K^+ \pi^-$ decays and $\bar{B}^0 \rightarrow K^- \pi^+$ decays. The resulting invariant mass distributions for the two charge conjugated final states are shown in Fig. 2. The asymmetry due to direct CP violation in this decay is clearly visible in the raw event yields. Production and detection asymmetries are small and after correcting for these, a preliminary result for the CP asymmetry of $A_{\text{CP}} = [\Gamma(\bar{B}^0 \rightarrow K^- \pi^+) - \Gamma(B^0 \rightarrow K^+ \pi^-)] / [\Gamma(\bar{B}^0 \rightarrow K^- \pi^+) + \Gamma(B^0 \rightarrow K^+ \pi^-)] = 0.074 \pm 0.033(\text{stat}) \pm 0.008(\text{syst})$ is found [4]. This result is in good agreement with the current world average of $A_{\text{CP}} = -0.098_{-0.011}^{+0.012}$ [5]. Note that the precision of the LHCb result is again limited by its statistical uncertainty. A significantly more precise result is expected from the 2011 data.

Another early benchmark analysis is the search for the very rare decay $B_s^0 \rightarrow \mu^+ \mu^-$. This decay is strongly suppressed in the Standard Model, which predicts a branching fraction of $\mathcal{B}(B_s^0 \rightarrow \mu^+ \mu^-) = (3.2 \pm 0.2) \times 10^{-9}$ [6]. The branching fraction can be significantly enhanced in many extensions of the Standard Model. Searches for $B_s^0 \rightarrow \mu^+ \mu^-$ have been performed at the Tevatron but the decay has not been observed yet. The best upper limit on the branching fraction so far has been reported by the CDF collaboration, $\mathcal{B}(B_s^0 \rightarrow \mu^+ \mu^-) < 3.6 \times 10^{-8}$ at 90% CL [7]. Based on a search for this decay in the 2010 data, LHCb has published an upper limit of $\mathcal{B}(B_s^0 \rightarrow \mu^+ \mu^-) < 4.3 \times 10^{-8}$ at 90% CL [8], which already approaches the best Tevatron result. A significantly improved LHCb result, based on the data sample collected in

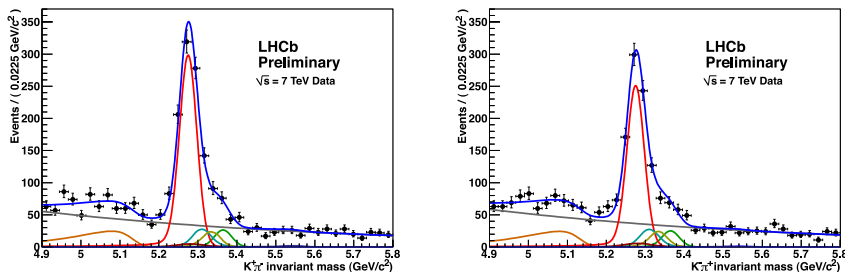


Figure 2: Invariant mass distributions for $K^+\pi^-$ (left) and for $K^-\pi^+$ (right).

spring 2011, will be shown at the summer conferences.

Both Tevatron experiments, CDF and D0, have reported measurements of the $B_s^0 - \bar{B}_s^0$ mixing phase, ϕ_s , which might hint at a possible discrepancy with the Standard Model prediction [9]. The statistical precision of these measurements is, however, still rather limited. The size of the LHCb data set collected in 2010 does not yet suffice to perform a competitive measurement of ϕ_s . As a proof of principle of the measurement, an analysis has nevertheless been performed with encouraging results [10]. A competitive ϕ_s measurement based on the data sample collected in spring 2011 will be shown at the summer conferences.

3 Physics potential

A few measurements with good sensitivity to possible contributions from New Physics have already been mentioned above. Another key measurement for LHCb is the precise determination of the CKM angle $\gamma = \arg(V_{ud}V_{ub}^*/V_{cd}V_{cb}^*)$. Various methods have been proposed that would allow a theoretically clean determination of γ , but they all require large samples of B meson decays to kaons and pions. Therefore γ is so far not well constrained by direct measurements. Using the 2011/2012 data samples, LHCb expects to determine γ to a precision of about 5° from pure tree decays such as $B^\pm \rightarrow D^0 K^\pm$ as well as from loop-induced Penguin decays such as $B^0 \rightarrow \pi^+\pi^-$ and $B_s^0 \rightarrow K^+K^-$. As New Physics is not expected to affect tree decays at a significant level, a comparison of the results obtained in these two approaches will provide a sensitive test for possible New Physics contributions in the loops. Moreover, a comparison of the measured value of γ with the value of γ obtained from Standard Model fits will test the CKM picture of CP violation in the b sector.

LHCb also has a strong and interesting physics programme in the charm sector. In particular, CP violation in $D^0 - \bar{D}^0$ mixing is predicted to be very small in the Standard Model. Experimentally, this field is not well explored so far and therefore provides excellent discovery potential.

Finally, the unique forward acceptance of the LHCb detector also provides for interesting measurements in other fields, such as electroweak physics, where the measurement of differential cross sections for W^\pm and Z^0 production and Drell-Yan processes can constrain the parton density functions of the proton. These measurements provide important input for example for the estimation of backgrounds in SUSY searches at ATLAS and CMS.

LHCb will collect a data sample of about 1 fb^{-1} by the end of 2011 and can expect up to

3 fb^{-1} by the end of 2012. These data sets will permit LHCb to perform sensitive searches for New Physics contributions in many analyses. These searches will either lead to the indirect discovery of New Physics beyond the Standard Model or permit to severely constrain the parameter space of New Physics models.

I would like to thank the organizers of the 7th Patras Workshop on Axions, WIMPs and WISPs for having given me the opportunity to present the beauty-ful physics of the LHCb experiment in the beautiful setting of the greek island of Mykonos.

References

- [1] LHCb collaboration, 2008 JINST 3 S08005.
- [2] CDF collaboration, Phys. Rev. Lett. 97 (2006) 242003, [arXiv:hep-ex/0609040].
- [3] LHCb collaboration, LHCb-CONF-2011-005.
- [4] LHCb collaboration, LHCb-CONF-2011-011.
- [5] E. Barberio et al. [Heavy Flavor Averaging Group], <http://www.slac.stanford.edu/xorg/hfag/rare/ichep10/acp/>.
- [6] A.J. Buras, Acta Phys. Polon. B41 (2010) 2487, [arXiv:1012.1447 [hep-ph]].
- [7] CDF collaboration, CDF public note 9892.
- [8] LHCb collaboration, Phys. Lett. B 699 (2011) 330, [arXiv:1103.2465 [hep-ex]].
- [9] CDF collaboration, CDF Public Note 10206; D0 collaboration, D0 Note 6098-CONF.
- [10] LHCb collaboration, LHCb-CONF-2011-006.

ATLAS Results on SUSY

Bilge M. Demirköz^{1,2}

¹Institut de Física d'Altes Energies (IFAE), Barcelona, Spain

²Middle East Technical University (METU), Ankara, Turkey
for the ATLAS collaboration

DOI: http://dx.doi.org/10.3204/DESY-PROC-2011-04/demirkoz_bilge

High luminosity data collected at a center-of-mass energy of 7 TeV at the Large Hadron Collider by ATLAS experiment has allowed it to search for supersymmetry (SUSY) and SUSY signatures with an unprecedented statistical precision and mass reach. We here present searches for different signatures in many channels, including jets plus missing transverse energy (E_T^{miss}), optionally with leptons, di-leptons plus E_T^{miss} , B -jets plus E_T^{miss} as well as electron plus muon resonance and slow meta-stable particle searches.

1 Introduction

The Large Hadron Collider has been providing proton-proton collisions to the experiments since the end of 2009 and, since March 2010, has been operating at 7 TeV center-of-mass. The peak instantaneous luminosity delivered to ATLAS at the time of the Patras workshop was $1.26 \times 10^{33} \text{ cm}^{-2} \text{ s}^{-1}$ in 2011 while it was $0.21 \times 10^{33} \text{ cm}^{-2} \text{ s}^{-1}$ in 2010. Reduction in β^* to 1.5 as well as the increase in the number of bunches in the collider to 1236 bunches and the increase in the bunch charge to 1.4×10^{11} allowed for this increase in luminosity. The data taking efficiency for ATLAS remains above 95% since the start of data-taking.

The ATLAS detector is a multipurpose particle physics apparatus with a forward-backward symmetric cylindrical geometry and nearly 4π coverage in solid angle [1]. A thin solenoid provides a 2 T magnetic field in the volume of inner tracking detectors, consisting of silicon pixel, silicon microstrip detectors and a transition radiation tracker. The surrounding calorimeters are of particular importance to analyses involving the transverse missing energy observable. In the pseudorapidity region $|\eta| < 3.2$, high-granularity liquid-argon (LAr) electromagnetic (EM) sampling calorimeters are used. An iron-scintillator tile calorimeter provides hadronic coverage over $|\eta| < 1.7$. The end-cap and forward regions, spanning $1.5 < |\eta| < 4.9$, are instrumented with LAr calorimetry for both EM and hadronic measurements. The muon spectrometer (MS) surrounds the calorimeters and consists of three large superconducting toroids, a system of precision tracking chambers, and detectors for triggering.

2 SUSY searches

Here we present results from data taken in 2010 and in two cases, updated with data taken in 2011. As the SUSY parameter space is very large, the search results here are presented for representative models.

2.1 Searches using Missing Transverse Energy

In R-parity conserving SUSY models, missing transverse energy, E_T^{miss} , is a very important observable as stable, neutral and weakly-interacting particles predicted by SUSY can escape the ATLAS detector without leaving behind any track and energy deposition. Especially noteworthy, a dark matter candidate, the lightest supersymmetric particle, would have a E_T^{miss} signature. In ATLAS, E_T^{miss} is measured using calorimeter cells over the full range of $|\eta| < 4$ and corrected for the energy of reconstructed physics objects, such as muons. Here we now discuss searches employing this observable.

2.1.1 Jets plus Missing Transverse Energy Search

A search for squarks and gluinos in final states containing jets, missing transverse momentum and no electrons or muons was first presented, with $35pb^{-1}$ of data [2]. This analysis has been updated with data collected in 2011, with a total integrated luminosity of $165pb^{-1}$ and extends the sensitivity of the search by including final state topologies with at least 4 jets [3]. In a large number of R-parity conserving models, squarks, \tilde{q} and gluinos, \tilde{g} can be produced in pairs, decay through $\tilde{q} \rightarrow q\chi_1^0$ and $\tilde{g} \rightarrow qq\chi_1^0$ to weakly-interacting neutralinos, leading to decays with jets and E_T^{miss} in the final state.

As no excess above the Standard model background was observed, 95% confidence level limits were set: gluino masses below 725 GeV are excluded in simplified models containing only squarks of the first two generations, a gluino octet and a massless neutralino. The exclusion increases to 1025 GeV for equal mass squarks and gluinos. In MSUGRA/CMSSM models with $\tan\beta = 10$, $A_0 = 0$ and $\mu > 0$, squarks and gluinos of equal mass are excluded for masses below 950 GeV, as shown in Fig. 1. While being model dependent, this search provides the highest mass reach limits out of all the searches presented in this paper.

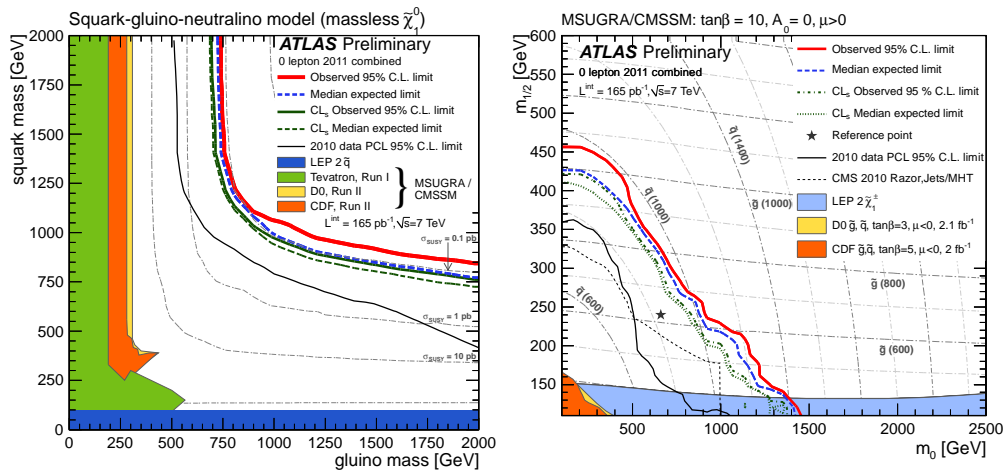


Figure 1: Results of the jets plus E_T^{miss} search. Left: Combined exclusion limits (solid red line) in the $(m_{\tilde{g}} ; m_{\tilde{q}})$ plane for the simplified squark–gluino model with massless χ_1^0 . Right: Combined exclusion limits in the $(m_0 ; m_{1/2})$ plane of mSUGRA for which $\tan(\beta) = 10$, $A_0 = 0$ and $\mu > 0$.

2.1.2 Jets plus Missing Transverse Energy with Leptons Search

In R-parity conserving SUSY models, the chargino decay into the lightest supersymmetric particle can produce a high-momentum lepton. The search for SUSY with jets, E_T^{miss} with one isolated electron or muon, at least three high- p_T jets and significant E_T^{miss} was first performed with $35pb^{-1}$ of data [4, 5] and was later updated with $165pb^{-1}$ of data [6].

The search for SUSY with jets, E_T^{miss} and two leptons was performed with $35pb^{-1}$ of data [7, 8]. Different search strategies, based on identical sign or opposite sign electrical charges was employed. Specifically, a flavour subtraction technique has been used to search for an excess beyond SM expectations of high p_T^{miss} events containing opposite charge identical flavour lepton pairs. Based on specific bench-mark models, limits are placed on the squark mass between 450 and 690 GeV for squarks approximately degenerate in mass with gluinos, depending on the supersymmetric mass hierarchy considered. The search for SUSY with jets, E_T^{miss} and multi-leptons was also performed with $34pb^{-1}$ of data [9].

2.1.3 B-jets plus Missing Transverse Energy with leptons search

Final states rich in b -jets can be produced by the decay of the gluino to sbottom, \tilde{b} or to stop, \tilde{t} . Search for supersymmetric particles in events with large missing transverse momentum and at least one heavy flavour jet candidate was performed using $35pb^{-1}$ of data [10]. No significant excess is observed with respect to the prediction for Standard Model processes. For R-parity conserving models in which sbottoms are the only squarks to appear in the gluino decay cascade, gluino masses below 590 GeV are excluded at the 95% confidence level. For stops, the limit is 520 GeV respectively.

2.2 Other searches

2.2.1 Search for electron plus muon resonance

Search for a heavy particle decaying into an $e^\pm\mu^\mp$ was performed, selecting an electron and muon with opposite signs with $p_T > 20$ GeV and requiring isolation, with $35pb^{-1}$ of data [11]. As no excess above the Standard Model background expectations was observed, 95% confidence-level limits were placed on two representative models. In an R-parity violating SUSY model, tau sneutrinos could produce such a signature and those with a mass below 0.75 TeV are excluded by this study, assuming single coupling dominance and the couplings $\lambda'_{311} = 0.11$ and $\lambda'_{312} = 0.07$. In a lepton flavor violating model, a Z' -like vector boson with masses of 0.70 to 1.00 TeV and corresponding cross sections times branching ratios of 0.175 to $0.183pb^{-1}$ is excluded.

2.2.2 Search for stable hadronizing squarks and gluinos

Coloured sparticles, predicted by SUSY, can hadronise into long-lived bound hadronic states, termed R-hadrons. A search for slow-moving charged particles was performed by triggering on E_T^{miss} , requiring isolation from jets in the event and a large ionisation energy loss in the pixel detector as well as requiring a long time-of-flight in the tile calorimeter, with $34pb^{-1}$ of data [12]. As no deviations from Standard Model background expectations was observed and 95% confidence-level limits can be set on the production cross-sections of squarks and gluinos. The influence of R-hadron interactions in matter was studied using a number of different models,

and lower mass limits for stable sbottoms, stops and gluinos are found to be at 294 GeV, 309 GeV and 562 GeV respectively.

2.2.3 Long-lived charged particle search

A search for heavy long-lived charged particles reaching the muon spectrometer, allowed by SUSY, specifically for meta-stable sleptons, squarks and gauginos, was also performed [13] with $37pb^{-1}$ of data. Requiring a late arrival time in the muon spectrometer, a well-measured Lorentz β factor and requiring it to be lower than 0.95, no excess above the estimated background was observed. Therefore, 95% confidence-level limits on $\tilde{\tau}$ and R-hadron production are set: Sleptons produced in electroweak processes are excluded up to a mass of 110 GeV. Stable $\tilde{\tau}$'s are excluded up to a mass of 136 GeV, in gravity-mediated SUSY breaking (GMSB) models with $N_5 = 3$, $m_{messenger} = 250$ TeV, $\text{sign}(\mu) = 1$ and $\tan\beta = 5$. Depending on the fraction of R-hadrons produced as \tilde{g} -balls, gluino R-hadrons in a generic interaction model are excluded up to masses of 530 GeV to 544 GeV.

3 Conclusion

The results presented here from ATLAS extend searches and provide more stringent constraints than the previous results from the Tevatron. The total integrated luminosity in 2011 by ATLAS was $5.25fb^{-1}$ and results are in the process of being updated. We would like to thank the LHC team for the excellent performance and the fast ramp of luminosity.

4 Bibliography

References

- [1] G. Aad *et al.* [ATLAS Collaboration], “The ATLAS Experiment at the CERN Large Hadron Collider,” JINST **3**, S08003 (2008).
- [2] G. Aad *et al.* [ATLAS Collaboration], “Search for squarks and gluinos using final states with jets and missing transverse momentum with the ATLAS detector in $\sqrt{s} = 7$ TeV proton-proton collisions,” Phys. Lett. B **701**, 186 (2011) [arXiv:1102.5290 [hep-ex]].
- [3] G. Aad *et al.* [ATLAS Collaboration], “Search for squarks and gluinos using final states with jets and missing transverse momentum with the ATLAS detector in $\sqrt{s} = 7$ TeV proton-proton collisions,” ATLAS-CONF-2011-086.
- [4] G. Aad *et al.* [ATLAS Collaboration], “Search for supersymmetry using final states with one lepton, jets, and missing transverse momentum with the ATLAS detector in $\sqrt{s} = 7$ TeV pp,” Phys. Rev. Lett. **106**, 131802 (2011) [arXiv:1102.2357 [hep-ex]].
- [5] G. Aad *et al.* [ATLAS Collaboration], “Combined exclusion reach of searches for squarks and gluinos using final states with jets, missing transverse momentum, and zero or one lepton, with the ATLAS detector in $\sqrt{s} = 7$ TeV proton-proton collisions,” ATLAS-CONF-2011-064.
- [6] G. Aad *et al.* [ATLAS Collaboration], “Search for supersymmetry with jets, missing transverse momentum and one lepton at $\sqrt{s} = 7$ TeV,” ATLAS-CONF-2011-090.
- [7] G. Aad *et al.* [ATLAS Collaboration], “Search for an excess of events with an identical flavour lepton pair and significant missing transverse momentum in $\sqrt{s} = 7$ TeV proton-proton collisions with the ATLAS detector,” Eur. Phys. J. C **71**, 1647 (2011) [arXiv:1103.6208 [hep-ex]].
- [8] G. Aad *et al.* [ATLAS Collaboration], “Search for supersymmetric particles in events with lepton pairs and large missing transverse momentum in $\sqrt{s} = 7$ TeV proton-proton collisions with the ATLAS experiment,” Eur. Phys. J. C **71**, 1682 (2011) [arXiv:1103.6214 [hep-ex]].

- [9] G. Aad *et al.* [ATLAS Collaboration], “SUSY Searches at ATLAS in Multilepton Final States with Jets and Missing Transverse Energy,” ATLAS-CONF-2011-039.
- [10] G. Aad *et al.* [ATLAS Collaboration], “Search for supersymmetry in pp collisions at $\sqrt{s} = 7\text{TeV}$ in final states with missing transverse momentum and b-jets,” Phys. Lett. B **701**, 398 (2011) [arXiv:1103.4344 [hep-ex]].
- [11] G. Aad *et al.* [ATLAS Collaboration], “Search for a heavy particle decaying into an electron and a muon with the ATLAS detector in $\sqrt{s} = 7\text{TeV}$ pp collisions at the LHC,” Phys. Rev. Lett. **106**, 251801 (2011) [arXiv:1103.5559 [hep-ex]].
- [12] G. Aad *et al.* [ATLAS Collaboration], “Search for stable hadronising squarks and gluinos with the ATLAS experiment at the LHC,” Phys. Lett. B **701**, 1 (2011) [arXiv:1103.1984 [hep-ex]].
- [13] G. Aad *et al.* [ATLAS Collaboration], “Search for Heavy Long-Lived Charged Particles with the ATLAS detector in pp collisions at $\sqrt{s} = 7\text{TeV}$,” Phys. Lett. B **703**, 428 (2011) [arXiv:1106.4495 [hep-ex]].

Proton EDM Simulations Using Fourth-Order Runge-Kutta Integration

Selcuk Haciomeroglu^{1,2}, Yannis K. Semertzidis¹

¹Brookhaven National Laboratory, (BNL), Physics Dept., Upton, NY 11973-5000, USA

²Istanbul Technical University, Istanbul 34469, Turkey

DOI: http://dx.doi.org/10.3204/DESY-PROC-2011-04/semertzidis_yannis

High intensity, polarized protons can be stored in an all-electric ring to probe the proton electric dipole moment. The expected sensitivity level is $10^{-29} e \cdot \text{cm}$, better than any planned hadronic EDM experiment by one to two orders of magnitude. The protons at their magic momentum of $0.7 \text{ GeV}/c$ keep their spin vectors aligned with their momentum vectors in any transverse electric field for the duration of the storage time. However, not all protons within the acceptance of the ring, are exactly at the magic momentum. An RF-cavity is used to eliminate the first order effects responsible for the spread of angles between the spin and momentum vectors. We have used particle simulations and fourth-order Runge-Kutta integration to determine the second order effects. The spin coherence time, a measure of the angle spreads, are found to be adequate for a total storage time of 10^3 s . Further improvements, using sextupole magnets and/or stochastic cooling, could bring another order of magnitude improvement in the statistical sensitivity.

1 Introduction

High intensity (of order 10^{11}) polarized proton and deuteron beams have been used successfully for several decades in storage rings around the world. The experience gained using those beams provides a unique opportunity in the study of the electric dipole moment (EDM) of the proton and deuteron. The storage ring EDM collaboration has recently completed the proposal for a proton EDM experiment with a sensitivity of $10^{-29} e \cdot \text{cm}$. The method is using protons at their magic momentum of $0.7 \text{ GeV}/c$ in an all-electric storage ring [1]. Together with the neutron [2], the proton and deuteron EDM experiments will be able to decipher the CP-violating source should one particle is found to have a non-zero EDM. At $10^{-29} e \cdot \text{cm}$, they are testing the electro-weak Baryogenesis model, and will constrain it severely in case they are found to be consistent with zero. For the experimental method and the physics reach of the proton, deuteron, and muon EDM experiments, see [1, 3, 4, 5, 6, 7].

Three discrete symmetries play an important role in the standard model (SM): Parity (P), time (T) reversal and charge (C) symmetry. The interaction energy of a particle under an electric field is given by: $H = -d(\vec{s}/s) \cdot \vec{E}$ where d is the magnitude of EDM, \vec{E} is the electric field vector and \vec{s} is the spin vector. This equation implies that the EDM vector is aligned with the spin vector, which has its origins from the requirement of non-degeneracy in quantum mechanics. Since \vec{E} is a polar vector and \vec{s} is an axial vector, the Hamiltonian is odd under P and T transformations. Therefore, a nonzero EDM means that both P and T symmetries

are violated. Assuming CPT conservation, T-violation means CP-violation as well. Andrei Sakharov [8] first pointed out that CP-violation is one of the essential ingredients needed to make the baryon-antibaryon asymmetric universe we observe today from an initially symmetric one. Even though CP-violation has been observed in weak decays it is not nearly enough, by some eight orders of magnitude, to explain this baryon-antibaryon asymmetry. Therefore, a much stronger source of CP-violation is needed and if a proton EDM is observed it could provide it. Physics beyond the SM predicts new CP-violating phases well within the sensitivity level of the proton EDM experiment. The CP-violating phase in the weak interactions predicts a much smaller EDM for the proton, in the range of $10^{-31} - 10^{-33} e \cdot \text{cm}$.

2 Frozen Spin Method

A charged particle in an electric field region will accelerate and get lost unless the electric field is compensated by another force. For particles in storage rings the electric field is compensated by the centripetal force. The storage ring EDM method can at the same time store a large number of polarized particles and arrange for maximum EDM sensitivity under certain conditions [1, 3, 4, 5, 7]. If the spin and the momentum of the particle precess at the same rate, then there will be a radial E-field in the particle rest frame acting on its EDM vector precessing it out of plane. The method, using high intensity proton beams (4×10^{10} per cycle) with small momentum spread $(dp/p)_{\text{rms}} = 2 \times 10^{-4}$, is found to hold the most promise [1].

The general T-BMT equations give the spin and velocity precession of a relativistic particle in the presence of both E and B fields:

$$\frac{d\vec{s}}{dt} = \frac{e}{m} \vec{s} \times \left[\left(\frac{g}{2} - \frac{1-\gamma}{\gamma} \right) \vec{B} - \left(\frac{g}{2} - 1 \right) \frac{\gamma}{\gamma+1} (\vec{\beta} \cdot \vec{B}) \vec{\beta} - \left(\frac{g}{2} - \frac{\gamma}{\gamma+1} \right) \frac{\vec{\beta} \times \vec{E}}{c} \right] \quad (1)$$

$$\frac{d\vec{\beta}}{dt} = \frac{e}{\gamma m} \left[\vec{\beta} \times \vec{B} + \frac{\vec{E}}{c} - \vec{\beta} \frac{(\vec{\beta} \cdot \vec{E})}{c} \right] \quad (2)$$

where β , e and m are the velocity, charge and mass of the particle respectively, $\gamma = \sqrt{1 - \beta^2}$, c is the speed of light and g is the g-factor for spin, which is $g = 2.792847356(23)$ for the proton. Setting $B = 0$, and assuming $(\vec{\beta} \cdot \vec{E} = 0)$, the so-called $g - 2$ precession rate, i.e., the precession rate of the angle between the spin and momentum vectors, is:

$$\vec{\omega}_a = \frac{e}{m} \left[\frac{1}{\gamma^2 - 1} - a \right] \frac{\vec{\beta} \times \vec{E}}{c} \quad (3)$$

where $a = (g - 2)/2$ is the anomalous magnetic moment. Setting $\gamma = \sqrt{1/a + 1}$ locks the angle between the spin and momentum vectors as a function of time. This method is called the “frozen spin” method. This specific case leads to a “magic” momentum value for the proton: $p_0 = m/\sqrt{a} = 0.707 \text{ GeV}/c$.

For a particle at rest, E-fields only couple to EDMs (d) and magnetic fields only to magnetic dipole moments (μ), with the spin precession given by: $d\vec{s}/dt = \vec{d} \times \vec{E} + \vec{\mu} \times \vec{B}$. When the magnetic field is zero and the particle is at its magic momentum, the spin precession is affected only by EDM: $d\vec{s}/dt = \vec{d} \times \vec{E}$ causing a *vertical* spin precession for the duration of the storage

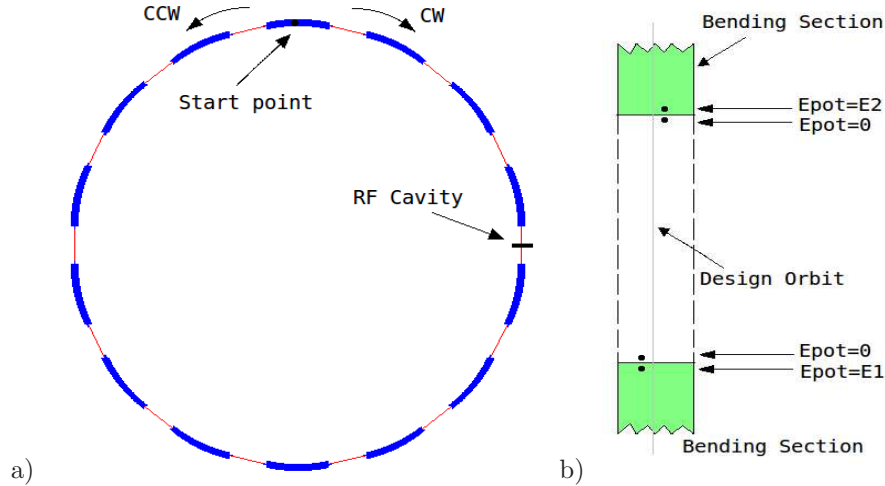


Figure 1: a) The ring includes 14 bending and straight sections, with one RF cavity. b) At the interface of bending and straight sections, kinetic and potential energy changes are made to keep the total energy conserved.

time. Since not all particles will be exactly at the “magic” momentum there is going to be a spread in the spin angles relative to their momentum vectors. The linear spread in angles is cancelled by using an RF-cavity in a straight section. Next we present a simulation that is sensitive to the second order effects.

The simulated ring is composed of 14 bending and straight sections (see Fig. 1 (a)). The assumed ring radius is $r = 40$ m and the radial electric field is 10.5 MV/m for a 3 cm plate separation. The electric field is provided by cylindrical plates, slightly modified to provide vertical focusing. The vertical tune was 0.2, while the E-field gradients comply with Maxwell’s equations up to fourth order. One of the straight sections includes an RF cavity. In the bending section, the position and spin of the particle are estimated by integrating Eqs. 1, 2 using the fourth order Runge-Kutta method [9]. At the boundaries of the straight sections, the fringe field is approximated with a sharp transition from a field region to no-field region (see Fig. 1 (b)). The potential energy of the particle is converted into kinetic energy at the entrance of the straight section. This is done by changing the longitudinal velocity of the particle, which is a good approximation. At the other end, when the particle reaches the bending section, its kinetic energy is again changed and shared again by kinetic and potential energy, according to its position. For example a particle at 1.5 cm away from the design orbit has a potential energy of about 150 keV. This corresponds to $dp/p = 3.5 \times 10^{-4}$.

Figure 2 shows the angle for $x_0 = z_0 = 0$ and $dp/p = 2 \times 10^{-4}$ for a ring with 28 m of total straight section length. It shows that the average spin precession rate is less than 0.004 rad/s for particles at the edge of the ring acceptance. Defining spin coherence time (SCT) as the time needed for the angle between spin and momentum to become 1 rad, Fig. 2 gives more than 250 seconds of SCT for particles off the “magic” momentum. Since those particles can be taken out at the polarimeter detector at early times, this finding supports a storage time of 10^3 s for each cycle without the need of compensating sextupoles. Using sextupoles and/or stochastic cooling the obtained SCT can be two orders of magnitude larger, further increasing the sensitivity of the

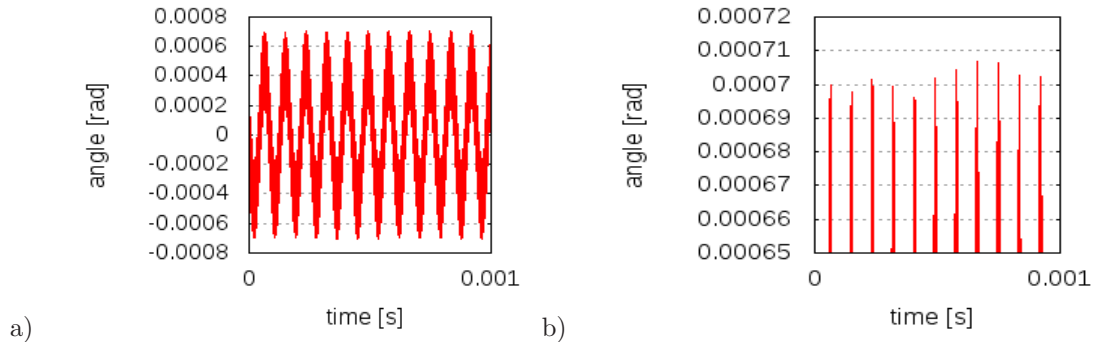


Figure 2: a) The angle between the spin and momentum vectors for $dp/p = 2 \times 10^{-4}$ and 28 m of total straight section length. b) Zoom-in the top region of (a) shows that the angle fluctuates but remains constant to about 0.25×10^{-5} radians over 1ms.

experiment by another order of magnitude. Finally, using the same tracking simulation, we have determined the acceptance of the ring to be: $\epsilon = x'^2 \frac{R}{Q_h} = (0.43 \times 10^{-3})^2 \times \frac{40}{1.3} = 5.6 \text{ mm mrad}$.

3 Conclusion

The simulation results show that the proposed frozen spin method, using “magic” momentum protons in an all-electric ring, provides a SCT that is adequate for a storage time of 10^3 seconds without the need of compensating sextupoles. In addition, for an all-electric ring with 3 cm aperture, the acceptance of the ring is found to be 5.6 mm mrad. In a future upgrade, applying compensating sextupoles and/or stochastic cooling could further improve the statistical sensitivity of the method by another order of magnitude.

References

- [1] V. Anastassopoulos *et al.* [Storage Ring EDM Collaboration], “A Proposal to Measure the Proton EDM with $10^{-29} e \cdot \text{cm}$ Sensitivity”, available from the collaboration web site: <http://www.bnl.gov/edm>.
- [2] There are several planned neutron EDM experiments: at the spallation neutron source (SNS) at Oak Ridge, Tennessee; at ILL at Grenoble, in France; at PSI, Villigen, Switzerland; and at more places under planning. Their sensitivity goal is between $10^{-27} e \cdot \text{cm}$ and $10^{-28} e \cdot \text{cm}$, limited mostly by statistics.
- [3] Y.K. Semertzidis *et al.*, “Sensitive Search for a Permanent Muon EDM”, proceedings of HIMUS99 workshop, Tsukuba, Japan, (1999), [arXiv:0012087 [hep-ph]].
- [4] Y.K. Semertzidis, “A New Method for a Sensitive deuteron EDM Experiment”, [arXiv:0308063 [hep-ex]].
- [5] F.J.M. Farley *et al.*, Phys. Rev. Lett. **93**, 052001 (2004), [arXiv:0307006 [hep-ex]].
- [6] Y.F. Orlov, W.M. Morse, and Y.K. Semertzidis, Phys. Rev. Lett. **96**, 214802 (2006).
- [7] <http://www.bnl.gov/edm> where the muon EDM Letter of Intent to J-PARC, and the deuteron, and proton EDM proposals are available.
- [8] A.D. Sakharov, JETP Lett. **5**, 24 (1967).
- [9] W.H. Press, S.A. Teukolsky, W.T. Vetterling, Numerical Recipes, (2007).

List of Authors

- Althaus, L., 158
Andreas, S., 60
Angloher, G., 11
Aprile, E., 15
Arias, P., 56
Asztalos, S. J., 47
Aune, S., 93
Avignone, F. T., 98
- Baker, O. K., 51
Barth, K., 93
Bauer, M., 11
Bavykina, I., 11
Belov, A., 93
Bento, A., 11
Betz, M., 76
Borghì, S., 93
Bräuninger, H., 93
Bradley, R., 47
Brax, P., 116
Bucci, C., 11
- Córsico, A., 158
Cadamuro, D., 139
Cantatore, G., 88, 93, 98
Carmona, J. M., 93, 98
Carosi, G., 47
Caspers, F., 76
Caspi, S., 98
Catalán, S., 158
Cetin, S. A., 93
Ciemiński, C., 11
Clarke, J., 47
Collar, J. I., 93
Crivelli, P., 35
Cudell, J. R., 147
- Döbrich, B., 82
Dafni, T., 93, 98, 120
Davenport, M., 93, 98
Demirköz, B. M., 174
- Derbin, A., 107, 112
Deuter, G., 11
Dudarev, A., 98
- Eleftheriadis, C., 93
Elias, N., 93
Erken, O., 43
Espriu, D., 143
Ezer, C., 93
- Fanourakis, G., 93, 98
Ferrer-Ribas, E., 93, 98
Friedrich, P., 93
- Gómez, H., 93, 98
Galán, J., 93, 98
García, J. A., 93, 98
GarcíaBerro, E., 158
Gardikiotis, A., 93, 120
Gasiór, M., 76
Gazis, E. N., 93
Gburek, S., 125
Georgiopolou, E., 120
Geralis, T., 93, 98
Gies, H., 82
Giomataris, I., 93, 98
Gironnet, J., 3
Gninenko, S., 93, 98
Gruber, E., 93
Guthörl, T., 93
- Haciomeroglu, S., 179
Hagmann, C., 47
Hartmann, R., 93
Hartnett, J. G., 64
Hasinoff, M., 93
Hauff, D., 11
Haug, F., 93
Hirshfield, J. L., 51
Hoffmann, D. H. H., 93, 98
Horns, D., 151

Hoskins, J., 47
 Hotz, M., 47
 Hutsemékers, D., 147

 Iguaz, F. J., 93, 98
 Irastorza, I. G., 93, 98
 Isaila, C., 11
 Isern, J., 158

 Jacoby, J., 93
 Jakovčić, K., 93, 98
 Janusz, S., 125
 Jiang, Y., 51
 Jochum, J., 11

 Königsmann, K., 93
 Karbstein, F., 82
 Karuza, M., 93
 Kayunov, A., 112
 Kazakov, S., 51
 Kiefer, M., 11
 Kim, J. E., 165
 Kimmerle, M., 11
 Kinion, D., 47
 Kishimoto, Y., 19
 Kotthaus, R., 93
 Krčmar, M., 93, 98
 Kuster, M., 93

 Lakić, B., 93, 98
 Lamanna, G., 31
 Lanfranchi, J.-C., 11
 LaPointe, M. A., 51
 Laurent, J. M., 93
 Li, H.-B., 7
 Lindner, A., 98, 129
 Liolios, A., 93
 Ljubičić, A., 93
 Lozza, V., 93
 Lutz, G., 93
 Luzón, G., 93, 98

 Malagon, A., 51
 Martin, A. J., 51
 Martin, C., 47
 Meyer, M., 151
 Morales, J., 93
 Moulin, E., 27
 Muratova, V., 107, 112

 Niinikoski, T., 93

 Nordt, A., 93

 Papaevangelou, T., 93, 98, 120
 Payez, A., 147
 Petricca, F., 11
 Pfister, S., 11
 Pivovarov, M. J., 93, 98
 Potzel, W., 11
 Povey, R. G., 64
 Pröbst, F., 11

 Raffelt, G., 93, 98
 Rashba, T., 93
 Redondo, J., 98, 129, 133, 139
 Reindl, F., 11
 Renau, A., 143
 Riege, H., 93
 Ringwald, A., 129
 Rodríguez, A., 93, 98
 Rosenberg, L. J., 47
 Rosu, M., 93
 Roth, S., 11
 Rottler, K., 11
 Russenschuck, S., 98
 Ruz, J., 93, 98
 Rybka, G., 47

 Sailer, C., 11
 Salaris, M., 158
 Savvidis, I., 93
 Schäffner, K., 11
 Schmalzer, J., 11
 Scholl, S., 11
 Schumann, M., 23
 Schwarz, M., 129
 Seidel, W., 11
 Semenov, D., 112
 Semertzidis, Y. K., 120, 179
 Shchelkunov, S., 51
 Shilon, I., 98
 Sikivie, P., 43, 47
 Silva, P. S., 93
 Slocum, P. L., 51
 Solanki, S. K., 93
 Steinkamp, O., 169
 Stewart, L., 93
 Stodolsky, L., 11
 Strandhagen, C., 11
 Strauss, R., 11
 Sullivan, N. S., 47

Szymkowiak, A., 51

Tam, H., 43
Tanner, D. B., 47
Tanzke, A., 11
Ten Kate, H., 98
Thumm, M., 76
Tobar, M. E., 64
Tomás, A., 93, 98
Torres, S., 158
Troitsky, S., 98, 102
Tsagri, M., 93, 120

Unzhakov, E., 112
Usherov, I., 11

Vafeiadis, T., 93
van Bibber, K., 47, 93, 98
Villar, J., 93, 98
Vogel, J. K., 93, 98
von Feilitzsch, F., 11
von Seggern, J.E., 72
von Sivers, M., 11

Wagner, A., 47
Walckiers, L., 98
Wawoczny, S., 11
Wester, W., 68
Wiedemann, G., 129
Willers, M., 11
Wong, H., 7

Yang, Q., 43
Yildiz, S. C., 93

Zöller, A., 11
Zioutas, K., 93, 98, 120



List of Participants

Abele, Hartmut – Atominstitut, TU Wien
Anastassopoulos, Vassilis – University of Patras
Andreas, Sarah – DESY
Aprile, Elena – Columbia University
Arias, Paola – DESY
Avignone, Frank – University of South Carolina
Baker, Keith – Yale University
Battesti, Rémy – CNRS-LNCMI
Baudis, Laura – University of Zürich
Bertone, Gianfranco – University of Zürich and IAP
Betz, Michael – CERN
Cadamuro, Davide – MPI für Physik, München
Cantatore, Giovanni – University of Trieste
Carmona, Jose Manuel – University of Zaragoza
Crivelli, Paolo – ETH Zürich
Cushman, Priscilla – University of Minnesota
Dafni, Theopisti – University of Zaragoza
Davenport, Martyn – CERN
Demirkoz, Bilge – University of Ankara
Derbin, Alexander – Nuclear Physics Institute, St. Petersburg
Döbrich, Babette – University of Jena
Ehret, Klaus – DESY
Espriu, Domenec – University of Barcelona
Finger, Michael – University of Prague
Finger, Miroslav – University of Prague
Gburek, Szymon – Polish Academy of Sciences
Gironnet, Johann – CNRS Lyon
Hasinoff, Michael – University of British Columbia
Irastorza, Igor – University of Zaragoza
Isern, Jordi – CSIC-IEEC
Jaeckel, Joerg – IPPP/Durham University
Karbstein, Felix – University of Jena
Keum, Yong-Yeon – Seoul University
Kharzeev, Dmitry – Stony Brook University
Kim, Jihn E. – Seoul University
Kishimoto, Yasuhiro – Kamoka Observatory, ICRR
Ko, Pyungwon – Korea Institute for Advanced Study
Lamanna, Giovanni – LAPP (CNRS/IN2P3)
Li, Hau-Bin – Academia Sinica, Taipei
Lindner, Axel – DESY
Malagon, Ana – Yale University
Manalaysay, Aaron – University of Zürich

Martin, Andrew – Yale University
Meyer, Manuel – University of Hamburg
Moore, Ben – University of Zürich
Moulin, Emmanuel – CEA Saclay
Muratova, Valentina – Nuclear Physics Institute, St. Petersburg
Payez, Alexandre – University of Liege
Povey, Rhys – University of Western Australia
Redondo, Javier – MPI für Physik, München
Ringwald, Andreas – DESY
Ruz Armendáriz, Jaime – CERN
Rybka, Gray – University of Washington
Sadoulet, Bernard – University of California, Berkeley
Schmidt-Wellenburg, Philipp – PSI
Schumann, Marc – University of Zürich
Schwarz, Matthias – Hamburger Sternwarte
Semenov, Dmitry – PNPI
Semertzidis, Yannis – Brookhaven National Laboratory
Sikivie, Pierre – University of Florida
Steinkamp, Olaf – University of Zürich
Strauss, Raimund – TU M'ünchen
Sulc, Miroslav – Technická Univerzita v Liberci
Suzuki, Yoichiro – Kamioka Observatory
Tanner, David – University of Florida
Touramanis, Christos – University of Liverpool
Troitsky, Sergey – Institute for Nuclear Research
Tsagri, Mary – CERN
Unzhakov, Evgeniy – PNPI
von Seggern, Eike – DESY
Wester, William – Fermilab
Zioutas, Konstantin – University of Patras

73 participants

Remote presentations from:

Brax, Philippe – CEA Saclay
van der Graaf, Harry – Nikhef

The article on the next page is reproduced with kind permission from CERN Courier.

Faces & Places

WORKSHOP

Casting light on the dark

More than 70 scientists from all over the world met on Mykonos, the Greek “island of the light”, to discuss current knowledge about the dark universe at the 7th PATRAS workshop on Axions, WIMPs and WISPs on 26 June – 1 July. As in previous meetings in the series, PATRAS 2011 brought together experimentalists and theorists to discuss the status of the field in an inspiring and friendly atmosphere.

The two major pillars of these meetings are the two best motivated candidates for particle dark matter – the axion and the weakly interacting massive particle (WIMP). Inspired by the possibilities that are opening up in ongoing axion searches and triggered by theoretical developments, particles with related properties have also become a focus of the workshop, so axion-like particles (ALPs) or more general, very weakly interacting slim (light) particles (WISPs) were covered in the range of presentations.

A few introductory talks set the scene. Pierre Sikivie of the University of Florida discussed axion dark matter and the special behaviour of this subelectron-volt particle. In particular, if axion dark-matter forms a Bose-Einstein condensate, it could lead to observable features in cosmological structures. This possibility sparked a lively discussion on how these features fare in the light of N-body simulations and observations. Such simulations are a speciality of Ben Moore of the University of Zurich, who determined the “frequency of elephants in the Galaxy” (or the number of Earth-Moon-like systems). Gianfranco Bertone, also currently at Zurich, focused on WIMP dark matter and explained that to pinpoint experimentally its major properties, mass and cross-section, with high precision, direct detection signals and signatures from collider experiments are necessary. This demonstrated that we truly live in exciting times as both direct-detection experiments and the LHC are delivering data at an astonishing rate. Jihn Kim of Seoul National University, one of the inventors of high-scale axion models, ventured beyond axions and showed how everything could be embedded into the bigger picture.

Direct dark-matter searches are a traditional focus of the workshop and there were presentations on the status of the EDELWEISS, XENON, CDEX/TEXONO,



The light shines on the participants at the 7th PATRAS workshop on the island of Mykonos, Greece. (Image credit: Marc Schumann.)

XMASS, CDMS, CRESS and DARWIN experiments and on their recent results. It became clear that the race to discover WIMP dark matter is on and it remains open as to whether the first hints will be from direct detection or the LHC. Indeed some direct detection experiments already report excess events, so one discussion session was devoted to the current situation, where signal claims of low-mass WIMPs by several experiments are challenged by the non-observations by several others. To resolve these issues, more efforts should go into co-ordinated background studies, a point that Priscilla Cushman of the University of Minnesota emphasized.

Experimental searches are developing rapidly for subelectron-volt (axion) dark matter and other particles, such as hidden photons and chameleons, which might provide a solution to the problem of dark energy as Philippe Brax, of Saclay, pointed out. This was evident in talks about several experiments – CAST, ADMX, the Yale cavity experiment, ALPS, GammeV, SHIPS and BMV/XAX – that in one way or another try to observe “light-shining through a wall” or even to convert dark matter into light. There are many more new and interesting ideas and experiments to shed light on very weak interactions, such as experiments with ultracold neutrons or, at somewhat higher energy scales, with electrons fired at

fixed targets. Talks on laboratory searches were complemented by presentations on astrophysical bounds on light particles, for example from the Sun or white dwarfs; the latter even provide a hint that such particles could be just around the corner.

The PATRAS programme traditionally also features recent results, new theoretical ideas, and exciting projects in particle and astroparticle physics, beyond the main focus of the conference. This year, there were several talks about the neutrino and in particular about the recent measurement of the last missing mixing angle by T2K (*CERN Courier* September 2011 p6), searches for electric dipole-moments and recent highlights from the ATLAS and LHCb experiments at the LHC.

As well as the inspiring talks and in-depth discussions, the beautiful venue, the delicious Greek food, an excursion to the famous ruins on the neighbouring island, Delos, and a memorable conference party, all made this workshop surpass the expectations of the participants and the organizers.

● The workshop was supported by CERN, DESY, the University of Patras, the Institute for Particle Physics Phenomenology (Durham University), and the University of Zurich. Further information and the slides of the presentations can be found at <http://axion-wimp.desy.de>. The next workshop will be held in Chicago in summer 2012.



7th Patras Workshop on Axions, WIMPs and WISPs
27 June-1 July 2011 · Mykonos · Greece

